

DCE
23

5th DOCTORAL
CONGRESS
IN ENGINEERING

Book of Abstracts



*DCE23 - Symposium on Chemical and
Biological Engineering*

DCE
23

5th DOCTORAL
CONGRESS
IN ENGINEERING

Book of Abstracts

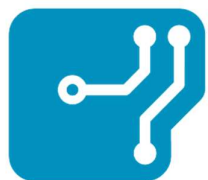
of the

Symposium on Chemical and Biological Engineering

Editors:

Alexandra Pinto, Cristiana Gomes, Joana Almeida, Joana Lopes,
Júlia Kessler, Mariana Bessa, Sara Ferreira, Susana Fernandes

Porto
June 2023



INESCTEC



APDL

**ADMINISTRAÇÃO DOS PORTOS
DOURO • LEIXÕES • VIANA**

ADDVOLT®

This volume contains the peer reviewed and accepted abstracts, presented at the Symposium on Chemical and Biological Engineering, of the 5th Doctoral Congress in Engineering – DCE23, held at FEUP-U.Porto, Porto, Portugal, between June 15th and 16th, 2023.

Title: Book of Abstracts of DCE'23 Symposium on Chemical and Biological Engineering

Edited by Alexandra Pinto, Cristiana Gomes, Joana Almeida, Joana Lopes, Júlia Kessler, Mariana Bessa, Sara Ferreira, Susana Fernandes

Published by: FEUP Edições

Digital version [Symposium on Chemical and Biological Engineering – DCE 2023 \(up.pt\)](#)

First edition June 2023

ISBN. 978-972-752-306-1

This book contains information obtained from authentic sources. Reasonable efforts have been made to publish reliable data information, but the authors, as well as the publisher, cannot assume responsibility for the validity of all materials or for the consequences of their use.

Trademark Notice: Product or corporate names may be trademarks or registered trademarks, and are used only for identification and explanation, without intent to infringe.

Copyright@FEUP and this Book of Abstracts

1. Welcome

Welcome to the Symposium on Chemical and Biological Engineering within the 5th Doctoral Congress in Engineering – DCE23 held on the 15th and 16th of July in Porto, at the Faculty of Engineering of the University of Porto (FEUP). The Organizing Committee for this Symposium was composed by students of the Doctoral Program in Chemical and Biological Engineering (PDEQB).

The Symposium on Chemical and Biological Engineering received in total 65 submissions. Out of these, and after a revision by the Scientific Committee, 32 proceeded to oral presentation and 30 for poster. There were 3 authors who, after submitting their abstracts, withdrew from participating in the Symposium. Besides the Oral Communications and Posters Sessions, the Symposium's Program also included one Invited Speaker, who has graduated from this Doctoral Program and now works in the industry. The speaker shared his experience and showed the versatility of Chemical and Biological Engineering.

Finally, all the presented works were contemplated to win the prizes of Best Oral Presentation and Best Poster. We acknowledge the Invited Speaker and all authors for their contributions, the prestigious Scientific Committee, the attendees and the financing companies and institutions for their support. We hope that the DCE will foster new connections, inspire novel ideas, and open the way for future advancements.

Porto, June 2023

Symposium on Chemical and Biological Engineering Organizing Committee

COMMITTEES	1
Organizing Committee	1
Scientific Committee	1
PROGRAMME.....	2
KEYNOTE SPEAKERS.....	6
List of the Symposium Keynote Speakers	6
ORAL PRESENTATIONS.....	7
Oral Communications to be presented in the Symposium	7
Macrostructured MWCNTs catalysts prepared by direct ink writing for oxalic acid ozonation	10
Combination of nanofiltration and ozonation to remove antineoplastic drugs from wastewaters.	13
Optimization of Catalytic Deoxygenation Reaction of Palmitic Acid for Production of Aviation Fuel Components	16
Dihydroxyacetone Separation from Glycerol Catalytic Oxidation Products in a Simulated Moving Bed Cascade: Proof-of-Concept	19
The photo-Fenton process for the treatment of wastewater from olive oil extraction industry	22
N-doped CNT-ZnO composite as supporting material of Cu-based catalysts for the Reverse Water-Gas Shift Reaction	25
Metal-free g-C ₃ N ₄ photoelectrocatalysts for degradation of pharmaceutical substances in the treatment of urban wastewater.....	28
Nanostructures and MOFs as electrochemical transducers for the voltammetric analysis of drugs in water	31
Value-added cereal-based products: incorporation of natural phenolic compounds in fresh pasta	34
Mono- and Bimetallic Carbon Nanotubes as Bifunctional Oxygen Electrocatalysts.....	37
Photocatalytic Ammonia Production using Immobilized GCN-T Catalysts	39
Graphitic carbon nitride immobilized onto ceramic foam for the degradation of sulfamethoxazole mediated by visible-light photocatalytic wet peroxide oxidation.....	42
Graphitic carbon nitride as a novel platform for Horseradish Peroxidase biocatalytic reactions with <i>in situ</i> H ₂ O ₂ production.....	45
Sustainability assessment of FAME production from vegetable oil: GREENSCOPE methodology....	48

Synthesis and modification of biochars for their usage as catalysts in water splitting reactions and adsorption coupled to Advanced Oxidation Processes.....	51
Hydrothermal carbonization for agro-industrial waste valorization: synthesis of Nitrogen-doped hydrochars as carbocatalysts for efficient removal of pharmaceuticals in water treatment.....	54
Controlling Supramolecular Chirality through Asymmetric Secondary Flows in Helical Microchannels	57
Numerical study of particle dynamics in high-efficiency gas-solid cyclone loaded with spherical steel shot	60
Towards an Optimization of the NETmix for Ozonation: Evaluation of the Effect of Channel Length on the Gas-Liquid Mass Transfer.....	63
Utilization of Moisture Barriers with Enhanced Tortuosity and Porous Attachments to Mitigate Burns Introduced by Impermeability: A Numerical Study	66
ChannelCOMB, 3D-Printed Device for Flow Distribution Uniformity in Mesostructured Reactors ..	69
Transition flow regimes in Baffled Reactors	72
Sustainable application of <i>Actinidia arguta</i> leaves as active ingredient in topical formulation: Development, optimization and <i>in vivo</i> evaluation	75
Precirol® ATO 5 and Miglyol® 612-based nanoparticles to target the brain and treat Alzheimer's disease.....	78
Valorization of a nutraceutical ingredient extracted from a chestnut by-product towards the implementation of Sustainable Development Goals	81
Spray drying microencapsulation of <i>Actinidia arguta</i> fruits and leaves extract	84
PNA-FISH applications for <i>Legionella</i> detection and localization in biofilms.....	87
Development of recombinase-aided amplification combined with nucleic acid lateral flow read-out for the diagnostic of RNA viruses – the detection of SARS-CoV-2 as an example	89
Biomimetic Surfaces from Cabbage Leaves: A Novel Approach to Prevent Biofilm Formation on Food Environments	92
Development of antifouling surfaces coated with chitosan from <i>Loligo opalescens</i> for marine applications	94
Incorporation of agro-industrial by-products extracts as an alternative to synthetic UV filters to develop a value-added sunscreen.....	97
Photoinactivation of clinical strains of <i>Staphylococcus aureus</i> using curcumin as photosensitizer agent.....	100

POSTERS	103
The antimicrobial and antibiofilm activity of novel phytochemicals against <i>Escherichia coli</i>	105
Delivery of Nucleic Acid Mimics into bacteria: effect of liposome composition in delivery efficiency	107
Metal-free sensitization of TiO ₂ for photocatalytic removal of pharmaceuticals under solar irradiation.....	109
Bioactivity and phenolic composition of chestnut shells extract before and after <i>in-vitro</i> simulated gastrointestinal digestion.....	111
Bioactive composition of goji berries extracted byUltrasound-Assisted Extraction: Validation of a mathematical model	113
Microparticles containing <i>Fragaria Vesca</i> leaf extract produced with biopolymeric matrices: Binary and ternary blends of alginate, pectin and carrageenan	115
Evaluating the Diffusion of NAMs Across the Bacterial Envelope.....	116
Continuous gas-liquid mass transfer in an oscillatory flow reactor provided with smooth periodic constrictions	118
Screening of supports and metal phases to obtain highly active catalysts for the CO ₂ conversion in C ₂ + products	120
Investigation of different gel polymer electrolytes forflexible electrochromic supercapacitors ...	123
Are parabens a hushed threat to drinking water microbiological quality?	126
Ecological brick production from water treatment sludge in brazil.....	128
Treatment of effluent from the olive pomace oil extraction industry by coagulation	131
<i>Delftia acidovorans</i> extracellular metabolites increase the biomass and metabolic activity of drinking water biofilms	134
Delivering antisense NAMs into bacteria using dendritic lipids.....	136
Selection of nucleic acid mimic (NAM) aptamers: from de novo SELEX to post-SELEX enhancement	138
CFD design of photocatalytic mesostructured reactors for ammonia production	141
Phenolic rich extracts from by-products: promising compounds for the development of value-added foods.....	144
Efficient wastewater treatment in olive pomace oil extraction industry using Fenton method....	147
Active and stable Iridium-based catalyst for conducting oxygen evolution reaction in a proton exchange membrane electrolyser.....	150

Identification of aromatic compounds in cocoa bean shells compared to natural cocoa powder..	153
Evaluating the impact of thermal disinfection on <i>Pseudomonas fluorescens</i> biofilm structures using a CDC biofilm reactor	156
Microparticles separation in microchannels	159
Looking for the Toxin.....	161
Direct contact membrane distillation-promoted persulfate activation as an innovative approach in water desalination.....	164
Photocatalytic activity of phosphorescent strontium aluminate doped with Eu^{2+} and Dy^{3+}	167
Development of different CuFe-MOF/PMS systems for selective treatment of wastewater pollutants	169
Reduction of critical raw materials in PEM water electrolysis catalysts for green hydrogen production	171
Carbon nanotube-supported bimetallic catalysts with high activity for the selective catalytic reduction of NO_x	175
Effectiveness of selected aldehydes as inhibitors of the LasI/LasR quorum sensing pathway and enhancers of antibiotic activity against <i>Pseudomonas aeruginosa</i> biofilms	178
Index of authors and the pages of this Book of Abstracts that they appear in	181

Organizing Committee

Chair: Alexandra Pinto | CEFT

Cristiana Gomes | LSRE-LCM

Joana Manuel Almeida | CEFT

Joana Lopes | LSRE-LCM

Júlia Kessler | LSRE-LCM

Mariana Bessa | LSRE-LCM

Sara Ferreira | LEPABE

Susana Fernandes | LEPABE

Scientific Committee

Alexandra Pinto | CEFT

Alexandre Ferreira | LSRE-LCM

Ana Mafalda Ribeiro | LSRE-LCM

António Ferreira | LEPABE

Cláudia Gomes da Silva | LSRE-LCM

Daniela Falcão | CEFT

Francisco Galindo-Rosales | CEFT

José Daniel Araújo | CEFT

José Pires | LEPABE

Luciana Gomes | LEPABE

Raquel Cristóvão | LSRE-LCM

Ricardo Santos | LSRE-LCM

Salomé Soares | LSRE-LCM

Vânia Oliveira | CEFT

15th June, Thursday

- 8:00-9:00 **Welcoming** (Reception)
- 9:00-9:30 **Opening session** (Auditorium)
- 9:30-10:00 **Industry Keynote lecture** (Auditorium)
- 10:00-11:00 **Round table:** Early Stage Research in Industry (Auditorium)
- **Coffee-break** -----
- 11:30-12:30 **Plenary Session:** Sustainable Engineering for an Intelligent World (11:30-13:00|Auditorium)
- **Coffee-break** -----
- Poster session**
- 13:00-15:00 Evaluated by António Ferreira and Daniela Falcão
Moderated by Mariana Bessa
- Session I | Innovative Materials, Reaction and Separation Processes**
- 15:00-16:30 Evaluated by Alexandra Pinto and Cláudia Gomes da Silva
Moderated by Joana Manuel Almeida
- José R.M. Barbosa, Maria João Regufe, João Restivo, Carla A. Orge, Alexandre F.P. Ferreira, Manuel F. R. Pereira, Ana Mafalda Ribeiro, Olívia S. G. P. Soares. Macrostructured MWCNTs catalysts prepared by direct ink writing for oxalic acid ozonation. #72
 - Teresa I. A. Gouveia, Ana Gorito, Beatriz Cristóvão, Vanessa Pereira, João Crespo, Arminda Alves, Fernando Pereira, Ana Rita Lado Teixeira Ribeiro, Adrian M. T. Silva and Mónica Santos. Combination of nanofiltration and ozonation to remove antineoplastic drugs from wastewaters. #81
 - Karoline K. Ferreira, Lucília Ribeiro and Fernando Pereira. Optimization of Catalytic Deoxygenation Reaction of Palmitic Acid for Production of Aviation Fuel Components. #89
 - Pedro M. Walgode, Rui P. V. Faria and Alírio E. Rodrigues. Dihydroxyacetone Separation from Glycerol Catalytic Oxidation Products in a Simulated Moving Bed Cascade: Proof-of-Concept. #130
 - Thais Theomaris Grabowski, Marlei Veiga dos Santos and Ramiro José Espinheira Martins. The photo-Fenton process for the treatment of wastewater from olive oil extraction industry. #145
 - Ana Rita Querido, Liliana P. L. Gonçalves, M. F. R. Pereira, and O. S. G. P. Soares. N-doped CNT-ZnO composite as supporting material of Cu-based catalysts for the Reverse Water-Gas Shift Reaction. #158
 - André Torres-Pinto, Aida M. Díez, M. Ángeles Sanromán, Cláudia G. Silva, Joaquim L. Faria, Marta Pazos, Adrián M.T. Silva. Metal free g-C₃N₄

photoelectrocatalysts for degradation of pharmaceutical substances in the treatment of urban wastewater. #338

- Sara Caruncho-Pérez, María Ignacio-Meijoeiro, Xoel Montes-Paradela, Marta Pazos, M. Ángeles Sanromán and Elisa González-Romero. Nanostructures and MOFs as electrochemical transducers for the voltametric analysis of drugs in water. #348

----- **Coffee-break** -----

17:00-18:30 Evaluated by Alexandra Pinto and Cláudia Gomes da Silva
Moderated by Joana Lopes

- Sandra M. Gomes, Daniela Albuquerque and Lúcia Santos. Value-added cereal-based products: incorporation of natural phenolic compounds in fresh pasta. #354
- Duarte J. Junqueira Magalhães, Rafael G. Morais, Rui S. Ribeiro, Natalia Rey-Raap, José Luís Figueiredo, M. Fernando R. Pereira. Mono- and Bimetallic Carbon Nanotubes as Bifunctional Oxygen Electrocatalysts. #355
- Amala Joy, Joana Cancela, Isabel Barbosa, Maria Sampaio, Joaquim Faria, Ricardo J. Santos and Claudia G. Silva. Photocatalytic Ammonia Production using Immobilized GCN-T Catalysts. #358
- Ana M. Chávez, André Torres-Pinto, Pedro M. Álvarez, Joaquim L. Faria, Cláudia G. Silva, Adrián M.T. Silva. Graphitic carbon nitride immobilized onto ceramic foam for the degradation of sulfamethoxazole mediated by photocatalytic wet peroxide visible-light assisted process. #359
- Rita A. M. Barros, Raquel O. Cristóvão, Maria Sampaio, Claudia G. Silva and Joaquim Faria. Graphitic carbon nitride as a novel platform for Horseradish Peroxidase biocatalytic reactions with in situ H₂O₂ production. #362
- Catarina M. Oliveira and José C. M. Pires. Sustainability assessment of FAME production from vegetable oil: GREENSCOPE methodology. #365
- Aida M. Díez, Veronica Laíño-Rodríguez, María Bolaños-Vázquez, M. Ángeles Sanromán and Marta Pazos. Synthesis and modification of biochars for their usage as catalysts in water splitting reactions and adsorption coupled to Advanced Oxidation Processes. #367
- Silvia Escudero-Curiel, Xacobe López Rodríguez, Marta Pazos, Ángeles Sanromán. Hydrothermal carbonization for agro-industrial waste valorization: synthesis of Nitrogen-doped hydrochars as carbocatalysts for efficient removal of pharmaceuticals in water treatment. #371

16th June, Friday

Session II | Transport Phenomena

Evaluated by Alexandre Ferreira and José Daniel Araújo

9:00-10:30

Moderated by Joana Manuel Almeida

- João Pedro Vale, Semih Sevim, Alessandro Sorrenti, Zoubir El-Hachemi, Salvador Pané, Andreas D. Flouris, Josep Puigmartí-Luis, Tiago Sotto Mayor. Controlling Supramolecular Chirality through Asymmetric Secondary Flows in Helical Microchannels. #14
- Pedro T. Pacheco, Manuel Alves, João Campos and Júlio Paiva. Numerical study of particle dynamics in high-efficiency gas-solid cyclone loaded with spherical steel shot. #66
- Paulo H. Marrocos, Luís Silva, Mateus Pituco, Isabel Fernandes, Ricardo J. Santos and Vítor Jorge Vilar. Towards an Optimization of the NETmix for Ozonation: Evaluation of the Effect of Channel Length on the Gas-Liquid Mass Transfer. #149
- André Fonseca Malaquias, João Miranda and João Campos. Utilization of Moisture Barriers with Enhanced Tortuosity and Porous Attachments to Mitigate Burns Introduced by Impermeability: A Numerical Study. #322
- Isabel Barbosa, João Costa, Yaidelin Manrique, Madalena Dias, Joaquim Faria, Ricardo J. Santos, Claudia G. Silva and Margarida Brito. ChannelCOMB, 3D-Printed Device for Flow Distribution Uniformity in Mesostructured Reactors. #325
- Sofia R. S. P. Brandão, Ricardo J. Santos and Margarida Brito. Transition flow regimes in Baffled Reactors. #364
- Ana Margarida Silva, Paulo Costa, Cristina Delerue-Matos and Francisca Rodrigues. Sustainable application of *Actinidia arguta* leaves as active ingredient in topical formulation: Development, optimization and in vivo evaluation. #23
- Débora Nunes, Joana A. Loureiro and Maria Carmo Pereira. Precirol® ATO 5 and Miglyol® 612-based nanoparticles to target the brain and treat the Alzheimer's disease. #46

----- Coffee-break -----

Session III | Biological Engineering and Biotechnology

Evaluated by António Ferreira and Vânia Oliveira

11:00-13:00

Moderated by Júlia Kessler

- Diana Pinto, Andreia Almeida, Anallely López-Yerena, Bruno Sarmiento, Rosa M. Lamuela-Raventós, Anna Vallverdú-Queralt, Cristina Delerue-Matos and Francisca Rodrigues. Valorization of a nutraceutical ingredient extracted from a chestnut by-product towards the implementation of Sustainable Development Goals. #55

- Filipa Teixeira, Ana Margarida Silva, Cristina Delerue-Matos, Berta M. A. N. Estevinho, Paulo Costa and Francisca Rodrigues. Spray drying microencapsulation of *Actinidia arguta* fruits and leaves extract. #67
- Ana Barbosa, Darla Goeres, Nuno Azevedo and Laura Cerqueira. PNA-FISH applications for *Legionella* detection and localization in biofilms. #327
- João Vindeirinho, Ricardo Oliveira, Eva Pinho, Nuno Azevedo, Raquel Guiomar, Ahmed Wahed and Carina Almeida. Development of recombinase-aided amplification combined with nucleic acid lateral flow read-out for the diagnostic of RNA viruses – the detection of SARS-CoV-2 as an example. #329

11:45

Invited speaker: José Nogueira (alumni PDEQB, current Hydrogen Business Manager in Bondalti). *Green Hydrogen as energy transition vector: an Industrial perspective*

- Fábio R.M. Carvalho, Luciana C. Gomes, Marta Lima, Rita Teixeira-Santos, Ana Azevedo, Mohsin Amin, Mette Burmølle, Jelmer Sjollema, Filipe Mergulhão and Kathryn Whitehead. Biomimetic Surfaces from Cabbage Leaves: A Novel Approach to Prevent Biofilm Formation on Food Environments. #343
- Marta Lima, Luciana C. Gomes, Rita Teixeira-Santos, Maria João Romeu, Jesus Valcarcel, José Vázquez, Miguel Cerqueira, Lorenzo Pastrana, Ana Bourbon, Ed.d. De Jong, Jelmer Sjollema and Filipe Mergulhão. Development of antifouling surfaces coated with chitosan from *Loligo opalescens* for marine applications. #369
- Mariana A. Messias, Sara Ferreira, Loleny Tavares and Lúcia Santos. Incorporation of agro-industrial by-products extracts as an alternative to synthetic UV filters to develop a value-added sunscreen. #353
- Ariana S. C. Gonçalves, Manuel Simões and Anabela Borges. Photoinactivation of clinical strains of *Staphylococcus aureus* using curcumin as photosensitizer agent. #372

----- **Coffee-break** -----

- 14:30-15:30 **Award Ceremony** (Auditorium)
- 15:30-16:00 **Keynote Lecture:** Prof. Manuel Heitor (Auditorium)
- 16:00-16:30 **Closing Session** (Auditorium)
- 16:30-17:00 **Cocktail/Porto d’Honra** (Coffee Lounge)

Symposium Keynote Speaker

José Nogueira, PhD, Bondalti

Topic: Green H₂ as an Energy Transition Vector: An Industry Perspective



José Nogueira is a Chemical Engineer from the Faculty of Engineering – University of Porto, with a PhD on solar electrochemistry from the same university. He joined Bondalti in 2021 with responsibility for Power-to-x and decarbonization projects development and management. Currently he is the Hydrogen Business Manager at Bondalti. José has more than 10 years of professional experience, divided by the industry and R&D research centers (BOSCH, EFACEC, FEUP, and UPTEC Innovation Centre) with roles in innovation, product and process development, and project management. His R&D track record includes 18 scientific publications and 2 international patents.

Oral Communications to be presented in the Symposium

- José R.M. Barbosa, Maria João Regufe, João Restivo, Carla A. Orge, Alexandre F.P. Ferreira, Manuel F. R. Pereira, Ana Mafalda Ribeiro, Olívia S. G. P. Soares. Macrostructured MWCNTs catalysts prepared by direct ink writing for oxalic acid ozonation. #72
- Teresa I. A. Gouveia, Ana Gorito, Beatriz Cristóvão, Vanessa Pereira, João Crespo, Arminda Alves, Fernando Pereira, Ana Rita Lado Teixeira Ribeiro, Adrian M. T. Silva and Mónica Santos. Combination of nanofiltration and ozonation to remove antineoplastic drugs from wastewaters. #81
- Karoline K. Ferreira, Lucilia Ribeiro and Fernando Pereira. Optimization of Catalytic Deoxygenation Reaction of Palmitic Acid for Production of Aviation Fuel Components. #89
- Pedro M. Walgode, Rui P. V. Faria and Alírio E. Rodrigues. Dihydroxyacetone Separation from Glycerol Catalytic Oxidation Products in a Simulated Moving Bed Cascade: Proof-of-Concept. #130
- Thais Theomaris Grabowski, Marlei Veiga dos Santos and Ramiro José Espinheira Martins. The photo-Fenton process for the treatment of wastewater from olive oil extraction industry. #145
- Ana Rita Querido, Liliana P. L. Gonçalves, M. F. R. Pereira, and O. S. G. P. Soares. N-doped CNT-ZnO composite as supporting material of Cu-based catalysts for the Reverse Water-Gas Shift Reaction. #158
- André Torres-Pinto, Aida M. Díez, M. Ángeles Sanromán, Cláudia G. Silva, Joaquim L. Faria, Marta Pazos, Adrián M.T. Silva. Metal free g-C₃N₄ photoelectrocatalysts for degradation of pharmaceutical substances in the treatment of urban wastewater. #338
- Sara Caruncho-Pérez, María Ignacio-Meijoeiro, Xoel Montes-Paradela, Marta Pazos, M. Ángeles Sanromán and Elisa González-Romero. Nanostructures and MOFs as electrochemical transducers for the voltametric analysis of drugs in water. #348
- Sandra M. Gomes, Daniela Albuquerque and Lúcia Santos. Value-added cereal-based products: incorporation of natural phenolic compounds in fresh pasta. #354
- Duarte J. Junqueira Magalhães, Rafael G. Morais, Rui S. Ribeiro, Natalia Rey-Raap, José Luís Figueiredo, M. Fernando R. Pereira. Mono- and Bimetallic Carbon Nanotubes as Bifunctional Oxygen Electrocatalysts. #355
- Amala Joy, Joana Cancela, Isabel Barbosa, Maria Sampaio, Joaquim Faria, Ricardo J. Santos and Claudia G. Silva. Photocatalytic Ammonia Production using Immobilized GCN-T Catalysts. #358
- Ana M. Chávez, André Torres-Pinto, Pedro M. Álvarez, Joaquim L. Faria, Cláudia G. Silva, Adrián M.T. Silva. Graphitic carbon nitride immobilized onto ceramic foam for the degradation of sulfamethoxazole mediated by photocatalytic wet peroxide visible-light assisted process. #359
- Rita A. M. Barros, Raquel O. Cristóvão, Maria Sampaio, Cláudia G. Silva and Joaquim Faria. Graphitic carbon nitride as a novel platform for Horseradish Peroxidase biocatalytic reactions with in situ H₂O₂ production. #362
- Catarina M. Oliveira and José C. M. Pires. Sustainability assessment of FAME production from vegetable oil: GREENSCOPE methodology. #365

- [Aida M. Díez](#), Veronica Laíño-Rodríguez, María Bolaños-Vázquez, M. Ángeles Sanromán and Marta Pazos. Synthesis and modification of biochars for their usage as catalysts in water splitting reactions and adsorption coupled to Advanced Oxidation Processes. #367
- [Silvia Escudero-Curiel](#), Xacobe López Rodríguez, Marta Pazos, Ángeles Sanromán. Hydrothermal carbonization for agro-industrial waste valorization: synthesis of Nitrogen-doped hydrochars as carbocatalysts for efficient removal of pharmaceuticals in water treatment. #371
- [João Pedro Vale](#), Semih Sevim, Alessandro Sorrenti, Zoubir El-Hachemi, Salvador Pané, Andreas D. Flouris, Josep Puigmartí-Luis, Tiago Sotto Mayor. Controlling Supramolecular Chirality through Asymmetric Secondary Flows in Helical Microchannels. #14
- [Pedro T. Pacheco](#), Manuel Alves, João Campos and Júlio Paiva. Numerical study of particle dynamics in high-efficiency gas-solid cyclone loaded with spherical steel shot. #66
- [Paulo H. Marrocos](#), Luís Silva, Mateus Pituco, Isabel Fernandes, Ricardo J. Santos and Vítor Jorge Vilar. Towards an Optimization of the NETmix for Ozonation: Evaluation of the Effect of Channel Length on the Gas-Liquid Mass Transfer. #149
- [André Fonseca Malaquias](#), João Miranda and João Campos. Utilization of Moisture Barriers with Enhanced Tortuosity and Porous Attachments to Mitigate Burns Introduced by Impermeability: A Numerical Study. #322
- [Isabel Barbosa](#), João Costa, Yaidelin Manrique, Madalena Dias, Joaquim Faria, Ricardo J. Santos, Claudia G. Silva and Margarida Brito. ChannelCOMB, 3D-Printed Device for Flow Distribution Uniformity in Mesostructured Reactors. #325
- [Sofia R. S. P. Brandão](#), Ricardo J. Santos and Margarida Brito. Transition flow regimes in Baffled Reactors. #364
- [Ana Margarida Silva](#), Paulo Costa, Cristina Delerue-Matos and Francisca Rodrigues. Sustainable application of *Actinidia arguta* leaves as active ingredient in topical formulation: Development, optimization and in vivo evaluation. #23
- [Débora Nunes](#), Joana A. Loureiro and Maria Carmo Pereira. Precirol® ATO 5 and Miglyol® 612-based nanoparticles to target the brain and treat the Alzheimer's disease. #46
- [Diana Pinto](#), Andreia Almeida, Anallely López-Yerena, Bruno Sarmento, Rosa M. Lamuela-Raventós, Anna Vallverdú-Queralt, Cristina Delerue-Matos and Francisca Rodrigues. Valorization of a nutraceutical ingredient extracted from a chestnut by-product towards the implementation of Sustainable Development Goals. #55
- [Filipa Teixeira](#), Ana Margarida Silva, Cristina Delerue-Matos, Berta M. A. N. Estevinho, Paulo Costa and Francisca Rodrigues. Spray drying microencapsulation of *Actinidia arguta* fruits and leaves extract. #67
- [Ana Barbosa](#), Darla Goeres, Nuno Azevedo and Laura Cerqueira. PNA-FISH applications for *Legionella* detection and localization in biofilms. #327
- [João Vindeirinho](#), Ricardo Oliveira, Eva Pinho, Nuno Azevedo, Raquel Guiomar, Ahmed Wahed and Carina Almeida. Development of recombinase-aided amplification combined with nucleic acid lateral flow read-out for the diagnostic of RNA viruses. #329

- Fábio R.M. Carvalho, Luciana C. Gomes, Marta Lima, Rita Teixeira-Santos, Ana Azevedo, Mohsin Amin, Mette Burmølle, Jelmer Sjollema, Filipe Mergulhão and Kathryn Whitehead. Biomimetic Surfaces from Cabbage Leaves: A Novel Approach to Prevent Biofilm Formation on Food Environments. #343
- Marta Lima, Luciana C. Gomes, Rita Teixeira-Santos, Maria João Romeu, Jesus Valcarcel, José Vázquez, Miguel Cerqueira, Lorenzo Pastrana, Ana Bourbon, Ed.d. De Jong, Jelmer Sjollema and Filipe Mergulhão. Development of antifouling surfaces coated with chitosan from *Loligo opalescens* for marine applications. #369
- Mariana A. Messias, Sara Ferreira, Loleny Tavares and Lúcia Santos. Incorporation of agro-industrial by-products extracts as an alternative to synthetic UV filters to develop a value-added sunscreen. #353
- Ariana S. C. Gonçalves, Manuel Simões and Anabela Borges. Photoinactivation of clinical strains of *Staphylococcus aureus* using curcumin as photosensitizer agent. #372

Macrostructured MWCNTs catalysts prepared by direct ink writing for oxalic acid ozonation

José R.M. Barbosa^{1,2*}, Maria João Regufe^{1,2}, João Restivo^{1,2}, Carla A. Orge^{1,2}, Alexandre F.P. Ferreira^{1,2}, Manuel F. R. Pereira^{1,2}, Ana Mafalda Ribeiro^{1,2}, Olívia S. G. P. Soares^{1,2}

¹Laboratory of Separation and Reaction Engineering – Laboratory of Catalysis and Materials (LSRE–LCM), Departamento de Engenharia Química, Faculdade de Engenharia, Universidade do Porto, 4200-465, Porto, Portugal

²ALiCE - Associate Laboratory in Chemical Engineering, Faculty of Engineering, University of Porto, Rua Dr. Roberto Frias, 4200-465 Porto, Portugal

*Corresponding author: jrbarbosa@fe.up.pt ORCID 0000-0001-6262-4167A

Abstract

Different emerging organic pollutants recalcitrant to conventional water treatment methods have been detected in watercourses at high concentrations in the recent years. R&D in catalytic ozonation has been reporting promising solutions; however, most of the used catalysts are applied in powder form. Looking forward to the introduction of these materials in the industry, their scale-up and handling are the major difficulties. Additive manufacturing (3D printing) can surpass the mentioned limitations. In this study macrostructured catalysts (MSCs) were developed, using multiwalled carbon nanotubes (MWCNTs) and different 'green' binders. The obtained results suggested that sodium carboxymethyl cellulose (CMC) is the most promising binder that guarantees a feasible mechanical strength, and thermal treatments improved the catalytic properties of the MSCs.

Author Keywords. Additive manufacturing, carbon materials, heterogeneous catalysis, ozonation

1. Introduction

Water pollution is a persistent issue nowadays and therefore deserves R&D in the search for solutions to mitigate it to avoid a future with the scarcity of water fit for consumption. Organic pollutants dissolved in water are compounds detected at hazardous concentrations; the major concern is that conventional water treatment processes cannot efficiently remove them (Gorito et al. 2017). Ozonation is a technology for removing organic pollutants in water, but it is insufficient to achieve efficient results. Heterogeneous catalytic ozonation is one of the most attractive alternatives because it can enhance the removal of highly refractory compounds (Soares et al. 2015). Carbon catalysts, such as multiwalled carbon nanotubes (MWCNTs), have been studied for heterogenous catalytic ozonation, and promising results have been reported (Rocha et al. 2011; Soares et al. 2015); however, most of these catalysts are used in powder form and suspended in a liquid phase or maintained in a fixed bed. Both approaches are not easy to scale-up and handle in industrial environments. Additive manufacturing, also known as 3D printing, in catalysis has been the target of several studies because it allows transforming powder catalysts into 3D macro structured catalysts (MSCs) that are adaptable for different operation conditions, easy to manipulate, and optimize the processes of mass transfer (Zhu et al. 2021). In this study, MSCs of MWCNTs through direct writing printing, one of the simplest techniques of 3D printing, were developed. Various 'green' binders at different concentrations were studied in the development of the printing inks. The catalytic performance was evaluated in a semi-batch reactor for oxalic acid catalytic ozonation in the liquid phase.

2. Materials and Methods

Commercial MWCNTs (Nanocyl, 90% puriss) were used as catalysts, carboxymethyl cellulose (CMC, VWR) and sodium alginate (ALG, CABOT) were used as 'green' binders and deionized water was used as a solvent to prepare the printing inks. Firstly, the MWCNTs were mixed with each binder at different mass ratios (5:1 and 1:1) using a ball-milling apparatus at 10 Hz during 30 min for 5:1 samples and 10 Hz during 60 min for 1:1 samples. Then, the resulting mixtures were wetted drop by drop and stirred until a workable rheology for printing was obtained (printing ink). MSCs pellets were developed by

direct ink writing (Ultimaker 2+ 3D-printer with an extrusion system, Discov3ry), putting the prepared inks into a syringe, and the printing process was carried out by applying controlled pressure. Thermal treatments were also performed to enhance the catalytic activity of the MSCs due to the possible blockage of the active sites by the presence of the binders. Two different temperatures were studied, considering thermogravimetric (TG) analysis of CMC and ALG: 250 °C and 500 °C for 1 h with a heating rate of 1 °C min⁻¹. The MSCs were named with the following code: MWCNT_XY_Z, wherein X is 20 or 50 corresponding to the mass fraction of binder, Y is CMC or ALG, and Z is 250 °C or 500 °C. The MSCs were also characterized to determine their textural properties (specific surface area) through N₂ physisorption at -196 °C, TG analysis to assess the thermal stability in an inert and oxidizing atmosphere at 900 °C and scanning electron microscopy/energy dispersive spectroscopy (SEM-EDS, FEI Quanta 400 FEG ESEM / EDAX Genesis X4M) to evaluate the MSCs morphology. For SEM-EDS analysis, the samples were coated with an Au/Pd thin film by sputtering using the SPI Module Sputter Coater equipment.

3. Discussion

The MSCs were mechanically stable independently of the type and concentration of binder. Nonetheless, CMC provided higher flexibility than ALG, whose structures collapsed when some light pressure was applied. It was also observed that higher concentrations of binder offered higher mechanical strength. The MSCs showed some decreases in the specific surface area, as expected due to the presence of the binders when compared with commercial MWCNTs (255 m² g⁻¹). For example, MWCNT_20CMC showed a specific surface area of 148 m² g⁻¹ and MWCNT_50CMC < 5 m² g⁻¹ (below the detection limit). The TG analysis showed high loss mass near 250 °C for both binders; therefore, the applied thermal treatments at 250 °C permitted an enhancement of the specific surface area, for example, MWCNT_20CMC_250 obtained 136 m² g⁻¹ and MWCNT_50CMC_250 51 m² g⁻¹. These results demonstrated that not all binder was degraded, but the thermal treatments at 500 °C permitted higher degradation; MWCNT_20CMC_500 showed a specific surface area of 190 m² g⁻¹ and MWCNT_50CMC_500 showed 126 m² g⁻¹. SEM analysis did not show differences due to the concentration and type of binder; however, differences were observed in MSCs after thermal treatment. The MSCs thermal treated at 250 °C showed cleaner surfaces due to the binder degradation, but at 500 °C, some crystallized structures were observed, as shown in Figure 1. SEM-EDS suggested that these structures are sodium (present in both binders) that have undergone a crystallization transition phenomenon at 500 °C.

The catalytic tests demonstrated that single ozonation (homogenous catalysis) of oxalic acid achieved a removal efficiency of 16% after 60 min of reaction, but using MSCs, higher removal efficiency values were obtained. Differences between the type of binder were observed in the catalytic performance of MSCs, in which CMC did not affect the results as negatively as ALG. As expected, the increase in binder concentration also negatively affected the catalytic performance. Furthermore, MWCNT_50CMC collapsed into powder during the reaction, demonstrating an unstable MSC. The thermal treated MSCs obtained the best results, and the most promising was MWCNT_20CMC_250, with a removal efficiency of 43% at 60 min of reaction and stable structures during the reaction.

4. Conclusions

Advances in the development of MSCs for water treatment were obtained in this work using commercial MWCNTs for oxalic acid heterogeneous catalytic ozonation. Two 'green' binders were used to prepare printing inks; however, the 3D-printed MSCs with CMC demonstrated higher mechanical strength and flexibility than with ALG. The presence of the binder decreased the specific surface area, but thermal treatments at 250 °C and 500 °C, considering TG analysis, permitted the degradation of the binder and consequently increased the specific surface area. This resulted in better catalytic performance, highlighting the MSCs MWCNT_20CMC_250 obtained a removal efficiency of 43% at 60 min of reaction (single ozonation achieved 16%).

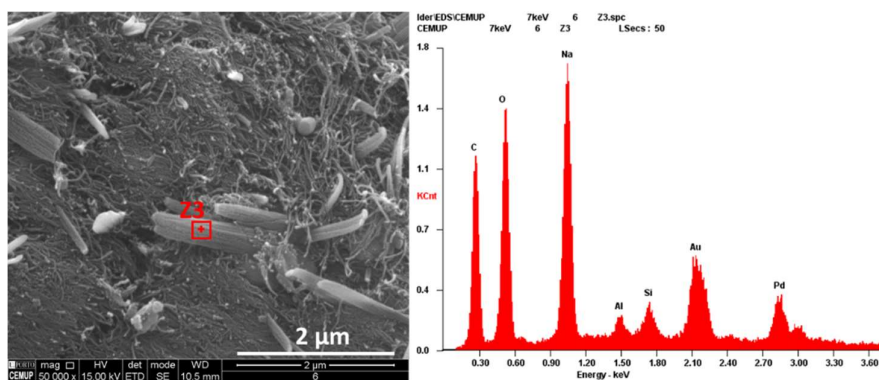


Figure 1: SEM-EDS analysis at a magnification of 50000× of MWCNT_20CMC_500

References

- Gorito, Ana M., Ana R. Ribeiro, C. M. R. Almeida, and Adrián M. T. Silva. 2017. "A review on the application of constructed wetlands for the removal of priority substances and contaminants of emerging concern listed in recently launched EU legislation." *Environmental Pollution* 227: 428-443. <https://doi.org/https://doi.org/10.1016/j.envpol.2017.04.060>.
- Rocha, Raquel P., Juliana P. S. Sousa, Adrián M. T. Silva, Manuel F. R. Pereira, and José L. Figueiredo. 2011. "Catalytic activity and stability of multiwalled carbon nanotubes in catalytic wet air oxidation of oxalic acid: The role of the basic nature induced by the surface chemistry." *Applied Catalysis B: Environmental* 104 (3-4): 330-336. <https://doi.org/10.1016/j.apcatb.2011.03.009>.
- Soares, O. S. G. P., A. G. Gonçalves, J. J. Delgado, J. J. M. Órfão, and M. F. R. Pereira. 2015. "Modification of carbon nanotubes by ball-milling to be used as ozonation catalysts." *Catalysis Today* 249: 199-203. <https://doi.org/https://doi.org/10.1016/j.cattod.2014.11.016>.
- Zhu, Jie, Peiwen Wu, Yanhong Chao, Jiangtao Yu, Wenshuai Zhu, Zhichang Liu, and Chunming Xu. 2021. "Recent advances in 3D printing for catalytic applications." *Chemical Engineering Journal*: 134341. <https://doi.org/10.1016/j.cej.2021.134341>.

Acknowledgments

This work is a result of: 2SMART NORTE-01-0145-FEDER-000054 funded by CCDR-N (Norte2020). This work was also financially supported by LA/P/0045/2020 (ALICE), UIDB/50020/2020 and UIDP/50020/2020 (LSRE-LCM) funded by national funds through FCT/MCTES (PIDDAC).

Combination of nanofiltration and ozonation to remove antineoplastic drugs from wastewaters

Teresa I.A. Gouveia^{1,2,*}, Ana M.Gorito^{2,3,4}, Maria B. Cristóvão^{5,6},
Vanessa J. Pereira^{5,7}, João G. Crespo⁶, Arminda Alves^{1,2}, M. Fernando
R. Pereira^{2,4}, Ana R. Ribeiro^{2,4}, Adrián M.T. Silva^{2,4}, Mónica S.F.
Santos^{1,2,8,9}

¹ LEPABE – Laboratory for Process, Environmental, Biotechnology and Energy Engineering, Faculty of Engineering, University of Porto, R. Dr. Roberto Frias, 4200-465 Porto, Portugal

² ALiCE – Associate Laboratory in Chemical Engineering, Faculty of Engineering, University of Porto, Rua Dr. Roberto Frias, 4200-465 Porto, Portugal

³ CIIMAR/CIMAR – Interdisciplinary Centre of Marine and Environmental Research, Universidade do Porto, Terminal de Cruzeiros do Porto de Leixões, Av. General Norton de Matos, 4450-208 Matosinhos, Portugal

⁴ LSRE-LCM – Laboratory of Separation and Reaction Engineering – Laboratory of Catalysis and Materials, Faculty of Engineering, University of Porto, Rua Dr. Roberto Frias, 4200-465 Porto, Portugal

⁵ iBET – Instituto de Biologia Experimental e Tecnológica, Apartado 12, 2781-901 Oeiras, Portugal

⁶ LAQV- REQUIMTE – Department of Chemistry, NOVA School of Science and Technology, Universidade NOVA de Lisboa, 2829-516 Caparica, Portugal

⁷ ITQB NOVA – Instituto de Tecnologia Química e Biológica António Xavier, Universidade Nova de Lisboa, Av. da República, 2780-157 Oeiras, Portugal

⁸ EPIUnit - Institute of Public Health, University of Porto, Rua das Taipas, n° 135, 4050-600 Porto, Portugal

⁹ Laboratory for Integrative and Translational Research in Population Health (ITR), University of Porto, Rua das Taipas, n° 135, 4050-600 Porto, Portugal

*Corresponding author: up201304237@fe.up.pt; <https://orcid.org/0000-0001-6641-1812>

Abstract

The presence of antineoplastic drugs in surface waters has been a topic of concern, since most of these pharmaceuticals are classified as hazardous agents by the National Institute for Occupational Safety and Health. As single treatments, nanofiltration (NF) and ozone (O₃)-based processes are not able to fully remove a pre-selected group of these compounds from wastewaters. Therefore, this work aims to study the combination of both technologies to produce a water stream suitable for human drinking purposes. NF+O₃, NF+O₃/H₂O₂ and NF+O₃/H₂O₂/UV were tested in a pilot-scale system (for nanofiltration experiments) and in a continuous-flow mode column (for O₃-based processes). Nanofiltration combined with O₃ and H₂O₂ was the most promising technology, removing all the target pharmaceuticals at an extent >98% from wastewater. The applicability of the clean water for drinking water purposes was corroborated by a risk assessment, where no risk was predicted neither for adults nor for children.

Author Keywords. cytotoxics, toxicity, emerging contaminants, nanofiltration, wastewater effluent, ozonation, drinking water.

1. Introduction

Cancer disease has been rising over the years and the World Health Organization expects an increase in worldwide cancer incidence that can rise from 19.3 M in 2020 to 30.2 M in 2040 (WHO 2021). Antineoplastic drugs are pharmaceuticals used in chemotherapy, which are then excreted by the patients and consequently released into the sewage systems. Since conventional treatments currently applied in wastewater treatment plants (WWTPs) are not effective for some of the antineoplastic drugs' removal (Luo et al. 2014), they end up being discharged into surface waters, potentially reaching aquatic organisms. Hence, to avoid the health concerns associated with exposure to these hazardous agents, effective treatment technologies to remove antineoplastic drugs should be tested using real wastewater effluents.

Membrane-based systems, like nanofiltration (NF), have recently attracted attention as a promising option for the removal of pharmaceuticals from wastewaters. Ozonation has also been considered an

interesting solution for the removal of pharmaceuticals due to its high oxidative potential and inexistence of a retentate requiring additional treatment (Gorito et al. 2021). However, if total removal of harmful compounds and toxicity is the goal, each technology applied alone may not be able to comply with that.

In this study, the performance of NF and O₃ alone and, for the first time, their combination was assessed for the degradation of ten antineoplastic drugs (bicalutamide, capecitabine, cyclophosphamide, flutamide, ifosfamide, megestrol, mycophenolate mofetil, mycophenolic acid, paclitaxel, and tamoxifen) and prednisone from real wastewaters. For the combined treatment, a NF permeate stream prevenient from a pilot-scale unit was used as feed for O₃-based processes (O₃, O₃/H₂O₂ and O₃/H₂O₂/UV). Additionally, considering the clean water potential for direct reuse as drinking water, the effects of the residual pharmaceuticals on human health were estimated by comparing the human exposure through ingestion over a lifetime with each pharmaceutical permitted daily doses (PDE), according to a previously published work (Gouveia et al. 2022).

2. Materials and Methods

Using real effluents from a secondary treatment of an urban WWTP, three experiments were conducted in a pilot-scale NF unit. In the NF system (model DK4040F30, Suez membranes, Lenntech, Delfgauw, Netherlands), a spiral wound Desal 5DK module was used. Details regarding the NF experiments can be found elsewhere (Cristóvão et al. (2022)). Following the NF tests, the NF permeate was collected and examined prior to being processed by O₃-based processes.

O₃-based degradation experiments (O₃, O₃/H₂O₂, and O₃/H₂O₂/UV) were carried out in a flow-through glass bubble column reactor in continuous operation. The collected matrices were fed at the bottom of the reactor by using a peristaltic pump (Watson-Marlow, UK) and collected after treatment at the outlet stream located at the top of the reactor. More information regarding the ozonation equipment can be found elsewhere (Gorito et al. (2021)). In the tests involving hydrogen peroxide (H₂O₂), this oxidant was immediately added as a single pulse to the spiked matrices under agitation, and the dosage of H₂O₂ was chosen in accordance with the stoichiometric amount with respect to matrix dissolved organic carbon (DOC) content. The effluents were pumped to the reactor at flow rate of 32 mL/min, for a hydraulic retention time of 10 min. After 30 minutes, treated samples were withdrawn after ensuring the steady state had been reached. To quench the reactions for extraction, 5 g/L of ascorbic acid was added to the collected samples (Wang et al. 2020). Inlet O₃ concentrations of 2.4 mg/L and 6.6 mg/L in the liquid phase after stabilization were used to treat NF permeate and WWTP effluents, respectively, which corresponds to an O₃ specific dose (g_{O_3}/g_{DOC}) of 0.4.

3. Discussion

NF treatment is incapable of completely remove all target pharmaceuticals or eliminating effluent toxicity. Although O₃-based processes showed better results than NF, mycophenolic acid was only degraded up to 61% for the three O₃-based treatments studied. Because the primary application defined for clean water from NF systems is human consumption, and in accordance with the "*as low as reasonably achievable*" principle, complete removal of antineoplastic drugs from water would be required. Among the combinations tested (NF+O₃, NF+O₃/H₂O₂ and NF+O₃/H₂O₂/UV), NF+O₃/H₂O₂ showed to be the best option, leading to the complete removal of the target drugs (>98%), being therefore not found in the treated water.

The remarkable efficacy of combining both strategies in the mineralization of the organic matter present in the wastewater is confirmed by the DOC abatement, which is around 92% from the WWTP effluent to the resulting clean water.

A human exposure to the target pharmaceuticals was evaluated by taking into account long-term use of drinking water produced from WWTP secondary effluents treated by the combined technology (NF+O₃/H₂O₂). It can be concluded the suggested treatment technique may be suitable for the production of drinking water from WWTP secondary effluents, since no risk from long-term ingestion of clean water by either children or adults was foreseen regarding the presence of the target compounds.

4. Conclusions

It was demonstrated that NF and O₃-based processes alone were not capable of completely remove all the target compounds from wastewaters. Since the main application defined for the clean water was human consumption, specifically drinking water purposes, a complete elimination of the target pharmaceuticals is needed and thus, none of these techniques itself would be the best option. Hence, the combination of NF with O₃-based processes (NF+O₃, NF+O₃/H₂O₂ and NF+O₃/H₂O₂/UV) was studied to increase the removal of the target compounds from WWTP secondary effluents.

When H₂O₂ and UV were coupled with O₃, all the pharmaceuticals were eliminated at >98%. As a result, it was determined that O₃/H₂O₂ was the best treatment to couple to NF in order to produce water meant for human consumption. An estimate of human exposure to the investigated pharmaceuticals through clean water consumption during a lifetime was made, and neither an adult risk nor a children risk was identified. Still, the possible presence of other hazardous compounds in wastewaters and the potential formation of by-products should be carefully considered.

References

- Cristóvão, M. B., J. Bernardo, A. Bento-Silva, M. Ressureição, M. R. Bronze, J. G. Crespo, and V. J. Pereira. 2022. "Treatment of anticancer drugs in a real wastewater effluent using nanofiltration: a pilot scale study." *Separation and Purification Technology*: 120565 <https://doi.org/10.1016/j.seppur.2022.120565>
- Gorito, Ana M., Joana F. J. R. Pesqueira, Nuno F. F. Moreira, Ana R. Ribeiro, M. Fernando R. Pereira, Olga C. Nunes, C. Marisa R. Almeida, and Adrián M. T. Silva. 2021. "Ozone-based water treatment (O₃, O₃/UV, O₃/H₂O₂) for removal of organic micropollutants, bacteria inactivation and regrowth prevention." *Journal of Environmental Chemical Engineering* 9 (4): 105315 <https://doi.org/10.1016/j.jece.2021.105315>
- Gouveia, Teresa I. A., Isabel H. Mota, Adrián M. T. Silva, Arminda Alves, and Mónica S. F. Santos. 2022. "Are cytostatic drugs in surface waters a potential threat?" *Science of The Total Environment* 853: 158559 <https://doi.org/10.1016/j.scitotenv.2022.158559>
- Luo, Yunlong, Wenshan Guo, Huu Hao Ngo, Long Duc Nghiem, Faisal Ibney Hai, Jian Zhang, Shuang Liang, and Xiaochang C. Wang. 2014. "A review on the occurrence of micropollutants in the aquatic environment and their fate and removal during wastewater treatment." *Science of The Total Environment* 473-474: 619-641 <https://doi.org/10.1016/j.scitotenv.2013.12.065>
- Wang, W. L., Z. Chen, Y. Du, Y. L. Zhang, T. H. Zhou, Q. Y. Wu, and H. Y. Hu. 2020. "Elimination of isothiazolinone biocides in reverse osmosis concentrate by ozonation: A two-phase kinetics and a non-linear surrogate model." *Journal of Hazardous Materials* 389: 10 <https://doi.org/10.1016/j.jhazmat.2019.121898>
- WHO. 2021. "Data and statistics." Accessed Accessed November 1, 2021. <https://www.euro.who.int/en/health-topics/noncommunicable-diseases/cancer/data-and-statistics>.

Acknowledgments

(i) Project POCI-01-0145-FEDER-031297 (CytoStraTech)—funded by FEDER funds through COMPETE2020—Programa Operacional Competitividade e Internacionalização (POCI) and by national funds (PIDDAC) through FCT/MCTES; (ii) NORTE-01-0145-FEDER-000069 (Healthy Waters) co-funded by European Regional Development Fund (ERDF), through North Portugal Regional Operational Programme (NORTE2020), under the PORTUGAL 2020 Partnership Agreement; (iii) 2022.08738.PTDC (DRopH2O) funded by national funds through FCT/MCTES (PIDDAC); (iv) UIDB/04750/2020 (EPIUnit) and LA/P/0064/2020 (ITR), funded by national funds through the FCT - Foundation for Science and Technology, I.P.; (v) LA/P/0045/2020 (ALiCE), Base Fundings UIDB/00511/2020 and UIDP/00511/2020 (LEPABE) and UIDB/50020/2020 and UIDP/50020/2020 (LSRE-LCM), funded by national funds through FCT/MCTES (PIDDAC); and (vi) iNOVA4Health (UIDB/04462/2020, UIDP/04462/2020) and LS4FUTURE Associated Laboratory (LA/P/0087/2020), a program financially supported by national funds through the FCT/MCTES. LAQV, financed by national funds from FCT/MCTES (UIDB/50006/2020 and UIDP/50006/2020), is gratefully acknowledged. TIAG and ARLR thank the FCT for the SFRH/BD/147301/2019 and 2022.00184.CEECIND grants, respectively.

Optimization of Catalytic Deoxygenation Reaction of Palmitic Acid for Production of Aviation Fuel Components

Karoline Kaiser Ferreira¹, Lucília S Ribeiro², Manuel Fernando Pereira³

¹LSRE-LCM - Laboratory of Separation and Reaction Engineering – Laboratory of Catalysis and Materials; ALiCE – Associate Laboratory in Chemical Engineering, Faculty of Engineering, University of Porto, Rua Dr. Roberto Frias, 4200-465 Porto, Portugal (up202103294@edu.fe.up.pt) ORCID 0000-0002-9618-7783

²LSRE-LCM - Laboratory of Separation and Reaction Engineering – Laboratory of Catalysis and Materials; ALiCE – Associate Laboratory in Chemical Engineering, Faculty of Engineering, University of Porto, Rua Dr. Roberto Frias, 4200-465 Porto, Portugal (lucilia@fe.up.pt) ORCID 0000-0003-0506-6183

³LSRE-LCM - Laboratory of Separation and Reaction Engineering – Laboratory of Catalysis and Materials; ALiCE – Associate Laboratory in Chemical Engineering, Faculty of Engineering, University of Porto, Rua Dr. Roberto Frias, 4200-465 Porto, Portugal (fpereira@fe.up.pt) ORCID 0000-0002-5447-2471

Abstract

Microalgae bio-oil is a renewable source and has great potential for the production of aviation fuel, contributing to the reduction of climate impacts. However, deoxygenation reactions are necessary to improve some of its physicochemical properties for its direct application as jet fuel. In this context, this work aims to define the optimal reaction parameters using a commercial catalyst (Co-Mo/Al₂O₃) to investigate the deoxygenation of a model bio-oil compound (palmitic acid). In the experiments performed, the best temperature and stirring rate were 350 °C and 150 rpm, respectively, achieving a 79 % conversion of palmitic acid and 67 % yield of hexadecane. The results also showed that the deoxygenation of the fatty acid occurs by hydrodeoxygenation.

Author Keywords. Palmitic Acid, Aviation Fuel, Reaction Optimization, Co-Mo/Al₂O₃, Hydrodeoxygenation

1. Introduction

Aviation has experienced a huge market expansion in the last two decades, being one of the most important global economic activities in the modern world. However, it contributes to the growth of greenhouse gases emissions and other pollutants as a result of the combustion of petrochemical-based aviation fuel (Lai et al. 2022). Moreover, the depletion of fossil resources and the limited access to them have raised the prices of the final products, further contributing to the investment in alternative fuels (Londoño-Pulgarin et al. 2021).

Thus, the use of low carbon emission fuels is the only pragmatic way to meet the goals of CO₂ emission reduction targets and accelerate the pace of decarbonizing the aviation sector (Wang et al. 2019; Londoño-Pulgarin et al. 2021).

Microalgae biomass stands out as a renewable source due to its high lipid content in fatty acids (C₁₄-C₂₂) and carbon number in the same range of aviation-fuel (C₈-C₁₆). Therefore, this feedstock has the potential to provide a bio-jet fuel using different emerging technologies (O'Neil, Knothe, and Reddy 2019). Currently, the production of bio-oil from microalgae by hydrothermal liquefaction (HTL) is the most promising path to obtain liquid hydrocarbons. However, its direct application as a fuel is hampered by the poor physical-chemical properties due to the presence of oxygenated compounds (Karatzos et al. 2017). In this context, it is crucial to develop systems to enhance the bio-oil physical-chemical properties allowing its use as a jet fuel. Catalytic systems for heteroatom removal are commonly found in the petrochemical industry in hydrotreatment units. Although those are well-established processes, there is still a lack of studies evaluating the optimal reaction conditions for the bio-oil deoxygenation. In this context, this work aims to define the optimal reaction parameters required to make microalgae bio-oil suitable for use as aviation fuel.

2. Materials and Methods

Catalytic reactions were carried out in a stainless batch reactor with 100 mL (Parr Instruments, USA Mod 4590), using the commercial catalyst Co-Mo/Al₂O₃. Palmitic acid (C₁₆H₃₂O₂), a microalgae model

compound, was used as substrate diluted in 50 mL of n-decane. The influence of the experimental conditions was evaluated by varying the temperature (220 – 370 °C), the hydrogen pressure (20 – 60 bar), the reaction time (0.5 – 6 h), the stirring rate (150 – 700 rpm), the catalyst load (0.1 – 0.4 g) and the palmitic acid concentration (5 – 15 g L⁻¹). The final liquid phase products were analyzed by a Dani GC-FID (model 1000) using a column TRB-5-RTX (30 m × 0.25 mm, 0.25 μm). Conversion of palmitic acid and yield of products were calculated as follows (Formulas 1 and 2, respectively):

$$\text{Conversion of palmitic acid} = \left(\frac{\text{moles of converted palmitic acid}}{\text{moles of initial palmitic acid}} \right) \times 100 \% \quad (1)$$

$$\text{Yield} = \left(\frac{\text{moles of products}}{\text{moles of initial palmitic acid}} \right) \times 100 \% \quad (2)$$

3. Discussion

The effect of the temperature was assessed, and the results are depicted in Figure 1. It was noted that palmitic acid starts converting into products from 260 °C, reaching a maximum conversion of 76 % at 350 °C. At this temperature, the highest hexadecane yield of 62 % was observed, and a small amount of pentadecane was also formed (yield 0.3 %). The results indicate that the deoxygenation followed mostly the hydrodeoxygenation route by the formation of the alkane corresponding to the carbon number of the fatty acid and water.

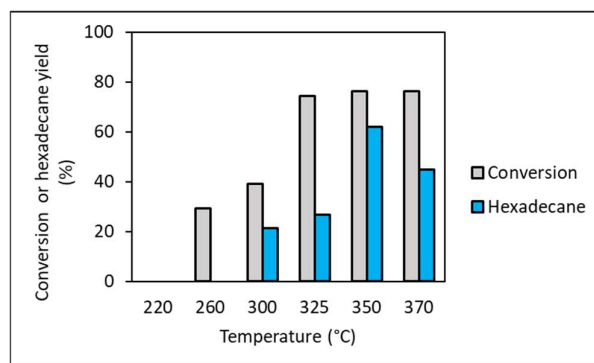


Figure 1: Influence of the temperature on the conversion of palmitic acid and yield of hexadecane after 4 h of reaction. Reaction conditions: 40 bar of H₂, 300 rpm, 0.25 g of Co-Mo/Al₂O₃ and 10 g L⁻¹ of palmitic acid in 50 mL of n-decane.

The effect of the stirring rate was also investigated over the same conditions at 350 °C. It was observed that experiments performed above 150 rpm have no mass transfer limitations, so that, this stirring rate was chosen to continue the study. Under these conditions, the hexadecane yield was 67 % and the conversion was 79 %. The effect of the remaining parameters described in section 2 is still being investigated.

4. Conclusions

The effect of temperature and stirring rate were evaluated for the deoxygenation reaction of palmitic acid. Under the best conditions found so far, a maximum conversion of 79 % palmitic acid was obtained with a yield of 67 % in hexadecane. The results also showed that deoxygenation of the substrate occurs via hydrodeoxygenation. However, the evaluation of the effects of the other reaction parameters is still under evaluation.

References

Karatzos, Sergios, J. Susan van Dyk, James D. McMillan, and Jack Saddler. 2017. "Drop-in Biofuel Production via Conventional (Lipid/Fatty Acid) and Advanced (Biomass) Routes. Part I." *Biofuels, Bioproducts and Biorefining*. John Wiley and Sons Ltd. <https://doi.org/10.1002/bbb.1746>.

- Lai, Y. Y., E. Christley, A. Kulanovic, C. C. Teng, A. Björklund, J. Nordensvärd, E. Karakaya, and F. Urban. 2022. "Analysing the Opportunities and Challenges for Mitigating the Climate Impact of Aviation: A Narrative Review." *Renewable and Sustainable Energy Reviews*. Elsevier Ltd. <https://doi.org/10.1016/j.rser.2021.111972>.
- Londoño-Pulgarin, Diana, Giovanni Cardona-Montoya, Juan C. Restrepo, and Francisco Muñoz-Leiva. 2021. "Fossil or Bioenergy? Global Fuel Market Trends." *Renewable and Sustainable Energy Reviews* 143 (June). <https://doi.org/10.1016/j.rser.2021.110905>.
- O'Neil, Gregory W., Gerhard Knothe, and Christopher M. Reddy. 2019. "Jet Biofuels from Algae." In *Biofuels from Algae*, 359–95. Elsevier. <https://doi.org/10.1016/B978-0-444-64192-2.00015-9>.
- Wang, Meng, Raf Dewil, Kyriakos Maniatis, John Wheeldon, Tianwei Tan, Jan Baeyens, and Yunming Fang. 2019. "Biomass-Derived Aviation Fuels: Challenges and Perspective." *Progress in Energy and Combustion Science*. Elsevier Ltd. <https://doi.org/10.1016/j.pecs.2019.04.004>.

Acknowledgments

This work is a result of project Move2LowC - Combustíveis de Base Biológica, with reference POCI-01-0247-FEDER-046117, co-funded by the European Regional Development Fund (ERDF), through the Operational Programme for Competitiveness and Internationalization (COMPETE 2020) and the Lisbon Regional Operational Programme (LISBOA 2020), under the PORTUGAL 2020 Partnership Agreement; and through COMPETE2020LA/P/0045/2020 (ALICE), UIDB/50020/2020 and UIDP/50020/2020 (LSRE-LCM) funded by national funds through FCT/MCTES (PIDDAC).

Dihydroxyacetone Separation from Glycerol Catalytic Oxidation Products in a Simulated Moving Bed Cascade: Proof-of-Concept

Pedro M. Walgode¹, Rui P. V. Faria², Alírio E. Rodrigues³

¹ALiCE LSRE-LCM, Faculdade de Engenharia, Universidade do Porto, Rua Dr. Roberto Frias, 4200-465 Porto, Portugal (pwalgode@fe.up.pt) 0000-0002-4341-7805

²ALiCE LSRE-LCM Faculdade de Engenharia, Universidade do Porto, Rua Dr. Roberto Frias, 4200-465 Porto, Portugal (ruifaria@fe.up.pt) ORCID 0000-0002-1216-0613

³ALiCE LSRE-LCM Faculdade de Engenharia, Universidade do Porto, Rua Dr. Roberto Frias, 4200-465 Porto, Portugal ORCID 0000-0002-0715-4761

Abstract

The separation of dihydroxyacetone from the main glycerol oxidation products was experimentally validated using a cascade of two Simulated Moving Bed (SMB) units, the FlexSMB-LSRE[®], using water and 5mM H₂SO₄ aqueous solution as eluent and a strong cation exchange resin as stationary phase. DHA was separated with 98.6% of purity, and the cascade showed a global productivity of 21.7 kg_{DHA} (m³_{adsorbent} day)⁻¹ and an eluent consumption of 5.7 m³_{eluent} kg_{DHA}⁻¹. An SMB model was validated using kinetic and equilibrium data from the fixed-bed column and SMB experimental data.

Author Keywords. Dihydroxyacetone Separation, Glycerol Valorization, Single-Cascade SMB, Strong Acid Cation Exchange Resins

1. Introduction

Glycerol (GLY), the main reaction by-product of the biodiesel industry, may be valorized by several well-known routes such as catalytic oxidation, yielding high-added-value products, including (DHA), which has major applications in the cosmetics industry. Several works on DHA production may be found in the literature (Katryniok et al. 2011). However, as far as we know there are no works concerning its purification from GLY catalytic oxidation in the liquid phase.

The cosmetics industry requires DHA with a minimum purity of 97%, therefore, DHA must be separated from the unreacted GLY and reaction by-products: oxalic acid (OXA), tartronic acid (TTA), glyceric acid (GCA), and glycolic acid (GCO). Adsorption isotherms of GLY and its oxidation products were determined at 293 K on a commercial polystyrene-divinylbenzene ion-exchange resin functionalized with sulfonic groups, the Dowex[®] 50WX-2 resin, in H⁺ form. All species presented a linear adsorption isotherm (except OXA, the least retained compound), with DHA and GLY being the most retained species. Adsorption isotherms of GLY and DHA in the Dowex[®] 50WX-2 resin in Ca²⁺ form were determined at 293 K, showing linear adsorption isotherm, with DHA being the most retained compound (M. Walgode et al. 2021).

Owing to the low separation selectivity of DHA from GLY in the resin in H⁺ form, ($\alpha = 1.04$), compared with the one in Ca²⁺ form ($\alpha = 1.28$), a DHA purification process on a cascade of two Simulated Moving Bed (SMB) units is herein proposed. DHA will be separated from the organic acids on an SMB packed with the resin in H⁺ form (SMB-H⁺), being collected in the extract stream together with part of the GLY, which will be fed to a second SMB packed with the resin in Ca²⁺ form (SMB-Ca²⁺) to separate DHA from GLY. The process was implemented on the gPROMS model builder V7.0.7 (PSE, UK) and experimentally performed on the FlexSMB-LSRE[®] with six fixed-bed columns (10 x 2 cm, 1-2-2-1 configuration) to separate the solution from the aerobic oxidation of a 1 M GLY aqueous solution with a commercial catalyst, Bi-doped Pt nanoparticles supported in activated carbon, in a semi-batch reactor (M. Walgode et al. 2021).

2. Materials and Methods

The columns were packed with resin and characterized by pulse injections of a tracer into the columns previously equilibrated in the eluent. A fixed-bed column model assuming axially dispersed plug flow model to describe the fluid flow and linear driving force for the mass transfer between the liquid and the solid, isothermal operation, homogeneous spherical particles with uniform size, constant fluid velocity, bed porosity, and bed length, and no bed radial gradients was implemented in the gPROMS software and validated using single and multi-component breakthrough experiments data (M.

Walgode et al. 2021). The model was extended to the SMB process, accounting the tubes, dead volumes, column filters, manifolds, and time switch delays of the FlexSMB-LSRE® unit, described elsewhere (Rodrigues 2015).

For each SMB, the regeneration region $\gamma_I^*, \gamma_{IV}^*$ was obtained by applying a safety factor of 15% to the γ_j^* (liquid and solid flow rate ratio in each SMB section) given by the equilibrium theory, while the separation region was obtained by running the FlexSMB-LSRE® model for different $\gamma_{II}^*, \gamma_{III}^*$ values, considering a minimum extract purity and DHA recovery in the extract stream.

The solution with the composition: 1.2 g_{OXA} L⁻¹, 12.9 g_{TTA} L⁻¹, 8.2 g_{GCA} L⁻¹, 6.9 g_{GCO} L⁻¹, 22.0 g_{GLY} L⁻¹, and 29.8 g_{DHA} L⁻¹ was fed to the SMB-H⁺ and 5mM H₂SO₄ aqueous solution as used as eluent. The flow rate of the inlet and outlet streams was measured at every SMB cycle, and the raffinate and extract streams were analyzed by HPLC. When the species' average concentration in both raffinate and extract streams did not change more than 5% during five successive cycles, cyclic steady state (CSS) conditions were reached. At this point, internal concentration profiles were obtained at 25%, 50%, and 75% of the t^* . The extract stream of the SMB-H⁺ was fed to the SMB-Ca²⁺ to separate DHA from GLY, using water as the eluent.

3. Discussion

The columns showed an average ε of 0.37 and an average Peclet number of 600. For the separation in the SMB-H⁺, a minimum DHA recovery in the extract of 85% and an extract purity on a GLY-free basis of 97% were defined. The operation point $\gamma_I^* = 2.88$, $\gamma_{II}^* = 2.44$, $\gamma_{III}^* = 2.47$, $\gamma_{IV}^* = 1.41$ and a t^* of 1.5 min were defined. The unit reached CSS conditions after 30 cycles (Figure 2 right). The internal concentration profiles at CSS were represented in Figure 2 left).

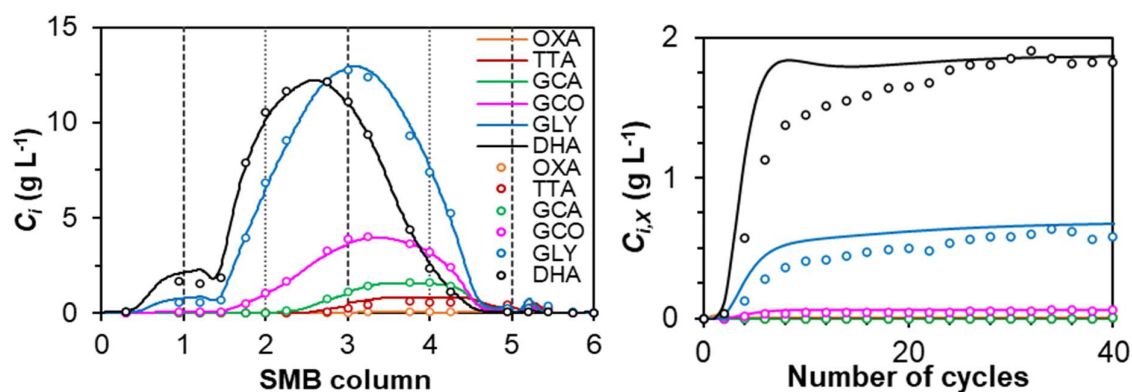


Figure 2. Left) SMB-H⁺ internal concentration profiles at CSS conditions. Right) Species' average concentration in the extract stream during the SMB-H⁺ run.

DHA recovery in the extract stream was 87.0% and the extract purity on GLY free basis was 96.8. The species' average concentration in the extract stream was 1.82 g L⁻¹ of DHA and 0.58 g L⁻¹ of GLY, and the main contaminant was GCO (0.06 g L⁻¹, 2.3%), see Figure 2 right.

The extract stream from the SMB-H⁺ was fed to the SMB-Ca²⁺. A minimum DHA recovery in the extract stream of 90% and an extract purity of 97% were considered for the separation region. The operation point $\gamma_I^* = 3.31$, $\gamma_{II}^* = 2.59$, $\gamma_{III}^* = 2.81$, $\gamma_{IV}^* = 2.07$ and a t^* of 2 min were defined. CSS conditions were achieved after 30 cycles (see Figure 3 right) and the internal concentration profiles at CSS were represented in Figure 3 left. with a DHA recovery in the extract stream of 89.0% and an extract purity of 98.6% and the species average concentration in the extract stream was 0.50 g L⁻¹ of DHA and 0.01 g L⁻¹ of GLY.

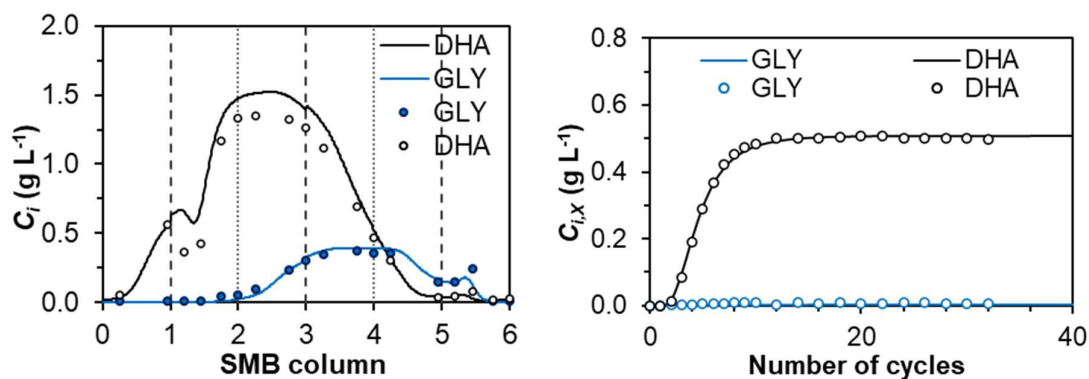


Figure 3. Left) SMB-Ca²⁺ internal concentration profiles at CSS conditions. Right) Species' average concentration in the extract stream during the SMB-Ca²⁺ run.

The model fitted well both the internal concentration profiles and the species' concentration in the outlet streams of both SMB experiments. The two-SMB cascade produced DHA with 98.6% of purity, and the cascade showed a global productivity of 21.7 kg_{DHA} (m³_{ads} day)⁻¹ and an eluent consumption of 5.7 m³_{ads} kg_{DHA}⁻¹.

4. Conclusions

The purification of DHA from the reactional mixture obtained during GLY aerobic oxidation with Pt-based catalysts was experimentally demonstrated on a lab-scale SMB unit, the FlexSMB-LSRE®. The FlexSMB model was validated together with the kinetic and equilibrium data previously obtained on the fixed-bed column.

References

- Katryniok, Benjamin, Hiroshi Kimura, Elżbieta Skrzyńska, Jean-Sébastien Girardon, Pascal Fongarland, Mickaël Capron, Rémy Ducoulombier, Naoki Mimura, Sebastien Paul, and Franck Dumeignil. 2011. "Selective catalytic oxidation of glycerol: perspectives for high value chemicals." *Green Chemistry* 13 (8): 1960-1979.
- M. Walgode, Pedro, Lucas C D. Coelho, Rui P V. Faria, and Alírio E. Rodrigues. 2021. "Dihydroxyacetone Production: From Glycerol Catalytic Oxidation with Commercial Catalysts to Chromatographic Separation." *Industrial & Engineering Chemistry Research*.
- Rodrigues, Alirio. 2015. *Simulated moving bed technology: principles, design and process applications*. 1st Edition ed., edited by Elsevier. Amsterdam: Butterworth-Heinemann.

Acknowledgments

This work was financially supported by LA/P/0045/2020 (ALiCE), UIDB/50020/2020, and UIDP/50020/2020 (LSRE-LCM), funded by national funds through FCT/MCTES (PIDDAC). It was also financed by a doctoral grant from FCT (SFRH/BD/143916/2019).

The photo-Fenton process for the treatment of wastewater from olive oil extraction industry

Marlei V. dos Santos¹, Thais T. Grabowski², Ramiro E. J. Martins^{2,3,4*}

¹Postgraduate Program of Environment and Sustainable Technologies, Federal University of Fronteira Sul, Av. Jacob Reinaldo Haupenthal, 1580, 97900-000, Cerro Largo, RS, Brazil.

²Technology and Management School, Polytechnic Institute of Bragança, Campus de Santa Apolónia, 5300-252, Bragança, Portugal.

³LSRE-LCM Laboratory of Separation and Reaction Engineering-Laboratory of Catalysis and Materials, Faculty of Engineering, University of Porto, Rua Dr. Roberto Frias, 4200-465, Porto, Portugal.

⁴ALICE - Associate Laboratory in Chemical Engineering, FEUP, Porto, Portugal.

*Corresponding author: e-mail address: rmartins@ipb.pt; ORCID ID 0000-0003-4327-7782.

Abstract

The olive oil industry in Europe is well-established, but the extraction of olive pomace generates a highly polluted effluent due to waste leaching and processing in the extraction units. To address this issue, this study aimed to treat the resulting pollutant effluent, known as olive oil extraction industry wastewater, using the photo-Fenton process. To optimize the process efficiency in removing organic matter (COD) and phenolic compounds (TPh), response surface methodology with Box-Behnken design was used. The variables considered were iron catalyst concentration, oxidant concentration, and UV irradiation time. The optimal conditions were determined to be $[\text{Fe}^{2+}] = 3 \text{ g L}^{-1}$, $[\text{H}_2\text{O}_2] = 23 \text{ g L}^{-1}$, and a photo reaction time of 60 min. The optimized process achieved removals of 93% (TPh) and 26% (COD) in the diluted sample (1:10) and 90% (TPh) and 39% (COD) in the raw sample.

Author Keywords. Olive oil extraction industry wastewater, Box-Behnken design, photo-Fenton, total phenolic compounds.

1. Introduction

The olive oil industry generates liquid and solid waste containing toxic phenolic compounds and high organic loads (Martins, Pietrobelli, and Mazur 2022). Advanced Oxidation Processes (AOPs), including Fenton and photo-Fenton, are recognized for their effectiveness in treating wastewater with high phenolic content (Domingues et al. 2022). The study aims to optimize the photo-Fenton process for treating wastewater from the olive oil extraction industry, using response surface methodology to determine optimal dosages of iron and hydrogen peroxide and photo-reaction time.

2. Materials and Methods

The photoreactor used had a total capacity of 0.7 L, and the olive oil extraction industry wastewater (OOEIW) sample was diluted 1:10 and adjusted to a pH of 3.5. The flow rate was maintained at 20 mL min^{-1} at predetermined times, and the treated samples were adjusted to a pH of 9.5 after the photoreaction time. The obtained results were averaged from at least two experiments.

The OOEIW has pH of 4.85, 6.6 g L^{-1} of total phenolic compounds (TPh), $85 \text{ g O}_2 \text{ L}^{-1}$ of chemical oxygen demand (COD), $12 \text{ g O}_2 \text{ L}^{-1}$ of biochemical oxygen demand, and 62 g L^{-1} of total solids.

3. Discussion

The study used a Box-Behnken design (BBD) to reduce the number of experimental trials while maintaining accuracy. The variables considered were H_2O_2 dosage, Fe^{2+} concentration, and reaction time, with TPh and COD removal as dependent variables. A second-order polynomial equation was used to fit the data, and ANOVA and regression surface analysis were used to determine the statistical significance of the model factors and responses. Table 1 shows the results obtained from the present experimental design.

Trial	Coded level of variable			Decoded level of variable			Removal (%)	
	X ₁	X ₂	X ₃	H ₂ O ₂ ^a (g L ⁻¹)	Fe ²⁺ ^b (g L ⁻¹)	t (min)	TPh	COD
1	-1	-1	0	10	1.5	60	53	9.7
2	1	-1	0	30	1.5	60	72	13
3	-1	1	0	10	4.5	60	55	8.7
4	1	1	0	30	4.5	60	81	19
5	-1	0	-1	10	3	30	41	7.7
6	1	0	-1	30	3	30	78	19
7	-1	0	1	10	3	90	60	15
8	1	0	1	30	3	90	89	19
9	0	-1	-1	20	1.5	30	73	11
10	0	1	-1	20	4.5	30	80	22
11	0	-1	1	20	1.5	90	83	14
12	0	1	1	20	4.5	90	60	16
13	0	0	0	20	3	60	77	18
14	0	0	0	20	3	60	77	15
15	0	0	0	20	3	60	77	16

^ag Oxidant L⁻¹ Effluent, ^bg catalyst L⁻¹ Effluent

Table 1: Results of TPh and COD removal (%) from olive oil extraction industry wastewater submitted to photo-Fenton (diluted sample 1:10).

Table 1 shows the reduction in TPh ranged from 41 - 89%, while COD showed removals of 7.7 - 22%. From the analyzes performed, it was found that for the removal of TPh, only the variable X1 [H₂O₂] has statistical significance ($t_{value} > 1.5$) and for the COD reduction, both the X1 [H₂O₂] and X2 [Fe²⁺] variables were significant. It was observed that X3 (photo reaction time) has no significant influence on the process used to remove TPh and COD, under the proposed conditions of the study.

The study of iron and hydrogen peroxide dosage is important in the Fenton reaction, which involves the decomposition of hydrogen peroxide into OH radicals in the presence of iron ions to degrade organic matter (Ertugay and Acar 2017). The amount of hydrogen peroxide required to treat an effluent increase with the organic load, but excessive hydrogen peroxide load can negatively impact organic pollutant degradation by enhancing the scavenging effect of OH radical by H₂O₂ (Ertugay and Acar 2017). The formation of stable organic Fe³⁺- complexes can limit the yield of organic pollutant mineralization, but this can be overcome by using UV irradiation to degrade the complexes (Malato et al. 2009). Increasing the amount of H₂O₂ increases TPh and COD removal, while increasing the concentration of Fe²⁺ increases COD removal until reaching an optimal point. Excessive iron can make the solution opaque, reducing light penetration, and hindering Fe³⁺ regeneration, decreasing the rate of degradation (Bhatkhande et al. 2004). As the dosage of H₂O₂ increases, there is a significant improvement in the removal efficiency of TPh, while the impact on COD removal is smaller. However, once an optimal concentration of H₂O₂ is achieved, further increases can lead to a decrease in COD removal due to the scavenging effect of H₂O₂ and the formation of HO₂ radicals (Ertugay and Acar 2017).

The study found that the best operational conditions for the photo-Fenton treatment of OOIEW were 60 min of treatment time, 23 g H₂O₂ L⁻¹ oxidant dosage, and 3 g Fe²⁺ L⁻¹ catalyst dosage. Using these conditions, the removal efficiencies of TPh and COD were 93% and 26%, respectively. In a subsequent experiment using the raw sample with these optimal conditions, the removal efficiencies of TPh and COD were 90% and 39%, respectively. The high efficiency of the photo-Fenton process in removing TPh was particularly noteworthy, as TPh is a significant pollutant in OOIEW due to its toxicity.

4. Conclusions

OOEIW is a wastewater hard to treat, with a high organic load and high toxicity. Through the experiments carried out it was possible to verify a high efficiency of the photo-Fenton process applied to the removal of TPH, with a removal of up to 90%. However, for COD, removals reached only 39%.

References

- Bhatkhande, Dhananjay S., Sanjay P. Kamble, Sudhir B. Sawant, and Vishwas G. Pangarkar. 2004. "Photocatalytic and Photochemical Degradation of Nitrobenzene Using Artificial Ultraviolet Light." *Chemical Engineering Journal* 102 (3): 283–90. <https://doi.org/10.1016/J.CEJ.2004.05.009>.
- Domingues, Eva, Eryk Fernandes, João Gomes, Sérgio Castro-Silva, and Rui C. Martins. 2022. "Advanced Oxidation Processes at Ambient Conditions for Olive Oil Extraction Industry Wastewater Degradation." *Chemical Engineering Science* 263 (December): 118076. <https://doi.org/10.1016/J.CES.2022.118076>.
- Ertugay, Nese, and Filiz Nuran Acar. 2017. "Removal of COD and Color from Direct Blue 71 Azo Dye Wastewater by Fenton's Oxidation: Kinetic Study." *Arabian Journal of Chemistry* 10 (February): S1158–63. <https://doi.org/10.1016/J.ARABJC.2013.02.009>.
- Malato, S., P. Fernández-Ibáñez, M. I. Maldonado, J. Blanco, and W. Gernjak. 2009. "Decontamination and Disinfection of Water by Solar Photocatalysis: Recent Overview and Trends." *Catalysis Today* 147 (1): 1–59. <https://doi.org/10.1016/J.CATTOD.2009.06.018>.
- Martins, Ramiro J. E., Juliana M. T. de A. Pietrobelli, and Andressa Mazur. 2022. "Effluent Characterization and Waterbody Monitoring from An Olive Pomace Oil Extractor Industry." *International Journal of Engineering Research & Technology* 11 (5): 120–23. <https://doi.org/DOI : 10.17577/IJERTV11IS050115>.

Acknowledgments

This work had financial support: i) Project NORTE-01-0247-FEDER-072124. Bagaço+Valor - Tecnologia Limpa para a Valorização dos Subprodutos do Bagaço na Indústria Extratora de Azeite, funded by the European Regional Development Fund (ERDF) and ii) LA/P/0045/2020 (ALiCE), UIDB/50020/2020 and UIDP/50020/2020 (LSRE-LCM), funded by national funds through FCT/MCTES (PIDDAC).

N-doped CNT-ZnO composite as supporting material of Cu-based catalysts for the Reverse Water-Gas Shift Reaction

Ana Rita Querido^{1,2,*}, Liliana P. L. Gonçalves^{1,2}, M. F. R. Pereira^{1,2}, and O. S. G. P. Soares^{1,2}

¹LSRE-LCM – Laboratory of Separation and Reaction Engineering – Laboratory of Catalysis and Materials, Faculty of Engineering, University of Porto, Rua Dr. Roberto Frias, 4200-465 Porto, Portugal.

²ALICE – Associate Laboratory in Chemical Engineering, Faculty of Engineering, University of Porto, University of Porto, Rua Dr. Roberto Frias, 4200-465 Porto, Portugal.

*anarnquerido@fe.up.pt

Abstract

Carbon dioxide (CO₂), a greenhouse gas, is a product of fossil fuel combustion, contributing to global warming. It is urgent to develop processes capable of decreasing CO₂ emissions. The Reverse Water-Gas Shift reaction (RWGS) converts CO₂ to CO, which mixed with H₂ forms syngas, the feedstock for most chemicals and synthetic fuels production. In this work Cu-based catalysts supported on pristine CNT and on composites of pristine and functionalized CNT:ZnO were developed and characterized for the RWGS reaction. The RWGS catalytic experiments were conducted between 100-600 °C and at 1 bar ($GHSV = 60\,000\text{ cm}^3\text{ g}^{-1}\text{ h}^{-1}$). The catalysts supported on pristine CNT achieved a CO₂ conversion of 17.6% whereas the catalyst supported on a composite of CNT:ZnO obtained a CO₂ conversion of 49.0%. N-doping CNT's surface enhanced CO₂ conversion up to 54.8%, with the catalyst stable for 93 h. All catalysts developed were 100% selective to CO.

Author Keywords. Reverse Water-Gas Shift reaction, CO₂ conversion, Carbon Nanotubes, metal oxides, Cu-based Catalyst.

1. Introduction

Carbon dioxide (CO₂) is one of the main products of fossil fuel combustion, and a greenhouse gas, contributing to global warming. Climate change is one of the world's most serious problems therefore, finding ways to reduce CO₂ emissions is critical (Din et al. 2019). The Reverse Water-Gas Shift (RWGS) reaction ((1), an endothermic reaction, has drawn interest from researchers as a route to reduce harmful CO₂ emissions. This reaction converts CO₂ into carbon monoxide (CO), which mixed with hydrogen (H₂) forms syngas, the feedstock of important chemical processes, such as Fischer-Tropsch synthesis (Chen et al. 2020).



Cu-based catalysts are the most used catalysts as they achieve excellent CO₂ conversion and CO selectivity and are less expensive than most metals (Liu et al. 2022). Nevertheless, Cu-based catalysts are susceptible to deactivation by sintering or reoxidation, at the high temperatures needed to achieve a good catalytic performance for the RWGS reaction (Chou, Loiland, and Lobo 2019). The most used catalysts' supports consist of metal oxides as they improve the activation of CO₂ on the surface of the catalyst and the active phase dispersion (Chen et al. 2020). Carbon nanotubes (CNT) have emerged as possible supports since they have a high specific surface area (providing better active phase dispersion) and a great resistance to structure changes by high temperatures, are less expensive than metal oxides and, it is possible to modify their surface by replacing some carbon atoms with other heteroatoms (e.g., N) (Serp and Figueiredo 2009).

In this work, Cu-based catalysts supported on pristine CNT, CNT:ZnO composite and N-doped CNT:ZnO composites were developed, characterized, and tested for the RWGS reaction.

2. Materials and Methods

To synthesize the composites, CNT materials (90% wt) and ZnO (10% wt) were co-ball-milled at a frequency of 20 vibrations per second for 30 min. To obtain N-doped CNT (CNT-N), commercial CNT and melamine were co-ball-milled for 4 h at a frequency of 15 vibrations per second. Then, the mixture

obtained was annealed at 600 °C for 1 h, under a N₂ flow. The catalysts were prepared by incipient wetness impregnation: the support was placed under ultrasonic vibration, and a solution of copper nitrate was added to achieve 15% wt of Cu. The samples were left under ultrasonic vibration for 90 min and then dried overnight. The catalysts were calcinated at the reduction temperature, under a N₂ flowrate. After 1 h, the gas was changed to H₂, and the catalysts were reduced for 3 h.

The catalytic experiments were carried out in a Microactivity XS15 reactor (PID Eng & Tech). The resulting gaseous products were analyzed using a GC 1000 gas chromatograph (DANI) equipped with a thermal conductivity detector (TCD) and a GS-CarbonPLOT capillary column. He was used as carrier gas while N₂ was used as internal standard. For the experiments, 100 mg of the catalyst was mixed with SiC and placed into a fixed bed quartz reactor. The reactor was fed with CO₂, H₂, and He ($GHSV = 60\,000\text{ cm}^3\text{ g}^{-1}\text{h}^{-1}$). A temperature ramping from 100 °C to 600 °C was performed to assess each catalyst's performance at different temperatures and at 1 bar. The stability of the best catalyst was assessed for 93 h.

The resultant catalysts and their supports were characterized by N₂ physisorption at -196 °C, elemental analysis (EA), temperature programmed desorption (TPD), hydrogen temperature programmed reduction (H₂-TPR), powder X-ray diffraction analysis (XRD), X-ray photoelectron spectroscopy (XPS), and transmission electron microscopy (TEM).

3. Discussion

Table 2 presents the catalytic results obtained for the developed catalysts. The performance of all catalysts achieves better results at the highest temperature, 600 °C, due to the endothermic nature of the RWGS reaction. The catalyst Cu/CNT-ZnO (90:10) surpassed the catalytic performance of the catalysts supported on pristine materials (Cu/ZnO and Cu/CNT), achieving a $X_{CO_2}=49.0\%$, demonstrating the benefits of combining the properties of CNT and ZnO. Furthermore, a Cu-based catalyst supported on N-doped CNT:ZnO composite was developed, and an even better catalytic performance was attained with $X_{CO_2}=54.8\%$. The N-groups present in the CNT's surface might enhance CO₂ adsorption, improving the overall performance of the catalysts (Shareman et al. 2010). Notably, all catalysts are 100% selective to CO and Cu/CNT-N-ZnO (90:10) presents excellent stability for 93 h.

Catalyst	X_{CO_2} (%)	S_{CO} (%)
Cu/ZnO	34.9	100
Cu/CNT	17.9	100
Cu/CNT-ZnO (90:10)	49.0	100
Cu/CNT-N-ZnO (90:10)	54.8	100

Table 2: CO₂ conversion and CO selectivity for the developed catalysts at 600 °C.

4. Conclusions

The main objective of this work was to assess the catalytic performance of Cu-based catalysts supported on CNT materials for the RWGS reaction. The catalytic performance was improved by the usage of a CNT:ZnO composite as supporting material – Cu/CNT-ZnO (90:10). Notably, it was possible to further enhance the catalytic performance by N-doping the CNT's surface – Cu/CNT-N-ZnO (90:10). This functionalization treatment led to the best performing catalyst with $X_{CO_2} = 54.8\%$, and a CO selectivity equal to 100%, at 600 °C. Adsorption of CO₂ was likely improved by this treatment with the catalytic performance achieving better results as well. Therefore, it is concluded that the catalytic performance of the RWGS reaction may benefit from combining the properties of CNT materials and metal oxides on composites, turning this approach an interesting toolbox for developing highly efficient catalysts for this reaction.

References

Chen, Xiaodong, Ya Chen, Chunyu Song, Peiyi Ji, Nannan Wang, Wenlong Wang, and Lifeng Cui. 2020. 'Recent Advances in Supported Metal Catalysts and Oxide Catalysts for the Reverse Water-Gas Shift Reaction'. *Frontiers in Chemistry*. Frontiers Media S.A. <https://doi.org/10.3389/fchem.2020.00709>.

- Chou, Chen Yu, Jason A. Loiland, and Raul F. Lobo. 2019. 'Reverse Water-Gas Shift Iron Catalyst Derived from Magnetite'. *Catalysts* 9 (9). <https://doi.org/10.3390/catal9090773>.
- Din, Israf Ud, Maizatul S. Shaharun, Mshari A. Alotaibi, Abdulrahman I. Alharthi, and A. Naeem. 2019. 'Recent Developments on Heterogeneous Catalytic CO₂ Reduction to Methanol'. *Journal of CO₂ Utilization*. Elsevier Ltd. <https://doi.org/10.1016/j.jcou.2019.05.036>.
- Liu, Hao Xin, Shan Qing Li, Wei Wei Wang, Wen Zhu Yu, Wu Jun Zhang, Chao Ma, and Chun Jiang Jia. 2022. 'Partially Sintered Copper–ceria as Excellent Catalyst for the High-Temperature Reverse Water Gas Shift Reaction'. *Nature Communications* 13 (1). <https://doi.org/10.1038/s41467-022-28476-5>.
- Serp, Philippe, and José Luís Figueiredo. 2009. *Carbon Materials For Catalysis*. Hoboken, New Jersey: John Wiley & Sons.
- Shafeeyan, Mohammad Saleh, Wan Mohd Ashri Wan Daud, Amirhossein Houshmand, and Ahmad Shamiri. 2010. 'A Review on Surface Modification of Activated Carbon for Carbon Dioxide Adsorption'. *Journal of Analytical and Applied Pyrolysis*. Elsevier B.V. <https://doi.org/10.1016/j.jaap.2010.07.006>.

Acknowledgments

This research was financially supported by Move2LowC project (n. 46117), cofinanced by Programa Operacional Competitividade e Internacionalização (POCI); Programa Operacional Regional de Lisboa, Portugal 2020 and the European Union, through the European Regional Development Fund (ERDF), and by Project HyGreen&LowEmissions, reference NORTE-01-0145-FEDER-000077, Co-financed by the European Regional Development Fund (FEDER), through the North Portugal Regional Operational Programme (NORTE2020); LA/P/0045/2020 (ALICE), UIDB/50020/2020 and UIDP/50020/2020 (LSRE-LCM), funded by national funds through FCT/MCTES (PIDDAC). O.S.G.P.S. acknowledges FCT funding under the Scientific Employment Stimulus - Institutional Call CEECINST/00049/2018.

Metal-free g-C₃N₄ photoelectrocatalysts for degradation of pharmaceutical substances in the treatment of urban wastewater

André Torres-Pinto^{1,2,3*}, Aida M. Díez³, M. Ángeles Sanromán³,
Cláudia G. Silva^{1,2}, Joaquim L. Faria^{1,2}, Marta Pazos³, Adrián M.T.
Silva^{1,2}

¹ LSRE-LCM - Laboratory of Separation and Reaction Engineering – Laboratory of Catalysis and Materials, Faculty of Engineering, University of Porto, Rua Dr. Roberto Frias, 4200-465 Porto, Portugal

² ALiCE - Associate Laboratory in Chemical Engineering, Faculty of Engineering, University of Porto, Rua Dr. Roberto Frias, 4200-465 Porto, Portugal

³ BIOSUV - Grupo de Bioingeniería y Procesos Sostenibles, CINTECX (Centro de Investigación en Tecnoloxías, Enerxía e Procesos Industriais), Departamento de Enxeñaría Química, Universidade de Vigo, Campus Lagoas Marcosende, 36310 Vigo, Spain

*Corresponding author: e-mail address: andretp@fe.up.pt; ORCID: 0000-0001-5337-4573

Abstract

Clean water scarcity is a topic requiring more attention. Research is being carried out towards the development of advanced technologies for the removal of recalcitrant contaminants present in effluents of urban wastewater treatment plants (WWTPs), such as persistent pharmaceutical compounds. In this sense, photocatalysis and electrocatalysis appear as alternatives that could answer the need for sustainable wastewater treatment processes. In particular, graphitic carbon nitride (g-C₃N₄) is a polymeric metal-free material that can be photo- and electro-activated and, therefore, allows the combination of two distinct technologies. In this work, we have synthesised g-C₃N₄ at different temperatures and assessed the electrochemical performance of the resulting materials. The best-performing electrocatalyst was then suspended in both simulated and real waters to evaluate its photo-, electro- and photoelectrocatalytic efficiency for removal of pharmaceutical compounds under different operating conditions, from matrix composition to electrode type.

Author Keywords. water treatment, advanced oxidation processes, carbon nitride, electrocatalysis, pharmaceuticals

1. Introduction

Clean water is one of the most esteemed resources. The widespread occurrence of organic contaminants in aquatic environments is leading to a worse supply of potable water. Conventional WWTPs are not capable to remove many recalcitrant organic micropollutants (MPs), such as several pharmaceutical compounds. These substances can provoke environmental damage and also pose a threat to human health, owing to their prevalence in waters, even in ones deemed potable for consumption (Papagiannaki *et al.* 2022). In this sense, wastewater treatment technologies are being developed in order to answer the necessities of current society. In particular, Advanced Oxidation Processes (AOPs) are reported as effective for the removal of MPs in different water compartments. Moreover, catalytic processes are well sought-after as they can reduce energy costs. Photocatalysis and electrocatalysis are being more and more investigated as they can employ external energy sources to promote oxidation reactions that lead to the full removal of MPs (Garcia-Segura and Brillas 2017). Among the possible materials, graphitic carbon nitride (commonly referred to as g-C₃N₄, and herein as GCN) is a metal-free photoelectrocatalyst capable of being activated by visible-light radiation and/or relatively low galvanostatic polarization. This catalyst can be easily synthesised through the thermal polymerisation of inexpensive precursors and shows a wide variety of applications, from pollutant degradation to hydrogen generation and bacterial inactivation (Ismael 2020). This is due to the capability of GCN to promote the formation of radical species through redox reactions in contact with dissolved oxygen, water, or other compounds, such as inorganic ions or organic degradation by-products (Velo-Gala *et al.* 2021). In this work, we have assessed different temperatures in the synthesis of GCN and tested the resulting electrochemical performance. The best-performing catalyst was employed for the photoelectrocatalytic removal of typical pharmaceutical compounds found in urban

wastewaters and, as consequence, surface waters (DCF – diclofenac, IBU – ibuprofen, and FLX – fluoxetine). A wide range of operating conditions was investigated, such as anode-to-cathode distance (ACD), type of electrolyte solution, cathode material, and water matrix.

2. Materials and Methods

The catalysts were prepared by a simple thermal calcination method, adapted from our previous publication (Torres-Pinto *et al.* 2022). Briefly, urea was placed in semi-closed quartz crucibles and heated under a static air atmosphere in a microwave muffle (CEM Corporation). The heating procedure consisted of a thermal treatment with distinct stages. The final powder product was washed with distilled water, filtered, and dried overnight at 60 °C. The materials were thoroughly characterised by scanning electron microscopy (SEM), Raman, X-ray photoelectron, infrared, ultraviolet-visible and steady-state photoluminescence emission spectroscopies, X-ray crystallography, nitrogen adsorption, voltammetry, and impedance studies. Electrochemical analyses were performed with a three-electrode open cell using an electrochemical workstation (Autolab PGSTAT302N, Metrohm). The reference electrode was Ag/AgCl, the counter electrode was a Pt wire, and the working electrodes were the GCN materials deposited onto a 1×1 cm² nickel foam. Photo- and electro-assisted catalytic reactions were carried out in a cylindrical borosilicate reactor using an ultraviolet lamp ($\lambda = 365$ nm) and an external galvanostatic power source. The anode was a boron-doped diamond rectangular plate, and the standard cathode was a titanium alloy sheet. Electrolytic, photolytic and adsorption reactions were completed as control experiments. The degradation experiments were performed using 250 mL of distilled water (DW) or secondary-treated urban wastewater (WW) with individual or mixed pharmaceuticals ($C_0 = 10$ ppm each) and dispersed GCN at a 0.5 g L⁻¹ load. Samples were periodically withdrawn, MPs concentration was analysed by high-performance liquid chromatography (HPLC) on an Agilent 1200 series coupled to a diode-array detector (DAD), and total organic carbon (TOC) was determined in a Multi N/C 2100 apparatus.

3. Discussion

The GCN materials were prepared under different synthesis temperatures, from 450 to 650 °C. The morphology of these catalysts was assessed by SEM, as observed in Figure 1. An increasingly higher processing temperature induced a more holey-like formation and seemingly more spaced-out layers. This distortion of the carbon nitride sheets may promote a higher surface area and greater availability of redox active sites. Higher temperatures show increasingly higher values of surface area (30, 44, and 89 m² g⁻¹, respectively for 450, 550 and 650 °C), while the average pore diameter decreases.

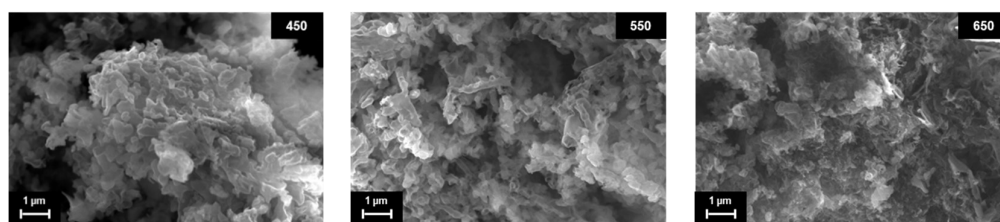


Figure 1: SEM images of GCN synthesised at 450, 550 and 650 °C (left to right).

The electrochemical activity of the synthesised materials was assessed for the oxygen evolution reaction (OER) in alkaline media, comparing to the bare nickel support and reference iridium oxide. The lowest OER overpotential, at 10 mA cm⁻², was registered for the GCN-550 material (190 mV) with a Tafel slope of 46.8 mV dec⁻¹, which surpasses that of the benchmark IrO₂ electrode (380 mV and 79.0 mV dec⁻¹). The mentioned catalyst was thoroughly characterised to understand the temperature effect on its activity, and preliminary results show that at 550 °C there is an adequate balance between crystallinity, porosity and surface chemistry.

The GCN-550 material was dispersed in aqueous solutions spiked with selected pharmaceutical compounds. Blank experiments were performed with DCF only in DW (Figure 2a) to demonstrate the enhanced synergistic effect of photochemical and electrochemical activation of GCN. DW and WW

were used as matrixes to verify the influence of natural organic matter (and other constituents) on the degradation of the three MPs in a mixture (Figure 2b). Typically, ionic strength and organic matter influence greatly the efficiency of different AOPs (Ribeiro *et al.* 2019). Herein, the degradation is slower with WW owing to the interference of organic matter and other possible WW constituents.

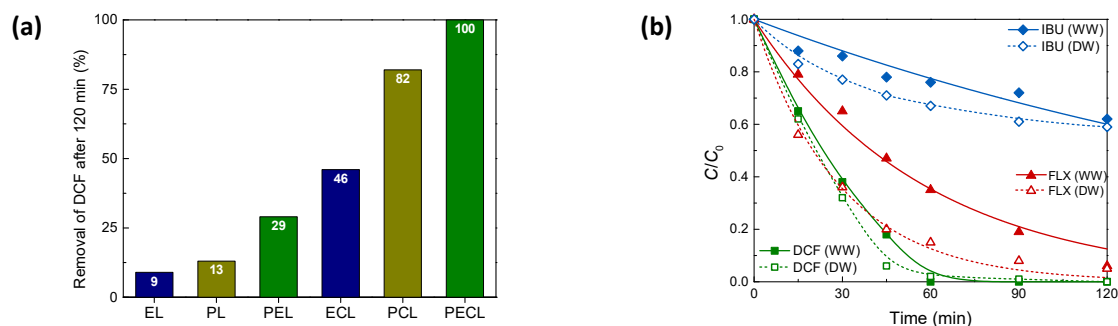


Figure 2: Removal of (a) DCF – diclofenac (EL – electrolysis, PL – photolysis, P/E/PECL – photo/electro/photoelectro-catalysis) after 120 min and (b) three MPs (DCF, IBU – ibuprofen and FLX – fluoxetine) in a mixture using distilled water (DW) and secondary-treated urban wastewater (WW) as matrices.

4. Conclusions

The processing temperature of GCN proved to be an important synthesis parameter in obtaining an efficient electrocatalyst, as it influences the surface area and morphological structure. The best-performing catalyst for OER (overpotential of 190 mV at 10 mA cm⁻²) was employed for the photoelectrocatalytic degradation of MPs in different conditions. It was observed that the combination of a photo-assisted and electrochemical processes performed much better than the individual catalytic technologies. Also, under more realistic conditions (*i.e.*, using a spiked secondary-treated urban wastewater as reaction media), the system proved rather efficient as the degradation only slightly decreased in comparison with distilled water as matrix.

References

- Garcia-Segura, S. and Brillas, E. 2017. "Applied photoelectrocatalysis on the degradation of organic pollutants in wastewaters." *J. Photochem. Photobiol.* 31: 1-35.
- Ismael, M. 2020. "A review on graphitic carbon nitride (g-C₃N₄) based nanocomposites: Synthesis, categories, and their application in photocatalysis." *J. Alloys Compd.* 846.
- Ribeiro, A. R. L., Moreira, N. F. F., Li Puma, G. and Silva, A. M. T. 2019. "Impact of water matrix on the removal of micropollutants by advanced oxidation technologies." *Chemical Engineering Journal* 363: 155-173.
- Papagiannaki, D., Belay, M. H., Gonçalves, N. P. F., Robotti, E., Bianco-Prevot, A., Binetti, R. and Calza, P. 2022. "From monitoring to treatment, how to improve water quality: The pharmaceuticals case." *Chem. Eng. J. Adv.* 10: 100245.
- Torres-Pinto, A., Silva, C. G., Faria, J. L. and Silva, A. M. T. 2022. "The effect of precursor selection on the microwave-assisted synthesis of graphitic carbon nitride." *Catal. Today*, in press.
- Velo-Gala, I., Torres-Pinto, A., Silva, C. G., Ohtani, B., Silva, A. M. T. and Faria, J. L. 2021. "Graphitic carbon nitride photocatalysis: the hydroperoxyl radical role revealed by kinetic modelling." *Catal. Sci. Technol.* 11(23): 7712-7726.

Acknowledgments

This work was financially supported by: LA/P/0045/2020 (ALiCE), UIDB/50020/2020 and UIDP/50020/2020 (LSRE-LCM), by project 2022.08738.PTDC (DRopH2O) funded by national funds through FCT/MCTES (PIDDAC), and by project PID2020-113667GB-I00 funded by MCIN/AEI/10.13039/501100011033. A.T.-P. acknowledges FCT for his scholarship SFRH/BD/143487/2019. A.M.D. is grateful to Xunta de Galicia for the financial support obtained (ED481B 2019/091) and to the project CINTECX-CHALLENGE 2023.

Nanostructures and MOFs as electrochemical transducers for the voltammetric analysis of drugs in water

Sara Caruncho-Pérez^{1,2,*}, María Ignacio-Meijoeiro¹, Xoel Montes-Paradela¹, Marta Pazos², M. Ángeles Sanromán², Elisa González-Romero^{1,*}

¹ Department of Analytical and Food Chemistry, Faculty of Chemistry, University of Vigo, Campus Lagoas-Marcosende, 36310 Vigo, Spain

² CINTECX – Universidade de Vigo, Campus Lagoas-Marcosende, University of Vigo, 36310 Vigo, Spain

*Corresponding author: e-mail address: sara.caruncho@uvigo.es and eromero@uvigo.es; ORCID ID 0000-0001-9286-855X and 0000-0001-8728-295X

Abstract

In this work the development of new sensing platforms is presented. For this purpose, different nanostructures and iron-based metal-organic frameworks (MOFs) are tested as modifiers of the working electrode of screen-printed carbon electrodes (SPCEs) with drugs of different classes, specifically alprazolam, clenbuterol, sulfamethizole, sulfamethoxazole and clonidine. SPCEs surfaces after being modified with MOFs were properly characterized with a redox probe to ensure the modification was successfully performed. Furthermore, in order to prove the application of the modified SPCEs, an analytical methodology based on voltammetric techniques was developed using clonidine as a model. After characterizing the electrochemical process that takes place, a calibration focused on the analysis of clonidine in water samples was performed.

Author Keywords. nanostructures, metal-organic frameworks, screen-printed carbon electrodes, voltammetry, drugs

1. Introduction

Nanomaterials are substances whose small dimensions make them abide by the laws of quantum mechanics, which gives them a wide range of applications in many fields such as medicine, catalysis, engineering and sensing, among others. In recent years the use of nanostructures as electrochemical transducers has increased significantly due to their high catalytic activity. Moreover, metal-organic frameworks (MOFs) have also received special attention because of their high porosity and tunability. Thus, new sensing platforms can be obtained by combining the unique properties of nanostructures and MOFs with the versatility of the screen-printed carbon electrodes (SPCEs) while minimizing the sample volume (Kaur 2022).

In this work, SPCEs modified with different nanostructures and MOFs are applied to the analysis of drugs of different classes, specifically anxiolytics (alprazolam), anabolics (clenbuterol), antibiotics (sulfamethoxazole and sulfamethizole) and antipsychotics (clonidine). The latter was selected as a model to demonstrate the viability of the modified SPCEs for the analysis of drugs at trace levels in water. In this sense, voltammetric techniques were chosen, specifically cyclic voltammetry (CV) and differential pulse voltammetry (DPV), and among the nanostructures tested as transducers the SPCEs modified with multi-walled carbon nanotubes (MWCNTs) showed the best response in terms of sensitivity and selectivity.

2. Materials and Methods

Alprazolam and clonidine were supplied by European Pharmacopeia and Sandoz, respectively. Sulfamethizole, sulfamethoxazole and clenbuterol were supplied by Sigma-Aldrich. All experiments were performed in electrolytic medium Na₂SO₄ (Panreac) 10 mM at a pH value of 3, and for this purpose different dilutions of H₂SO₄ (Fluka) were used. The redox probe used to characterize the modified SPCEs' surface was K₃[Fe(CN)₆] (Fluka). The o-phenylenediamine (o-PD) for the electropolymerization was obtained from Sigma-Aldrich.

Voltammetric measurements were performed with a potentiostat-galvanostat PGSTAT12 (Autolab, software GPES 4.9.05) and PGSTAT30 (Autolab, software NOVA 2.1.2) and DropSens Connector for

SPCE (Metrohm-Dropsens). The electrochemical cell consists of a SPCE composed of a graphite working electrode (modified or not), a carbon counter electrode and an Ag pseudoreference electrode. Electropolymerization was carried out by CV, applying 15 cycles from -0.4 to 0.7 V at 100 mV s⁻¹ with step potential 5 mV (Baradoke 2019).

3. Discussion

The voltammograms obtained during the working electrode material studies for alprazolam, clotiapine, clenbuterol, sulfamethoxazole and sulfamethizole are collected in Figure 4. It can be observed that the peaks of both antibiotics do not seem to be affected by the modifications neither in intensity nor in potential, whereas the other three drugs do show significant differences.

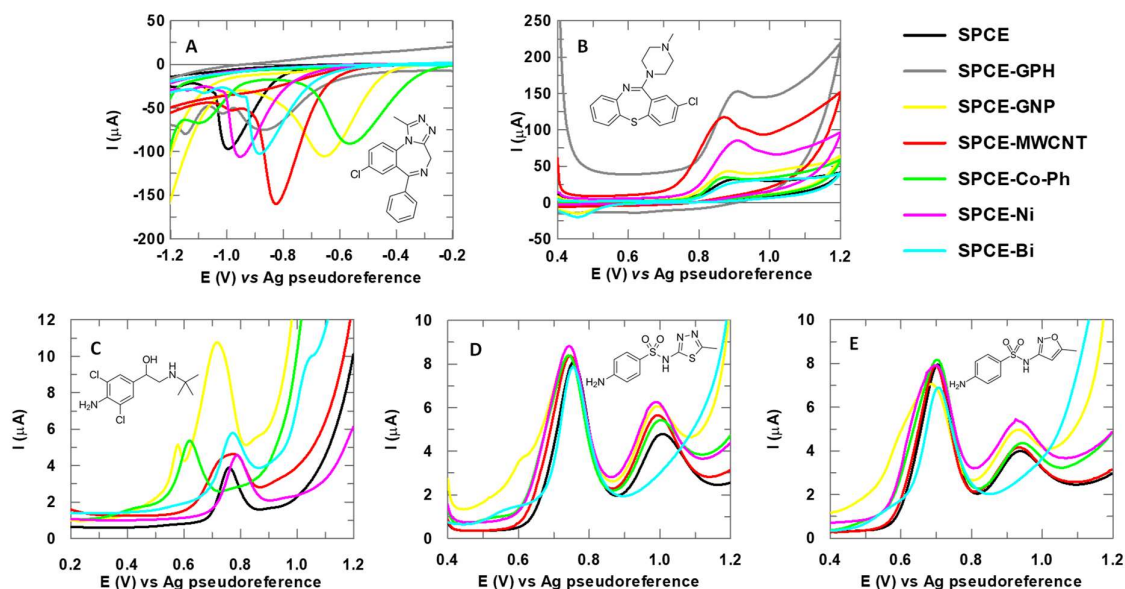


Figure 4. Voltammograms obtained during the working electrode material studies for A) alprazolam, B) clotiapine, C) clenbuterol, D) sulfamethoxazole and E) sulfamethizole. Abbreviations: GPH, graphene; GNP, gold nanoparticles; MWCNT, multi-walled carbon nanotubes; Co-Ph, cobalt (II) phtalocyanine; Ni, NiO; Bi, BiO.

As far as MOFs are concerned, they were tested on sulfamethizole. For this purpose, SPCEs were modified with an iron-based MOF and different co-modifiers. On the one hand, some nanostructures were studied, specifically carbon nanofibers (CNF) and magnetic iron nanoparticles (FeNP). On the other hand, *o*-PD polymerization was used to help immobilize the MOF following two different strategies. First, *o*-PD was electropolymerized followed by MOF incorporation by drop-casting. Second, MOF was added before electropolymerization. These experiments can be observed in Figure 5. The SPCEs modified surfaces were characterized with the Fe(CN)₆³⁻/[Fe(CN)₆]⁴⁻ system acting as a redox probe. In all cases, the redox probe confirmed the presence of the modifiers on the SPCE surface, but when it comes to sulfamethizole the expected electrocatalytic effect was not achieved in terms of sensitivity.

Finally, clotiapine was selected as an example to test the application of MWCNTs as sensing platforms. First, the electrochemical process was studied by CV, concluding that clotiapine undergoes an irreversible oxidation reaction that is governed by diffusion but with a significant adsorption component. Then, a calibration via external standard was performed by DPV, obtaining a linear range from 10.02 to 100.2 μmol L⁻¹ with limits of detection and quantification of 1.8 and 6.2 μmol L⁻¹, respectively, thus demonstrating the high sensitivity achieved with MWCNTs.

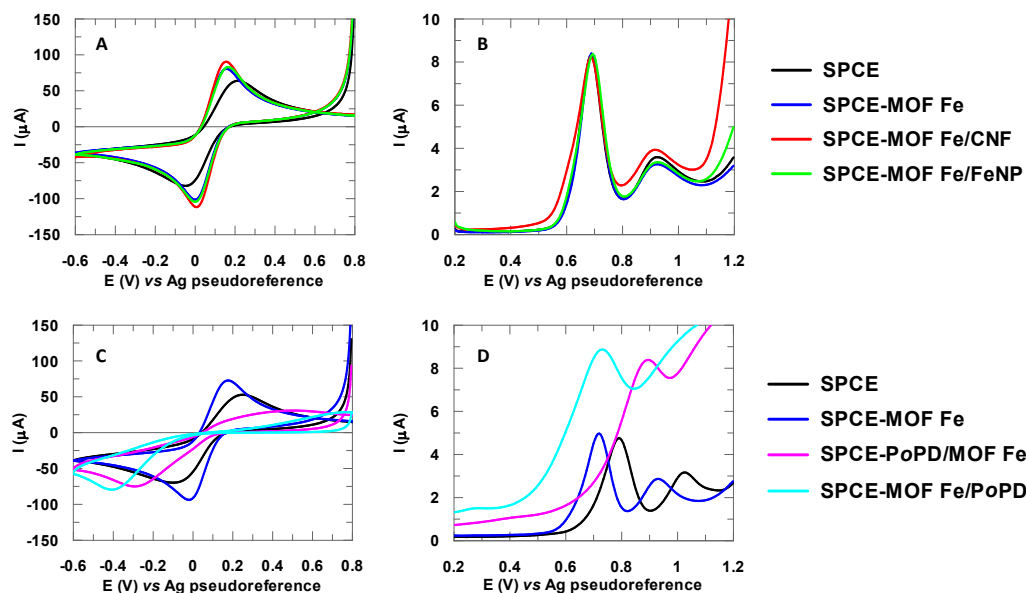


Figure 5. Voltammograms obtained with the iron-based MOF modified SPCEs. A) SPCEs modified with MOF and nanostructures for redox probe and B) sulfamethizole. C) SPCEs modified with MOF and *o*-PD for redox probe and D) sulfamethizole. The pink and light blue lines correspond to the first and second strategies mentioned above, respectively.

4. Conclusions

Both nanomaterials and MOFs were successfully applied as modifiers of the SPCEs surface, what proves their application as electrochemical transducers for drug sensing. Specifically, MWCNTs showed an excellent performance when it comes to clotiapine analysis at trace levels. As far as MOFs are concerned, their incorporation to the SPCEs surface was demonstrated with the redox probe. It must be taken into account that the optimal proportion of the co-modifiers was not studied yet, so further investigation will be carried out to improve the catalytic activity of the materials before developing an analytical method.

References

- Baradoke, A., Pastoriza-Santos, I. and González-Romero, E. 2019. "Screen-printed GPH electrode modified with Ru nanoplates and PoPD polymer film for NADH sensing: Design and characterization". *Electrochimica Acta* 300: 316-323. <https://doi.org/10.1016/j.electacta.2019.01.128>
- Kaur, H., Siwal, S., Chauhan, G., Saini, A., Kumari, A. and Thakur, V. 2022. "Recent advances in electrochemical-based sensors amplified with carbon-based nanomaterials (CNMs) for sensing pharmaceutical and food pollutants". *Chemosphere* 304: 135182. <https://doi.org/10.1016/j.chemosphere.2022.135182>

Acknowledgments

This research has been financially supported by Project PID2020-113667GB-I00 funded by the Spanish Ministry of Sciences and Innovation MCIN/AEI/10.13039/501100011033 and European Union Next Generation EU/ PRTR (PDC2021-121394-I00 and PCI2022-132941).

Value-added cereal-based products: incorporation of natural phenolic compounds in fresh pasta

Sandra M. Gomes^{1,2*}, Daniela Albuquerque³, Lúcia Santos^{1,2}

¹LEPABE - Laboratory for Process Engineering, Environment, Biotechnology and Energy, Faculty of Engineering, University of Porto, Rua Dr. Roberto Frias, 4200-465 Porto, Portugal

²ALICE - Associate Laboratory in Chemical Engineering, Faculty of Engineering, University of Porto, Rua Dr. Roberto Frias, 4200-465 Porto, Portugal

³FEUP - Faculty of Engineering, University of Porto, Rua Dr. Roberto Frias, 4200-465 Porto, Portugal

*Corresponding author: scgomes@fe.up.pt; ORCID ID 0000-0001-9654-2899

Abstract

Moringa oleifera is a plant, rich in bioactive compounds, that can be incorporated in cereal-based products to improve their nutritional profile and biological value. In this work, these compounds were extracted with ethanol using a solid-liquid extraction method. The extract presented a total phenolic content of $79.0 \pm 20.3 \text{ mg}_{\text{GAE}} \text{ g}_{\text{extract}}^{-1}$ and IC50 values of $633.1 \pm 11.5 \text{ mg L}^{-1}$ and $201.7 \pm 5.8 \text{ mg L}^{-1}$ for DPPH and ABTS, respectively. The extract was incorporated into fresh pasta with different levels of substitution (1.25% and 2%). The addition of *Moringa oleifera* leave extract increased the antioxidant activity of the supplemented pastas and its water absorption index and cooking loss.

Author Keywords. By-products, Bioactive compounds, Antioxidants, Food fortification, Cereal-based products

1. Introduction

Cereal-based products, such as bread and pasta, are staple foods widely consumed around the world. Despite its high content in carbohydrates, cereal-based products lack other nutrients and minerals. Nowadays, there is an increased demand for foods with higher nutritional value and health benefits, which can be achieved with the addition of functional ingredients from natural sources (Hodas, Zorzenon, and Milani 2021).

M. oleifera, a tree native to India, is rich in bioactive compounds such as phenols, flavonoids, and carotenoids, presenting antioxidant, anti-inflammatory, and anticancer properties (Vonghirundecha et al. 2022). Due to its composition, *M. oleifera* extracts can be used as natural additives to fortify cereal-based products such as pasta, namely fresh pasta. The incorporation of such extracts can add beneficial biological properties to the product, while their antioxidant activity can increase food shelf-life. Hence, *M. oleifera* extracts can be a promising natural additive to improve the nutritional and biological value of cereal-based products and replace synthetic preservatives.

2. Materials and Methods

Moringa oleifera leaf powder was provided by Agostinho Neto University, Luanda, Angola. The phenolic-rich extract was obtained using a solid-liquid extraction method with a Soxhlet extractor. The extraction parameters were as follows: extraction solvent – ethanol; extraction time – 2 h; sample-to-solvent ratio – 1:40 (m/V). After the extraction, a rotary evaporator was used to evaporate the solvent and then a gentle stream of nitrogen (2 mbar) was applied until the extract was completely dry. The Folin-Ciocalteu method was applied to determine the total phenolic content (TPC) of the extract (Silva et al. 2007). Briefly, the sample solution (1 g L⁻¹ in ethanol), was incubated with Folin-Ciocalteu reagent and sodium carbonate for 2 h and the absorbance was analysed at 750 nm. The results were expressed in mg of gallic acid equivalents (GAE)/g of dried extract. The antioxidant activity was studied following two protocols: 2,2-diphenyl-1-picrylhydrazyl (DPPH) method (Bobo-García et al. 2015) and 2,2-azinobis (3-ethyl-benzothiazolin-6-sulfonic acid) (ABTS) method (Xiao et al. 2020). For that, sample solutions with different concentrations were prepared: 1.5-8 g L⁻¹ for DPPH and 0.1-2.5 g L⁻¹ for ABTS. Then, the sample was incubated with the radical solution for 40 minutes, in the case of DPPH, and for 15 minutes, in the case of ABTS. After incubation, the absorbance was analysed at 515 nm and 734 nm for DPPH

and ABTS, respectively. Finally, the radical inhibition percentages were calculated to determine the IC₅₀ values, i.e. the extract concentration to inhibit 50% of the radical.

Fresh pasta was produced using 100 g of wheat flour, 1 egg, 0.7 g of olive oil and 0.2 g of salt. The pasta was fortified with *M. oleifera* extract (1.25% and 2% substitution level of wheat flour). The antioxidant capacity was evaluated as previously described. The water absorption and cooking loss were determined according to the literature (Kamble et al. 2022), with some modifications: 5 g of pasta was cooked for 5 min in 100 mL of boiling water.

3. Discussion

In this work, phenolic-rich extracts were obtained using a solid-liquid extraction. The solvent used was ethanol since it is Generally Recognized As Safe (GRAS), an important aspect for food applications, and due to its polarity. The extraction yield was 77.3 % and the extract presented a TPC of $79.0 \pm 20.3 \text{ mg}_{\text{GAE}} \text{ g}_{\text{extract}}^{-1}$. The TPC can vary according to the extraction conditions and the plant origin. The value obtained in the present work is similar to the one obtained in another study ($74.87 \text{ mg}_{\text{GAE}} \text{ g}_{\text{extract}}^{-1}$), where the phenolic compounds were extracted with 80% ethanol using mechanical agitation (Tai et al. 2018). Regarding the antioxidant capacity, the extract presented an IC₅₀ value of $633.1 \pm 11.5 \text{ mg L}^{-1}$ for DPPH and $201.7 \pm 5.8 \text{ mg L}^{-1}$ for ABTS, which indicates a higher radical scavenging activity towards ABTS, since the concentration necessary to inhibit 50% of the free radical is lower. The results obtained demonstrate the antioxidant potential of *M. oleifera* extract. Therefore, the extract was incorporated into fresh pasta to study its impact on the physicochemical properties of the product and the results are shown in Table 1.

Property	NC	FP1.25	FP2	
% Inhibition	DPPH	10.5 ± 1.2	11.7 ± 1.6	21.5 ± 1.4
	ABTS	47.2 ± 10.5	69.0 ± 4.9	92.6 ± 4.1
Water absorption (%)	59.1%	70.3%	85.5%	
Cooking loss (%)	2.0%	2.4%	2.5%	

Table 3: Physicochemical properties of fresh pasta. NC: negative control (pasta without additives); FP1.25: pasta with 1.25% *M. oleifera* extract; FP2: pasta with 2% *M. oleifera* extract

The results obtained support that the incorporation of *M. oleifera* extract into fresh pasta increases its antioxidant activity. Moreover, the pasta supplemented with 2% of extract presented a higher antioxidant capacity, for both ABTS and DPPH, than the one with 1.25%. The water absorption index increased significantly, from 59.1% to 85.5%, with the supplementation with *M. oleifera* extract. The water absorption is a good indicator of the pasta quality, as it can indicate a greater efficiency in satiating hunger and giving a feeling of satiety. The cooking loss also increased slightly, from 2.0% to 2.5%, with an increase of the extract content in the pastas. A low cooking loss indicates a high cooking performance with little loss of solids. These results are consistent with the ones obtained in the literature where an increase in the water absorption and cooking loss in pastas supplemented with *M. oleifera* pod powder was reported (Kamble et al. 2022).

4. Conclusions

The *M. oleifera* extract presented antioxidant activity against DPPH and ABTS, demonstrating its antioxidant properties and potential to be incorporated in food products. The supplemented fresh pastas presented a significantly increase in the antioxidant activity compared to the control pasta, due to the bioactive compounds that are present in the extract. Also, the water absorption index increased with the supplementation with *M. oleifera* extract and the cooking loss only increased slightly, indicating a good quality pasta. These results demonstrate the potential use of *M. oleifera* extracts as a natural source of phenolic compounds to improve the physical and biological properties of cereal-based food.

References

- Bobo-García, G., G. Davidov-Pardo, C. Arroqui, P. Virseda, M. R. Marín-Arroyo, and M. Navarro. 2015. "Intra-laboratory validation of microplate methods for total phenolic content and antioxidant activity on polyphenolic extracts, and comparison with conventional spectrophotometric methods." *J Sci Food Agric* 95 (1): 204-9. <https://doi.org/https://doi.org/10.1002/jsfa.6706>.
- Hodas, F., M. R. T. Zorzenon, and P. G. Milani. 2021. "Moringa oleifera potential as a functional food and a natural food additive: a biochemical approach." *An Acad Bras Cienc* 93 (suppl 4): e20210571. <https://doi.org/10.1590/0001-3765202120210571>.
- Kamble, Dinkar B., Khalid Bashir, Rakhi Singh, and Savita Rani. 2022. "Effect of Moringa oleifera pod addition on the digestibility, cooking quality, and structural attributes of functional pasta." *Journal of Food Processing and Preservation* 46 (1): e16163. <https://doi.org/https://doi.org/10.1111/jfpp.16163>.
- Silva, Adrián M. T., Ekaterini Nouli, Nikolaos P. Xekoukoulotakis, and Dionissios Mantzavinos. 2007. "Effect of key operating parameters on phenols degradation during H2O2-assisted TiO2 photocatalytic treatment of simulated and actual olive mill wastewaters." *Appl Catal B* 73 (1): 11-22. <https://doi.org/https://doi.org/10.1016/j.apcatb.2006.12.007>.
- Tai, Truong Kim, Jittima Thongklay, Pisipong Meunprasertdee, Papadchaya Kornthattalim, and Thammarat Kaeawmanee. 2018. "A Comparison of Three Extraction Methods for Phenolic Compounds and Antioxidant Activities from Moringa oleifera Leaves." *Chiang Mai J Sci* 45 (7): 2779 - 2789.
- Vonghirundecha, Phanita, Sasitorn Chusri, Pisipong Meunprasertdee, and Thammarat Kaewmanee. 2022. "Microencapsulated functional ingredients from a Moringa oleifera leaf polyphenol-rich extract: Characterization, antioxidant properties, in vitro simulated digestion, and storage stability." *LWT* 154: 112820. <https://doi.org/https://doi.org/10.1016/j.lwt.2021.112820>.
- Xiao, Fan, Tao Xu, Baiyi Lu, and Ruihai Liu. 2020. "Guidelines for antioxidant assays for food components." *Food Front* 1 (1): 60-69. <https://doi.org/https://doi.org/10.1002/fft.10>.

Acknowledgments

This work was financially supported by: (i) Project MORfood (541163254/2019) funded by Foundation for Science and Technology (FCT) and Aga Khan Development Network (AKDN) and (ii) LA/P/0045/2020 (ALiCE), UIDB/00511/2020 and UIDP/00511/2020 (LEPABE), funded by national funds through FCT/MCTES (PIDDAC)

Mono- and Bimetallic Carbon Nanotubes as Bifunctional Oxygen Electrocatalysts

Duarte J. Junqueira Magalhães^{1,2}, Rafael G. Morais^{1,2}, Rui S. Ribeiro^{1,2},
Natalia Rey-Raap³, José Luís Figueiredo^{1,2}, M. Fernando R. Pereira^{1,2}

¹ LSRE-LCM – Laboratório de Processos de Separação e Reacção - Laboratório de Catálise e Materiais, Faculdade de Engenharia, Universidade do Porto, R. Dr. Roberto Frias s/n, 4200-465 Porto, Portugal.

² ALiCE - Associate Laboratory in Chemical Engineering, Faculty of Engineering, University of Porto, Rua Dr. Roberto Frias, 4200-465 Porto, Portugal.

³ Instituto de Ciencia y Tecnología del Carbono, INCAR-CSIC, Francisco Pintado Fe 26, 33011 Oviedo, Spain.

(up201207138@edu.fe.up.pt)

Abstract

This work aimed to develop carbon nanotube (CNT) supported electrocatalysts for electrochemical energy conversion, targeting the oxygen reactions occurring in a unitized regenerative fuel cell (URFC). A monometallic catalyst obtained by impregnation of CNT with nickel(II) nitrate followed by thermal treatment at 260 °C under H₂ (CNT_{Ni_260H2}) displayed the best performance in the oxygen evolution reaction (OER), whereas CNT doped with iron(II) phthalocyanine (CNT_{FePc}) showed the best performance in the oxygen reduction reaction (ORR). A bifunctional catalyst prepared by physically mixing these samples in a 1:1 mass ratio (CNT_{Ni_260H2}/CNT_{FePc}) exhibited better electrocatalytic activity than a commercial benchmark electrocatalyst for OER and an ORR performance similar to that of the widely used Pt/C electrocatalyst. Ultimately, CNT_{Ni_260H2}/CNT_{FePc} presented the lowest potential gap of all the synthesized samples and benchmark catalysts, thus demonstrating its great potential to replace noble metals and be tested at a larger scale.

Author Keywords. Oxygen evolution reaction, Oxygen reduction reaction, Unitized regenerative fuel cell, Nickel, Iron(II) phthalocyanine.

1. Introduction

Modern energy supply in our society is mostly based on fossil fuels, which depends on finite resources that will be depleted in the near future. The high consumption of these fuels and consequent emissions of carbon dioxide have adverse impacts on climate change. Thus, the use of energy obtained from renewable sources is crucial to fight global warming and ensure the sustainability of the planet. Therefore, it is essential to optimize systems for energy storage when renewable energy production exceeds energy consumption and for its reconversion into electrical energy when demand surpasses instant production.

Currently, noble metals are widely used as catalysts for electrochemical energy conversion, but are associated with high costs. Carbon materials are a good alternative, as they are significantly less expensive than noble metals. Therefore, the objective of this study was to prepare highly active bifunctional electrocatalysts for the oxygen reactions occurring in a unitized regenerative fuel cell (URFC). To achieve this objective, iron phthalocyanine (FePc) and/or nickel species were incorporated onto carbon nanotubes (CNT) and tested towards the oxygen evolution and reduction reactions (OER and ORR, respectively).

2. Materials and Methods

Electrocatalysts for OER were prepared by incorporating nickel(II) nitrate hexahydrate on CNT by incipient wetness impregnation (IWI) followed by thermal treatments in two different atmospheres (N₂ and/or H₂) and at various temperatures. CNT were also modified by incorporation of FePc by IWI followed by a thermal treatment under N₂ atmosphere at 500 °C for 2 h (CNT_{FePc}). This Fe-doped CNT sample has been previously tested as ORR electrocatalyst, displaying a performance similar to that of the benchmark Pt/C catalyst. The Ni-doped samples were electrochemically characterized to determine their OER activities. Afterwards, the best-performing Ni-doped CNT (CNT_{Ni_260H2}) and CNT_{FePc} were

physically mixed using a 1:1 mass ratio (CNT_{Ni_260H2}/CNT_{FePc}). The electrochemical measurements (cyclic voltammetry – CV, linear sweep voltammetry – LSV, and stability tests) were performed using 0.1 mol L⁻¹ of KOH as the electrolyte in a conventional 3-electrode cell. To determine the bifunctionality of the catalysts for the oxygen reactions, the potential gap (ΔE), which corresponds to the difference between the OER potential at 10 mA cm⁻² (E_{10}), and the ORR half-wave potential ($E_{1/2}$) was calculated.

3. Discussion

The prepared carbon electrocatalysts were tested in the OER. The OER electroactivity of the samples treated under H₂ atmosphere was higher than their N₂-treated counterparts, in which CNT_{Ni_260H2} achieved a very low E_{10} (1.59 V). Nevertheless, the best performance among all samples was obtained with the bimetallic catalyst (CNT_{Ni_260H2}/CNT_{FePc}), an E_{10} as low as 1.57 V being obtained. This performance is even slightly better than that of RuO₂ ($E_{10} = 1.58$ V) – a conventional electrocatalyst for OER. Regarding ORR, CNT_{Ni_260H2} presents a poor performance towards this reaction. Nonetheless, CNT_{Ni_260H2}/CNT_{FePc} displays an excellent performance in the ORR, surpassing that of Pt/C ($E_{1/2}$ of 0.91 V vs 0.83 V, respectively), with negligible by-product formation. Regarding stability during the ORR, CNT_{Ni_260H2} performed better than CNT_{FePc}, but worse than Pt/C. However, the stability of the bimetallic catalyst formed by the mixture of these two samples is quite close to that of Pt/C, which is a good indication of its long-term performance as ORR electrocatalyst. Concerning oxygen bifunctionality, all the prepared samples led to a ΔE lower than that of Pt/C, which indicates that these catalysts are better suited to be used in a URFC. Among all samples prepared, the bimetallic sample stands out (CNT_{Ni_260H2}/CNT_{FePc}) with a ΔE of 0.66 V, which represents almost half the value obtained for Pt/C.

4. Conclusions

The highest electrocatalytic activity towards OER among the monometallic catalysts was obtained with sample CNT_{Ni_260H2}. The bimetallic electrocatalyst (CNT_{Ni_260H2}/CNT_{FePc}), which consists of a physical mixture of the catalysts with the best performance in OER and ORR, demonstrated the highest bifunctionality towards the oxygen reactions occurring in a URFC (*i.e.*, ORR and OER), even surpassing that of the commercial noble metal-containing catalysts typically used at industrial scale. Therefore, the prepared materials have high potential as a viable alternative to replace noble metal-based electrocatalysts.

References

Morais, R. G., Rey-Raap, N., Figueiredo, J. L., Pereira, M.F.R. 2023. "Optimization of cobalt CNT towards the oxygen evolution reaction and its synergy with iron (II) phthalocyanine as bifunctional oxygen electrocatalyst". In *Catalysis Today* 418. Accessed 26 March, 2023. DOI: 10.1016/j.cattod.2023.114057.

Acknowledgments

This work was financially supported by project BiCat4Energy (PTDC/EQU-EQU/1707/2020), funded by national funds (PIDDAC) through FCT/MCTES; LA/P/0045/2020 (ALiCE), UIDB/50020/2020 and UIDP/50020/2020 (LSRE-LCM) funded by national funds through FCT/MCTES (PIDDAC). D.J.J.M. expresses gratitude for the "Bolsa de Iniciação à Investigação no Verão_com_Ciencia_2022_LSRE-LCM", conducted at LSRE-LCM, funded by national funds through FCT – Fundação para a Ciência e Tecnologia, under the program "Verão com Ciência 2022". R.G.M. acknowledges the research grant from FCT (2020.06422.BD).

Photocatalytic Ammonia Production using Immobilized GCN-T Catalysts

Amala Joy^{1,2}, Joana Cancela^{1,2}, Isabel S.O. Barbosa^{1,2}, Maria J.

Sampaio^{1,2}, Joaquim L. Faria^{1,2}, Ricardo J. Santos^{1,2}, Cláudia G. Silva^{1,2}

¹Laboratory of Separation and Reaction Engineering–Laboratory of Catalysis and Materials (LSRE-LCM), Faculty of Engineering, University of Porto, Rua Dr. Roberto Frias, 4200-465 Porto, Portugal

²Associate Laboratory in Chemical Engineering (ALiCE), Faculty of Engineering, University of Porto, Rua Dr. Roberto Frias, 4200-465 Porto, Portugal

*Corresponding author: cgsilva@fe.up.pt

Abstract

Ammonia is mainly used for manufacturing fertilizers with the world's food production relying on it. It is also a promising indirect hydrogen carrier, much easier to store and transport. Introducing a zero-carbon process to produce ammonia allows for its use as a sustainable energy carrier. This work involves the application of heterogeneous photocatalysis for ammonia production using renewable resources like visible light, N₂, water, and metal-free catalysts. Graphite-like carbon nitride (GCN), a metal-free semiconductor easily synthesized from C- and N-rich precursors, can be tailored toward specific applications. The immobilization of such materials in 3D structures fabricated by additive manufacturing using GCN-T/PVDF films contributes to accelerating the technological effectiveness of photocatalysis as a more sustainable alternative ammonia production method.

Author Keywords. Ammonia, Heterogeneous photocatalyst, Graphitic carbon nitride, Additive Manufacturing.

1. Introduction

Ammonia is a significant component in modern agriculture and food production, with an annual production of approximately 200 million tons, mostly used in manufacturing fertilizers (Smith and Torrente-Murciano 2021). However, the use of natural gas to produce H₂ and the high energy consumption to extract nitrogen from air has caused environmental concerns, with industrial NH₃ production contributing to 1-2% of global energy demand and emitting over 200 million tons of CO₂ annually (Qandil, Othman, and Beithou 2023). To address these concerns, carbon neutral NH₃ production is of utmost importance since ammonia can offer a promising and easily transportable alternative to hydrogen.

Heterogeneous photocatalysis is a sustainable method for NH₃ production using renewable energy sources such as solar light or low-energy consumption radiation sources to reduce the carbon footprint. The overall process consists of the photocatalytic reduction of dinitrogen and water to ammonia and oxygen (Zhang et al. 2019).

Graphite-like carbon nitride (g-C₃N₄) is a metal-free semiconductor that can be activated by visible light radiation, making it a good candidate for photocatalytic NH₃ production. Nevertheless, its use as a powder in slurry photoreactors can cause technical problems and need time-consuming and costly separation of the catalyst (Sampaio et al. 2023).

Herein, a metal-free photocatalyst (GCN-T) immobilized in the form of a film (GCN-T/PVDF) over a 3D-printed structure was successfully tested in a batch photoreactor for ammonia production.

2. Materials and Methods

Photocatalyst Preparation

The bulk g-C₃N₄ preparation was produced using DCN as a precursor. The obtained powder sample was washed and dried. After that, the bulk material was undergone of a second thermal treatment at 500 °C, which was employed for 2 h to obtain the exfoliated GCN-T material. GCN-T was immobilized in a 3D-printed structure, which was previously coated with a PVDF film acting as an adherent agent for the photocatalyst.

Photocatalytic Experiments

The photocatalytic production of ammonia was carried out under visible irradiation using the tubular-shaped 3D printed structure supporting the GCN-T/PVDF film inside the photoreactor (Figure 1a). In a typical experiment, the catalytic structure was supported by a glass refrigeration tube, which maintained a constant temperature on the system and was placed inside a cylindrical glass reactor filled with 100 mL of ultra-pure water, which was continuously stirred and purged with N₂. A 4-UV LED system ($\lambda_{\text{max}} = 420 \text{ nm}$) was placed around the reactor. Figure 1b shows a schematic of the experimental setup.

Ammonia concentration analysis was conducted using Nessler's reagent method by measuring the absorbance of the solution over time in a JASCO V-560 spectrometer.

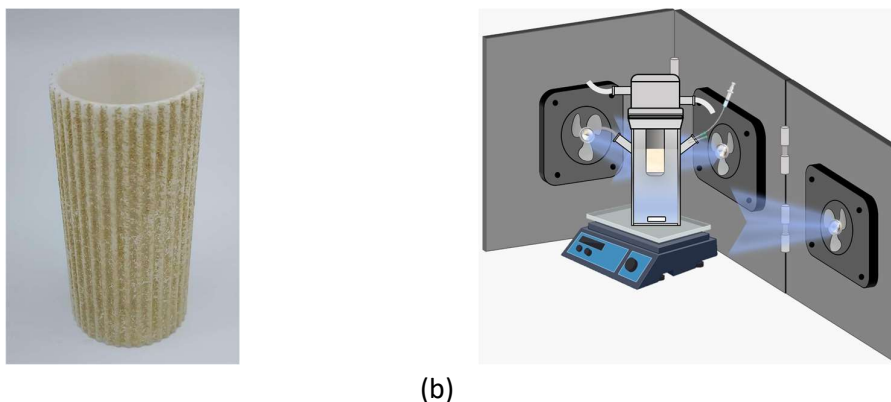


Figure 1: (a) 3D-printed structure coated with GCN-T and (b) Experimental setup for the photocatalytic ammonia synthesis.

Several experiments were conducted to test the efficiency of different scavengers, namely alcohols, to increase the efficiency of the photocatalytic reduction of dinitrogen to ammonia.

3. Results and Discussion

A comparison between several scavengers is in **Erro! A origem da referência não foi encontrada.**, which shows ammonia rate generation for ethanol, methanol, and isopropyl alcohol.

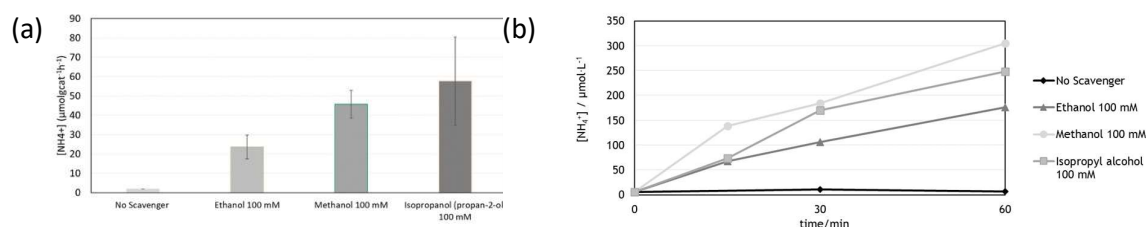


Figure 2: (a) Ammonia rate generation using different scavengers and (b) ammonia concentration evolution along the time.

Comparing the results from Figure 2(a), hole scavengers can enhance the photocatalytic activity of the system for ammonia synthesis. Isopropanol was proven to promote the best ammonia rate generation ($\sim 60 \mu\text{mol}\cdot\text{g}_{\text{cat}}^{-1}\cdot\text{h}^{-1}$). From Figure 2(b), it is observed that ammonia concentration in the solution increase almost linearly with time.

4. Conclusions

A batch reactor with an immobilized metal-free photocatalyst was successfully employed for photocatalytic ammonia synthesis under visible light using alcohols as effective hole scavengers. This system avoids the separation of the catalyst from the solution and opens up the possibility of using

solar light for reaction activation, both accounting for the sustainability of the proposed ammonia production route.

References

- Qandil, Ahmed, Ali Othman, and Nabil Ibrahim Beithou. 2023. "Experimental Analysis of Atmospheric Water Harvester Using Ammonia Vapour Absorption System." *Journal of Ecological Engineering* 24 (2): 221-229. <https://doi.org/10.12911/22998993/156612>.
- Sampaio, Maria J., Ana R. L. Ribeiro, Cláudia M. R. Ribeiro, Rita A. Borges, Marta F. Pedrosa, Adrián M. T. Silva, Cláudia G. Silva, and Joaquim L. Faria. 2023. "A technological approach using a metal-free immobilized photocatalyst for the removal of pharmaceutical substances from urban wastewaters." *Chemical Engineering Journal* 459. <https://doi.org/10.1016/j.cej.2023.141617>.
- Smith, Collin, and Laura Torrente-Murciano. 2021. "The potential of green ammonia for agricultural and economic development in Sierra Leone." *One Earth* 4 (1): 104-113. <https://doi.org/https://doi.org/10.1016/j.oneear.2020.12.015>.
- Zhang, Shuai, Yunxuan Zhao, Run Shi, Geoffrey I. N. Waterhouse, and Tierui Zhang. 2019. "Photocatalytic ammonia synthesis: Recent progress and future." *EnergyChem* 1 (2): 100013. <https://doi.org/https://doi.org/10.1016/j.enchem.2019.100013>.

Acknowledgments

This work was financially supported by LA/P/0045/2020 (ALiCE), UIDB/50020/2020 and UIDP/50020/2020 (LSRE-LCM), and the project SuN2Fuel 2022.04682.PTDC - funded by national funds through FCT/MCTES (PIDDAC). I.S.O. Barbosa acknowledges her FCT grant UI/BD/151092/2021.

Graphitic carbon nitride immobilized onto ceramic foam for the degradation of sulfamethoxazole mediated by visible-light photocatalytic wet peroxide oxidation

Ana M. Chávez^{1,2,3*}, André Torres-Pinto^{2,3}, Pedro M. Álvarez¹, Joaquim L. Faria^{2,3}, Cláudia G. Silva^{2,3}, Adrián M.T. Silva^{2,3}

¹Departamento de Ingeniería Química y Química Física, Instituto Universitario del Agua, Cambio Climático y Sostenibilidad (IACYS), Universidad de Extremadura, 06006 Badajoz, Spain.

²LSRE-LCM – Laboratory of Separation and Reaction Engineering – Laboratory of Catalysis and Materials (LSRE-LCM), Faculdade de Engenharia, Universidade do Porto, Rua Dr. Roberto Frias s/n, 4200-465 Porto, Portugal.

³ALICE – Associate Laboratory in Chemical Engineering, Faculdade de Engenharia, Universidade do Porto, Rua Dr. Roberto Frias s/n, 4200-465 Porto, Portugal.

*Corresponding author: achavez@fe.up.pt; ORCID ID 0000-0001-8781-5154

Abstract

Graphitic carbon nitride (CN) photocatalyst was immobilized onto a ceramic foam (AF) by thermal condensation of urea, which is an advantage for the process scale-up. A high photocatalytic activity under visible-light illumination was observed for sulfamethoxazole (SMX) degradation. Moreover, adding hydrogen peroxide (H₂O₂) enhanced the SMX mineralization. Definitively, a CN-F35 sample (35 mg CN per 1 g AF) demonstrated excellent efficiency for SMX degradation (80 %), H₂O₂ conversion (55 %) and removal of intermediates, when using the visible-light photocatalytic wet peroxide process in continuous flow dead-end regime for 24 h.

Author Keywords. Ceramic foam, carbon nitride, hydrogen peroxide, photocatalysis, water treatment.

1. Introduction

Pharmaceuticals have been widely detected in the aquatic environment (Barbosa et al. 2016). Considering their long-term impacts, one of the alternatives for their removal in water and wastewater treatment is to employ advanced oxidation processes (AOPs), which are based on the generation of reactive oxygen species (ROS). In particular, photocatalytic oxidation (PCO) is an AOP that may be performed using energy-efficient lighting sources (*e.g.*, visible-light LEDs). PCO can be assisted by adding different oxidizing agents, such as H₂O₂ (*i.e.*, the so-called photocatalytic wet peroxide oxidation process - PCWPO).

Graphitic carbon nitride (CN) has gained significant interest in heterogeneous photocatalysis since it is a metal-free catalyst with outstanding photocatalytic activity under visible-light illumination. It has associated with inexpensive synthesis procedures and chemical stability. Most research has been performed using powdered CN suspended in water; however, immobilized photocatalysts are more suitable solutions for the process scale-up (Fouad et al. 2021).

The main aim of this work consisted on immobilizing CN in a ceramic support with photocatalytic activity for being used in PCWPO in continuous regime for the removal of sulfamethoxazole (SMX) in water.

2. Materials and Methods

Material synthesis

A ceramic alumina/silica foam (*ca.* 69 % Al₂O₃, 27 % SiO₂, 1.8 % MgO and <2.3 % other oxides, 20 ppi) was used as supporting material. CN was deposited onto AF by a thermal condensation procedure adapted from the literature (Lima et al. 2017) and using dissolved urea as a precursor. The resulting samples were labeled as CN-Fx, where x corresponds to the theoretical amount of CN immobilized per gram of AF (*e.g.*, 35 mg in the case of the CN-F35 sample). The CN-based foams were cleaned with purified water, sonicated for 5 min and dried with compressed air before being used in the experiments.

Experiments

The PCO activity of immobilized CN-foams was tested by using 4 visible-light LEDs with a maximum emission at 415 nm, illuminating a 25 mL cylindrical reactor where a CN-foam was placed. A 100 mL solution containing sulfamethoxazole (30 mg L^{-1}) was fed to the reactor at 5 mL min^{-1} (hydraulic retention time, HRT = 5 min), and the outlet stream was recirculated to the feed reservoir. The PCWPO experiments followed the same procedure, but added H_2O_2 into the feed reservoir. Different H_2O_2 concentrations were tested (5, 10, 25 and 50 mM). The catalytic activity and stability of the CN-F35 sample for both PCO and PCWPO were also investigated in a continuous dead-end regime at 0.5 mL min^{-1} (HRT = 50 min). Liquid samples were collected and analyzed by high-performance liquid chromatography (HPLC), ionic chromatography and spectrophotometric methods.

3. Discussion

Regardless of the initial H_2O_2 dose tested under recirculation mode with the CN-F35 sample, the same efficiency was observed for the degradation of SMX (results not shown) and more than 90 % of H_2O_2 is continuously consumed at these conditions. **Erro! A origem da referência não foi encontrada.** presents the % of nitrogen (N) and sulfur (S) in SMX respectively transformed into nitrite/nitrate or sulfate for the different H_2O_2 doses tested. The concentration of some short-chain organics acids (SCOAs) is also shown in the table. As observed, there is a significant increase in the concentrations of these by-products when using 25 mM of H_2O_2 . In contrast, photocatalysis without H_2O_2 (PCO) only transformed *ca.* 6 % of the organic N and S-content.

$\text{H}_2\text{O}_{2,0}$ mM	% N	% S	Acetate ($\text{mg}\cdot\text{L}^{-1}$)	Formate ($\text{mg}\cdot\text{L}^{-1}$)	Oxalate ($\text{mg}\cdot\text{L}^{-1}$)
0	5.8	6.6	<Q.L.	<Q.L.	<Q.L.
5	7.3	8.1	0.5	0.4	0.4
10	11	18	0.8	0.9	0.5
25	29	42	2.5	1.7	2.0
50	40	36	2.3	1.6	1.6

Table 4: Yields of N/S-species and concentration of SCOAs quantified in PCO and PCWPO degradation of SMX under recirculation mode in 360 min (<Q.L.: below quantification limit).

Figure 6 depicts the data obtained in the PCO of SMX (left) and when adding H_2O_2 (25 mM) – PCWCO (right) in a continuous flow dead-end regime. PCWPO reached 80 % of SMX removal, 20 % of mineralization (TOC - total organic carbon removal) and 55 % of H_2O_2 conversion in steady state.

Moreover, 12 and 32 % of N- and S-content in SMX generated inorganic species (mainly nitrates and sulfates, respectively) – results not shown. Oxalate was quantified in over 1.2 mg L^{-1} , which might explain the slight drop in the pH to 4.1. In comparison, PCO achieved a lower removal of SMX (40 %) and <1 % N, <6 % S and < 0.2 mg L^{-1} oxalate.

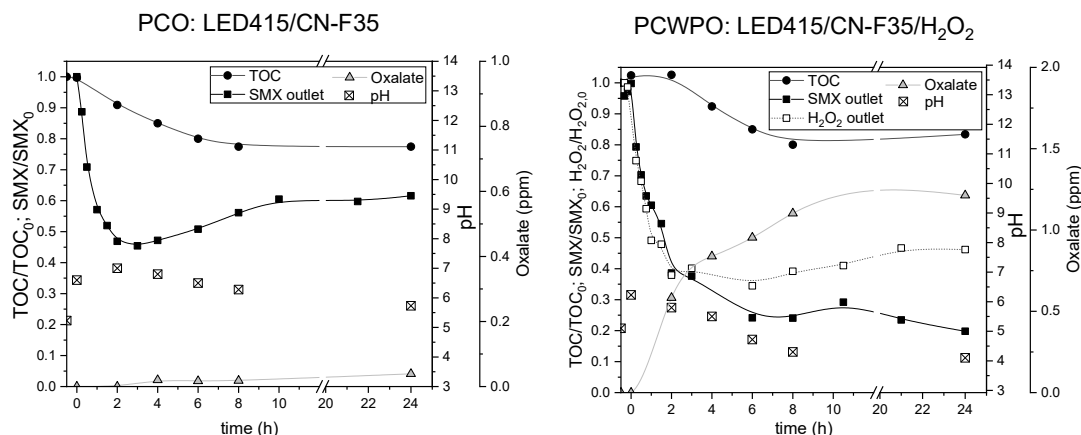


Figure 6: Evolution of SMX and TOC normalized concentrations, and pH and oxalate formed during PCO (left) and PCWPO, including the normalized consumed H₂O₂ (right), in continuous dead-end regime with CN-F35.

4. Conclusions

Graphitic carbon nitride was easily immobilized onto ceramic alumina/silica foams and demonstrated a high photocatalytic activity under visible-light illumination. Adding hydrogen peroxide led to an improvement in sulfamethoxazole mineralization (i.e., by-product degradation). The immobilized photocatalyst CN-F35 demonstrated stability after 24 hours in the visible-light photocatalytic wet peroxide oxidation (PCWPO) process under a continuous flow dead-end regime.

References

- Barbosa, Marta O., Nuno F.F. Moreira, Ana R. Ribeiro, Manuel F.R. Pereira, and Adrián M.T. Silva. 2016. "Occurrence and Removal of Organic Micropollutants: An Overview of the Watch List of EU Decision 2015/495." *Water Research* 94: 257–79. <https://doi.org/10.1016/j.watres.2016.02.047>.
- Fouad, Kareem, Mohamed Bassyouni, Mohamed Gar Alalm, Mamdouh, and Y. Saleh. 2021. "Recent Developments in Recalcitrant Organic Pollutants Degradation Using Immobilized Photocatalysts." *Applied Physics A* 127: 612. <https://doi.org/10.1007/s00339-021-04724-1>.
- Lima, Maria J., Adrián M.T. Silva, Cláudia G. Silva, and Joaquim L. Faria. 2017. "Graphitic Carbon Nitride Modified by Thermal, Chemical and Mechanical Processes as Metal-Free Photocatalyst for the Selective Synthesis of Benzaldehyde from Benzyl Alcohol." *Journal of Catalysis* 353: 44–53. <https://doi.org/10.1016/J.JCAT.2017.06.030>.

Acknowledgments

A.M.C. is grateful to Ministerio de Ciencia, Innovación y Universidades of Spain through Universidad de Extremadura (UEX) for her postdoctoral fellowship "Ayudas para la recualificación del sistema universitario español. Modalidad Margarita Salas" for young Ph.D. researchers (MS-17, UEX, call 2021). This work was also supported by LA/P/0045/2020 (ALICE), UIDB/50020/2020 and UIDP/50020/2020 (LSRE-LCM), funded by national funds through FCT/MCTES (PIDDAC), and Project NORTE-01-0145-FEDER-000069 (Healthy Waters) supported by NORTE 2020, under the PORTUGAL 2020 Partnership Agreement, through ERDF. A.T-P. gratefully acknowledges FCT for his scholarship SFRH/BD/143487/2019.

Graphitic carbon nitride as a novel platform for Horseradish Peroxidase biocatalytic reactions with *in situ* H₂O₂ production

Rita A. M. Barros^{1,2*}, Raquel O. Cristóvão^{1,2}, Maria J. Sampaio^{1,2},
Cláudia G. Silva^{1,2}, Joaquim L. Faria^{1,2}

¹LSRE-LCM - Laboratory of Separation and Reaction Engineering – Laboratory of Catalysis and Materials, Faculty of Engineering, University of Porto, Rua Dr. Roberto Frias, 4200-465 Porto, Portugal

²ALICE – Associate Laboratory in Chemical Engineering, Faculty of Engineering, University of Porto, Rua Dr. Roberto Frias, 4200-465 Porto, Portugal

*Corresponding author: e-mail address: up201604653@edu.fe.up.pt; ORCID ID 0000-0002-5627-0785

Abstract

Thermally exfoliated graphitic carbon nitride (GCN-T) was synthesized and used as support material for the immobilization of Horseradish Peroxidase (HRP). The surface chemical composition and excellent biocompatibility of GCN-T make it an effective support for enzyme immobilization, while its capacity for *in situ* photocatalytic H₂O₂ production can enhance the enzyme's catalytic efficiency. HRP was successfully immobilized onto GCN-T through a simple physical adsorption method. The highest activity of the bioconjugate was obtained at pH 6, with an initial enzyme concentration of 40 mg/L and an immobilization time of 60 min. The results showed excellent performance of the GCN-T as support of HRP with a maximum enzyme loading of 269 U per g of adsorbent. The bioconjugate was further evaluated regarding reusability and performance under different pH, and thermal and storage stabilities. The *in situ* generation of H₂O₂ by GCN-T under visible light was also explored and optimized, proving its great potential for various biocatalytic applications using peroxidases.

Author Keywords. Horseradish peroxidase, hydrogen peroxide, immobilization, graphitic carbon nitride.

1. Introduction

Peroxidases (EC 1.11.1.7) belong to the enzymatic group of oxidoreductases that catalyze the oxidation of a wide range of organic and inorganic substances by using hydrogen peroxide (H₂O₂) (Azevedo et al. 2015). They can be found in many different types of organisms and have applications in various fields, including the use in immunoassays, water treatment (Bian et al. 2021), as food preservatives, and production of biofuels (Junge, Fernandes, and Sá 2018). From the industrial point of view, peroxidases have the advantage of using H₂O₂ as an economically viable and easily synthesized electron acceptor. However, its practical application at a large scale is still restricted by low stability under environmental conditions and lack of reusability. Besides, at high concentrations, exogenous H₂O₂ can have a negative effect on peroxidases by causing oxidative damage to the enzyme.

In recent years, graphitic carbon nitride (GCN) has gained particular attention as a semiconductor that operates under visible light (Ismael 2020). Made of earth-abundant elements, GCN has outstanding biocompatibility, thermal and chemical stability, photocatalytic activity, and tunable functionalization, all of which provide a unique set of interesting properties for its use in various fields. Besides, it is the most studied metal-free photocatalyst for H₂O₂ production.

Therefore, the aim of this work is to increase the performance of horseradish peroxidase (HRP) by the simultaneous enzyme immobilization on a photocatalyst and the *in situ* production of the ideal H₂O₂ concentration. For this purpose, HRP was immobilized by physical adsorption onto thermally exfoliated graphitic carbon nitride (GCN-T). The bioconjugate was then studied regarding reusability, pH, thermal, and storage stabilities. Furthermore, the photocatalytic generation of H₂O₂ by GCN-T was explored and optimized under different conditions. Overall, this study combines the synergetic effect of enzyme immobilization for improved stability under different conditions, together with the simultaneous *in situ* production of H₂O₂, which is an indispensable chemical to drive the enzymatic reaction.

2. Materials and Methods

The synthesis of bulk GCN was performed by the thermal decomposition of dicyandiamide at 550 °C. A second thermal treatment at 500 °C was applied to the bulk material to obtain the exfoliated materials, denoted as GCN-T. The immobilization of HRP onto GCN-T by physical adsorption was studied by adding different concentrations of HRP solutions to 2 mg of GCN-T. HRP activity was studied by measuring the absorbance at 510 nm (OceanOptics USB2000+ UV-vis spectrophotometer). The assay mixture consisted of 0.1 M phosphate buffer pH 7.4, 9.6 mM 4-aminoantipirene (4-AAP), 0.1 M phenol, 2 mM H₂O₂, and free enzyme or bioconjugate. One unit of HRP activity was defined as the conversion of 1 μmol of H₂O₂ per minute at pH 7.4 and 25 °C. The photocatalytic efficiency of the GCN-T was studied in a glass reactor containing 50 mL of aqueous glucose solution. The reactions occurred under magnetic stirring and the incidence of visible light ($\lambda_{\text{max}} = 413 \text{ nm}$). The reactions were performed in continuous air saturation, with 15 min of air bubbling in the dark to achieve adsorption-desorption equilibrium. Different operating conditions were investigated: initial concentration of glucose (5 to 35 mM), pH (4 to 8), and catalyst load (0.5 to 1.5 g/L). Samples were periodically withdrawn, filtered, and analyzed by a colorimetric method for the determination of the amount of H₂O₂ produced (Eisenberg 1943).

3. Discussion

The immobilization of HRP onto GCN-T was evaluated by optimizing several parameters, namely, the pH, the time of contact, and the enzyme concentration. The results show that the maximum activity of the bioconjugate was obtained at pH 6, with an initial enzyme concentration of 40 mg/L and an immobilization time of 60 min. The results demonstrate the excellent performance of the GCN-T as support of HRP with a maximum enzyme loading of 269 U per g of material (Figure). The effect of H₂O₂ on the HRP activity was also evaluated, showing that concentrations above 1.5 mM have a negative effect on the enzyme's catalytic activity, possibly caused by oxidative damage of the enzyme. Regarding the photocatalytic reactions, after 2 hours and under the optimal conditions (catalyst load of 1.3 g/L, glucose concentration of 35 mM, and pH of 7.35), the amount of H₂O₂ produced was 0.53 mM. These results confirm the photocatalytic efficiency of GCN-T for the *in situ* generation of H₂O₂ and further use in combination with HRP.

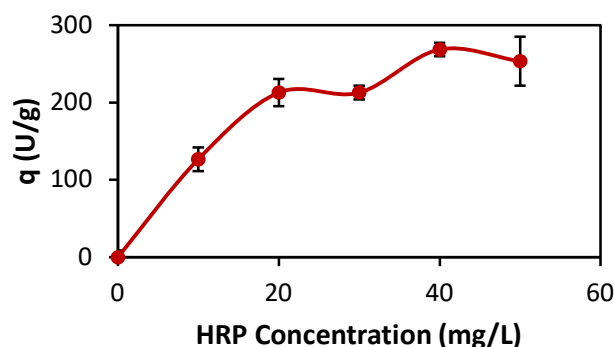


Figure 1: Amount of HRP adsorbed per g of GCN-T (q).

4. Conclusions

The immobilization of HRP onto GCN-T was successfully achieved by a simple physical adsorption method. GCN-T proved to be a stable and biocompatible support for HRP immobilization, while *in situ* H₂O₂ production prevents the enzyme from suffering oxidative stress, enhancing its catalytic activity. Future tests will involve the evaluation of the efficiency of the photobiocatalyst in a reaction medium with *in situ* H₂O₂ production for the degradation of contaminant compounds. Further, the surface modification of GCN-T with ligands that strengthen the bonds between the enzyme and the support will also be considered.

References

- Azevedo, Renato M., João B. Costa, Philippe Serp, José M. Loureiro, Joaquim L. Faria, Cláudia G. Silva, and Ana P.M. Tavares. 2015. "A Strategy for Improving Peroxidase Stability via Immobilization on Surface Modified Multi-Walled Carbon Nanotubes." *Journal of Chemical Technology and Biotechnology* 90 (9): 1570–78. <https://doi.org/10.1002/jctb.4698>.
- Bian, Jiyong, Xiaoqiang An, Wei Jiang, Ruiping Liu, Chengzhi Hu, and Huijuan Liu. 2021. "Defect-Enhanced Activation of Carbon Nitride/Horseradish Peroxidase Nanohybrids for Visible-Light-Driven Photobiocatalytic Water Purification." *Chemical Engineering Journal* 408 (March). <https://doi.org/10.1016/j.cej.2020.127231>.
- Eisenberg, George M. 1943. "Colorimetric Determination of Hydrogen Peroxide." *Ind. Eng. Chem. Anal. Ed.* 15 (5): 327–28. <https://doi.org/https://doi.org/10.1021/i560117a011>.
- Ismael, Mohammed. 2020. "A Review on Graphitic Carbon Nitride (g-C₃N₄) Based Nanocomposites: Synthesis, Categories, and Their Application in Photocatalysis." *Journal of Alloys and Compounds* 846: 156446. <https://doi.org/10.1016/j.jallcom.2020.156446>.
- Junge, N. H., D. L.A. Fernandes, and J. Sá. 2018. "Phototriggering Lignin Peroxidase with Nanocatalysts to Convert Veratryl Alcohol to High-Value Chemical Veratryl Aldehyde." *Materials Today Sustainability* 1–2 (December): 28–31. <https://doi.org/10.1016/j.mtsust.2018.11.001>.

Acknowledgments

This work was financially supported by: LA/P/0045/2020 (ALiCE) and UIDB/50020/2020 - UIDP/50020/2020 (LSRE-LCM) funded by national funds through FCT/MCTES (PIDDAC). The authors also thank the projects ClimActic (NORTE-01-0145-FEDER-000071). R.A.M. Barros acknowledges FCT for her PhD grant 2022.12055.BD. MJS acknowledges FCT funding under the Scientific Employment Stimulus - Institutional Call (CEECINST/00010/2021).

Sustainability assessment of FAME production from vegetable oil: GREENSCOPE methodology

Catarina M. Oliveira^{1,2,*}, José C.M. Pires^{1,2}

¹LEPABE—Laboratory for Process Engineering, Environment, Biotechnology and Energy, Faculty of Engineering, University of Porto, Rua Dr. Roberto Frias, 4200-465 Porto, Portugal

²ALICE—Associate Laboratory in Chemical Engineering, Faculty of Engineering, University of Porto, Rua Dr. Roberto Frias, 4200-465 Porto, Portugal

*Corresponding author: e-mail address: up201704157@edu.fe.up.pt; 0009-0003-6358-5157

Abstract

Fatty acid methyl esters (FAME) application as biodiesel has grown in interest as an alternative to petroleum-based diesel fuel due to reduced CO₂ emissions. FAME is produced industrially by the transesterification of vegetable oils with methanol and using NaOH as a catalyst. The industrial production of FAME still faces some challenges, such as undesirable reactions and intense energy requirements. In this work, a sustainability assessment of FAME production from vegetable oil was performed based on the Gauging Reaction Effectiveness for the Environmental Sustainability of Chemistries with a multi-Objective Process Evaluator (GREENSCOPE) methodology. A sensibility analysis of the process operating conditions (e.g., oil input flow rate) was performed to evaluate process sustainability. Several scenarios with oil input flow rates ranging from 500 to 2 000 kg/h were studied. An overall sustainability improvement was observed with the increase in oil input flow rate. The maximum process sustainability value tended towards approximately 77%.

Author Keywords. Sustainability Assessment, GREENSCOPE, Biofuel, Vegetable Oil

1. Introduction

Global energy security has been heightened by the depletion of fossil fuel supplies and price volatility (Amin 2019). Moreover, burning fossil fuels has resulted in significant greenhouse gas emissions, contributing to climate change. Growing global energy and fuel demand due to a rising world population has prompted the development of alternative renewable energy and fuel sources. Biodiesel has been suggested as a viable, renewable, and biodegradable alternative to traditional fossil fuels as an energy source (Douvartzides et al. 2019). The increased interest in biodiesel arises from its comparable physical characteristics to petroleum-based diesel fuel, which allows its direct application in engines with minimal modifications required (Amin 2019). Additionally, its blending with petroleum-based diesel fuel can potentially reduce harmful emissions such as CO₂, hydrocarbons, and particulate matter.

Fatty acid methyl esters (FAME) are produced from the transesterification of plant oils (edible and non-edible) and animal fats, which are subsequently purified to blend or use as biodiesel. The most common industrial production of FAME involves the transesterification of edible plant oils (triglycerides) with methanol via a homogenous alkali catalyst and glycerol as a byproduct (Amin 2019). High yields have been reported for short reaction times at low temperatures (Amin 2019). Nevertheless, feedstock quality can affect its yield, requiring a pretreatment step. FAME is suitable to be used as a biodiesel source, but issues such as low oxidative stability, increased NO_x emissions, and high feedstock viscosity need to be addressed (Douvartzides et al. 2019). The production of FAME requires the performance of catalyst and byproduct separation, which are difficult and intense energy processes that can question the economic and environmental viability of the process (Amin 2019).

Process sustainability assessment has been proposed by several methodologies to improve the performance of chemical production processes. In this work, a sustainability evaluation of FAME production through the transesterification of vegetable oil with methanol using NaOH as a catalyst was performed by Gauging Reaction Effectiveness for the Environmental Sustainability of Chemistries with a multi-Objective Process Evaluator (GREENSCOPE) methodology. The objective of the present study was to evaluate the impact of varying operating conditions on the sustainability of chemical processes.

2. Materials and Methods

The production of FAME was simulated in *Aspen Plus* based on the process proposed by Zhang et al. (2003) for a FAME production capacity of 8 500 t/y (oil input flow rate of 1 050 kg/h), with a purity of 99.7 %. The transesterification reaction kinetics considered were suggested by Salehi et al. (2019).

The process sustainability assessment was performed based on the GREENSCOPE methodology proposed by Ruiz-Mercado et al. (2012), coded in *Visual Basic for Applications (Microsoft Excel)*. This methodology aims to assess the impact of producing a desired product while fulfilling environmental demands and maximising economic return by using a sustainability measurement scale. The GREENSCOPE methodology was carried out by determining indicators capable of characterising the studied process in the areas of environment, efficiency (material), energy, and economy (four E's) (Ruiz-Mercado et al. 2012). Additionally, a global indicator for each of the 4 areas of interest and the overall process was determined by the weighted average of the calculated indicators. A sensibility analysis of process operating conditions, such as oil input flow rate, was carried out to evaluate the opportunities for sustainability improvement in the 4 areas and the global production process. The performed variations were accommodated by changing process operating parameters while maintaining FAME purity.

3. Discussion

The sustainability assessment was performed by calculating the indicators proposed by the GREENSCOPE methodology and determining a global process sustainability weighted average for the different scenarios. In this work, several indicators were calculated: (i) 61 for environmental impact; (ii) 26 for efficiency of material; (iii) 8 for energy use; and (iv) 33 for economic profits of the work. The potential for process sustainability improvement was evaluated by varying operating conditions (e.g., oil input flow rate). Several scenarios ranging from 500 to 2 000 kg/h were studied. The base case scenario of the process considered had an oil input flow rate of 1 050 kg/h. The global weighted average for each area and the overall process are shown in Table 5.

Oil input flow rate (kg/h)	Environmental	Efficiency	Energy	Economic	Global
500	74.34	80.89	64.51	51.02	69.05
1000	77.39	82.97	68.50	65.05	74.78
1050	77.56	82.99	70.06	65.52	75.09
1500	78.68	83.13	71.12	68.30	76.43
2000	79.07	81.83	72.97	69.72	76.84

Table 5: Sustainability performance in percentage (%) determined by the GREENSCOPE methodology for each area and the global production process.

An overall sustainability performance improvement was observed by increasing the oil input flow rate. The observed improvement in overall process sustainability tends towards a value of approximately 77 %. The same trend behaviour is observed for each of the quantified areas at various maximum values.

For each of the considered scenarios, it is observed that the economic impact has the highest potential for sustainability improvement. Nevertheless, the economic impact had the highest sustainability improvement, an increase of approximately 19 %, due to the variation in oil input flow rate.

The material efficiency had a decline in sustainability from 82.99 % for an oil input flow rate of 1 050 kg/h (base case scenario) to 81.83 % in the scenario with a 2 000 kg/h oil input flow rate. This outcome arises from the inability of the process to balance the additional FAME output with the extra need for resources.

Globally, these results demonstrate the potential to improve process sustainability by increasing oil input flow rate; however, these sustainability benefits must be carefully evaluated since they might not be sufficient to motivate a change in the FAME production process.

4. Conclusions

FAME has been considered as an alternative to petroleum-based diesel fuel. In this work, the sustainability assessment of the production of FAME from vegetable oil in the presence of methanol using NaOH as a catalyst was studied through the GREENSCOPE methodology. A sensibility analysis of the oil input flow rate was performed, ranging from 500 to 2 000 kg/h. The increase in oil input flow rate was found to allow for sustainability improvements in the FAME production process. A maximum overall process sustainability value tends towards approximately 77%.

References

- Amin, Ashraf. 2019. "Review of diesel production from renewable resources: Catalysis, process kinetics and technologies." *Ain Shams Engineering Journal* 10 (4): 821-839. <https://doi.org/10.1016/j.asej.2019.08.001>.
- Douvartzides, Savvas L., Nikolaos D. Charisiou, Kyriakos N. Papageridis, and Maria A. Goula. 2019. "Green Diesel: Biomass Feedstocks, Production Technologies, Catalytic Research, Fuel Properties and Performance in Compression Ignition Internal Combustion Engines." *Energies* 12 (5): 809. <https://doi.org/10.3390/en12050809>.
- Ruiz-Mercado, Gerardo J., Raymond L. Smith, and Michael A. Gonzalez. 2012. "Sustainability Indicators for Chemical Processes: I. Taxonomy." *Industrial & Engineering Chemistry Research* 51 (5): 2309-2328. <https://doi.org/10.1021/ie102116e>.
- Salehi, Abozar, Abdolreza Karbassi, Barat Ghobadian, Amir Ghasemi, and Amir Doustgani. 2019. "Simulation process of biodiesel production plant." *Environmental Progress & Sustainable Energy* 38 (6): e13264. <https://doi.org/https://doi.org/10.1002/ep.13264>.
- Zhang, Y., M. A. Dubé, D. D. McLean, and M. Kates. 2003. "Biodiesel production from waste cooking oil: 1. Process design and technological assessment." *Bioresource Technology* 89 (1): 1-16. [https://doi.org/https://doi.org/10.1016/S0960-8524\(03\)00040-3](https://doi.org/https://doi.org/10.1016/S0960-8524(03)00040-3).

Acknowledgments

This work was financially supported by: (i) LA/P/0045/2020 (ALiCE) and UIDB/00511/2020-UIDP/00511/2020 (LEPABE) funded by national funds through FCT/MCTES (PIDDAC); (ii) Project PhotoBioValue (ref. PTDC/BTA-BTA/2902/2021), funded by FEDER funds through COMPETE2020-Programa Operacional Competitividade e Internacionalização (POCI) and by national funds (PIDDAC) through FCT/MCTES; and (iii) project "HyGreen&LowEmissions - Tackling Climate Change Impacts: the role of Green Hydrogen production, storage and use, together with low emissions energy systems", with the reference NORTE-01-0145-FEDER-000077, supported by Norte Portugal Regional Operational Programme (NORTE 2020), under the PORTUGAL 2020 Partnership Agreement, through the European Regional Development Fund (ERDF).

Synthesis and modification of biochars for their usage as catalysts in water splitting reactions and adsorption coupled to Advanced Oxidation Processes

Aida M. Díez¹, M. Bolaños-Vázquez¹, V. Laíño-Rodríguez¹, M.A. Sanromán¹, M. Pazos¹

¹ BIOSUV Research Group, CINTECX, University of Vigo, As Lagoas Marcosende s/n, Vigo, Spain
*Corresponding author: adiez@uvigo.gal; 0000-0002-7007-748X

Abstract

Energy detriment and water pollution increase are the modern world problems. In order to cope with them, the utilization of water splitting processes is an alternative for the generation of energy-valuable products such as H₂ or H₂O₂. On the other hand, the utilization of adsorption coupled to Advanced Oxidation Process (AOPs) is a recent option for the elimination of pollutants from wastewaters. Thus, the pollutants are eliminated quickly due to adsorption and then the spent adsorbents can be regenerated by applying AOPs, avoiding the spent adsorbent disposal. These processes require the utilization of efficient adsorbents and catalysts which are usually expensive and environmentally unfriendly. This study presents the synthesis of biochars from agroindustry residues so they can be used as adsorbents and catalysts for both AOPs and water splitting reactions. The results demonstrate agroindustry residues can be fitted into circular economy by their utilization on these environmentally-friendly processes.

Author Keywords. Oxygen/Hydrogen Evolution Reaction, Oxygen Reduction Reaction, regeneration of catalytic adsorbents, radicals generation

1. Introduction

Pollution and energy sources shortage have become a pressing global concern, threatening the environment and human wellbeing (Wang et al., 2019). To mitigate the pollution issue, adsorption has emerged as a promising and sustainable technique for pollutant removal. Carbon-based materials have garnered significant attention as effective adsorbents due to their unique properties, including high surface area, porosity, and chemical reactivity.

One of the main concerns with spent adsorbents is their proper disposal, as they can pose environmental risks if not handled appropriately, as adsorbed pollutants onto carbon-based materials can leach into the environment. Therefore, effective regeneration methods are essential to ensure the safe and sustainable handling of spent adsorbents (Escudero-Curiel et al., 2021).

Advanced Oxidation Processes (AOPs) are presented as an alternative for the treatment of the spent adsorbents. These processes are based on the generation of radical species such as SO₄^{•-} or HO[•] which attack quickly and non-selectively the organic matter. Thanks to the small size of these particles, they pass throughout the adsorbent, degrading the retained pollutant within the structure. For carbon-based materials regeneration one can consider peroxydisulfate (PDS) considering it can be activated by carbon-based materials, leading to SO₄^{•-} radicals (Wang et al., 2019).

On the other hand, in order to abate the energy demand, water splitting processes are presented as an alternative. In this process, water is broken by the application of an overpotential into O₂ (Oxygen Evolution Reaction-OER) and into H₂ (Hydrogen Evolution Reaction-HER). One of the challenges in water splitting reactions is the need for efficient and cost-effective catalysts to facilitate the electrochemical reactions, considering the expensive benchmark catalysts for OER and HER, which are respectively, IrO₂ and Pt/C. Biochars have been presented as an alternative catalyst (Chen et al., 2022). In this study, several agroindustry residues are thermally treated to synthesize biochars which can be used as both water splitting catalysts and AOPs-catalytic-adsorbents.

2. Materials and Methods

Biochar synthesis

The agroindustry residues (spent coffee, spinach stem, rice bran and potato, corn, banana and chestnut peels) were washed, dried and grounded prior to synthesis.

Then, they were placed in a tubular furnace (Aero-360) was used and N₂ was fixed at 2 L/min. Initially, 400 or 800°C were essayed, although the best performant materials were further optimized. In all cases, the residues were heat-treated for 2 h, having reached the fixed temperature at a rate of 10°C/min, attaining the so-called biochars.

These materials were washed 5 times hydrothermally (121 °C, 15 min) in the ratio 1 g/125 mL distilled water. With that, the porous were cleaned and the excess of ions and organic matter, removed (Escudero-Curiel et al., 2021).

In order to improve HER performance, MoO₂/Mo₂C addition was done as previously reported (Chen et al., 2022).

Water splitting reactions

HER, OER and Oxygen Reduction Reaction (ORR) were evaluated. In all cases, Hg₂Cl₂ was used as the reference electrode. HER and ORR were carried out under acid conditions (0.5 M H₂SO₄) and using carbon paper as the working electrode where the biochars where placed (0.25 mg/cm²) and carbon stick as the counter electrode. In the case of alkaline OER (1 M NaOH), Ni-foam was used as the working electrode and Pt wire as the counter electrode.

Adsorption and AOPs tests

The removal of 30 ppm of fluoxetine was evaluated. For that, 10 mg of the as-prepared carbon-based materials were mixed with 50 mL of the fluoxetine solution in a glass tube which was placed in a rotary shaker. Adsorption tests were left for 24 h at 80 rpm. For PDS regeneration, 2 mM was added to the reactor tubes and a sample was taken after 1 h of reaction.

3. Discussion

Water splitting reactions

In the case of water splitting reactions, banana biochar-800°C provided the best results (Table 1). With this, it is proved that these metal-free materials can be used as water splitting catalysis.

On the case of acid HER, the addition of MoO₂/Mo₂C, provided a significant enhancement (Table 1). This was due to the metal addition, which favoured H⁺ reduction (Chen et al., 2022).

On the case of acid ORR, a big oxidation peak at 0.6 V appeared when bubbling O₂ due to H₂O₂ generation.

Material	Process	Overpotential (mV)			Tafel slope (mV/dec ⁻¹)
		10 mA	50 mA	100 mA	
Banana-800°C	OER	408	455	*473 (74.2 mA)	58.4
Banana-800°C:Mo	HER	194	*298 (35 mA)	-	178.8

Table 6: Results for water splitting reactions (0.25 mg/cm²)

Adsorption and AOPs tests

Some of the attained biochars demonstrated a good adsorption degree (Table 2). PDS regeneration was essayed, which has showed activation by biochars (Wang et al., 2019). Consequently, fluoxetine was removed and in the case of the optimal banana-biochar synthesized at 220°C, it could be reused up to five times with a detriment of 10%, which is within acceptable values explained by the structure oxidation due to the generated radical attack. This can be seen on the slight modifications found in FTIR and XPS results.

Material	Uptake (mg/g)	PDS regeneration (%)
Banana-220°C	146.48	82.4
Banana-400°C	69.67	26.0
Banana-800°C	57.68	0.5
Spinach-400°C	93.05	43.1
Corn-800°C	51.61	40.4
Chesnut-800°C	9.72	33.3

Table 2: Best adsorption and PDS regeneration results for the synthesized materials.

4. Conclusions

Different agroindustry residues have been used for the synthesis of biochars, which were further used as adsorbents and catalysts for both AOPs and water splitting processes. This paves the way for a circular economy approach, where the residues are not only eliminated, but used for environmentally-friendly aims.

References

- Chen, X., Sun, J., Guo, T., Zhao, R., Liu, L., Liu, B., Wang, Y., Li, J., & Du, J. 2022. "Biomass-derived carbon nanosheets coupled with MoO₂/Mo₂C electrocatalyst for hydrogen evolution reaction". *International Journal of Hydrogen Energy* 30959–30969. DOI: 10.1016/J.IJHYDENE.2021.12.173
- Escudero-Curiel, S., Acevedo-García, V., Sanromán, M. Á., & Pazos, M. 2021. "Eco-approach for pharmaceutical removal: Thermochemical waste valorisation, biochar adsorption and electro-assisted regeneration". *Electrochimica Acta* 389: 138694-138706. DOI: 10.1016/J.ELECTACTA.2021.138694
- Wang, H., Guo, W., Liu, B., Wu, Q., Luo, H., Zhao, Q., Si, Q., Sseguya, F., & Ren, N. 2019. "Edge-nitrogenated biochar for efficient peroxydisulfate activation: An electron transfer mechanism". *Water Research* 160:405–414. DOI:10.1016/J.WATRES.2019.05.059

Acknowledgments

The researcher Aida M. Díez is grateful to Xunta de Galicia (ED481B 2019/091) and to the project CINTECX-CHALLENGE 2023 for the financial support.

Hydrothermal carbonization for agro-industrial waste valorization: synthesis of Nitrogen-doped hydrochars as carbocatalysts for efficient removal of pharmaceuticals in water treatment

Silvia Escudero-Curiel^{1,*}, Xacobe López Rodríguez¹, Marta Pazos¹
Ángeles Sanromán¹

¹CINTECX. Universidade de Vigo, Department of Chemical Engineering. Campus As Lagoas-Marcosende, 36310 Vigo, Spain.

*Presenting author (sescudero@uvigo.gal) ORCID 0000-0002-5454-9379

Abstract

Transitioning to a circular economy is necessary to reduce resource consumption and waste generation. Waste valorization, such as the hydrothermal carbonization (HTC) process, can convert agro-industrial waste into hydrochar (HC), which can be utilized as a carbocatalyst in advanced oxidation processes (AOPs), particularly peroxymonosulfate (PMS)-based systems, for water treatment. Functionalization with nitrogen can enhance HC's efficiency. This study evaluated the valorization of alperujo (A) and banana peel (B) residues into N-HCs for removing Reactive Black 5 (RB5) dye. N-HCs derived from A were more effective than those derived from B. N-HCA functionalized with EDC crosslinker achieving an 80% removal of RB5. Active surface complexes were responsible for the outcome. Based on these results, N-HCA-EDC was also evaluated to remove Sulfamethoxazole (SMX) achieving a promising 70% removal. This study shows the potential of waste valorization through HTC to produce efficient N-HCs for water treatment, highlighting the importance of implementing circular economy strategies to reduce waste and increase resource efficiency.

Author Keywords. Hydrochar, carbocatalyst, nitrogen-functionalization, wastewater treatment.

1. Introduction

The unsustainable rate of resource consumption and waste generation is one of the biggest challenges that the planet is facing today. To tackle this problem, transitioning to a circular economy model has become mandatory. The circular economy model emphasizes the importance of reusing, recycling, and adding value to existing materials and products. By valorizing waste, we can extend the life cycle of products and transform waste into energy or raw materials, thereby reducing the negative impact of waste on the environment.

Nevertheless, waste is not the only residual product of human activity that poses a threat to the environment. One of the most alarming is water pollution due to the presence of pharmaceuticals and other organic compounds which poses a significant hazard to ecosystems and human health. Effective regulations and processes for degrading these contaminants are essential. Traditional methods of water decontamination are often insufficient in achieving the desired level of purity. Among the new processes most studied for decontamination are AOPs. When combined with other processes, such as adsorption or biological processes, they have been shown to have significant potential in terms of economic efficiency due to the reduction in the use of chemicals and energy.

AOPs that rely on sulfate, such as the use of PMS, require the use of catalysts. However, metallic catalysts, which are commonly used in Fenton-like processes, often produce secondary contamination through leaching or sludge generation, leading to additional costs and operational problems. As a result, there has been growing interest in developing greener alternatives to traditional methods, such as carbon-based catalysts or carbocatalysts. A source of carbocatalysts can be found in agro-industrial waste, which can be valorized into HC using HTC. HC has the potential to be an excellent starting material for generating carbocatalysts, offering a solution to two environmental problems at once by promoting a circular economy and fighting water pollution.

While the catalytic activity of pristine HCs is generally lower than that of metallic catalysts, they can be easily modified to enhance their electronic and physicochemical properties, making them more

suitable for catalysis. By incorporating certain elements into the carbon atom matrix, the surface charge balance can be broken, inducing polarization of bonds at the point of inclusion, resulting in a more favorable material for chemical catalysis (Dai et al. 2012). Doping with heteroatoms as Nitrogen for functionalization helps to modify the surface properties of HCs, thereby favoring electron transfer mechanisms that trigger different pathways of PMS activation. Figure 1 shows the possible PMS activation by a N-HC.

This study has specific objectives that include valorizing two abundant agro-industrial wastes using HTC to produce N-HC as nitrogen-doped carbocatalysts. The next objective is to evaluate the catalytic capacity of the N-HC in the PMS activation for the removal of a model organic contaminant, RB5 and a pharmaceutical, SMX. Lastly, the mechanism of action of the N-HC in N-HC/PMS systems will be elucidated.

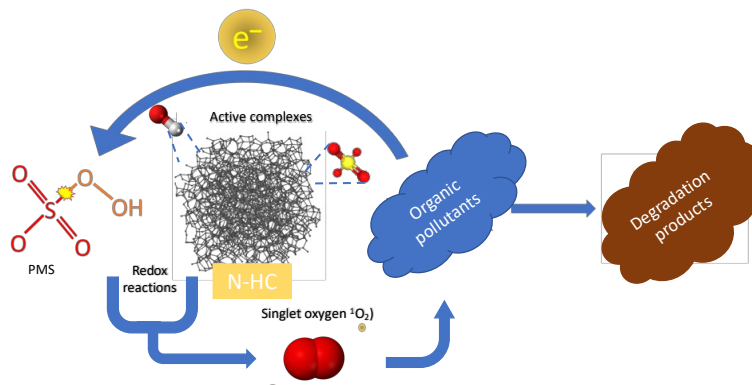


Figure 1: Possible PMS/N-HC activation mechanisms.

2. Materials and Methods

The HC precursors utilized in this study were Alperujo (A), the primary waste product of olive oil production, and banana peel (B), which were kindly supplied by local companies (Aceites Abril S.L. and FreshCut S.L., respectively). The chemicals RB5, SMX, PMS, Polyethyleneimine (PEI), glutaraldehyde (GTA), and 1-ethyl-3-(3-dimethylaminopropyl)carbodiimide (EDC) were provided from Merck and TCI Europe N.V.

The synthesis of HCs involved using A and B as HC precursors, in a 1:3 solid:liquid ratio, and heating them in a cylindrical stained steel hydrothermal reactor for 2.5 h at 220 °C. After cooling, the reactors were opened, and the HCs were washed, filtered, and stored. To functionalize the HCs with nitrogen (N-HC), two post-treatments were applied: with GTA or EDC crosslinkers after adding PEI. The catalytic capacity of the resulting N-HCs was evaluated by adding a catalyst load of 0.1 g/L and 2 mM PMS to 50 mL of 0.05 mM RB5 or SMX solution in cylindrical, amber-colored reactor tubes and agitating for 2 hours. Quenching experiments were also conducted by adding one of the quenchers NaN_3 , KI, or methanol to the catalytic evaluation assays. Adsorption controls and controls of PMS activity alone were also performed.

3. Discussion

The performance of the carbocatalysts obtained from A was found to be significantly higher compared to those obtained from B. While the adsorption exhibited by both A and B materials was low, it improved considerably for all N-HCs. This improved adsorption can enhance the interaction between active complexes on the surface and pollutants (Navalon et al. 2014), leading to a higher catalytic capacity. N-HCs synthesized using EDC as the crosslinker showed the highest yield in removing RB5, suggesting that this compound is more effective in introducing nitrogen into the HC structure, leading to better performance in the N-HC/PMS system. In order to understand how PMS is activated, it is essential to determine the dominant oxidizing species in the N-HC/PMS system. N-HCA-EDC was found to be the most effective material in removing RB5, achieving an 80% removal rate, and was therefore used in scavenger experiments to identify the active species. The results showed that the majority of

the decolorizing capacity of the N-HC/PMS system was due to the active complexes, with singlet oxygen coming in second. These findings support the notion that the non-radical pathway is the main mode of PMS activation by N-HCA-EDC. In addition, it is noteworthy that the catalytic performance of N-HCA-EDC was also evaluated for the removal of SMX, achieving a removal efficiency of 70%, which further confirms the potential of this material as an efficient catalyst for the removal of organic contaminants.

4. Conclusions

N-HCs enhance waste treatment and circular economy principles by functionalizing carbon materials to improve catalytic activity. Nitrogen doping using EDC as a crosslinker significantly boosts N-HCs' catalytic performance, activating PMS in N-HC/PMS systems. This sustainable, low-cost approach offers an eco-friendly alternative to metal-based catalysts that generate high waste and use non-renewable resources.

References

- Dai, Liming, Dong Wook Chang, Jong-Beom Baek, y Wen Lu. 2012. "Carbon Nanomaterials for Advanced Energy Conversion and Storage". *Small* 8 (8): 1130–66. <https://doi.org/10.1002/sml.201101594>.
- Navalon, Sergio, Amarajothi Dhakshinamoorthy, Mercedes Alvaro, y Hermenegildo Garcia. 2014. "Carbocatalysis by Graphene-Based Materials". *Chemical Reviews* 114 (12): 6179–6212. <https://doi.org/10.1021/cr4007347>.

Acknowledgments

This research has been financially supported by MCIN / AEI /10.13039/501100011033 (Project PID2020-113667GB-I00 and PDC2021-121394-I00). Silvia Escudero-Curiel thanks Universidade de Vigo for her grant.

Controlling Supramolecular Chirality through Asymmetric Secondary Flows in Helical Microchannels

João Pedro Vale^{1,2}, Semih Sevim^{3,4}, Alessandro Sorrenti^{3,5,6}, Zoubir El-Hachemi⁵, Salvador Pané⁴, Andreas D. Flouris⁷, Josep Puigmartí-Luis^{*,6,8,9}, Tiago Sotto Mayor^{*,1,2}

¹Transport Phenomena Research Centre (CEFT), Engineering Faculty, Porto University, Rua Dr. Roberto Frias, 4200-465 Porto, Portugal

²Associate Laboratory in Chemical Engineering (ALICE), Engineering Faculty, Porto University, Rua Dr. Roberto Frias, 4200-465 Porto, Portugal

³Institute of Chemical and Bioengineering, Department of Chemistry and Applied Biosciences, ETH Zurich, Zurich 8093, Switzerland

⁴Multi-Scale Robotics Lab, ETH Zurich, Tannenstrasse 3, CH-8092 Zurich, Switzerland.

⁵Depart. de Química Inorgànica i Orgànica, University of Barcelona, 08028 Barcelona, Spain

⁶Institut de Química Teòrica i Computacional, University of Barcelona, 08028 Barcelona, Spain

⁷FAME Laboratory, Department of Exercise Science, University of Thessaly, Greece

⁸Depart. de Ciència dels Materials i Química Física, Univ. of Barcelona, 08028 Barcelona, Spain

⁹Institució Catalana de Recerca i Estudis Avançats (ICREA), Pg. Lluís Companys 23, 08010 Barcelona, Spain

* Corresponding authors: josep.puigmarti@ub.edu; tiago.sottomayor@fe.up.pt

Abstract

The chirality of a molecule influences its properties and function. Therefore, the ability to control chirality can have significant implications for the development of new materials and drugs. Here, we demonstrate the chirality transfer from the macroscopic chiral shape of a 3D helical microchannel to the chirality of supramolecular nanoassemblies. Chiral information is transferred top-down thanks to the interplay between asymmetric secondary flows and precise spatiotemporal control of reagent concentration. Our results show that it is possible to enantioselectively control molecular processes at the nanoscale by modulating the reactor geometry.

Author Keywords. Chirality, chiral symmetry breaking, secondary flow, microfluidics.

1. Introduction

Chirality is a property of molecules that cannot be overlapped with their mirror image. When a group of molecules have the same chirality, they are said to have homochirality, which is a fundamental characteristic of living matter. However, the origin of homochirality is still unknown and a subject of intense research, given its key role in determining the function of molecules and supramolecular assemblies (Ruiz-Mirazo, Briones, and De La Escosura 2014).

An enantiomeric excess reflects the degree to which a sample contains one chiral form in greater amounts than the other. This excess can spontaneously emerge during the self-assembly of an achiral molecule into a chiral aggregate due to a chiral symmetry breaking process (Liu, Zhang, and Wang 2015). Importantly, external influences such as circularly polarized light (Kim et al. 2015) or mechanical forces (Ribó et al. 2001) can bias a spontaneous symmetry breaking process towards a deterministic state. This means that the process can be biased to dictate the chiral form that is predominantly created, while, if no bias were applied, the enantiomeric excess would result from a stochastic process. Yet, in these processes, the mixing of reagents and the nucleation/aggregation events have not been controlled, nor has the role of mass transport in chiral selection phenomena been investigated. Addressing this limitation is fundamental given that spatial and temporal control over the reagents mixing is known to have a strong effect on the outcome of self-assembly processes (Sevim et al. 2018). Here, we demonstrate that we can rationally control a chiral symmetry breaking process occurring in a helical microchannel by manipulation of the secondary flows generated within it. Our numerical simulations of fluid flow and mass transport inside the device show how the mass transport is influenced by the asymmetry of the secondary flows. Furthermore, our results are confirmed by microfluidic experiments and circular dichroism (CD) spectroscopy.

2. Materials and Methods

We considered two helical microchannels in simulations and experiments: one with a short pitch (1.5 mm) and another with a long pitch (7.5 mm). Both geometries were prepared and 3D-printed in their right-handed (R) and left-handed (L) forms, resulting in four devices R_{short} , R_{long} , L_{short} , L_{long} (see representation of the R geometries in Figure a-b). An achiral porphyrin in aqueous solution was injected at the central inlet (red region in Figure a-b) and was focused by a flow of NaCl in aqueous HCl (blue region in Figure a-b). Because porphyrin molecules aggregate into chiral structures spontaneously, they can be used to investigate chiral symmetry breaking phenomena. Numerical simulations of flow and mass transport along these microfluidic devices were performed using ANSYS Fluent. CD spectroscopy was used in microfluidic experiments to measure the chirality of the aggregates created inside the devices.

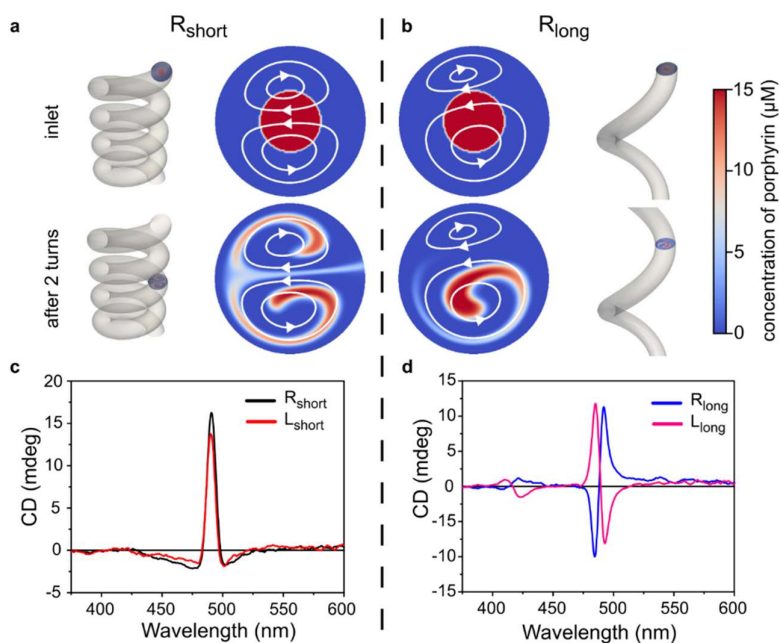


Figure 1. Mass transport and 2D representation of the 3D secondary flows forming inside the (a) R_{short} and (b) R_{long} devices. Representative CD spectra in (c) short-pitch and (d) long-pitch devices.

3. Discussion

In helical microchannels, secondary flows with three-dimensional counter-rotating vortices are formed due to the centrifugal forces acting on the fluid when it is made to turn. Simulations showed that, while the vortices are symmetric in the short-pitch device (Figure a), they are asymmetric in the long-pitch device (Figure b). Also, and as expected, the flow pattern in L_{short} and L_{long} devices mirror those in the corresponding R_{short} and R_{long} devices. More importantly, the different flow patterns in the short and long devices implied that the porphyrin was exposed to distinct flow conditions in both devices. While in the R_{short} device the porphyrin was exposed to both counter-rotating vortices (Figure a), in the R_{long} device the porphyrin was only exposed to the lower vortex (Figure b), and its counter-clockwise rotation. We were able to expose the porphyrin to a single vortex by leveraging the asymmetry of the secondary flow, and in doing so, we ensured that the protonation of the porphyrin and the consequent nucleation events occurred under one rotation. We evaluated the progress of the aggregation and the generation of an enantiomeric excess via CD spectroscopy. Aggregates formed with the R_{short} and the L_{short} devices produced similar CD spectra, indicating equivalent supramolecular chirality (Figure c). Yet, CD spectra from the samples obtained with the R_{long} and the L_{long} devices were similar in magnitude but opposite in sign (Figure d), indicating the formation of aggregates with opposite chirality. This shows that, by making the protonation / nucleation events occur under the influence of a single vortex,

the long-pitch devices induced a deterministic bias in the supramolecular chirality of the porphyrin aggregates. In other words, the long-pitch devices allowed to select the chiral sign of the aggregates. Importantly, aggregates with inverted chiral sign can be obtained using a helical microchannel with opposite handedness (R or L), to induce a flow field with mirrored secondary flow.

4. Conclusions

We showed that chirality can be transferred top-down from the 3D macroscopic handedness of the fluidic reactor to the supramolecular level of porphyrin aggregates when protonation / nucleation events are made to occur in a single vortex. These findings point towards the possibility of enantioselectively controlling molecular processes such as self-assembly via modulation of the geometry and operating conditions of fluidic reactors.

References

- Kim, Jisung, Jinhee Lee, Woo Young Kim, Hyungjun Kim, Sanghwa Lee, Hee Chul Lee, Yoon Sup Lee, Myungeun Seo, and Sang Youl Kim. 2015. "Induction and Control of Supramolecular Chirality by Light in Self-Assembled Helical Nanostructures." *Nature Communications* 6. <https://doi.org/10.1038/ncomms7959>.
- Liu, Minghua, Li Zhang, and Tianyu Wang. 2015. "Supramolecular Chirality in Self-Assembled Systems." *Chemical Reviews* 115 (15): 7304–97. <https://doi.org/10.1021/cr500671p>.
- Ribó, Josep M., Joaquim Crusats, Francesc Sagués, Josep Claret, and Raimon Rubires. 2001. "Chiral Sign Induction by Vortices During the Formation of Mesophases in Stirred Solutions." *Science* 292 (5524): 2063–66. <https://doi.org/10.1126/science.1060835>.
- Ruiz-Mirazo, Kepa, Carlos Briones, and Andrés De La Escosura. 2014. "Prebiotic Systems Chemistry: New Perspectives for the Origins of Life." *Chemical Reviews* 114 (1): 285–366. <https://doi.org/10.1021/cr2004844>.
- Sevim, S., A. Sorrenti, C. Franco, S. Furukawa, S. Pané, A. J. DeMello, and J. Puigmartí-Luis. 2018. "Self-Assembled Materials and Supramolecular Chemistry within Microfluidic Environments: From Common Thermodynamic States to Non-Equilibrium Structures." *Chemical Society Reviews* 47 (11): 3788–3803. <https://doi.org/10.1039/C8CS00025E>.

Acknowledgments

This work is supported by LA/P/0045/2020 (ALiCE), UIDB/00532/2020 and UIDP/00532/2020 (CEFT), funded by Portugal through FCT/MCTES (PIDDAC), and by the EU, from the Horizon 2020 FETOPEN project SPRINT (No. 801464). Additionally, this work is supported by the European Research Council Starting Grant microCrysFact (ERC-2015-STG No. 677020), the Swiss National Science Foundation (project no. 200021_181988), and grant PID2020-116612RB-C33 funded by MCIN/AEI /10.13039/501100011033.

Numerical study of particle dynamics in high-efficiency gas-solid cyclone loaded with spherical steel shot

Pedro Pacheco^{1,2*}, Manuel A. Alves^{1,2}, João Campos^{1,2}, Júlio Paiva^{1,2,3}

¹ Centro de Estudo de Fenómenos de Transferência (CEFT), Departamento de Engenharia Química, Faculdade de Engenharia, Universidade do Porto, Rua Dr. Roberto Frias, 4200-465 Porto, Portugal

² Associate Laboratory in Chemical Engineering (ALiCE), Departamento de Engenharia Química, Faculdade de Engenharia, Universidade do Porto, Rua Dr. Roberto Frias, 4200-465 Porto, Portugal.

³ Advanced Cyclone Systems, SA, Rua de Vilar, 235, 3^oE, 4050-626 Porto, Portugal

* up201304015@edu.fe.up.pt

Abstract

This work explores fluid and particle dynamics in a high-efficiency gas-solid cyclone loaded with spherical steel particles using a numerical model based on computational fluid dynamics (CFD) coupled with the discrete element method (DEM). The methods used to simulate the fluid and solid phases and the obtained results are presented, focusing on the mechanics of particle collisions and trajectories. The results demonstrate that the CFD-DEM technology is well-suited for the numerical simulation of gas-solid cyclones loaded with abrasive spherical steel particles, and that the analysis of particle dynamics provides important insights into relevant mechanical processes.

Author Keywords. Cyclone separator, CFD-DEM, particle dynamics.

1. Introduction

Cyclone separators are an economical and convenient solution for gas-solid separation. They are simple to fabricate, can operate continuously, and have reduced maintenance requirements compared to alternatives, such as filter separation units (Hoffman et al. 2007). Their separation efficiency depends on the characteristics of the solid phase and on the fluid flow field which, by extension, is heavily dependent on the geometry of the flow manifold. The use of numerical techniques to model the operation of cyclones has been growing over the last two decades with the significant increase in available computing power. These numerical tools have provided powerful insights into the physics and phenomenology of gas-solid cyclones.

Numerical modelling of cyclones is still a significant challenge, as the fluid phase is characterized by a very high degree of turbulence and swirl, requiring sophisticated turbulence modelling and high-resolution computational grids. Furthermore, the solid phase may be composed of $10^8 - 10^9$ individual particles with complex shapes and significant particle-fluid-particle and particle-particle interactions (Dehdarinejad and Bayareh 2021). In this work, we explore fluid and particle dynamics in high-efficiency cyclones loaded with spherical steel abrasive using a numerical model based on computational fluid dynamics (CFD) coupled with the discrete element method (DEM).

2. Methods

To simulate fluid and solid phases in a high-efficiency gas-solid cyclone, we used the opensource code CFDEM[®]-coupling-PFM for coupled CFD-DEM simulation (Pietsch et al. 2016). The fluid was modelled using the finite volume method to solve the Navier-Stokes equations for incompressible fluid flow, incorporating the Wall Adapting Local Eddy-viscosity method to model the sub-grid scale turbulence (Hreiz et al. 2011). The Navier-Stokes equations are modified to consider the presence of a solid phase and include particle-fluid coupling as a source term, encompassing sub-models for pressure gradient force, viscous force, and drag through the Koch-Hill model (Zhou et al. 2010). The solid phase was modelled using DEM to solve Newton's laws of motion for translational and rotational movement of each particle in the ensemble. The Hertzian contact model was used to calculate particle-particle and particle-wall interaction forces.

The CFD mesh was composed of 2.1 million elements. The inlet velocity was set as 28 m/s and the average pressure at the outlet was set to the atmospheric pressure. Spherical steel shot is modelled with the material properties of high carbon steel, and injected at a mass flowrate of 7 kg/h

corresponding to a particle injection rate of nearly 30000 particles per second. Injected particles had a radius ranging from 70 to 145 μm obeying a Rosin-Rammler distribution.

3. Results and Discussion

Figure shows instantaneous snapshots of particle positions in the cyclone, colored by linear and angular velocity magnitude. Note that angular velocity refers to the spin of the particles. Particles are injected with the same velocity as the gas flow (28 m/s) without any rotational motion. The high linear momentum causes them to strike the inlet target zone, directly opposite to the inlet, with little effect from the fluid phase. This initial impact dissipates most of their linear kinetic energy, with the average linear kinetic energy per particle decreasing by two orders of magnitude after collision. Part of the dissipated linear kinetic energy is transferred into rotational kinetic energy due to the internal curvature of the cyclone wall. As can be seen in **Figureb**, the angular velocity shortly after the initial impact can exceed 15000 rad/s, equivalent to a full revolution roughly every 0.4 ms.

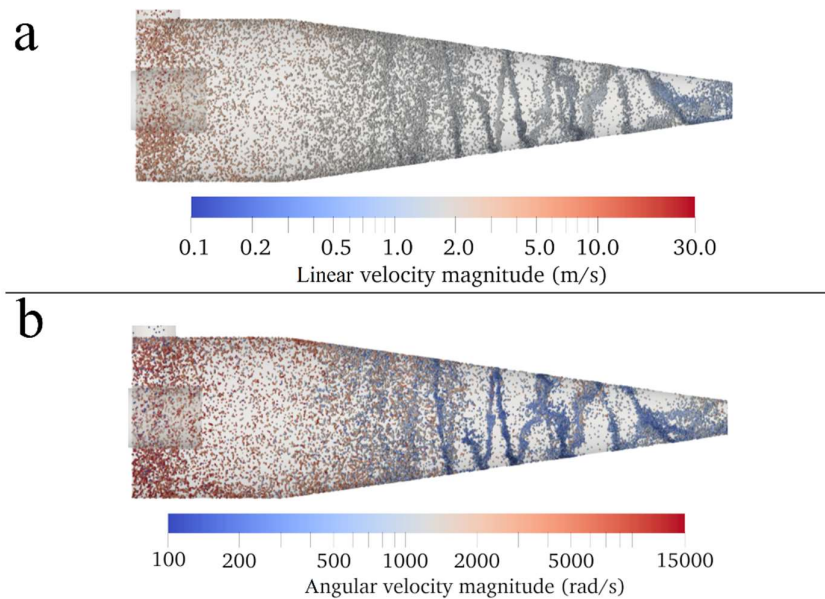


Figure 1: XZ plane views of particle snapshots colored by linear (a) and angular (b) velocity magnitudes, with logarithmic scale

Following this initial impact, particles follow a nearly ballistic trajectory as they collide successively against the walls, with each collision dissipating linear momentum. This dissipation is stronger in the direction normal to the wall, with each successive collision leading to a weaker elastic rebound. As particle momentum decreases with each collision, momentum transfer from the gas to each particle becomes more dynamically relevant. These two effects act in *tandem* confining particle trajectories to the wall, traveling in a tightly wound spiral, and experiencing linear and rotational deceleration caused by sliding and rolling friction. This behavior, together with the effect of local geometry in the transition zone between the cylindrical and conical sections of the cyclone, lead to the accumulation of particles in strands, which become denser and denser as the particles move towards the collection bin.

Conclusions

CFD-DEM technology is well-suited for the numerical simulation of gas-solid cyclones loaded with spherical steel particles, as judged by the physical realism of simulation results. A thorough analysis of particle dynamics throughout the cyclone was conducted, showcasing the relevant mechanical processes.

References

- Dehdarinejad, Ehsan, and Morteza Bayareh. 2021. "An overview of numerical simulations on gas-solid cyclone separators with tangential inlet." *ChemBioEng Reviews* 8 (4): 375-391.
- Hoffman, Alex C. and Louis E. Stein. 2007. *Gas Cyclones and Swirl Tubes: Principles, Design and Operation*. 2 ed. New York: Springer.
- Hreiz, Rainier, Caroline Gentric, and Noël Midoux. 2011. "Numerical investigation of swirling flow in cylindrical cyclones." *Chemical Engineering Research and Design* 89 (12): 2521-2539. <https://doi.org/https://doi.org/10.1016/j.cherd.2011.05.001>.
- Pietsch, Swantje, Stefan Heinrich, Frank Kleine-Jäger, Michael Schönherr, and Katja Karpinski. 2016. "CFDEM® modelling of particle coating in a three-dimensional prismatic spouted bed."
- Zhou, Z. Y., S. B. Kuang, K. W. Chu, and A. B. Yu. 2010. "Discrete particle simulation of particle–fluid flow: model formulations and their applicability." *Journal of Fluid Mechanics* 661: 482-510. <https://doi.org/10.1017/S002211201000306X>.

Acknowledgments

This work was financially supported by: Base Funding - UIDB/00532/2020 and Programmatic Funding - UIDP/00532/2020 of CEFT - funded by national funds through the FCT/MCTES (PIDDAC); PhD grant of P. T. Pacheco was funded by Advanced Cyclone Systems, S.A; and ALiCE through project LA/P/0045/2020.

Towards an Optimization of the NETmix for Ozonation: Evaluation of the Effect of Channel Length on the Gas-Liquid Mass Transfer

Paulo Henrique Marrocos^{1,2}, Luís Silva^{1,2}, Mateus Pituco^{1,2}, Isabel Fernandes^{1,2}, Ricardo Santos^{1,2}, Vítor Vilar^{1,2}

¹LSRE-LCM – Laboratory of Separation and Reaction Engineering – Laboratory of Catalysis and Materials, Faculty of Engineering, University of Porto, Rua Dr. Roberto Frias, 4200-465 Porto, Portugal

²ALICE – Associate Laboratory in Chemical Engineering; Faculty of Engineering, University of Porto, Rua Dr. Roberto Frias, 4200-465 Porto, Portugal

*Corresponding author: vilar@fe.up.pt; ORCID: 0000-0003-0943-2144

Abstract

The innovative geometry of the micro/meso-structured static mixer NETmix provides a powerful gas/liquid mixing intensity, enabling its use for ozonation through a sidestream configuration. Thus, this work aims the enhancement of the NETmix for ozonation by evaluating the influence of the mixer's channel length on the gas-liquid mass transfer. This assessment was done by the construction of three similar NETmix units, differing only in their channel length - it was considered 1 mm, 2 mm and 4 mm -, and the measurement of the volumetric mass transfer coefficient for each NETmix at a selection of gas and liquid flowrates. It was shown a significant influence of the channel length on the gas-liquid mass transfer, whereby there was an increase of 17% in the volumetric mass transfer coefficient when the length was reduced from 4 mm to 1 mm.

Author Keywords. Ozonation, Gas-liquid Mass Transfer, NETmix Static Mixer, Optimization

1. Introduction

Ozonation is a powerful method for water/wastewater treatment due to the oxidation potential of ozone molecules enabling the degradation of persistent organic molecules and disinfection. Traditionally it is used bubbling devices, such as fine bubble diffusers, to combine two processes in the same contact chamber: transferring the ozone gas into the water/wastewater to be treated, along with the reaction process. Although common, this approach carries several disadvantages, such as a large footprint. An alternative approach considers the use of a sidestream configuration, consisting in the splitting-off a fraction of the main flow, into which the ozone is mixed by efficient equipment such as a venturi or a static mixer, and subsequently, this stream saturated with ozone is injected back into the main flow, consequently reducing the total size of the equipment (Rakness 2005).

The micro/meso-structured static mixer, the NETmix, consists of a network of unit cells composed by a cylindrical chamber connected to four prismatic half-channels, each at a 45° of the flow direction. Due to its innovative geometry, the NETmix presents interesting mixing capabilities for one-phase and two-phase flows (Costa et al. 2022), displaying a huge potential for ozone dissolution using a sidestream configuration. Hence, this work aims to investigate the effect of a NETmix geometrical property, the channel length, on the gas-liquid mass transfer, to optimize its application for ozone dissolution.

2. Materials and Methods

In order to evaluate the effect of the NETmix channel length (L_{ch}) on the gas-liquid mass transfer, three NETmix units, made of acrylic, were conceived, each of which was identical in their depth ($w = 2$ mm), chamber diameter ($D = 6.75$ mm) and channel width ($d = 1$ mm), differing only in L_{ch} . Hence, in this work, it was adopted 4 inlets and 9 rows of chambers, in addition to three values of channel length: 1 mm, 2 mm and 4 mm. As such, the gas-liquid mass transfer for each NETmix unit was assessed by the measurement of the volumetric mass transfer coefficient ($k_L a$) associated to co-current downwards gas-liquid flows at chosen values of liquid and gas flowrates (Q_L and Q_G , respectively). To perform these measurements, it was used a dissolved oxygen desorption method through nitrogen injection technique, as described by (Al Taweel et al. 2005). The experimental

apparatus utilized is displayed in Figure 1a. Consequently, for each experiment, 5 dm³ of demineralized water, saturated with oxygen, was placed inside a jacketed tank at 20 °C. Once the desired temperature was attained, the water was pumped into the NETmix through a venturi injector, in which it was simultaneously injected nitrogen gas, thus initiating the desorption of the dissolved oxygen in the liquid. Thereafter, samples of the gas-liquid mixture were collected at the outlet of the NETmix at fixed time intervals. Subsequently, a dissolved oxygen probe was utilized to measure the dissolved O₂ concentration ($C_{Out}^{O_2}$) associated with each sample, by which the related $k_L a$ to the evaluated condition was computed, as given by Equation 1. This equation was used to calculate the $k_L a$ value for each sample, whereby an average of the computed values was used as the result associated to the gas/liquid flowrate conditions at which the experiment was performed.

$$k_L a = -\frac{1}{\tau_L} \ln \left[\left(1 + \frac{Q_L}{Q_G H} \right) \left(\frac{C_{Out}^{O_2}}{C_{In}^{O_2}} \right) - \frac{Q_L}{Q_G H} \right] \quad (1)$$

In which $C_{In}^{O_2}$ is the dissolved oxygen concentration at the venturi inlet; H , the Henry coefficient for oxygen based on molar concentrations, measured to be 27 at room temperature (Al Taweel et al. 2005); and τ_L , the liquid passage time, given by Equation 2.

$$\tau_L = \frac{1 - \alpha_G}{Q_L} V_{NETmix} \left(1 + \frac{Q_L}{Q_G H} \right) \quad (2)$$

Whereby V_{NETmix} is the NETmix volume and α_G is the gas hold-up, which was numerically estimated through CFD simulations. As such, the described procedure was performed for liquid and gas flowrates both ranging from 30 Ndm³·h⁻¹ to 60 Ndm³·h⁻¹, for each of the three NETmix units.

3. Results and Discussion

According to Higbie's penetration theory, the liquid-side mass transfer coefficient $k_L = 2\sqrt{D_g/(\pi\theta)}$, in which D_g is the diffusion coefficient of the gas species in the liquid and θ is the time during which the body of gas is in contact with the liquid.

Therein, θ is often interpreted as the inverse of a surface renewal rate S , such that $S = 1/\theta$, meaning that a body of gas in contact with a high velocity liquid leads to lower exposure times, and, consequently, larger surface renewal rates: hence, Higbie's theory predicts an enhancement of the mass transfer in these situations due to an increase in k_L . As a consequence of the micro/meso scale of the NETmix, this mass transfer enhancement phenomenon is expected to occur, however, as the mixer is associated to different length scales between the chambers and the channels, the strength of the phenomenon is also expected to vary between these two elements of the unit cell. The liquid velocities around the bubbles at the channels are much larger than at the chambers due to the minimal space available for its flow, leading to small θ and, consequently, large values of surface renewal at the channel. Thus, the surface renewal rate in the NETmix - and, by extension, the gas-liquid mass transfer - is controlled by the dimensions of the channel. As is displayed in Figure 1b, the average and respective standard deviations of the results, obtained from the experiments varying the injected gas and liquid flowrates, of the ratio of the $k_L a$ measurements for channel lengths 1 mm and 2 mm in relation to those for 4 mm confirm that the variation of L_{ch} leads to a significant effect on the mass transfer. Hence, these results show that reducing the channel length, thus reducing θ and increasing S , leads to a gas-liquid mass transfer enhancement of the NETmix, which is in agreement with Higbie's theory.

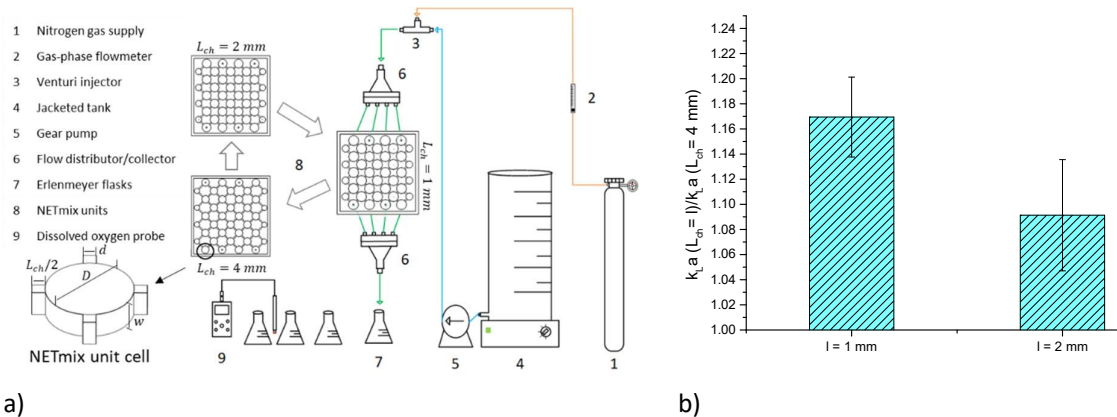


Figure 1 – a) Illustration of the experimental setup used in this work, along with each NETmix unit employed; b) average and standard deviation results of the ratio of the k_{La} measurements, encompassing all flowrate conditions tested, for 1 mm and 2 mm channel length in relation to measurements for 4 mm length.

4. Conclusions

This study evaluated the effect of the channel length of a NETmix static mixer on the gas-liquid mass transfer through the measurement of the volumetric mass transfer coefficient as a function of three values of channel lengths - 1 mm, 2 mm and 4 mm – for various gas and liquid flowrates. The results confirmed that the channel length of the NETmix has a significant role on the gas-liquid mass transfer, in which the reduction of the length led to an enhancement of the transfer: there was a 17% increase on the volumetric mass transfer coefficient as the length was reduced from 4 mm to 1 mm.

References

- Costa, Marcelo F., Carlos M. Teixeira, Armandina M. Lopes, João P. Araújo, Madalena M. Dias, Ricardo J. Santos, and José Carlos B. Lopes. 2022. "Carbon Capture and Storage Toward Industrialization: A Novel Continuous Process for the Production of Carbon Dioxide Clathrates." *Energy Technology* 10 (6).
- Rakness, Kerwin L. 2005. *Ozone in Drinking Water Treatment: Process Design, Operation, and Optimization*. American Water Works Association. First Ed. American Water Works Association.
- Taweel, A. M. Al, J. Yan, F. Azizi, D. Odedra, and H. G. Goma. 2005. "Using In-Line Static Mixers to Intensify Gas-Liquid Mass Transfer Processes." *Chemical Engineering Science* 60 (22): 6378–90.

Acknowledgments

This work is financially supported by national funds through the FCT/MCTES (PIDDAC), under the project PTDC/EAM-AMB/4702/2020 (OZONE4WATER), LA/P/0045/2020 (ALiCE), UIDB/50020/2020 and UIDP/50020/2020 (LSRE-LCM). P.H. Marrocos acknowledges FCT - Fundação para a Ciência e Tecnologia - for his PhD scholarship (2022.10437.BD). V. Vilar acknowledges the FCT Individual Call to Scientific Employment Stimulus 2017 (CEECIND/01317/2017).

Utilization of Moisture Barriers with Enhanced Tortuosity and Porous Attachments to Mitigate Burns Introduced by Impermeability: A Numerical Study

André Fonseca Malaquias^{1,2*}, João Mário Miranda^{1,2}, J.B.L.M. Campos^{1,2}

¹ CEFT – Transport Phenomena Research Center, Faculty of Engineering, University of Porto, Rua Dr. Roberto Frias, 4200-465 Porto, Portugal

² ALiCE – Associate Laboratory in Chemical Engineering, Faculty of Engineering, University of Porto, Rua Dr. Roberto Frias, 4200-465 Porto, Portugal

*Corresponding author: e-mail address: up201007676@up.pt ; ORCID ID 0000-0002-3644-2658

Abstract

Firefighters suffer local burns in areas where attachments (such as trims) are present in the outer surface of the Fire Protective Clothing (FPC). Moisture presence in the FPC could be the reason behind the occurrence of these burns (1). However, little is known about the mechanisms by which such occurs. Possible solutions to this problem could be making the attachments porous or even increasing moisture barrier tortuosity in the positions where attachments are present. Thus, in this work, a numerical study is carried out utilizing a heat and mass transport model for textiles to measure the thermal performance of FPC, incorporating porous attachments and moisture barriers with enhanced tortuosity. Second-degree burn times are computed utilizing the Henriques criterion for different attachment porosities, moisture barrier tortuosity, initial water distributions, and heat flux exposures. The observed tendencies are also discussed in terms of the identified heat and mass transfer mechanisms.

Author Keywords. Firefighting, scald burns, Porous attachments, Tortuosity, Moisture

1. Introduction

Fire protective clothing usually consists of three main layers; an outer shell, moisture barrier, and thermal inner. Each layer has a specific function. Namely the outer shell serves primarily to provide mechanical resistance, whilst the moisture barrier and thermal inner serve to provide protection against hazard liquids and thermal insulation, respectively. Fire protective clothing may become wet due to a variety of reasons during its use in everyday deployments. The firefighter may sweat profusely during strenuous tasks or be hose sprayed during fire suppression (Prasad et al. 2002). Consequently, the presence of water in the FPC introduces the possibility of steam production inside of it, especially when facing high heat intensity exposures. On one hand, water phase change lowers the temperatures in the FPC suit, but on the other, hot steam is formed. Such diffuses towards the environment and the skin elevating the risk of scald burn occurrence (Fonseca Malaquias et al. 2022). The presence of trims or attachments may hinder water vapor from diffusing towards the environment and thus the risk of scald burn occurrence becomes greater. Potential solutions to mitigate this problem include either making the attachments porous or increasing the moisture barrier tortuosity. The effectiveness of these solutions in mitigating the occurrence of scald burns are investigated in this study.

2. Materials and Methods

Based on Gibson's model, a heat and mass transport model for hygroscopic porous media is utilized to compute the heat and mass debits in the different layers of the FPC (Gibson 1994; Fonseca Malaquias et al. 2022). The FPC is assumed to be constituted by an outer shell, moisture barrier, and thermal inner. The model is implemented in COMSOL Multiphysics® 6.0. Pennes' bioheat model (Pennes 1948) is utilized to simulate the heat transport in the skin, along with the Henriques burn criterion, to compute second-degree burn times (Henriques 1947). A parametric study is performed where attachment porosity is varied between 0 (impermeable) and 1 (no attachment present), moisture barrier tortuosity between 2.87 and 23.0 (i.e., an 8-fold increase), outer shell and thermal inner wetness levels between 0 and 100 %, and radiative heat flux between 5 kW/m² and 80 kW/m². A mesh

of 1540 elements is utilized. A backward differentiation formula solver is utilized to calculate the time steps taken according to a relative and absolute tolerance of 10^{-3} for all variables except temperature and gas phase volume fraction (i.e., 10^{-2}). The tolerance criterion is limited by a maximum time step of 0.1 s. A Newton-dampened solver is utilized to solve the resulting discretized algebraic equations from the PDE system at each time step.

3. Discussion

Figure 7a shows the second-degree burn times obtained for different outer shell wetness levels. As can be seen, the attachment porosities which promote second-degree burns vary with wetness level. For example, if the outer shell is fully saturated with water (i.e., 100%), an attachment with a porosity above a threshold value of 0.4 will have a negligible effect on second-degree burn time, while the opposite is true if it is below this value. This threshold value tends to decrease with outer shell wetness level such that for shallow wetness levels (i.e., 20%), the introduction of an attachment, even if impermeable, does not decrease second-degree burn time. A possible way of countering the adverse effects on second-degree burn time introduced by the attachment is to increase the tortuosity of the moisture barrier (Figure 7b). However, as can be seen, such a solution is only effective in particular conditions. For example, increasing moisture barrier tortuosity 2-fold is only beneficial for situations where a fully saturated outer shell is present and the porosity of the attachment is 0.2 (i.e., Figure 7b, 2x/1x_100%).

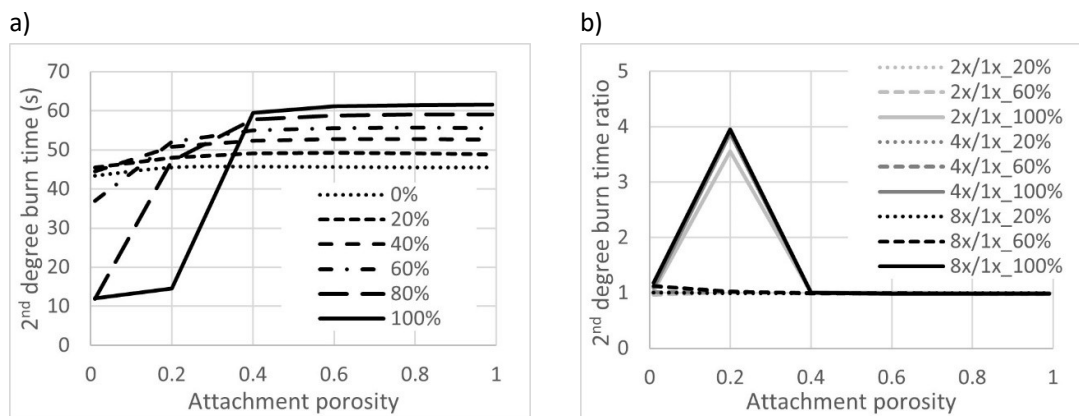


Figure 7: Parameters obtained assuming a 20 kW/m² heat exposure: a) Second-degree burn times obtained in function of attachment porosity, and for the various indicated outer shell wetness levels b) Ratio between second-degree burn times obtained for the indicated tortuosity values (e.g., 2x/1x_20% reads second-degree burn time obtained with a 2-fold tortuosity increase divided by second-degree burn time obtained with original tortuosity value of 2.87, for an outer shell wetness level of 20%)

4. Conclusions

Adding attachments, such as trims, to the outer surface of the fabric is inevitable due to FPC requirements. Such may introduce hindrance of moisture transport towards the environment and therefore promote scald burns on the firefighter. It is thus of imperative importance to find solutions to hinder this effect. Two possible solutions (increasing attachment porosity or increasing moisture barrier tortuosity) have been investigated. It is demonstrated that, depending on the exposure scenario, it might be beneficial to use porous attachments with specific porosity values. Increasing the moisture barrier tortuosity might be beneficial or prejudicial depending on the water distribution in the FPC (at the attachment position) and the heat flux exposure considered. The data generated could aid in the design or modification of current attachments and FPC so that firefighters are less likely to suffer local scald burns.

References

- Fonseca Malaquias, André, S F Neves, and J B L M Campos. 2022. "The Impact of Water on Firefighter Protective Clothing Thermal Performance and Steam Burn Occurrence in Firefighters." *Fire Safety Journal* 127 (November 2021). <https://doi.org/10.1016/j.firesaf.2021.103506>.
- Gibson, Phillip. 1994. "Governing Equations for Multiphase Heat and Mass Transfer in Hygroscopic Porous Media With Applications to Clothing Materials."
- Henriques, F. C. 1947. "Studies of Thermal Injury V. The Predictability and the Significance of Thermally Induced Rate Processes Leading to Irreversible Epidermal Injury." *Archives of Pathology* 43: 489–502.
- Pennes, Harry H. 1948. "Analysis of Tissue and Arterial Blood Temperatures in the Resting Human Forearm." *Journal of Applied Physiology* 1 (2): 93–122. <https://doi.org/10.1152/jappl.1948.1.2.93>.
- Prasad, K., Twilley, W. H., & Lawson, J. R. 2002. "Thermal Performance of Fire Fighters' Protective Clothing: Numerical Study of Transient Heat and Water Vapor Transfer." *National Institute of Standards and Technology Gaithersburg, MD 20899-8660*, 1–32. <https://doi.org/https://doi.org/10.6028/NIST.IR.6881>.

Acknowledgments

This work was financially supported by LA/P/0045/2020 (ALICE), UIDB/00532/2020 and UIDP/00532/2020 (CEFT), funded by national funds through FCT/MCTES (PIDDAC).

ChannelCOMB, 3D-Printed Device for Flow Distribution Uniformity in Mesostructured Reactors

Isabel S.O. Barbosa^{1,2}, João M. Costa^{1,2}, Yaidelin A. Manrique^{1,2},
Madalena M. Dias^{1,2}, Joaquim L. Faria^{1,2}, Ricardo J. Santos^{1,2},
Cláudia G. Silva^{1,2}, Margarida S.C.A. Brito^{1,2}

¹Laboratory of Separation and Reaction Engineering–Laboratory of Catalysis and Materials (LSRE-LCM), Faculty of Engineering, University of Porto, Rua Dr. Roberto Frias, 4200-465 Porto, Portugal

²Associate Laboratory in Chemical Engineering (ALiCE), Faculty of Engineering, University of Porto, Rua Dr. Roberto Frias, 4200-465 Porto, Portugal

*Corresponding author: mbrito@fe.up.pt

Abstract

ChannelCOMB, a consecutive flow distributor, was constructed by additive manufacturing (AM) for experimental validation. The feasibility of using AM was experimentally analyzed for two techniques: stereolithography (SLA) and fused deposition modeling (FDM). For the best ChannelCOMB configuration, SLA printing shows a maximum of ca. 4 % in flow deviation, while FDM has a maximum of ca. 15 %. Thus, the SLA technique promotes better flow uniformity due to the fabrication tolerance and material permeability. The results also show that the experimental flow distribution measured for the best ChannelCOMB configuration printed by SLA can be well predicted by both computational fluid dynamics simulations and a model based on resistance analogues proposed in a previous work.

Author Keywords. Additive Manufacturing, ChannelCOMB device, Flow Distribution Uniformity, Mesostructured Reactors

1. Introduction

Flow distribution uniformity is crucial for the successful performance of reactions in meso and micro-channel reactors operating as continuous flow systems (Barbosa et al. 2021). The flow distribution ensures that all the channels operate under similar conditions of flow regime, mass, and heat transfer. The flow distribution through several channels can be ensured by arrays of flow controllers or by manifold devices that split the flow through the channels. Recent and fast prototyping tools enable to construct accurate devices geometries optimized through computational fluid dynamics (CFD) and the experimental evaluation of their performance (Parra-Cabrera et al. 2018). This work focuses on two widespread AM technologies: SLA and FDM. In order to understand the influence of FDM and SLA 3D printing processes for flow distribution uniformity, several ChannelCOMB geometries were tested and compared (Barbosa et al. 2021; Barbosa et al. 2023).

2. Materials and Methods

ChannelCOMB Device

Figure 1 shows a sketch of ChannelCOMB and the respective parameters. In this device, the fluid is injected from a single inlet in a prismatic channel that has an expansion into a prismatic chamber where the flow is distributed to an array of ten evenly spaced channels (Barbosa et al. 2021).

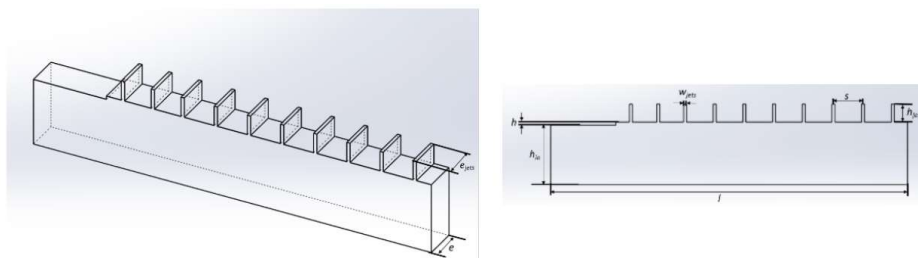


Figure 1: ChannelCOMB sketch

The dimensions of geometric parameters of the three tested devices are listed in Table 1.

	ChannelCOMB10	ChannelCOMB20	ChannelCOMBOptim
l / mm	120	120	120
h_{in} / mm	20	20	20
h_{jets} / mm	6	6	6
h / mm	1	1	1
w_{jets} / mm	1	1	1
e / mm	10	20	20
e_{jets} / mm	10	20	1
s / mm	10	10	10

l – device length, h_{in} – inlet height, h_{jets} – outlet channel height, h – chamber expansion height, w_{jets} – outlet channel width, e – reactor depth, e_{jets} – outlet channels depth and s - spacing between the outlet channels.

Table 1: ChannelCOMB Dimensions

The ChannelCOMB was analysed according to its ability for the uniform flow rate distribution for Re numbers (59 and 196) and several geometric parameters, namely ChannelCOMB10, ChannelCOMB20 and ChannelCOMBOptim. In a previous work, the ability of ChannelCOMB to uniformly distribute the inlet flow rate throughout the ten outlet channels was numerically demonstrated by a Resistance Analogue Model and CFD simulation, showed that the best design was obtained using ChannelCOMBOptim.

Flow rate distribution were assessed by the calculation of % Deviation, which is given by:



$$\% \text{ Deviation} = \frac{|Q_i - \bar{Q}|}{\bar{Q}} \times 100$$

where Q_i is the flow rate in channel i and \bar{Q} is the average flow rate.

1.1. Additive Manufacturing Techniques

Two additive manufacturing techniques were applied in the construction of ChannelCOMB: FDM and SLA and the differences between them in the uniform flow distribution were accessed. Also, three configurations of ChannelCOMB labelled as ChannelCOMB10, ChannelCOMB20 and ChannelCOMBOptim were considered for this study. The characteristics of 3D printing processes are described in Table 2.

Table 2: Characteristics of FDM and SLA 3D printing processes for ChannelCOMB construction.

	FDM	SLA
3D Printer	BEETHEFIRST+ from Beeverycreative [®]	Form 2 from Formlabs [®]
Printing Material	PLA (polylactic acid) Filament	Clear V4 from Formlabs
Fabrication' Tolerance	100 μ m	50 μ m
ChannelCOMB		

3. Results and Discussion

A general comparison between SLA and FDM is in Figure 2, which shows the maximum and average %deviation of the mean flow rate as a function of flow rate.

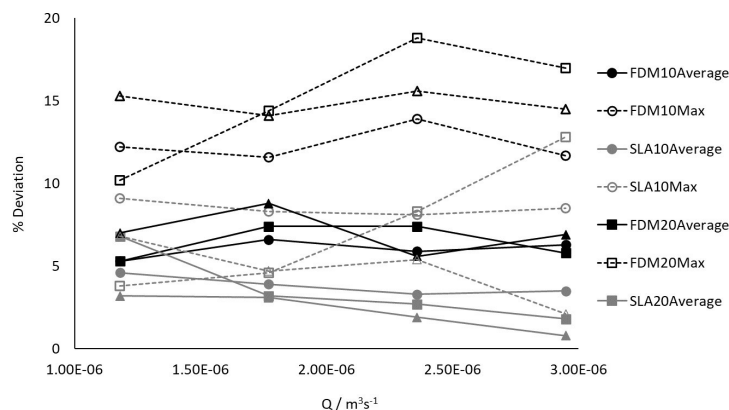


Figure 2: Maximum and average deviation for ChannelCOMB devices for both techniques: SLA and FDM.

Comparing the SLA and FDM results in Figure 2, the flow distribution uniformity seems to be influenced by the manufacturing techniques' accuracy. All the devices printed using SLA (coloured by grey), which is the technique with lower tolerance (50 μm), present a lower %deviation for all flow rates tested, meaning that SLA promotes a better flow distribution uniformity. Therefore, SLA has the capability of printing more high-resolution parts than FDM. Nevertheless, FDM is the most suitable technique in terms of printing simplicity because the process basically consists of heating the polymer filament to a semi-solid state and depositing it on the print bed.

4. Conclusions

As conclusion, the flow distribution uniformity is influenced by the manufacturing techniques and therefore, it would be recommended to resort to SLA technique to construct a flow distribution applied to micro/milli reactors, which are very sensible to differences in flow distribution.

References

- Barbosa, Isabel S. O., João M. Costa, Yaidelin A. Manrique, Madalena M. Dias, Joaquim L. Faria, Ricardo J. Santos, Cláudia G. Silva, and Margarida S. C. A. Brito. 2023. "ChannelCOMB Device for Mesostructured Reactors and Networks of Reactors." *Chemical Engineering & Technology*. <https://doi.org/10.1002/ceat.202200560>.
- Barbosa, Isabel S. O., Ricardo J. Santos, Cláudia G. Silva, and Margarida S. C. A. Brito. 2021. "Consecutive Flow Distributor Device for Mesostructured Reactors and Networks of Reactors." *Chemical Engineering and Processing - Process Intensification* 167. <https://doi.org/10.1016/j.cep.2021.108541>.
- Parra-Cabrera, C., C. Achille, S. Kuhn, and R. Ameloot. 2018. "3D printing in chemical engineering and catalytic technology: structured catalysts, mixers and reactors." *Chem Soc Rev* 47 (1): 209-230. <https://doi.org/10.1039/c7cs00631d>.

Acknowledgments

This work was financially supported by LA/P/0045/2020 (ALiCE), UIDB/50020/2020 and UIDP/50020/2020 (LSRE-LCM), and the project SuN2Fuel 2022.04682.PTDC - funded by national funds through FCT/MCTES (PIDDAC). I.S.O. Barbosa acknowledges her FCT grant UI/BD/151092/2021.

Transition flow regimes in Baffled Reactors

Sofia Brandão^{1,3*}, Margarida Brito^{2,3}, António Ferreira^{2,3}, Ricardo Santos^{1,3}

¹Laboratory of Separation and Reaction Engineering – Laboratory of Catalysis and Materials, Faculdade de Engenharia, Universidade do Porto, Rua Dr. Roberto Frias, 4200-465 Porto, Portugal

²LEPABE - Laboratory for Process Engineering, Environment, Biotechnology and Energy, Faculdade de Engenharia, Universidade do Porto, Rua Dr. Roberto Frias, 4200-465 Porto, Portugal

³ALiCE – Associate Laboratory in Chemical Engineering, Faculdade de Engenharia, Universidade do Porto, Rua Dr. Roberto Frias, 4200-465 Porto, Portugal

*Corresponding author: rsantos@fe.up.pt; ORCID ID: 0000-0002-9133-218

Abstract

This work focuses on the identification of different flow regimes in Baffled Reactors operating without external stimuli. It seeks full comprehension of the mixing mechanisms and dynamics for subsequent optimization of the active mixing parameters when applying the external oscillatory stimulus. Computational Fluid Dynamics (CFD) simulations were performed to understand the flow behavior under different operational Reynolds (Re) numbers. Different 3D geometries were studied, a planar and a cylindrical form containing smooth periodic constrictions (SPC). For the planar geometry, the influence of the reactor's depth on the flow dynamics was also assessed. The dominant flow scales and the flow natural oscillation frequency at different regimes were identified through spectral analysis.

Author Keywords. Baffled Reactors, Flow Regimes, CFD, Turbulence Scales

1. Introduction

Oscillatory Baffled Reactors (OBRs) are a type of Oscillatory Flow Reactors (OFRs) composed of a tube with equally spaced baffles, to which an oscillatory flow is imposed. Application of these devices has been widely reported on batch processes, but recent studies focus on continuous operation, such as continuous crystallizations of active pharmaceutical ingredients (Cruz et al. 2021). However, the control of mixing scales in OBRs is not yet mastered, which, for instance, compromises the nucleation stage during crystallization (Avila et al. 2021).

Characterization of flow regimes in reactors, such as CIJs and NETmix, has been widely studied at LSRE-LCM since it enables control of mixing scales and the improvement of mixing efficiency (Erkoç et al. 2016). Efficient mixing occurs when the flow transitions from a segregated regime (no mixing) to a chaotic state where vortex shedding promotes convective mixing, while keeping the Re within the laminar flow range.

This work aims to provide a complete description of flow regimes in Baffled Reactors (BRs), i.e., OBRs without external stimuli. The natural frequencies of oscillation were identified to enhance the frequencies applied in the oscillatory stimulus, improving the control of mixing scales (Erkoç et al. 2016; Okkels and Tabeling 2004). Computational Fluid Dynamics (CFD) simulations were conducted using a planar and a cylindrical configuration with Smooth Periodic Constrictions (SPC) (Ferreira et al. 2015).

2. Materials and Methods

The flow fields were obtained through laminar transient 3D CFD simulations using the commercial package Ansys Fluent 2021 R2. **Erro! A origem da referência não foi encontrada.** shows the cylindrical and planar BR and the respective dimensions. Periodic Boundary Conditions (PBCs) were imposed at the inlet and outlet, and a no-slip boundary condition was set on the walls. The following continuity and Navier-Stokes equations are solved for an incompressible and isothermal flow,

$$\nabla \cdot \vec{v} = 0 \quad (1)$$

$$\rho \left(\frac{\partial \vec{v}}{\partial t} + \vec{v} \cdot \nabla \vec{v} \right) = -\nabla p + \mu \nabla^2 \vec{v} \quad (2)$$

where \vec{v} is the velocity vector and p is the static pressure. The working fluid is water at 25 °C, the convergence criterium was the residuals below 10^{-5} , and the Courant number was set to 0.5 for all simulations.

3. Discussion

The Reynolds numbers tested, $Re = \rho d_h v / \mu$, range from 40 to 1500. Figure 8b and Figure 8c show the streamlines obtained from the 3D CFD simulations at different Re numbers for both geometries.

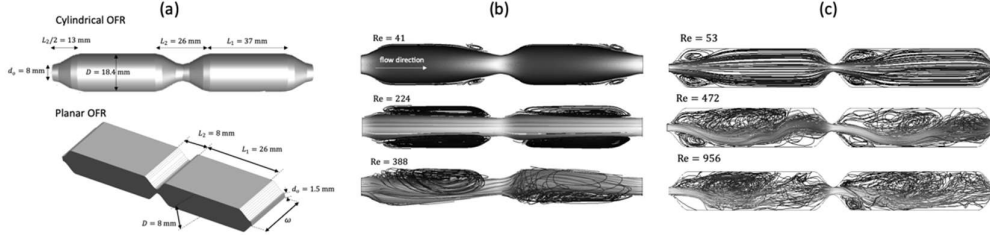


Figure 8: (a) Geometries tested; (b) streamlines for cylindrical BR and (c) streamlines for planar BR with $\omega = 15$ mm.

Cylindrical BR. Figure 8b shows that, at $Re = 41$, a segregated flow regime is identified since no dynamic flow structures are formed. At $Re = 224$, two symmetrical vortices are formed in each chamber, but a steady flow with recirculation zones is observed. At $Re = 388$, the symmetry is broken. The consecutive expansions and contractions generate a vortex within each chamber with the size of the respective chamber. At this Re number, the flow transitions from a steady to a chaotic state, marked by convective mixing.

Figure 9 shows the turbulence spectra of velocity fluctuations at the midpoint of each chamber for a cylindrical geometry at $Re = 437$.

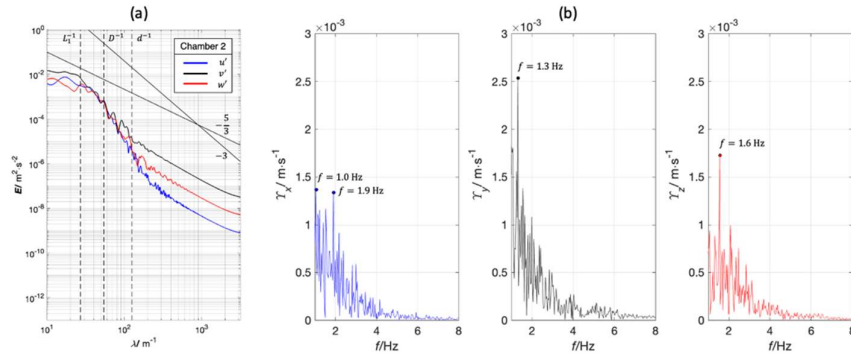


Figure 9: (a) Power and (b) frequency spectra for cylindrical BR at $Re = 437$.

Figure 9a shows that there is a change in the slope at d^{-1} , showing that turbulence is fed by a small scale, the inlet jet, that feeds larger vortices. This is an inversion of the 3D turbulent energy cascade where larger scales inject energy into smaller ones (Gonçalves et al. 2017). Figure 9b shows that the flow natural frequencies are between 1 and 2 Hz, corresponding to the formation of the vortices with characteristic lengthscale L_1^{-1} . The Strouhal number ($St = f D_h / v_{in}$) ranges from 1.8 to 3.4, which falls within the commonly cited range of $0.15 < St < 4$ for cylindrical BRs according to Avila et al. (2021).

Planar BR. Figure 8c shows that for the planar BR the flow transition occurs between Re of 472 and 956. At $Re = 472$, a jet crossing the reactor and the formation of vortices in each chamber are identified. At $Re = 956$, a complex chaotic flow pattern is generated, promoting mixing by flow engulfment in the chambers.

Figure 10 shows the turbulence spectra for the planar BR with $\omega = 15$ mm at $Re = 956$. Figure 10a shows an inversion of the energy cascade at a scale of d^{-1} . Figure 10b shows that the flow natural frequencies are between 2 - 5 Hz, which translates in St of 0.26 and 0.80. The scales associated to these

St are below D^{-1} , which correspond to the larger vortices fed by the jets, containing most of the turbulent energy.

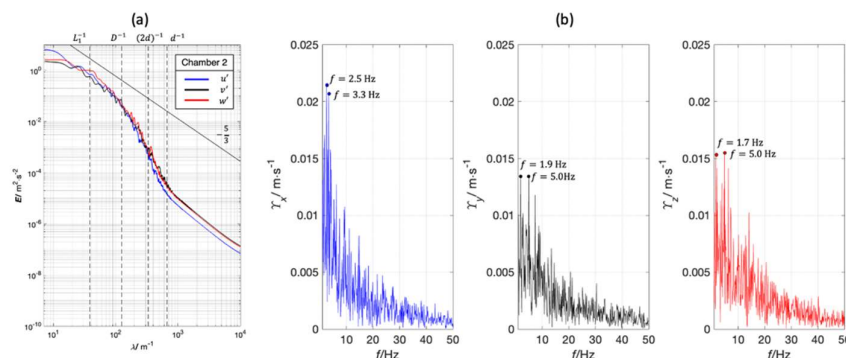


Figure 10: (a) Power and (b) frequency spectra for planar BR with $\omega = 15$ mm at $Re = 956$.

Results obtained for the different depths of the planar BR tested, indicate that the presence of wall effect hinders the onset of vortex shedding, leading to transition regimes occurring at higher Reynolds numbers.

4. Conclusions

Re marking the transition between flow regimes were identified for a cylindrical and a planar BR with SPC. The flow transitions from steady to chaotic occurs at $Re = 400$ for the cylindrical BR and at $Re = 500$ for the planar. The Strouhal number of the unforced flow rounds 1.8 - 3.4 for the cylindrical and 0.29 - 0.40 for the planar reactor. The inversion of the turbulent energy cascade that was reported in CIJs was also clearly observed in both BRs studied. Finally, deeper planar geometries favor the onset of dynamic chaotic flow.

References

- Avila, Marco, Beatrice Kawas, David Frederick Fletcher, Martine Poux, Catherine Xuereb, and Joelle Aubin. 2021. "Design, Performance Characterization and Applications of Continuous Oscillatory Baffled Reactors." *Chemical Engineering and Processing - Process Intensification*. <https://doi.org/10.1016/J.CEP.2021.108718>.
- Cruz, Patrícia, Carlos Alvarez, Fernando Rocha, and António Ferreira. 2021. "Tailoring the Crystal Size Distribution of an Active Pharmaceutical Ingredient by Continuous Antisolvent Crystallization in a Planar Oscillatory Flow Crystallizer." *Chemical Engineering Research and Design* 175 (November): <https://doi.org/10.1016/J.CHERD.2021.08.030>.
- Erkoç, Ertugrul, Cláudio P Fonte, Madalena M Dias, José Carlos B Lopes, and Ricardo J Santos. 2016. "Numerical Study of Active Mixing over a Dynamic Flow Field in a T-Jets Mixer—Induction of Resonance." *Chemical Engineering Research and Design* 106: 74–91. <https://doi.org/https://doi.org/10.1016/j.cherd.2015.12.002>.
- Ferreira, António, F Rocha, J A Teixeira, and A A Vicente. 2015. "Apparatus for Mixing Based on Oscillatory Flow Reactors Provided with Smooth Periodic Constrictions."
- Gonçalves, Nelson D., Hélder M. Salvador, Cláudio P. Fonte, Madalena M. Dias, José Carlos B. Lopes, and Ricardo J. Santos. 2017. "On the 2D Nature of Flow Dynamics in Opposed Jets Mixers." *AIChE Journal* 63 (6): 2335–47. <https://doi.org/10.1002/AIC.15566>.
- Okkels, F., and P. Tabeling. 2004. "Spatiotemporal Resonances in Mixing of Open Viscous Fluids." *Physical Review Letters* 92 (3): 4. <https://doi.org/10.1103/PHYSREVLETT.92.038301>.

Acknowledgments

This work was financially supported by: LA/P/0045/2020 (ALiCE), UIDB/50020/2020 e UIDP/50020/2020 (LSRE-LCM), UIDB/00511/2020 and UIDP/00511/2020 (LEPABE) by national funds through FCT/MCTES (PIDDAC) and by NORTE-01-0145-FEDER-000077 – funded by Comissão de Coordenação e Desenvolvimento Regional do Norte (CCDRN).

Sustainable application of *Actinidia arguta* leaves as active ingredient in topical formulation: Development, optimization and *in vivo* evaluation

Ana Margarida Silva^{1,2}, Paulo C. Costa^{3,4}, Cristina Delerue-Matos¹,
Francisca Rodrigues¹

¹REQUIMTE/LAQV, ISEP, Polytechnic of Porto, Rua Dr. António Bernardino de Almeida 431, 4249-015 Porto, Portugal, (ana.silva@graq.isep.ipp.pt; cmm@isep.ipp.pt; francisca.rodrigues@graq.isep.ipp.pt) ORCID 0000-0002-1823-9816; 0000-0002-3924-776X; 0000-0001-8803-0041

²Faculty of Sciences, University of Porto, Rua do Campo Alegre, s/n, 4169-007, Porto, Portugal, (ana.silva@graq.isep.ipp.pt) ORCID 0000-0002-1823-9816

³REQUIMTE/UCIBIO, MedTech-Laboratory of Pharmaceutical Technology, Department of Drug Sciences, Faculty of Pharmacy, University of Porto, Rua de Jorge Viterbo Ferreira, 228, 4050-313 Porto, Portugal, (pccosta@ff.up.pt) ORCID 0000-0002-1152-3398

⁴Associate Laboratory i4HB—Institute for Health and Bioeconomy, Faculty of Pharmacy, University of Porto, Rua de Jorge Viterbo Ferreira, 228, 4050-313 Porto, Portugal, (pccosta@ff.up.pt) ORCID 0000-0002-1152-3398

Abstract

The interest for new and sustainable cosmetic ingredients has increased, and, consequently, the valorization and re-use of food by-products constitute a trend. The proposed study aims to develop and optimize a topical formulation with *Actinidia arguta* leaves extract and evaluate its *in vivo* safety and moisture efficacy in human healthy volunteers. The formulation was developed by a mathematical model, namely response surface methodology (RSM), and the independent variables studied were the amount of carbomer, glycerin and decyl oleate, while the dependent variables were pH, viscosity, and particle size. According to the mathematical model, the optimal formulation contains 0.329% of carbomer, 15% of glycerin and 13.796% of decyl oleate. *In vivo* studies performed in human volunteers through a patch and hydration tests attested the safety and moisturizing capacity of the optimal formulation.

Author Keywords. *Actinidia arguta* leaves, topical formulation, response surface methodology, safety, and efficacy studies.

1. Introduction

Circular economy is an essential point of sustainable development that supports the efficient use of resources, waste minimization, primary resources reduction, and long-term value retention (Morseletto 2020). On the last decade, the interest in new topical ingredients based on sustainable principles is a trend, mainly due to their novelty, efficacy and low price (Rodrigues et al. 2013). In this sense, food by-products arise as an alternative to cosmetic ingredients due to their richness in bioactive compounds, particularly antioxidants. Among them, *A. arguta* leaves, one of the main by-products generated during kiwiberry production, have attracted a lot of attention (Silva, Costa, et al. 2021). Recently, our research team reported that the hydroalcoholic extract of *A. arguta* leaves obtained by Microwave-Assisted Extraction (MAE) is a source of polyphenols (particularly caffeoylquinic acids, proanthocyanidins, quercetin derivatives and kaempferol) with high antioxidant/antiradical activities (Silva, Pinto, et al. 2021). Also, Silva *et al.* demonstrated that the extract is safe for cosmeceutical application through skin (EpiSkin™) and ocular (SkinEthic™ HCE) models validated by the European Commission (Silva et al. 2022). In this sense, the aim of this study is to develop and optimize a topical formulation with *A. arguta* leaves extract as active ingredient by Response Surface Methodology (RSM). *In vivo* studies, namely patch and hydration tests, were executed to ensure the safety and efficacy of the topical formulation.

2. Materials and Methods

The leaves were provided by Mini-Kiwi Farm in October 2021 and extracted by MAE, according to Silva *et al.* (Silva, Pinto, et al. 2021).

The formulation was developed with water, decyl oleate, glycerin, cetearyl alcohol (and) sodium cetearyl sulfate, isoamyl cocoate, phenoxyethanol (and) decylene glycol (and) caprylyl glycol, carbomer, and triethanolamine (if the mixture had an acid pH), applying a single-phase methodology.

In order to determine the optimal composition of the formulation, a Box–Behnken design (BBD) with three central points was employed and a total of 15 experiences were designed by the Design Expert software. The three independent variables studied were the amount of thickener (carbomer; X_1 , 0.1-0.5 %), humectant (glycerin; X_2 , 9-15 %) and emollient (decyl oleate; X_3 , 12-18 %). Three dependent variables were evaluated, namely pH (Y_1), viscosity (Y_2), and particle size (Y_3).

The skin irritation potential of the optimal formulation containing the *A. arguta* leaves extract was assessed in 13 healthy volunteers through occlusive patch test. After 48 hours of occlusion, the patch was removed, and the clinical observations were assessed after 30 minutes and 48 hours. The moisturizing effect was also investigated in 10 healthy volunteers that applied the product on the inner side of the right forearm. For that, Corneometer® CM 825 was employed before and after 1, 2, 3 and 4 hours of the product' application.

3. Discussion

The effects of carbomer, glycerin, and decyl oleate on pH, viscosity, and particle size were evaluated to determine the optimal formulation conditions (Figure 1). The results demonstrated that carbomer had a significant influence on pH. In the same way, the increase of glycerin led to a higher pH. Regarding viscosity, carbomer and decyl oleate had a significant effect on viscosity, being perceptible that a high quantity of carbomer led to a higher viscosity. Regarding particle size, the reduction of carbomer and glycerin led to a decrease. Considering the responses obtained, the predicted optimal quantities achieved were 0.329% of carbomer, 15% of glycerin and 13.796% of decyl oleate. The optimal formulation presented a pH value of 5.72, a viscosity of 342.57 Pa.s and a particle size of 6.88 μm .

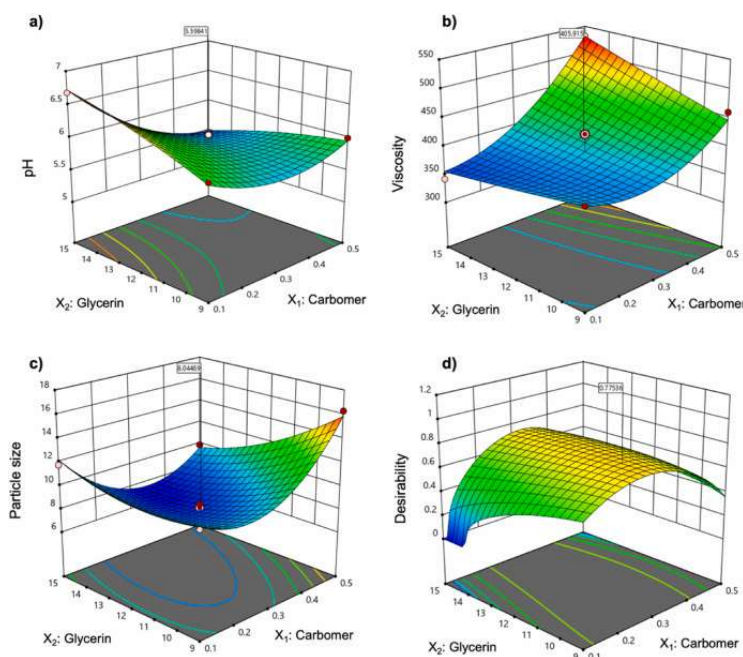


Figure 1: Response surface plots for interaction effects of carbomer (X_1) and glycerin (X_2) on pH (a), viscosity (b) and particle size (c) and on the desirability index for combined responses of factors.

In addition, a patch test was performed in 13 healthy human volunteers to evaluate the optimal formulation safety. The results confirmed the absence of irritations or allergic reactions (oedema and erythema), being well tolerated by all volunteers. Regarding hydration, 10 healthy human volunteers were enrolled in the study and, 4 hours after application, the skin hydration significantly increased. It was perceptible that the percentage of hydration augmented 28.5 % and 24.3 %, respectively, after 1 and 4 hours of application. Oppositely, a decrease of 3.3% was observed for the control product after 4 hours. The results achieved for the present study support the moisturizing effect of the topical formulation optimized. Most important, considering that dry skin normally induces wrinkles formation,

the topical formulation developed may prevent skin aging (Poomanee et al. 2021). In fact, a good hydration contributes to a healthy and moisturized skin, promoting the cutaneous barrier strength and the integrity and delay of the skin aging process (Ahmed et al. 2020).

4. Conclusions

In this study, a topical formulation was optimized through RSM methodology. The formulation containing *A. arguta* leaves extract demonstrated a typical behavior of a water in oil emulsion, promoting a good compatibility with skin's pH and easy penetration in the skin. The *in vivo* safety study proved the absence of allergy and irritancy after the product application in human volunteers, supporting a very good skin compatibility. Besides that, the topical formulation improved the skin hydration. Further anti-wrinkles studies should be performed to attest the anti-aging capacity of the formulation.

References

- Ahmed, Idris Adewale, Maryam Abimbola Mikail, Norhisam Zamakshshari, and Al-Shwyeh Hussah Abdullah. 2020. "Natural anti-aging skincare: role and potential." *Biogerontology* 21 (3): 293-310.
- Morseletto, Piero. 2020. "Targets for a circular economy." *Resources, Conservation and Recycling* 153: 104553.
- Poomanee, Worrapan, Watcharee Khunkitti, Wantida Chaiyana, Nutjeera Intasai, Wei-Chao Lin, Shang-Chian Lue, and Pimporn Leelapornpisid. 2021. "Multifunctional biological properties and phytochemical constituents of *Mangifera indica* L. seed kernel extract for preventing skin aging." *Toxicological Research* 37 (4): 459-472.
- Rodrigues, Francisca, Ana Palmeira-de-Oliveira, José das Neves, Bruno Sarmento, Maria Helena Amaral, and Maria Beatriz Oliveira. 2013. "Medicago spp. extracts as promising ingredients for skin care products." *Industrial Crops and Products* 49: 634-644.
- Silva, Ana Margarida, Paulo C Costa, Cristina Delerue-Matos, Piotr Latocha, and Francisca Rodrigues. 2021. "Extraordinary composition of *Actinidia arguta* by-products as skin ingredients: A new challenge for cosmetic and medical skincare industries." *Trends in Food Science & Technology* 116: 842-853.
- Silva, Ana Margarida, Juliana Garcia, Stefano Dall'Acqua, Paulo Costa, Cristina Delerue-Matos, and Francisca Rodrigues. 2022. "Eco-friendly insights on kiwiberry leaves valorization through in-vitro and in-vivo studies." *Industrial Crops and Products* 184: 115090.
- Silva, Ana Margarida, Diana Pinto, Iva Fernandes, Victor de Freitas, María de la Luz Cádiz-Gurrea, Paulo Costa, Cristina Delerue-Matos, and Francisca Rodrigues. 2021. "An Insight into Kiwiberry Leaf Valorization: Phenolic Composition, Bioactivity and Health Benefits." *Molecules* 26 (8): 2314.

Acknowledgments

The authors are thankful to MiniKiwi Land and DS Produtos Químicos for providing, respectively, the *A. arguta* leaves and the raw materials for the formulation development.

This work received financial support from project EXPL/BAA-GR/0663/2021 – Kiwi4Health – Exploring the Eco-Innovative Re-Use of Kiwiberry, supported by national funds by FCT/MCTES. Ana Margarida Silva is thankful for the Ph.D. grant (SFRH/BD/144994/2019) financed by POPH-QREN and subsidized by the European Science Foundation and Ministério da Ciência, Tecnologia e Ensino Superior. Francisca Rodrigues (CEECIND/01886/2020) is thankful for her contract financed by FCT/MCTES—CEEC Individual Program Contract.

Precirol® ATO 5 and Miglyol® 612-based nanoparticles to target the brain and treat Alzheimer's disease

Débora Nunes^{1,2}, Joana A. Loureiro^{1,2}, and Maria Carmo Pereira^{1,2,*}

¹LEPABE—Laboratory for Process Engineering, Environment, Biotechnology and Energy, Faculty of Engineering, University of Porto, Rua Dr. Roberto Frias, 4200-465 Porto, Portugal

²ALiCE—Associate Laboratory in Chemical Engineering, Faculty of Engineering, University of Porto, Rua Dr. Roberto Frias, 4200-465 Porto, Portugal

*Corresponding author: mcsp@fe.up.pt; ORCID ID 0000-0001-8505-3432

Abstract

Alzheimer's disease (AD) is a neurodegenerative condition considered the most common form of dementia. Memantine is an approved drug for AD that continues to be a palliative pharmaceutical strategy with several drawbacks that compromise its biological efficacy. Herein, nanostructured lipid carriers (NLCs) composed of Precirol® ATO 5 and Miglyol® 612 were produced as carriers of memantine to improve its therapeutic effectiveness. The NPs' surface was modified with brain-targeting molecules. The targeting-NLCs exhibited appropriate physicochemical characteristics for brain drug delivery, great memantine encapsulation efficiency, and physical stability for at least six months. The proposed nanocarriers may be a potential AD therapeutic strategy, and future *in vitro* and *in vivo* studies will be carried out to validate the efficacy of the drug delivery system.

Author Keywords. Drug delivery system, Brain targeting, Blood-brain barrier, Neurodegenerative disease, Memantine.

1. Introduction

The leading cause of dementia, Alzheimer's disease (AD), is a progressive neurological condition affecting about 75% of the world's people (Anand, Gill, and Mahdi 2014). As the global population ages, AD is becoming more prevalent, and in 2050, the incidence of AD is anticipated to reach 140 million people. Memantine is the most used drug approved to treat moderate-to-severe dementia in AD. In addition to being merely palliative, the therapeutic activity of memantine fails due to its low bioavailability, weak pharmacokinetic and pharmacodynamic properties and inability to cross the blood-brain barrier (BBB) (Sharif et al. 2018). Thus, higher dosages and frequent administrations are required to maintain the plasma levels within the therapeutic range, which causes toxicity in the remaining tissues and unwanted side effects. A plausible strategy to overcome these problems is using nanoparticles (NPs) since their surface could be modified with specific molecules for a targeted administration, overcoming the BBB and enabling drug release in the brain. Thus, the unintended side effects of the unspecific distribution over various tissues could be reduced (Begines et al. 2020).

Therefore, the present study aims the development of nanostructured lipid carriers (NLCs) loaded with memantine as a therapeutic approach for AD. The NP's surface was functionalized with targeting molecules to improve brain drug delivery and transport memantine across the BBB.

2. Materials and Methods

NLCs were prepared with a lipid phase of Precirol® ATO 5 (175 mg), Miglyol® 612 (75 mg), and memantine (0 or 10 mg), and a water phase of 2.175 mL of 10% (w/v) solution of Pluronic® F-127. NLCs were produced by combining the shear homogenization and the ultrasonication methods. First, the lipid and aqueous phases were separately heated at 80 °C allowing the lipid to melt completely. Then, the lipid phase was dispersed in the aqueous phase. The NPs were formed in a high-shear mixing device and then submitted to ultrasonication to reduce their size. Finally, NPs were left to cool down at room temperature allowing lipid crystallization. NPs conjugation with Tf was prepared by replacing 1% of the lipid with DSPE-PEG-NH₂ before melting. Due to its lipophilic nature, DSPE was incorporated into the NPs matrix, while the hydrophilic PEG and the terminal amine group were exposed on the surface to make it possible to bind the protein. An activated Tf solution was added to the NPs conjugated with DSPE-PEG-NH₂ for reaction.

The NPs were characterized using the dynamic light scattering (DLS) technique. The memantine encapsulation was quantified using high-performance liquid chromatography, while spectrophotometry was carried out to quantify the amount of Tf conjugated on the surface of the lipid NPs. The Tf conjugation was also confirmed by Fourier Transform Infrared Spectroscopy (FTIR) analysis. The morphology of NPs was analyzed by transmission electron microscopy (TEM).

3. Discussion

The NPs were characterized by mean diameter, polydispersity index (PDI), zeta potential and encapsulation efficiency (EE). The results are presented in Table 1 for the different formulations.

Formulation	Mean diameter (nm)	PDI	Zeta Potential (mV)	EE (%)	Number of Tf molecules per NP
NLCs	133 ± 15	0.20 ± 0.02	-24 ± 3	-	-
NLCs-memantine	197 ± 16 **	0.19 ± 0.02	-10 ± 3 *	46 ± 6	-
NLCs-Tf	123 ± 13	0.18 ± 0.02	-14 ± 2 *	-	30 ± 6
NLCs-Tf-memantine	141 ± 0	0.18 ± 0.01	-15 ± 6	56 ± 2	38 ± 8

Table 1: Characterization of NLCs before and after memantine encapsulation and Tf conjugation (mean ± SD, n = 3). * and ** Denotes statistically significant (p < 0.05) and highly significant differences (p < 0.01) compared to the unloaded and unconjugated formulation.

The NPs were under 200 nm in mean diameter, essential for systemic administration and BBB penetration. Memantine was found to increase the size of NLCs (p < 0.01), whereas conjugation with Tf had no significant effect on that parameter (p > 0.05). This increase in the mean diameter agrees with the literature, where some studies have reported that the incorporation of drugs into lipid NPs leads to an increase in the mean diameter due to the rearrangement of the lipid matrix (Loureiro et al. 2017). Despite that, the NPs remained in a size range suitable to cross the BBB. PDI was about 0.2 for all formulations, showing no evidence of aggregation and an appropriate size distribution. According to the results, the NPs have zeta potential values high enough to ensure good NPs stabilization and prevent aggregation.

The findings revealed a conjugation of 30 ± 6 molecules of Tf per NLC, demonstrating an efficient conjugation of Tf, which agrees with the literature that used the same method for Tf conjugation (Neves et al. 2021). The conjugation of NPs with Tf was confirmed by FTIR analysis of both functionalized and nonfunctionalized NPs, as depicted in Figure 1 A). The spectra of the Tf and Tf- conjugated NLCs show one prominent band that matches the C=O stretching vibrations (1650 cm⁻¹) present in the peptide bonds between amino acids of Tf protein, supporting the conjugation of the NPs with Tf. TEM images (Figure 1 B and C) revealed that NPs have a spherical shape and a size of less than 200 nm, which agrees with the physicochemical characterization obtained by DLS. Additionally, the images revealed no visible aggregation of NPs, a suitable indicator of their stability. No significant differences in morphology were observed between NPs with or without memantine or Tf.

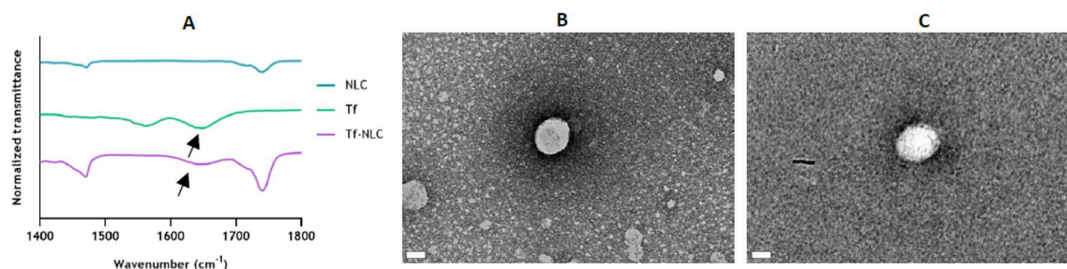


Figure 1: A) Infrared spectra obtained by FTIR for NLCs before and after conjugation with Tf. A Tf sample was analyzed as a control. B) TEM images of NLCs and

4. Conclusions

NLCs were successfully created as carriers for memantine, with diameters of less than 200 nm, which is the size required to be used systemically and pass through the BBB. Memantine was successfully encapsulated, and NPs were functionalized with Tf without any apparent changes in their physicochemical properties. The production of spherical NPs with homogeneous shapes and no discernible aggregation was seen in TEM images.

References

- Anand, R., K. D. Gill, and A. A. Mahdi. 2014. "Therapeutics of Alzheimer's disease: Past, present and future." *Neuropharmacology* 76 Pt A:27-50. doi: 10.1016/j.neuropharm.2013.07.004.
- Begines, Belén, Tamara Ortiz, María Pérez-Aranda, Guillermo Martínez, Manuel Merinero, Federico Argüelles-Arias, and Ana Alcuía. 2020. "Polymeric Nanoparticles for Drug Delivery: Recent Developments and Future Prospects." *Nanomaterials* 10 (7). doi: 10.3390/nano10071403.
- Loureiro, Joana A., Stephanie Andrade, Ana Duarte, Ana R. Neves, Joana F. Queiroz, Cláudia Nunes, Emmanuel Sevin, Laurence Fenart, Fabien Gosselet, Manuel A. N. Coelho, and Maria C. Pereira. 2017. "Resveratrol and Grape Extract-loaded Solid Lipid Nanoparticles for the Treatment of Alzheimer's Disease." *Molecules* 22 (2). doi: 10.3390/molecules22020277.
- Neves, A. R., L. van der Putten, J. F. Queiroz, M. Pinheiro, and S. Reis. 2021. "Transferrin-functionalized lipid nanoparticles for curcumin brain delivery." *Journal of Biotechnology* 331:108-117. doi: 10.1016/j.jbiotec.2021.03.010.
- Sharif, Yousra, Fareed Jumah, Louis Coplan, Alec Krosser, Kassem Sharif, and R. Shane Tubbs. 2018. "Blood brain barrier: A review of its anatomy and physiology in health and disease." *Clinical Anatomy* 31 (6):812-823. doi: 10.1002/ca.23083.

Acknowledgments

This work was financially supported by LA/P/0045/2020 (ALiCE), UIDB/00511/2020 and UIDP/00511/2020 (LEPABE), funded by national funds through FCT/MCTES (PIDDAC); Project 2SMART - engineered Smart materials for Smart citizens, with reference NORTE-01-0145-FEDER-000054, supported by Norte Portugal Regional Operational Program (NORTE 2020), under the PORTUGAL 2020 Partnership Agreement, through the European Regional Development Fund (ERDF). National funds through the FCT/MCTES (PIDDAC) under the project EXPL/NAN-MAT/0209/2021. FCT supported D.N. through a doctoral grant (UI/BD/150946/2021).

Valorization of a nutraceutical ingredient extracted from a chestnut by-product towards the implementation of Sustainable Development Goals

Diana Pinto^{1,2}, Andreia Almeida¹, Anallely López-Yerena^{3,4}, Bruno Sarmiento^{5,6,7}, Rosa Lamuela-Raventós^{3,4}, Anna Vallverdú-Queralt^{3,4}, Cristina Delerue-Matos¹, Francisca Rodrigues^{1,*}

¹REQUIMTE/LAQV, Instituto Superior de Engenharia do Porto, 4249-015 Porto, Portugal; ²Faculdade de Ciências, Universidade do Porto, Rua do Campo Alegre, 4169-007 Porto, Portugal; ³Nutrition, Food Science and Gastronomy Department, School of Pharmacy and Food Science, University of Barcelona, Barcelona, Spain; ⁴Consorcio CIBER, M.P. Fisiopatología de la Obesidad y la Nutrición (CIBEROBn), Instituto de Salud Carlos III (ISCIII), Madrid, Spain; ⁵IS – Institute for Research and Innovation in Health, University of Porto, 4200-135 Porto, Portugal; ⁶INEB – Institute of Biomedical Engineering, University of Porto, 4200-135 Porto, Portugal; ⁷CESPU – Institute for Research and Advanced Training in Health Sciences and Technologies, 4585-116 Gandra, Portugal. * francisca.rodrigues@graaq.isep.ipp.pt

Abstract

Chestnut (*Castanea sativa*) shells (CS) are a promising source of bioactive molecules. This study explores the effects of its oral administration (in two different concentrations, 50 and 100 mg/kg b.w.) in rats regarding *in-vivo* antioxidant properties, anti-hemolytic activity, blood glucose and serum lipids levels, and metabolomic profiling of blood serum by LC-ESI-LTQ-Orbitrap-MS. The *in-vivo* studies revealed an upmodulating of antioxidant enzymes activities, downmodulating of lipid peroxidation, anti-hemolytic, and mild hypoglycemic and hypolipidemic effects. Metabolomic profiling was characterized by phenolic acids, flavonoids, and lignans, along with phase I and II metabolites.

Author Keywords. *Castanea sativa*, phenolic compounds, *in-vivo*, bioactivity, metabolomic, nutraceutical.

1. Introduction

The intake of food supplements and nutraceuticals has steadily increased owing to their pivotal role in the daily diet of society for health-promoting purposes, mainly ascribed to the phytochemicals possessing outstanding antioxidant effects (Pinto et al. 2023). The demand for antioxidants from natural sources, such as CS, has intensified with industries searching for new bioactive molecules in close alliance with the Sustainable Development Goals from the Agenda 2030 (Pinto et al. 2021). The CS generated during chestnut processing are an abundant by-product, not entirely depleted by their reuse as biomass that may lead to disposal problems. Previous research investigated the *in-vitro* bioactivity and phytochemical composition of CS extracts, attesting the antioxidant, anti-inflammatory and antimicrobial effects, mainly attributed to vitamin E, amino acids, and polyphenols (Pinto et al. 2023; Pinto et al. 2021). This study aims to explore the effects of its daily oral administration to rats regarding polyphenols *in-vivo* bioactivity and bioavailability in blood serum.

2. Materials and Methods

The *in-vivo* studies were performed to appraise the effects of the daily oral administration of CS extract (50 and 100 mg/kg per body weight (b.w.)) on male Wistar rats (200 ± 50 g, 5–6 weeks old) provided by Jackson Laboratory (Bar Harbor, ME, USA), housed under standard conditions (21±2 °C; 45–55% humidity; 12 h/12 h light/dark) and fed *ad libitum*. Animals were separated into three groups (*n*=6 per group): a control group treated with water (4 mL/kg b.w.); and two treatment groups with 50 and 100 mg/kg b.w. The CS extract was administered by gastric gavage once daily for 7 days. The *in-vivo* antioxidant activity, anti-hemolytic properties, blood glucose and lipids levels as well as the metabolomic profiling of the blood serum targeted on polyphenols by LC-ESI-LTQ-Orbitrap-MS were evaluated. After the 7 days, the animals were sacrificed by pentobarbital overdose (50 mg/kg b.w.) and the blood was collected by cardiac puncture and centrifuged (2000 g, 15 min, 4 °C) to obtain serum.

3. Discussion

The animals body weight ranged from 175 to 225 g during the experiment. The results proved the *in-vivo* antioxidant properties in the blood serum from rats treated with both doses of CS extract through upmodulating antioxidant enzymes activities and downregulating lipid peroxidation, along with anti-hemolytic properties ($IC_{50} = 34.71 \mu\text{g/mL}$) and protective effects against rising blood glucose and lipids levels (Table 3; Figure; Table 3).

Groups	SOD (U/g protein)	CAT (U/g protein)	GSH-Px (U/g protein)	LPO (nmol MDA/mg protein)
CS 50 mg/kg b.w.	148 ± 19 ^a	25 ± 4 ^b	26 ± 7 ^{b,c}	18 ± 2 ^a
CS 100 mg/kg b.w.	127 ± 14 ^{a,b}	26 ± 3 ^{a,b}	65 ± 13 ^a	7.6 ± 2 ^b
Control (water)	109 ± 7 ^b	31 ± 3 ^a	23 ± 8 ^c	16 ± 3 ^a

Table 1: *In-vivo* antioxidant activity of blood serum from rats. SOD, superoxide dismutase. CAT, catalase. GSH-Px, glutathione peroxidase. LPO, lipid peroxidation. MDA, malondialdehyde.

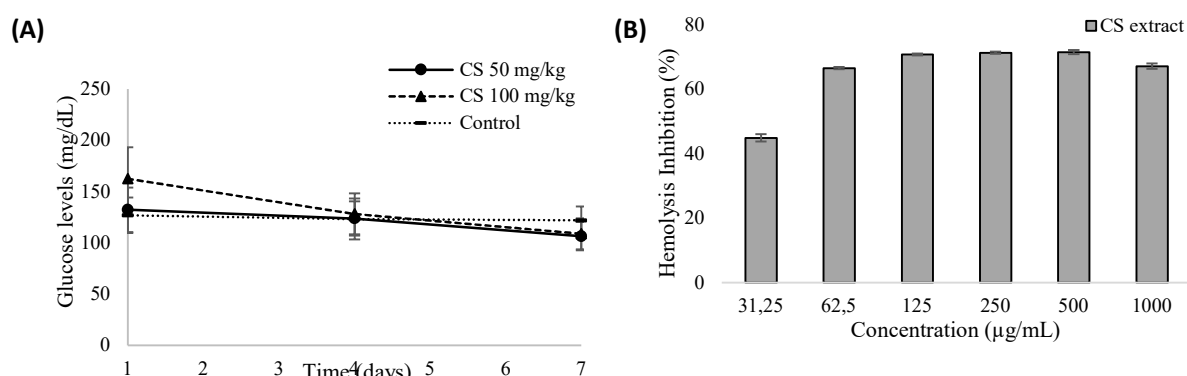


Figure 1: Blood glucose levels (A) and anti-hemolytic effects (B). * denotes $p < 0.05$.

Groups	Triglycerides (mg/dL)	Total cholesterol (mg/dL)	HDL-c (mg/dL)	LDL-c (mg/dL)
CS 50 mg/kg b.w.	205 ± 36 ^{a,b}	84 ± 11 ^b	70 ± 9 ^a	24 ± 6 ^b
CS 100 mg/kg b.w.	177 ± 17 ^b	98 ± 2 ^a	72 ± 8 ^a	19 ± 5 ^b
Control (water)	275 ± 61 ^a	95 ± 7 ^{a,b}	48 ± 8 ^b	40 ± 6 ^a

Table 2: Blood serum lipids levels from rats treated with CS extract and water (control). HDL-c, high-density lipoprotein cholesterol. LDL-c, low-density lipoprotein cholesterol.

Phenolic acids, flavonoids, and lignans were quantified in the blood serum, along with phase I and II metabolites. Hydroxyphenylpropionic acid (HPPA) and 3-hydroxybenzoic acid were the major polyphenols, while HPPA-O-sulfate was the main metabolite (Table 3).

Compounds/metabolites	Concentration (nmol/mL blood serum)		
	Control (water)	CS extract 50 mg/kg b.w.	CS extract 100 mg/kg b.w.
3-Hydroxybenzoic acid	n.i.	206 ± 48 ^a	163 ± 31 ^b
Protocatechuic acid	n.i.	1.7 ± 0.5 ^a	0.86 ± 0.3 ^b
Dihydrogallic acid	n.i.	1.8 ± 0.5 ^a	1.6 ± 0.4 ^a
Syringic acid	n.i.	3.2 ± 1 ^a	2.7 ± 0.8 ^a
Hippuric acid	7.2 ± 1 ^b	13 ± 2 ^a	13 ± 3 ^a
Caffeic acid-O-sulfate	n.i.	0.15 ± 0.02 ^a	0.13 ± 0.02 ^b
Dihydrocaffeic acid	n.i.	2.0 ± 0.3 ^a	1.8 ± 0.4 ^a
Dihydrocaffeic acid-O-sulfate	n.i.	0.93 ± 0.2 ^a	1.0 ± 0.2 ^a
Dihydrocaffeic acid-O-glucuronide	n.i.	0.04 ± 0.01 ^a	0.04 ± 0.01 ^a
Methyl-ferulic acid-O-sulfate	n.i.	0.44 ± 0.08 ^a	0.36 ± 0.05 ^b
Dihydroferulic acid-O-sulfate	n.i.	2.4 ± 0.4 ^a	2.5 ± 0.5 ^a
Dihydroferulic acid-O-glucuronide	n.i.	0.24 ± 0.07 ^b	0.32 ± 0.1 ^a
p-Coumaric acid	n.i.	0.26 ± 0.04 ^a	0.23 ± 0.03 ^b
Hydroxyphenylpropionic acid	n.i.	319 ± 63 ^a	334 ± 60 ^a
Hydroxyphenylpropionic acid-O-sulfate	n.i.	225 ± 61 ^a	220 ± 65 ^a
(Epi)catechin-O-sulfate	n.i.	1.3 ± 0.4 ^b	1.5 ± 0.1 ^a
Secoisolariciresinol	n.i.	0.33 ± 0.08 ^a	0.34 ± 0.07 ^a

Table 3: Metabolic profile of phenolics in rats blood serum. n.i., non-identified. CS, chestnut shells.

4. Conclusions

The *in-vivo* studies corroborated the outcomes accomplished on the *in-vitro* assays, proposing a novel approach for the industrial valorization of CS as an appealing source of antioxidant compounds for nutraceuticals.

References

- D. Pinto, A. Almeida, A. López-Yerena, S. Pinto, B. Sarmiento, R. Lamuela-Raventós, A. Vallverdú-Queralt, C. Delerue-Matos, and F. Rodrigues. 2023. Appraisal of a new potential antioxidants-rich nutraceutical ingredient from chestnut shells through *in-vivo* assays – A targeted metabolomic approach in phenolic compounds. *Food Chemistry*, 404:134546. Accessed 28 March, 2023. DOI: 10.1016/j.foodchem.2022.134546.
- D. Pinto, E. Vieira, A. Peixoto, C. Freire, V. Freitas, P. Costa, C. Delerue-Matos, and F. Rodrigues. 2021. Optimizing the extraction of phenolic antioxidants from chestnut shells by subcritical water extraction using response surface methodology. *Food Chemistry*, 334:127521. Accessed 29 March, 2023. DOI: 10.1016/j.foodchem.2020.127521.

Acknowledgments

This work received financial support from the projects PTDC/ASP-AGR/29277/2017, 5537 DRI, Sérvia 2020/21 from Portuguese-Serbia Bilateral Cooperation, UIDB/50006/2020, supported by FCT/MCTES and FEDER throughout COMPETE 2020 (POCI-01-0145-FEDER-029277). D.P. is thankful for her Ph.D. grant (SFRH/BD/144534/2019) financed by FCT/MCTES, POPH-QREN, EU and FSE. F.R. (CEECIND/01886/2020) is thankful for her contract financed by FCT/MCTES—CEEC Individual 2020 Program Contract. A.V.-Q. thanks the Spanish Ministerio de Ciencia, Innovación y Universidades for the Ramon y Cajal contract (RYC-2016-19355).

Spray drying microencapsulation of *Actinidia arguta* fruits and leaves extract

Filipa Teixeira¹, Ana Margarida Silva¹, Cristina Delerue-Matos¹, Berta Estevinho^{2,3}, Paulo C. Costa^{4,5}, Francisca Rodrigues¹

¹REQUIMTE/LAQV, ISEP, Polytechnic of Porto, Rua Dr. António Bernardino de Almeida 431, 4249-015 Porto, Portugal (filipamrt237@gmail.com; ana.silva@graq.isep.ipp.pt; cmm@isep.ipp.pt; francisca.rodrigues@graq.isep.ipp.pt) ORCID 0000-0002-9287-8771; 0000-0002-1823-9816; 0000-0002-3924-776X; 0000-0001-8803-0041

²LEPABE, Departamento de Engenharia Química, Faculdade de Engenharia da Universidade do Porto, Rua Dr. Roberto Frias, 4200-465 Porto, Portugal (berta@fe.up.pt) ORCID 0000-0002-1564-6010

³ALiCE—Associate Laboratory in Chemical Engineering, Faculty of Engineering, University of Porto, Rua Dr. Roberto Frias, 4200-465 Porto, Portugal (berta@fe.up.pt) ORCID 0000-0002-1564-6010

⁴REQUIMTE/UCIBIO, MedTech-Laboratory of Pharmaceutical Technology, Department of Drug Sciences, Faculty of Pharmacy, University of Porto, Rua de Jorge Viterbo Ferreira, 228, 4050-313 Porto, Portugal (pccosta@ff.up.pt) ORCID 0000-0002-1152-3398

⁵Associate Laboratory i4HB—Institute for Health and Bioeconomy, Faculty of Pharmacy, University of Porto, Rua de Jorge Viterbo Ferreira, 228, 4050-313 Porto, Portugal (pccosta@ff.up.pt) ORCID 0000-0002-1152-3398

Abstract

Actinidia arguta fruits (commonly known as kiwiberry), as well as its by-products (such as leaves), have an outstanding content of phenolic compounds with pro-healthy properties, such as antioxidant and anti-inflammatory effects. The aim of this study is to develop, by spray drying, microparticles of *A. arguta* fruits and leaves extracts prepared by ultrasound-assisted extraction (UAE). The microparticles size and distribution, antioxidant/antiradical activities, swelling capacity and moisture content were evaluated. The effect on the viability of TR146 and HSC-3 cell lines was also evaluated. The data obtained suggests that the kiwiberry leaves extract microparticles are the most promising in what concerns to activity and safety.

Author Keywords. Spray drying. *Actinidia arguta*. Microparticles. Ultrasound-assisted extraction.

1. Introduction

Actinidia arguta is a perennial vine rich in phenolic compounds (such as phenolic acids, carotenoids, and organic acids) with outstanding therapeutic properties, namely antioxidant, and anti-inflammatory activities (Macedo et al. 2023). During the fruit production, different by-products are generated, particularly leaves, which are also rich in polyphenols (Silva et al. 2022). Nevertheless, polyphenols are extremely sensitive and have low bioavailability in the human body, being necessary to develop suitable delivery systems, such as microparticles, to allow the protection of the active ingredients, reducing reactivity with external factors, and allowing a controlled release (Ribeiro, Estevinho, and Rocha 2019). The present study aims to develop, by spray-drying, microparticles of *A. arguta* fruits and leaves extracts prepared by ultrasound-assisted extraction (UAE) and compare them regarding physicochemical

parameters (size and distribution), antioxidant/antiradical activities, swelling capacity, moisture content, and effect on the viability of TR146 and HSC-3 cell lines. To the best of our knowledge, this is the first study that encapsulates *A. arguta* extracts.

2. Materials and Methods

A. arguta fruits and leaves were harvested in October 2021 in Mini-Kiwi Farm (Vila Nova de Famalicão, Portugal). Kiwiberries UAE was performed according to Macedo et al. (2023), while leaves were extracted following Silva et al. (2022). Microparticles were prepared using a minispray dryer BÜCHI B-290 and Eudragit RS30D (1%) as encapsulating agent. Different microparticles were prepared: empty

microparticles (RS30D), kiwiberry extract microparticles (RS30D + KB) and *A. arguta* leaves extract microparticles (RS30D + AAL). The active microparticles were prepared by mixing 2 mL of each extract with 200 mL of the encapsulating agent (3%, v/v). All solutions were fed into the spray dryer at a flow rate of 4 mL/min (15%) and an inlet and outlet temperature of 115 °C and 55 –60 °C, respectively (Ribeiro, Estevinho, and Rocha 2019). Microparticles size and distribution were investigated through a Mastersizer™ 3000 laser diffraction analyzer and scanning electron microscopy (SEM). The antiradical/antioxidant activities were assessed by the 2,2-diphenyl-1-picrylhydrazyl (DPPH) radical scavenging and ferric reducing antioxidant power (FRAP) assays. Swelling capacity and moisture content were also evaluated by infrared moisture. *In vitro* cell studies were conducted on TR146 and HSC-3 cell lines, both oral cell lines, by a 3-(4,5-dimethylthiazol-2-yl)-2,5-diphenyltetrazolium bromide (MTT) assay.

3. Discussion

The empty microparticles presented a yield of 49.6%, while RS30D + KB and RS30D + AAL achieved yields of 44.9% and 35.1%, respectively. Regarding size, the empty microparticles ranged between 0.31 and 5.95 µm, while the RS30D + KB varied between 0.33 to 8.62 µm and the RS30D + AAL ranged from 1.85 to 6.33 µm. The swelling capacity and the moisture content were also evaluated (**Table 1**).

Microparticles	Moisture content (%)	Swelling capacity (%)
RS30D	4.48 ± 1.70 ^b	17.20 ± 3.36 ^a
RS30D + KB	16.93 ± 2.55 ^a	4.98 ± 0.35 ^b
RS30D + AAL	7.34 ± 0.47 ^b	12.34 ± 1.82 ^{a,b}

Table 1: Moisture content and swelling capacity of produced microparticles.

Results are expressed as mean ± standard deviation ($n = 3$). Different letters in the same column mean significant differences ($p < 0.05$).

The SEM images showed a spherical morphology like a biconcave disc for all microparticles. **Table 2** summarizes the antioxidant/antiradical activities of the different microparticles. Although RS30D + KB showed no significant differences in either assay when compared to empty microparticles, the same could not be said for RS30D + AAL. These microparticles demonstrated significant antioxidant and antiradical activities ($p < 0.05$), which may indicate that the leaves extract encapsulation is more promising.

Microparticles	FRAP (µmol FSE/g)	DPPH (mg TE/g)
RS30D	28.43 ± 3.72 ^a	2.48 ± 0.40 ^a
RS30D + KB	30.30 ± 3.21 ^a	2.15 ± 0.27 ^a
RS30D + AAL	81.72 ± 4.31 ^b	4.90 ± 0.60 ^b

Table 2: Antiradical and antioxidant activities of the formulated microparticles evaluated, respectively, by DPPH and FRAP assays. Results are expressed as mean ± standard deviation ($n = 3$). Different letters in the same column mean significant differences ($p < 0.05$).

In vitro cell assays revealed that any microparticles reduced cell viability in both oral cell lines used (HSC-3 and TR146) (**Figure 1**).

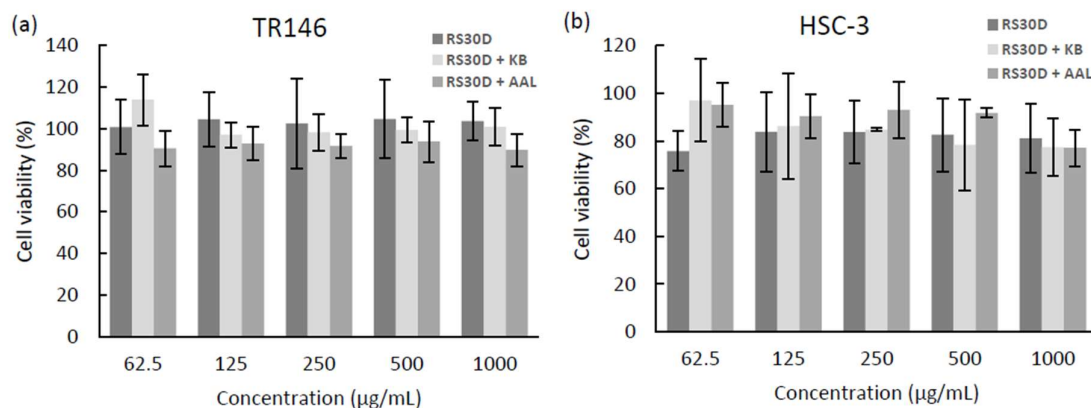


Figure 1: Effect of all formulated microparticles on the viability of TR146 (a) and HSC-3 (b) cell lines measured by MTT assay (n = 3).

4. Conclusions

The results obtained suggest that RS30D + AAL are the most promising in what concerns to activity, being safe on oral cell lines. LC-MS analysis should be performed to assess the encapsulation efficiency, along with studies regarding the *in vitro* controlled release in order to evaluate the release of bioactive compounds over time.

References

- Macedo, Catarina, Ana Margarida Silva, Ana Sofia Ferreira, María de la Luz Cádiz-Gurrea, Álvaro Fernández-Ochoa, Antonio Segura-Carretero, Cristina Delerue-Matos, Paulo Costa, and Francisca Rodrigues. 2023. "Insights into the polyphenols extraction from *Actinidia arguta* fruit (kiwiberry): A source of pro-healthy compounds". *Scientia Horticulturae* 313:111910. Accessed 25 March, 2023. DOI: 10.1016/j.scienta.2023.111910.
- Ribeiro, A. Marisa, Berta N. Estevinho, and F. Rocha. 2019. "Spray Drying Encapsulation of Elderberry Extract and Evaluating the Release and Stability of Phenolic Compounds in Encapsulated Powders". *Food and Bioprocess Technology* 12 (8):1381-1394. Accessed 21 March, 2023. DOI: 10.1007/s11947-019-02304-z.
- Silva, Ana Margarida, Juliana Garcia, Stefano Dall'Acqua, Paulo Costa, Cristina Delerue-Matos, and Francisca Rodrigues. 2022. "Eco-friendly insights on kiwiberry leaves valorization through in-vitro and in-vivo studies". *Industrial Crops and Products* 184:115090. Accessed 25 March, 2023. DOI: 10.1016/j.indcrop.2022.115090.

Acknowledgments

The authors are thankful to MiniKiwi Land for the samples. This work received financial support from project EXPL/BAA-GR/0663/2021 – Kiwi4Health – Exploring the Eco-Innovative Re-Use of Kiwiberry, supported by national funds by FCT/MCTES. Filipa Teixeira is thankful for the scholarship from project EXPL/BAA-GR/0663/2021. Ana Margarida Silva is thankful for the Ph.D. grant (SFRH/BD/144994/2019) and Francisca Rodrigues (CEECIND/01886/2020) is thankful for her contract financed by FCT/MCTES—CEEC Individual Program Contract. This work was financially supported by LA/P/0045/2020 (ALICE), UIDB/00511/2020 and UIDP/00511/2020 (LEPABE), funded by national funds through FCT/MCTES (PIDDAC); Also, Berta Estevinho acknowledges FCT for the contract based on the "Lei do Emprego Científico" (DL 57/2016 – norma transitória).

PNA-FISH applications for *Legionella* detection and localization in biofilms

Ana Barbosa^{1,2}, Darla M. Goeres³, Nuno F. Azevedo^{1,2}, Laura Cerqueira^{1,2}

¹LEPABE - Laboratory for Process Engineering, Environment, Biotechnology and Energy, Faculty of Engineering, University of Porto, Rua Dr. Roberto Frias, 4200-465 Porto, Portugal (up202204092@edu.fe.up.pt) (nazevedo@fe.up.pt) ORCID (0000-0001-5864-3250) (lcerqueira@fe.up.pt) (0000-0001-8452-4749)

²ALICE - Associate Laboratory in Chemical Engineering, Faculty of Engineering, University of Porto, Rua Dr. Roberto Frias, 4200-465 Porto, Portugal (up202204092@edu.fe.up.pt) (nazevedo@fe.up.pt) ORCID (0000-0001-5864-3250) (lcerqueira@fe.up.pt) (0000-0001-8452-4749)

³Center for Biofilm Engineering, Montana State University, Bozeman, MT 59717-3980, USA (darla_g@montana.edu) (0000-0002-6320-9616)

Abstract

Legionella pneumophila is an intracellular waterborne pathogen that represents a serious public health problem when is present in artificial water systems. Fluorescence *in situ* hybridization using Nucleic Acid Mimics (NAM-FISH) represents a promising molecular approach that can be applied for detection. When coupled to spectral imaging using high-resolution CLSM can also provide insights on biofilm's spatial biogeography. This work intends to explore the development of PNA probes for the detection of *L. pneumophila* in water samples and also to demonstrate the adaptation of PNA-FISH to target mRNA for gene expression studies.

Author Keywords. Biofilm, *Legionella pneumophila*, water systems, spatial organization.

1. Introduction

In most anthropogenic water systems, *Legionella pneumophila*, an opportunistic waterborne pathogen, is one of the most monitored agents, posing a serious public health problem. This bacterium ubiquitously found in natural freshwater can colonize a range of manmade water systems including cooling towers, spas, or hospitals (Chauhan and Shames 2021). Despite the outstanding developments in *Legionella* identification, current technologies do not fully answer the needs of industrial entities for *Legionella* monitoring. Fluorescence *in situ* hybridization using Nucleic Acid Mimics (NAM-FISH) represents a promising and versatile approach, where fluorescently labelled NAMs such as peptide nucleic acids (PNA), are used to penetrate microbial cells and hybridize with specific rRNA sequences (Nácher-Vázquez, Santos, et al. 2022). Our group already has reported the design of several PNA probes for the detection of different pathogens in food, clinical and environmental samples (e.g. *Listeria* spp., *Helicobacter pylori*, *Legionella* spp.) (Rocha et al. 2019; Cerqueira et al. 2013; Nácher-Vázquez, Barbosa, et al. 2022). Furthermore, under the scope of the ERA Chair e.Biofilm project, we want to explore the use of PNA probes for *Legionella* biofilm studies. Indeed, NAM-FISH is a powerful and versatile technique for bacterial detection that can also be applied in biofilm studies (Almeida et al. 2011). In addition, the adaptation of this approach to target mRNA will allow the study of gene expression in individual cells, either in suspension or in biofilms, combining spatial and functional information of cells in their original environment. The main goal of this work will be to explore the development of PNA probes for the detection of *L. pneumophila* in water samples. Moreover, we will demonstrate that adapting PNA-FISH to target mRNA and combining it with spectral imaging using high-resolution CLSM will allow us to study gene expression in individual cells both in suspension and in biofilms, thus combining spatial and functional information from cells *in situ*.

2. Materials and Methods

Several temperatures, ranging from 55 °C to 63 °C, with a 30% formamide concentration were studied to evaluate the signal-to-noise ratio of the rRNA PNA probe. After that, the specificity and sensitivity values were assessed using 22 *L. pneumophila* and 24 non-*L. pneumophila* strains. Additionally, the design of probes targeting the genes involved in the formation of the *L. pneumophila* biofilm is being developed using bioinformatics tools.

3. Discussion

The optimal conditions for hybridization were achieved at 60 °C for 60 min. Also, the results showed a positive fluorescence signal for the target (100% sensitivity) but none of the non-target strains were positive (100% specificity). Currently, the filtration/centrifugation protocols for water samples treatment prior to hybridization are being performed to optimize and simplify the detection protocols when low concentrations of bacteria are present (based on ISO protocol 11731:2017). The hybridization conditions of the mRNA probes are also being optimized in planktonic growth under different conditions.

4. Conclusions

These results emphasize the PNA-FISH method remains a good alternative for rapid and accurate detection. Here we also intend to present a preliminary model for the use of mRNA PNA-FISH to study the regulatory network of *L. pneumophila* that is used to provide information about gene expression in single cells either in the planktonic or sessile state, recording both spatial and functional information. Indeed, rethinking current *Legionella* research and management paradigms is crucial to provide additional information that could improve the efficiency of *Legionella* control and proliferation strategies.

References

- Almeida, Carina, Nuno F Azevedo, Sílvia Santos, Charles W Keevil, and Maria J Vieira. 2011. "Discriminating multi-species populations in biofilms with peptide nucleic acid fluorescence in situ hybridization (PNA FISH)." *PLoS one* 6 (3): e14786. <https://doi.org/10.1371/journal.pone.0014786>.
- Cerqueira, Laura, Ricardo M Fernandes, Rui M Ferreira, Mónica Oleastro, Fátima Carneiro, Catarina Brandão, Pedro Pimentel-Nunes, Mário Dinis-Ribeiro, Céu Figueiredo, and Charles W Keevil. 2013. "Validation of a fluorescence in situ hybridization method using peptide nucleic acid probes for detection of *Helicobacter pylori* clarithromycin resistance in gastric biopsy specimens." *Journal of Clinical Microbiology* 51 (6): 1887-1893. <https://doi.org/10.1128/JCM.00302-13>.
- Chauhan, D., and S. R. Shames. 2021. "Pathogenicity and Virulence of *Legionella*: Intracellular replication and host response." *Virulence* 12 (1): 1122-1144. <https://doi.org/10.1080/21505594.2021.1903199>.
- Nácher-Vázquez, Montserrat, Ana Barbosa, Inês Armelino, Andreia Sofia Azevedo, Gonçalo Nieto Almeida, Cristina Pizarro, Nuno Filipe Azevedo, Carina Almeida, and Laura Cerqueira. 2022. "Development of a novel peptide nucleic acid probe for the detection of *Legionella* spp. in water samples." *Microorganisms* 10 (7): 1409. <https://doi.org/10.3390/microorganisms10071409>.
- Nácher-Vázquez, Montserrat, Bruno Santos, Nuno Filipe Azevedo, and Laura Cerqueira. 2022. "The role of Nucleic Acid Mimics (NAMs) on FISH-based techniques and applications for microbial detection." *Microbiological Research*: 127086. <https://doi.org/10.1016/j.micres.2022.127086>.
- Rocha, R., J. M. Sousa, L. Cerqueira, M. J. Vieira, C. Almeida, and N. F. Azevedo. 2019. "Development and application of Peptide Nucleic Acid Fluorescence in situ Hybridization for the specific detection of *Listeria monocytogenes*." *Food Microbiol* 80: 1-8. <https://doi.org/10.1016/j.fm.2018.12.009>.

Acknowledgments

This work was supported by LA/P/0045/2020 (ALiCE), UIDB/00511/2020, and UIDP/00511/2020 (LEPABE), funded by national funds through the FCT/MCTES (PIDDAC); Project FLUDS - Desenvolvimento de sistemas baseados em espectroscopia de fluorescência para detecção microbiana, with reference NORTE-01-0247-FEDER-046970, co-funded by the European Regional Development Fund (ERDF), through the North Portugal Regional Operational Programme (NORTE2020), under the PORTUGAL 2020 Partnership Agreement; Project e.Biofilm – "Creation of a group of Excellence on Engineered Biofilms", Grant Agreement number 101087568, financed by the European Commission in the scope of the Horizon Europe Framework Programme; PhD fellowship 2022.11840.BD is supported by national funds through FCT – Fundação para a Ciência e a Tecnologia.

Development of recombinase-aided amplification combined with nucleic acid lateral flow read-out for the diagnostic of RNA viruses – the detection of SARS-CoV-2 as an example

João Vindeirinho^{1,2,3}, Ricardo Oliveira^{1,2,3}, Eva Pinho^{1,2,3}, Nuno Azevedo^{2,3}, Raquel Guiomar⁴, Ahmed Abd El Wahed⁵, Carina Almeida¹
2 3 6

¹INIAV, I.P, National Institute for Agrarian and Veterinarian Research, Rua dos Latidos, Lugar da Madalena, 4485-655 Vairao, Portugal

²LEPABE-Laboratory for Process Engineering, Environment, Biotechnology and Energy, Faculty of Engineering, University of Porto, Rua Dr. Roberto Frias, 4200-465 Porto, Portugal

³ALiCE-Laboratory for Process Engineering, Environment, Biotechnology and Energy, Faculty of Engineering, University of Porto, Rua Dr. Roberto Frias, 4200-465 Porto, Portugal

Abstract

SARS-CoV-2 accelerated the adoption of affordable, easy-to-use and accurate nucleic acid tests. Nucleic Acid Lateral Flow Assays (NALFAs) are simple, fast and cost-effective assays that can use reporter- and capture- oligonucleotide probes to effectively detect target nucleic acid sequences by naked eye, following an isothermal nucleic acid amplification step. In this context, there is a promising NALFA approach that relies in the tailing of DNA amplicons during the step of amplification, with single strand DNA sequences (ssDNA), allowing their interaction with the NALFA's capture and reporter oligonucleotide probes.

In this work, Reverse Transcription Recombinase-Aided Amplification (RT-RAA) was chosen to produce tailed amplicons and then combined with an in-house developed NALFA (RT-RAA-NALFA), as described above, to evaluate its potential as a high-performance solution for end-point detection of RNA viruses.

SARS-CoV-2 was used as a model. The limit of detection of this assay was found to be 10-10² copies of RNA/μL, which is suitable for use in point-of-care detection of SARS-CoV-2 and other viruses.

These results show a promising option for the development of a point-of-care device, contributing to mitigate large outbreaks caused by RNA viruses like SARS-CoV-2.

Author Keywords. Nucleic Acid Lateral Flow Assays, Oligonucleotide probes, Isothermal Amplification, Reverse Transcription Recombinase-Aided Amplification, RNA detection

1. Introduction

Real time RT-PCR turned to be the gold standard for the detection of SARS-CoV-2. However, such technique is expensive, time-consuming, and mostly laboratory-based, not being feasible for point-of-care diagnostic. There has been an effort to find alternative technologies that can be used to perform an analogue nucleic acid amplification test at the point of-care.

Lateral Flow Assays are simple devices based on the interaction of an analyte in a liquid medium with a specific molecule immobilized on a membrane, which can deliver very fast results, when built to directly detect protein antigens; a method that has also been widely used for the detection of SARS-CoV-2. Nonetheless, drawbacks associated with the detection of protein antigens by LFA include false negatives, reflecting low sensitivity and the use of inadequate testing times, since early protein antigen testing can omit the infection(L. *et al.*, 2022).

NALFAs are usually based on the interaction of an oligonucleotide probe immobilized on the membrane with a second oligonucleotide probe, conjugated by distinct methods with colored nanoparticles (like AuNPs). In this work, a sandwich NALFA assay is proposed, in which the amplicons are tailed with ssDNA tails in the 5' extremities of the forward and reverse primers, enabling the simultaneous capture on the strip by hybridizing with complementary ssDNA capture probes and the colorimetric signaling by hybridizing with complementary ssDNA reporter probes linked to AuNPs(Jauset-Rubio *et al.*, 2016).

RT-RAA is an isothermal amplification method compatible with the addition of ssDNA tails to primers, which can be performed in only 15 minutes, enabling early detection of the infection and making it suitable to establish the desired strategy (Wu *et al.*, 2020).

2. Materials and Methods

Tailed primers for the RdRp gene of SARS-CoV-2 were adapted from published literature (El Wahed *et al.*, 2021). Complementary ssDNA tails were added to the 5' end of the primers, for the recognition by NALFA, while employing gold nanoparticles (AuNPs) as reporter probes; the sequences of both capture and reporter probes were also adapted from literature (Jauset-Rubio *et al.*, 2016) (Magriñá *et al.*, 2019). Two sequences of probes (and respective complementary tails), with two distinct lengths were tested. The RT-RAA amplification protocol with tailed primers was optimized and agarose gel electrophoresis was used as read-out. The NALFA strips were assembled in-house, by using commercial grade components. The capture probes' immobilization on the strips was performed based on the anchor system biotin-streptavidin. A streptavidin solution (5mg/mL) and biotinylated ssDNA capture probes (1.5mg/mL) were conjugated in PBS, ensuring 1:4 streptavidin:biotin ratio. Then, test and control probes, were added to the strip, while pipetting a fixed volume and allowing to air dry for one hour. The NALFA limit of detection was assessed using synthetic RNA as start-point, following RT-RAA with tailed primers.

3. Results

Optimization of the amplification protocol with tailed primers

A pair of primers, already reported in literature for the diagnostic of SARS-CoV-2 (but using a distinct approach) was chosen as a starting point. A first RT-RAA assay was performed, using only the primers without tails. Four types of tailed primers (two distinct sequences, with two lengths) were simultaneously tested, for evaluating what was the best pair.

Upon the selection of the best pair, new optimization rounds followed, assessing the best concentration of primers, temperature and finally the ideal duration of the reaction.

Optimization of NALFA strips

Distinct parameters of NALFA strips were optimized. The volume of probe to immobilize on the strip, the volume and proportion of running buffer, the concentration of AuNPs, or the volume of amplicons to use were the targets of optimization.

Assessment of the limit of detection

The limit of detection of the NALFA strips was accessed, following the test of decreasing copy numbers of SARS-CoV-2 RNA standard (10^5 10^4 10^3 10^2 10^1 10^0 copies/ μ L). When testing three replicates, the limit of detection was found to be in the range 10 - 10^2 copies/ μ L.

4. Discussion

The amplification efficiency of tailed primers was lower than the non-tailed primers, with some pairs of primers tested not yielding amplification; this shows that the tails interfered with the amplification process, although the use of the strategy was still viable if the parameters of the amplification reaction were optimized for the best set of primers. Following the optimization of the aforementioned parameters, the amplification efficiency was improved, being suitable to combine with the NALFA read-out.

The optimal conditions for the detection of RdRp gene by NALFA were found (3.2 section), contributing for the optimal performance of the assay. The limit of detection of the assay was 10-100 copies of RNA/ μ L, which is fit for SARS-CoV-2 diagnostic.

5. Conclusions

The RT-RAA together with NALFA colorimetric device comprehends a simple diagnostic approach, which can be integrated in a device for the detection of SARS-CoV-2 at the point-of-care, exhibiting a suitable limit of detection. The analysis of specificity and sensitivity is still in progress. Furthermore, this assay shows to be promising for simple, end-point detection of other RNA viruses.

References

- Jauset-Rubio, M., Svobodová, M., Mairal, T., McNeil, C., Keegan, N., Saeed, A., et al. (2016) Ultrasensitive, rapid and inexpensive detection of DNA using paper based lateral flow assay. *Scientific Reports* **6**: 37732.
- L., R.M., Agha, M., Nicholas, G., Alec, B., Lydia, G.J., Tong, Y., et al. (2022) Limitations of Molecular and Antigen Test Performance for SARS-CoV-2 in Symptomatic and Asymptomatic COVID-19 Contacts. *Journal of Clinical Microbiology* **60**: e00187-22.
- Magriñá, I., Jauset-Rubio, M., Ortiz, M., Tomaso, H., Simonova, A., Hocek, M., and O’Sullivan, C.K. (2019) Duplex Electrochemical DNA Sensor to Detect Bacillus anthracis CAP and PAG DNA Targets Based on the Incorporation of Tailed Primers and Ferrocene-Labeled dATP. *ACS omega* **4**: 21900–21908.
- El Wahed, A.A., Patel, P., Maier, M., Pietsch, C., Rüster, D., Böhlken-Fascher, S., et al. (2021) Suitcase Lab for Rapid Detection of SARS-CoV-2 Based on Recombinase Polymerase Amplification Assay. *Analytical Chemistry* **93**: 2627–2634.
- Wu, T., Ge, Y., Zhao, K., Zhu, X., Chen, Y., Wu, B., et al. (2020) A reverse-transcription recombinase-aided amplification assay for the rapid detection of N gene of severe acute respiratory syndrome coronavirus 2(SARS-CoV-2). *Virology* **549**: 1–4.

Acknowledgments

This section is conventionally used to thank persons and granting agencies for their help and support. in the revision version of the manuscript this section must be omitted: it gives too much information about the authors to the reviewers.

Biomimetic Surfaces from Cabbage Leaves: A Novel Approach to Prevent Biofilm Formation on Food Environments

Fábio M. Carvalho^{1,2}, Luciana C. Gomes^{1,2}, Marta Lima^{1,2}, Rita Teixeira-Santos^{1,2}, Ana Azevedo^{1,2}, Mohsin Amin³, Mette Burmølle⁴, Jelmer Sjollema⁵, Filipe J. Mergulhão^{1,2} and Kathryn A. Whitehead³

¹LEPABE-Laboratory for Process Engineering, Environment, Biotechnology and Energy, Faculty of Engineering, University of Porto, Rua Dr. Roberto Frias, 4200-465 Porto, Portugal.

²ALiCE - Associate Laboratory in Chemical Engineering, Faculty of Engineering, University of Porto, Rua Dr. Roberto Frias, 4200-465 Porto, Portugal.

³Microbiology at Interfaces, Faculty of Science and Engineering, Manchester Metropolitan University, Manchester M1 5GD, United Kingdom.

⁴Department of Microbiology, University of Copenhagen, Copenhagen, Denmark.

⁵Department of Biomedical Engineering, University of Groningen, University Medical Center Groningen, Groningen, The Netherlands.

Author Keywords. Biomimetic surfaces, Plant leaves, Biofouling, Conditioning film, Food industry.

1. Introduction

Contamination of food contact surfaces is a significant public health concern with severe economic impacts. The effectiveness of standard hygiene procedures is often limited against foodborne pathogens due to their high resistance. Therefore, there is an urgent need for new strategies capable of restricting bacterial proliferation. One approach that has recently gained attention is the development of antifouling surfaces that delay bacterial adhesion, either by antimicrobial coatings or modification of the surface properties. This study aimed to (1) produce and characterize biomimetic surfaces inspired by the topographies and physicochemical characteristics of various plant leaves with self-cleaning and superhydrophobic properties – White cabbage, Tenderheart, Cauliflower and Leek – and (2) evaluate their antifouling activity by attachment, adhesion, and retention assays, the three key phenomena involved in the initiation of biofilm formation. Furthermore, the effect of casein conditioning films on biofilm formation was evaluated as the accumulation of organic matter on surfaces can alter their chemical, physicochemical, and topographic properties.

2. Materials and Methods

The biomimetic surface replicas were synthesised by a moulding technique using wax and characterised by water contact angle measurements (hydrophobicity), Optical Profilometry (roughness), Scanning Electron Microscopy (morphology), and Fourier Transform Infrared Spectroscopy (chemistry). For the microbiological analysis, attachment (spray plus wash assay), adhesion (spray assay), and retention (1-h static incubation) assays were performed using *Escherichia coli*. The culturable cells were enumerated by colony-forming units (CFU), and the surfaces were analysed by Scanning Electron Microscopy. Additionally, 72-h biofilms were formed in 12-well microtiter plates under static conditions and were analysed for the number of culturable cells by CFU, biofilm thickness by Optical Coherence Tomography, and biofilm architecture by Confocal Laser Scanning Microscopy.

3. Discussion

The results showed that, although the macro- and micro-topographies of the original surfaces were well reproduced on the biomimetic surfaces, the presence of nanotopographies was less evident. However, all biomimetic surfaces were more efficient at reducing the number of bacteria bound to the surface than the corresponding original leaves. On the attachment of *E. coli* to biomimetic surfaces, the White Cabbage (the roughest and most hydrophobic surface) showed the highest reduction in cell numbers, approximately 1 Log CFU/cm², compared with the natural White Cabbage, followed by Tenderheart and Cauliflower; biomimetic and natural Leek surfaces did not show significant differences. For the adhesion assays, Tenderheart was the biomimetic surface with the lowest number of *E. coli* cells, and the only one presenting significant reductions from the natural leaves. Following the retention assays, all biomimetic surfaces were significantly more efficient than natural leaves,

exhibiting a reduction of approximately 2 Log CFU/cm². Also, White Cabbage, Tenderheart, and Leek replicas showed lower *E. coli* numbers than the flat control surface. Regarding the biofilm assays, a significant decrease in the number of culturable cells was observed on *E. coli* biofilms formed on both 5% (w/v) casein-conditioned surfaces (up to 50% reduction) and non-conditioned biomimetic surfaces (up to 89% reduction) compared to the flat control, revealing their antifouling properties. Moreover, both unconditioned and conditioned biomimetic surfaces were able to reduce biofilm thickness by up to 26% and 35%, respectively, compared to unconditioned and conditioned flat surfaces.

4. Conclusions

This study highlights moulding as a reliable technique for reproducing the structure of vegetable leaves. The results suggest that these biomimetic surfaces are promising for preventing the initial settlement of bacteria and the development of mature biofilms. The findings of this study have important implications for developing more effective food contact surfaces to enhance food safety and combat foodborne pathogens.

Acknowledgments

This work was financially supported by LA/P/0045/2020 (ALiCE), UIDB/00511/2020 and UIDP/00511/2020 (LEPABE) and project 2022.05314.PTDC, funded by national funds through FCT/MCTES (PIDDAC); project SurfSAFE supported by the European Union's Horizon 2020 Research and Innovation Programme under grant agreement no. 952471; project HealthyWaters (NORTE-01-0145-FEDER-000069) was supported by Norte Portugal Regional Operational Programme (NORTE 2020), under the PORTUGAL 2020 Partnership Agreement, through the European Regional Development Fund (ERDF). Fábio M. Carvalho, Marta Lima and Ana Azevedo thank the Portuguese Foundation for Science and Technology (FCT) for the financial support of their PhD grants: 2022.12705.BD, 2022.11196.BD, and 2020.07427.BD, respectively.

Development of antifouling surfaces coated with chitosan from *Loligo opalescens* for marine applications

Marta Lima^{1,2}, Luciana C. Gomes^{1,2}, Rita Teixeira-Santos^{1,2}, Maria J. Romeu^{1,2}, Jesus Valcarcel³, José A. Vázquez³, Miguel A. Cerqueira⁴, Lorenzo Pastrana⁴, Ana I. Bourbon⁴, Ed.d. De Jong⁵, Jelmer Sjollema⁵, Filipe J. Mergulhão^{1,2,*}

¹LEPABE-Laboratory for Process Engineering, Environment, Biotechnology and Energy, Faculty of Engineering, University of Porto, Rua Dr. Roberto Frias, 4200-465 Porto, Portugal; up201604683@fe.up.pt (M.L.)

²ALiCE - Associate Laboratory in Chemical Engineering, Faculty of Engineering, University of Porto, Rua Dr. Roberto Frias, 4200-465 Porto, Portugal

³Grupo de Reciclado y Valorización de Materiales Residuales (REVAL), Instituto de Investigaciones Marinas (IIM-CSIC), C/Eduardo Cabello, 6, CP36208 Vigo, Galicia, Spain

⁴International Iberian Nanotechnology Laboratory, Department of Life Sciences, Av. Mestre José Veiga s/n, 4715-330 Braga, Portugal

⁵Department of Biomedical Engineering University of Groningen, University Medical Center Groningen, Groningen, The Netherlands

*Corresponding author: filipem@fe.up.pt

Abstract

Marine biofouling is often associated with biofilm formation on submerged surfaces, which causes economic and environmental problems. Although several biocides and cleaners have been used to control biofouling, new eco-friendly antifouling approaches are required. Chitosan (CS) is a polysaccharide widely used due to its outstanding properties, namely its antimicrobial activity. This work aimed to produce and characterise poly(lactic acid) (PLA)-CS surfaces with CS of different molecular weight (Mw) at different concentrations for application in marine paints. The antimicrobial performance of these surfaces was assessed against *Cobetia marina* for 7 weeks under controlled hydrodynamic conditions. All CS surfaces exerted a significant antimicrobial action by reducing the number of culturable cells up to 69% compared to control, being this activity dependent on CS Mw. Optical Coherence Tomography analysis corroborated these results, showing reductions in biofilm thickness of up to 36%. Overall, CS coatings represent a promising approach to reducing biofouling in marine environments.

Author Keywords. Chitosan, marine biofouling, marine waste, biofilm formation, antifouling coatings

1. Introduction

In marine environments, natural and artificial submerged structures are quickly colonised by marine organisms in a process known as biofouling (Faria et al. 2020). This natural and complex process is responsible for several economic, industrial, environmental, and health problems (Tian et al. 2020). The attachment of fouling organisms to marine vessels increases drag resistance, which leads to higher fuel consumption and environmental pollution, changes the physicochemical properties of the surfaces, and contributes to species invasion (Tian et al. 2020; Lacoursière-Roussel et al. 2016). Since biofilm formation is one of the first steps of this process, a potential strategy to delay macrofouling is to prevent adhesion and biofilm formation by marine bacteria. Although several biocides, cleaners, and antifouling agents have been used to mitigate biofilm formation, their negative impact on marine ecosystems and human health (Amara et al. 2018) stresses the need to develop novel sustainable and eco-friendly approaches to prevent marine biofouling in ship hulls such as bio-based coatings. Chitosan (CS) is a polysaccharide obtained by deacetylation of chitin, which can be extracted from marine sources and microorganisms. Besides the use of CS enables the valorization of fish processing industry waste, CS has been widely used due to its interesting biological properties, namely the antimicrobial activity, which depends on a set of properties such as molecular weight (Mw), degree of deacetylation, concentration, and source (Kong et al. 2010; Chandrasekaran, Kim, and Chun 2020). The present study

aimed to (i) produce and characterise poly(lactic acid) (PLA) surfaces coated with CS of different Mw and concentrations obtained from the *Loligo opalescens* pen, and (ii) evaluate the antifouling activity of these surfaces against *Cobetia marina* under nutritional conditions, temperature, and hydrodynamics that mimics the conditions typically found in some marine environments.

2. Materials and Methods

A combination of enzymatic and alkaline treatments was used to extract CS from *Loligo opalescens* pens, which was depolymerised into derivatives of different molecular weight (Mw). After dip coating the PLA films with 0.5% and 1% (w/v) of CS and its derivatives, the physical and chemical properties of the produced surfaces were assessed by Atomic Force Microscopy, contact angle measurements, and Scanning Electron Microscopy. The antifouling assays were performed with *Cobetia marina* for 7 weeks at 25 °C under controlled hydrodynamic conditions that mimic a ship in a harbor. Våatanen Nine Salt Solution (VNSS) medium was prepared as previously described (Holmström et al. 1998) and used to simulate the nutritional conditions found in marine environments. The biofilms formed were analysed by colony-forming unit counts to determine the number of culturable cells and by Optical Coherence Tomography (OCT) to analyse the biofilm thickness and architecture.

3. Discussion

The analysis of biofilm composition revealed that PLA films coated with 0.5% and 1% (w/v) CS exerted a significant antimicrobial effect by reducing the number of culturable cells by up to 58% and 69%, respectively, compared to the control. Regardless of the CS concentration, the results suggest that CS coatings with lower Mw CS had higher antimicrobial activity since the most active surfaces were those coated with CS1, CS2, and CS3 with 186, 129, and 61 kDa, respectively (Lima et al. 2022).

OCT imaging was used to assess the thickness and architecture of *C. marina* biofilms. Regarding biofilm thickness, significant reductions were observed for all functionalized surfaces compared with PLA. This antifouling effect was higher on biofilms developed on PLA-CS1, PLA-CS2 and PLA-CS3 surfaces, achieving thickness reductions of up to 36%. In general, no significant differences between the concentrations of 0.5% and 1% (w/v) CS were observed in biofilm culturability and thickness. Concerning *C. marina* biofilm architecture, regardless of the CS concentration, biofilms developed on PLA-CS surfaces presented visible differences in their structures compared with those grown on PLA films. Biofilms formed on the functionalized surfaces were more homogeneous and compact, while those formed on the control surface presented more prominent and irregular structures. These results were corroborated by the biofilm cell counts and thickness, revealing that both native CS and its derivatives prevented *C. marina* biofilm development (Lima et al. 2022).

4. Conclusions

CS coatings showed long-term and Mw-dependent antifouling performance against *C. marina* biofilms under the marine environmental conditions mimicked in this work. Overall, the incorporation of CS in marine paints may be a promising eco-friendly antifouling approach to reduce biofouling on ship hulls, simultaneously contributing to the valorization of marine waste.

References

- Amara, I., W. Miled, R. B. Slama, and N. Ladhari. 2018. "Antifouling processes and toxicity effects of antifouling paints on marine environment. A review." *Environ Toxicol Pharmacol* 57: 115-130. <https://doi.org/10.1016/j.etap.2017.12.001>.
- Chandrasekaran, Murugesan, Ki D. Kim, and Se C. Chun. 2020. Antibacterial Activity of Chitosan Nanoparticles: A Review. *Processes* 8 (9). <https://doi.org/10.3390/pr8091173>.
- Faria, Sara I., Rita Teixeira-Santos, Luciana C. Gomes, Elisabete R. Silva, João Morais, Vítor Vasconcelos, and Filipe J. M. Mergulhão. 2020. "Experimental Assessment of the Performance of Two Marine Coatings to Curb Biofilm Formation of Microfoulers." *Coatings* 10 (9): 893. <https://www.mdpi.com/2079-6412/10/9/893>.
- Holmström, C., S. James, B. A. Neilan, D. C. White, and S. Kjelleberg. 1998. "Pseudoalteromonas tunicata sp. nov., a bacterium that produces antifouling agents." *Int J Syst Bacteriol* 48 Pt 4: 1205-12. <https://doi.org/10.1099/00207713-48-4-1205>.
- Kong, M., X. G. Chen, K. Xing, and H. J. Park. 2010. "Antimicrobial properties of chitosan and mode of action: a state of the art review." *Int J Food Microbiol* 144 (1): 51-63. <https://doi.org/10.1016/j.ijfoodmicro.2010.09.012>.

Lacoursière-Roussel, Anaïs, Dan Bock, Melania Cristescu, Frédéric Guichard, and Christopher McKindsey. 2016. "Effect of shipping traffic on biofouling invasion success at population and community levels." *Biol Invasions* 18. <https://doi.org/10.1007/s10530-016-1258-3>.

Lima, Marta, Luciana C. Gomes, Rita Teixeira-Santos, Maria J. Romeu, Jesus Valcarcel, José Antonio Vázquez, Miguel A. Cerqueira, Lorenzo Pastrana, Ana I. Bourbon, Ed D. de Jong, Jelmer Sjollema, and Filipe J. Mergulhão. 2022. "Assessment of the Antibiofilm Performance of Chitosan-Based Surfaces in Marine Environments." *Int J Mol Sci* 23 (23): 14647. <https://www.mdpi.com/1422-0067/23/23/14647>.

Tian, Limei, Yue Yin, Huichao Jin, Wei Bing, E. Jin, Jie Zhao, and Luquan Ren. 2020. "Novel marine antifouling coatings inspired by corals." *Mater Today Chem* 17: 100294. <https://doi.org/10.1016/j.mtchem.2020.100294>.

Acknowledgments

This work was financially supported by: LA/P/0045/2020 (ALiCE), UIDB/00511/2020 and UIDP/00511/2020 (LEPABE) were funded by national funds through the FCT/MCTES (PIDDAC); project HealthyWaters (NORTE-01-0145-FEDER-000069) was supported by Norte Portugal Regional Operational Programme (NORTE 2020), under the PORTUGAL 2020 Partnership Agreement, through the European Regional Development Fund (ERDF); CVMAR + I—Industrial Innovation and Marine Biotechnology Valorization” project was funded by INTERREG V Espanha Portugal (POCTEP) (0302_CVMAR_I_1_P). The research was also supported by the SurfSAFE project funded by the European Union’s Horizon 2020 research and innovation programme under grant agreement No. 952471. A.I.B. thanks the Portuguese Foundation for Science and Technology (FCT) for the financial support of her work contract through the Scientific Employment Stimulus— Individual Call (ref. 2020.03447.CEECIND). R.T.-S. acknowledges the receipt of a junior researcher fellowship from the Project PTDC/CTM-COM/4844/2020 (NanoCAT) supported by national funds through the FCT/MCTES (PIDDAC). M.L. and M.J.R. also acknowledge FCT for their PhD grants (2022.11196.BD and SFRH/BD/140080/2018, respectively). J.A.V. and J.V. also thank Xunta de Galicia by Xunta de Galicia (Grupos de Potencial Crecimiento, IN607B 2018/2019) for the financial support. Support from the EURO-MIC COST Action (CA20130) is acknowledged.

Incorporation of agro-industrial by-products extracts as an alternative to synthetic UV filters to develop a value-added sunscreen

Mariana Messias^{1,2*}, Sara M. Ferreira^{1,2}, Loleny Tavares^{3,4}, Lúcia Santos^{1,2}

¹LEPABE – Laboratory for Process Engineering, Environment, Biotechnology and Energy, Faculty de Engineering, University of Porto, Rua Dr. Roberto Frias, 4200-465 Porto, Portugal

²ALiCE – Associate Laboratory in Chemical Engineering, Faculty de Engineering, University of Porto, Rua Dr. Roberto Frias, 4200-465 Porto, Portugal

³ESAN – School of Design, Management and Production Technologies Northern Aveiro, University of Aveiro, Estrada do Cercal 449, 3720-509, Oliveira de Azeméis, Santiago de Riba-UI, Portugal

⁴CICECO-Aveiro – Institute of Materials, Campus Universitário de Santiago, University of Aveiro, 3810-193 Aveiro, Portugal

*Corresponding author: e-mail address: up201806148@edu.fe.up.pt ; ORCID ID 0009-0005-2183-5394

Abstract

The negative impact of synthetic UV filters in sunscreens is a growing concern, as studies have found that these compounds can be harmful and toxic to aquatic organisms and humans, which causes a necessity to find new, safe and non-pollutant compounds to act as UV filters. Plant extracts containing phenolic compounds have shown promise and sustainable alternative to synthetic UV filters to produce sunscreen formulations due to their high antioxidant capacity and UV filters properties. However, these compounds are very sensitive to light and pH, and the microencapsulation technology arises as solution to protect them when incorporated in cosmetic formulations. This project consists in producing a sunscreen incorporating microencapsulated onion peel extract. The characterization of the extract revealed a great antioxidant capacity and a significant presence of quercetin. The following steps are to microencapsulate the extract, incorporate it in the formulation and evaluate the performance of the sunscreen.

Author Keywords. Sunscreen, onion peel, phenolic compounds, UV filters, microencapsulation.

1. Introduction

Prolonged exposure to sunlight is harmful for the skin, being the cause of several skin diseases, such as skin cancer, solar burn and hyperpigmentation. Sunscreens appear as the solution for people to safely benefit from the sunlight without harming their skin. Nowadays, most sunscreens available on the market have synthetic UV filters in their formulations. However, some synthetic UV filters have been proved to be toxic to marine species and human body, which lead to them being removed from the market (Jesus et al. 2022).

In recent years, there has been growing interest among the scientific community in plant extracts containing polyphenols as a natural alternative to synthetic UV filters. Polyphenols are known to be rich in antioxidants and present a strong photo-protection capacity. Although having these properties, polyphenolic compounds are highly sensitive to light, pH, temperature and oxygen, being easily oxidized and losing their bioactive interest. A protector of these compounds is then necessary, and microencapsulation is presented as a possible solution.

An interesting source of plant extracts are agricultural by-products as they are cheap to obtain and rich in bioactive compounds and by incorporating them in cosmetics we are contributing to the circular economy model (Ferreira, Gomes, and Santos 2023). Hence, this works proposes to formulate a sunscreen with microencapsulated onion peel extract incorporated and evaluate its properties.

2. Materials and Methods

The onion peel extract was obtained by performing a solid-liquid extraction for 2 hr, using a Soxhlet apparatus. The solvent used was ethanol. The antioxidant capacity was evaluated by carrying out the Total Phenolic Content method (TPC), the DPPH (2,2-diphenyl-1-picrylhydrazyl) and the ABTS (2,2-azinobis (3-ethyl-benzothiazolin-6-sulfonic acid)) assays. To analyze the photo-protection capacity of

the OP extract, it was studied its Sun Protection Factor (SPF), using a spectrophotometer method. The quantification of the main phenolic compounds present in the extract was achieved by high-performance liquid chromatography- diode array (HPLC-DAD). All the tests performed were done according to the protocols of (Ferreira, Gomes, and Santos 2023).

3. Discussion

The values obtained for the characterization of the extract are presented in **Table 1**.

TPC ($\text{mg}_{\text{GAE}} \text{g}^{-1}_{\text{extract}}$)		585.23 \pm 10.43
DPPH	TE ($\text{mg}_{\text{TE}} \text{g}^{-1}_{\text{extract}}$)	199.71 \pm 1.16
	IC ₅₀ (mg L^{-1})	31.01 \pm 1.98
ABTS ($\text{mg}_{\text{TEAC}} \text{g}^{-1}_{\text{extract}}$)		381.45 \pm 8.05
HPLC-DAD	Quercetin (mg/g dried extract)	2.46
	Resveratrol (mg/g dried extract)	0.24

The results are expressed as mean \pm standard deviations of 4 independent measurements. TPC: total phenolic content; GAE: gallic acid equivalents; IC₅₀: the concentration of extract necessary to inhibit 50% of DPPH radical; TE: Trolox equivalents; TEAC: Trolox equivalent antioxidant capacity.

Table 1 : Characterization of the Onion Peel Extract regarding its antioxidant capacity and compounds identified by HPLC-DAD.

The TPC value obtained is within the range of the literature values, but it is closer to the higher values of the literature which demonstrates a high phenolic content in this extract (Benito-Román et al. 2020). It is also important to evidence the value of the half maximal inhibitory concentration (IC₅₀), which represents the concentration of extract needed to inhibit 50 % of the DPPH present in solution. The obtained value is inferior to 50 mg L^{-1} , which means this extract is considered a very strong antioxidant (Fitrasyah et al. 2021).

Quercetin and resveratrol were the found to be the main phenolic compounds present in the onion peels extract, which is in accordance with the literature.

The sun protection factor was analyzed for different concentration of onion peel (OP) extract and was compared to a synthetic UV filter serving as positive control (oxybenzone), as presented in **Table 2**. The absorbance spectra are illustrated in **Figure 11**.

Sample	Concentration (mg mL^{-1})	SPF
Oxybenzone (positive control)	0.010	5.39
Onion Peel Extract (OP)	0.045	3.73
Onion Peel Extract (OP)	0.095	9.04
Onion Peel Extract (OP)	0.010	0.89

Table 2 : Sun Protection Factor for different concentration of Onion Peel Extract.

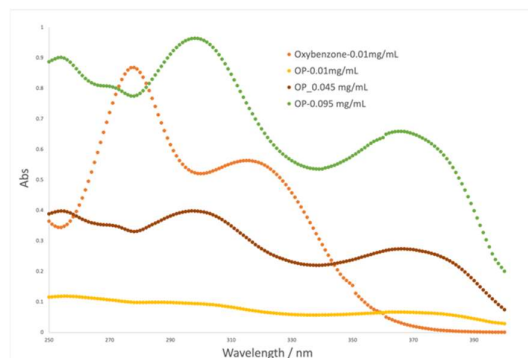


Figure 11 : Absorbance spectra of the several solutions.

It is observed that, the onion peel extract can achieve the same and higher values of SPF than the value for the synthetic UV filter. However, the onion peel extract needs to be in a more concentrated solution to achieve the same values of SPF. Nevertheless, the fact that it presents good results in terms of its photo-protection capacity means this extract presents itself as a good alternative for a UV filter. In **Figure 11**, it is shown that OP absorbs in the same UV region as oxybenzone, and also at higher values of wavelength (350 – 390 nm), in which oxybenzone does not absorb, possibly providing protection against a wider range of UV radiation than the synthetic compound.

To protect phenolic compounds when incorporating them in cosmetic formulations, a microencapsulation method, based on the protocol presented by (Kalogeropoulos et al. 2010), is being optimized. The microparticles, containing the onion peel extract, will be incorporated in a sunscreen formulation and its physicochemical properties, stability and SPF value will be studied across 4 weeks. The results will be compared to a formulation containing the non-microencapsulated extract.

4. Conclusions

The results of the characterization of the OP extract revealed that the extract is a promising alternative to synthetic UV filters used in cosmetic formulations. This suggests that several by-products from the agri-cultural sector may be reused to develop value-added products. After defining the microencapsulation protocol, the following step is to incorporate the OP extract in the formulation and evaluate its photo-protection capacity, as well as the performance of the sunscreen along the time.

References

- Benito-Román, Óscar, Beatriz Blanco, María T. Sanz, and Sagrario Beltrán. 2020. Subcritical Water Extraction of Phenolic Compounds from Onion Skin Wastes (*Allium cepa* cv. Horcal): Effect of Temperature and Solvent Properties. *Antioxidants* 9 (12). doi:10.3390/antiox9121233.
- Ferreira, Sara M., Sandra M. Gomes, and Lúcia Santos. 2023. A Novel Approach in Skin Care: By-Product Extracts as Natural UV Filters and an Alternative to Synthetic Ones. *Molecules* 28 (5). doi:10.3390/molecules28052037.
- Fitrasyah, Siti Ika, Ariani Ariani, Nurdin Rahman, Nurulfuadi Nurulfuadi, Ummu Aiman, Devi Nadila, Fendi Pradana, Aulia Rakhman, and Diah Ayu Hartini. 2021. "Analysis of Chemical Properties and Antioxidant Activity of Sambiloto (*Andrographis paniculata* Nees.) Leaf Tea Formula as a Functional Drink in Preventing Coronavirus Diseases and Degenerative Diseases." *Open Access Macedonian Journal of Medical Sciences (OAMJMS)* 9 (A):196-201. doi: 10.3889/oamjms.2021.5872.
- Jesus, Ana, Emília Sousa, Maria T. Cruz, Honorina Cidade, José M. Sousa Lobo, and Isabel F. Almeida. 2022. UV Filters: Challenges and Prospects. *Pharmaceuticals* 15 (3). doi:10.3390/ph15030263.
- Kalogeropoulos, Nick, Konstantina Yannakopoulou, Aristeia Gioxari, Antonia Chiou, and Dimitris P. Makris. 2010. "Polyphenol characterization and encapsulation in β -cyclodextrin of a flavonoid-rich *Hypericum perforatum* (St John's wort) extract." *LWT - Food Science and Technology* 43 (6):882-889. doi: <https://doi.org/10.1016/j.lwt.2010.01.016>.

Acknowledgments

This work was financially supported by: LA/P/0045/2020 (ALiCE), UIDB/00511/2020 and UIDP/00511/2020 (LEPABE) and funded by the project S4Hort_Soil&Food – Sustainable practices for Soil health & horticultural products quality improvement in the Entre Douro e Minho Region, with reference NORTE-01-0145-FEDER-000074, co-financed by the European Regional Development Fund (ERDF), through the North Portugal Regional Operational Programme (NORTE2020), under the PORTUGAL 2020 Partnership Agreement.

Sara M. Ferreira would like to thank the Portuguese Foundation for Science and Technology (FCT) for her PhD grant (2022.10910.BD).

Photoinactivation of clinical strains of *Staphylococcus aureus* using curcumin as photosensitizer agent

Ariana S. C. Gonçalves^{1,2}, Manuel Simões^{1,2,3*}, Anabela Borges^{1,2,3*}

¹LEPABE—Laboratory for Process Engineering, Environment, Biotechnology and Energy, Faculty of Engineering, University of Porto, Rua Dr. Roberto Frias, 4200-465 Porto, Portugal

²ALICE—Associate Laboratory for Innovation in Chemical Engineering, Faculty of Engineering, University of Porto, Rua Dr. Roberto Frias, s/n, 4200-465 Porto, Portugal

³DEQ—Department of Chemical Engineering, Faculty of Engineering, University of Porto, Rua Dr. Roberto Frias, s/n, 4200-465 Porto, Portugal.

*Corresponding authors: Manuel Simões-(mvs@fe.up.pt) ORCID 0000-0002-3355-4398; Anabela Borges-(apborges@fe.up.pt) ORCID 0000-0001-6929-6805

Abstract

Phytochemicals present excellent physicochemical properties that allow their application as photosensitizers. Herein, the efficacy of blue light to photoactivate curcumin (CU) and in turn promote its antimicrobial activity against two clinical strains of *Staphylococcus aureus* (CECT 976 and MJMC568-B), including methicillin-resistant (MRSA), was investigated. Additionally, the photodynamic antimicrobial effect of this plant secondary metabolite on the improvement of less effective antibiotics (mupirocin-Mup, methicillin-Met, tetracycline-Tet and tobramycin-Tob) was explored. The obtained results reveal that the photoactivation (420 nm, 30 mW/cm², 10 min) of CU leads to a 32-fold reduction in its minimum inhibitory concentration (200 µg/mL). Only the combination of CU with Tob and Mup, showed a synergistic effect. These combinations were photoactivated and the CU-Tob combination promoted 100% of photoinactivation for MRSA strain. Photoactivated CU-Tob combination demonstrated for the first time a great antimicrobial potential for the treatment of *S. aureus* infections.

Author Keywords. Antibiotic Combinations, Bacterial Infections, Multi-Drug Resistance, Curcumin, Phytochemicals, Photosensitizers Agents.

1. Introduction

Antimicrobial photodynamic inactivation (aPDI) has been widely studied as a promising strategy to face the global problem of antibiotic resistance amongst clinical relevant bacterial pathogens (Borges et al. 2015). This approach explores the induction of cell cytotoxicity through the production of reactive oxygen species (ROS) (Gonçalves et al. 2023). This process involves the transition from a low energy level (ground state) to a high energy level (excited state). The reduced photosensitizer can interact with oxygen through a redox reaction, leading to ROS production molecules that cause irreversible damage to cellular structures, including the membrane and DNA, which can lead to cell death (Gonçalves et al. 2023). In this context, the identification of natural photosensitizers from plants, *i.e.* phytochemicals, emerged as an attractive eco-friendly and cost-effective way to effectively suppress bacterial resistance mechanisms.

The aim of this study is to develop innovative antimicrobial strategies using curcumin (CU) to develop a novel and natural system for photoinactivation of two clinical strains of *Staphylococcus aureus*. This approach also focuses on the activity recovery of less effective antibiotics based on a combinatorial approach.

2. Materials and Methods

Bacterial strains and antibacterial compounds

S. aureus CECT 976 and MJMC568-B were used in this study. *S. aureus* MJMC568-B (methicillin-resistant-MRSA) was isolated from patients with diabetic feet at the Centro Hospitalar de Trás-os-Montes e Alto Douro (Portugal). *S. aureus* CECT 976 (methicillin-susceptible-MSSA) was used as model microorganism. A stock solution of CU, mupirocin (Mup), methicillin (Met), tetracycline (Tet), and tobramycin (Tob) (Sigma-Aldrich) were prepared in dimethyl sulfoxide (DMSO, Sigma)/distilled water (Met and Tob) and was stored at -20 °C until use.

Minimum inhibitory and bactericidal concentrations determination

The minimum inhibitory concentration (MIC) of each compound to be tested was firstly determined using the broth microdilution method (Borges et al. 2013). For each bacterium, different concentrations of CU (6.25-1000 µg/mL) and antibiotics (0.0625-1024 µg/mL) were used. Subsequently, the minimum bactericidal concentration (MBC) was assessed by plating 10 µL of the well contents on plate count agar.

Antibiotic-potential assay

The synergistic activity of the phytochemical-antibiotic combinations were assessed by disc diffusion test (DDT) and checkerboard assay (CKB) (Abreu et al. 2014). In DDT, CU was incorporated into Mueller–Hinton agar at 1/10×MIC. Sterile blank discs were placed on the agar plates and were impregnated with 15 µL of each antibiotic (at concentration recommended by the CLSI guidelines). In CKB, CU and each antibiotic was tested at concentrations ranging from 1/64 to 2×MIC. Readings at 600 nm were measured spectrophotometrically.

aPDI assay

The antimicrobial photodynamic capabilities of CU and their photoactivated combinations were tested using an LED emitting visible light at 420 nm during 10 min, with a power density of 30 mW/cm², under a laminar-flow hood in the dark. Cells were incubated for 30 min before irradiation (37°C, 150 rpm). After irradiation, the cells were incubated for 6 hours (37°C, 150 rpm). The culturability of the cells was assessed after 30 min and 6 hours of incubation. The control groups were maintained in the dark.

3. Results and Discussion

Antimicrobial resistance (AMR) is one of the greatest threats to global health. Phytochemicals can act as antibacterial agents through different mechanisms of action (Borges et al. 2015). Particularly, the ROS production capacity of phytochemicals when photoactivated has shown positive results. CU has been extensively studied as a photosensitizer (Gonçalves et al. 2023). However, the photoactivation of CU-antibiotic combinations is still largely unexplored. Therefore, the aim of this study was to evaluate the antimicrobial photodynamic activity of CU and its combinatorial effect with 4 conventional topical antibiotics against two clinical isolates of *S. aureus* (CECT 976 and MJMC568-B). For this purpose, the MIC and MBC values of all tested compounds were firstly evaluated (see Table 3). The MIC and MBC values for *S. aureus* MJMC568-B are higher than those determined for *S. aureus* CECT 976. These results are supported by the higher antibiotic resistance usually displayed by the clinical strains (Luo et al. 2018). The results of the antibiotic potentiation tests showed that CU-Mup and CU-Tob had a synergistic effect. This potentiation may be due to increased cell membrane damage and oxidative stress promoted by CU (Kali et al. 2016).

The results of the photoactivation of CU showed that its irradiation (10 min) resulted in a 32-fold reduction in MIC values compared to the same condition without irradiation. These results suggest that CU has remarkable photodynamic capabilities and that it can enhance its antimicrobial activity when exposed to blue light.

Photoactivation of CU-Tob and CU-Mup combinations in the aPDI assay showed that both combinations caused a decrease in culturable cells. However, the CU-Tob combination showed the best results (approximately 4 and 9 log (P<0.0001) reductions (CFU/mL) for *S. aureus* CECT 976 and MJMC568-B, respectively). In the case of aPDI of *S. aureus* MJMC568-B, the combination CU-Tob allowed 100% inactivation of the culturable cells (see Figure 1). The photoactivated CU-Tob combination showed excellent ability to photoinactivate the clinical strain MRSA and simultaneously restore the antimicrobial activity of Tob.

Compound	<i>S. aureus</i> CECT 976		<i>S. aureus</i> MJMC568-B	
	MIC	MBC	MIC	MBC
CU	200	>1000	200	>1000
Mup	8	8	16	512
Met	4	64	512	512
Tet	8	32	8	128
Tob	4	4	64	256

Table 1: MIC and MBC values of CU and selected antibiotics against *S. aureus* strains. The MIC and MBC values are represented in $\mu\text{g/mL}$.

4. Conclusions

In this study it was demonstrated for the first time that photoactivation of the CU-Tob led to promising antimicrobial effects against *S. aureus*. This study also highlights the potential of photoactivated CU to restore the antibacterial activity of less effective antibiotics. Further studies are underway to investigate the antimicrobial mechanisms of action of the photoactivated combinations.

References

- Abreu, Ana Cristina, Sofia C Serra, Anabela Borges, Maria José Saavedra, António J Salgado, and Manuel Simões. 2014. "Evaluation of the best method to assess antibiotic potentiation by phytochemicals against *Staphylococcus aureus*." *Diagnostic Microbiology and Infectious Disease* 79 (2):125-134.
- Borges, Anabela, Carla Ferreira, Maria J Saavedra, and Manuel Simões. 2013. "Antibacterial activity and mode of action of ferulic and gallic acids against pathogenic bacteria." *Microbial drug resistance* 19 (4):256-265.
- Borges, Anabela, Maria J Saavedra, and Manuel Simoes. 2015. "Insights on antimicrobial resistance, biofilms and the use of phytochemicals as new antimicrobial agents." *Current medicinal chemistry* 22 (21):2590-2614.
- Gonçalves, Ariana SC, Miguel M Leitão, Manuel Simões, and Anabela Borges. 2023. "The action of phytochemicals in biofilm control." *Natural Product Reports*.
- Kali, Arunava, Devaraj Bhuvaneshwar, Pravin MV Charles, and Kunigal Srinivasaiah Seetha. 2016. "Antibacterial synergy of curcumin with antibiotics against biofilm producing clinical bacterial isolates." *Journal of basic and clinical pharmacy* 7 (3):93.
- Luo, Kui, Fuye Shao, Kadijatu N Kamara, Shuaiyin Chen, Rongguang Zhang, Guangcai Duan, and Haiyan Yang. 2018. "Molecular characteristics of antimicrobial resistance and virulence determinants of *Staphylococcus aureus* isolates derived from clinical infection and food." *Journal of Clinical Laboratory Analysis* 32 (7):e22456.

Acknowledgments

This work was supported by LA/P/0045/2020 (ALiCE), UIDP/00511/2020 (LEPABE) and FCT – Portuguese Foundation for Science and Technology through the Scientific Employment Stimulus—Individual Call—[CEECIND/00823/2021] and PhD fellowship (2022.10913.BD).

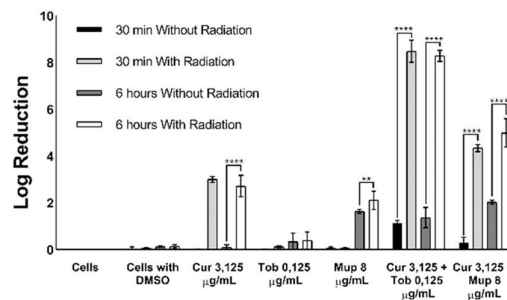


Figure 2: Photoinactivation of *S. aureus* MJMC568-B by CU-Tob and CU-Mup combinations (420 nm, 30 mW/cm², 10 min) after 30 min and 6 hours of incubation.

5. Posters to be displayed in the Symposium

- Mariana Sousa, Ana C. Afonso, Lília Soares Teixeira, Anabela Borges, Maria José Saavedra, Lúcia Chaves Simões and Manuel Simões: The antimicrobial and antibiofilm activity of novel phytochemicals against *Escherichia coli*. #21
- João P. Santos, Nuno Guimarães, Eva Pinho, Rita S. Santos and Nuno Azevedo: Delivery of Nucleic Acid Mimics into bacteria: effect of liposome composition in delivery efficiency. #24
- Manuel Peñas-Garzón, Almudena Gómez-Avilés, Javier Álvarez-Conde, Jorge Bedia, Eva M. García-Frutos and Carolina Belver: Metal-free sensitization of TiO₂ for photocatalytic removal of pharmaceuticals under solar irradiation. #38
- Diana Pinto, Manuela M. Moreira, Anna Vallverdú-Queralt, Cristina Delerue-Matos and Francisca Rodrigues: Bioactivity and phenolic composition of chestnut shells extract before and after *in-vitro* simulated gastrointestinal digestion. #56
- Filipa Teixeira, Ana Margarida Silva, Cristina Delerue-Matos and Francisca Rodrigues: Bioactive composition of goji berries extracted by Ultrasound-Assisted Extraction: Validation of a mathematical model. #68
- Yara B. Bastos, Antónia Gonçalves, Berta M.A.N. Estevinho and Fernando Rocha: Microparticles containing *Fragaria vesca* leaf extract produced with biopolymeric matrices: Binary and ternary blends of alginate, pectin and carrageenan. #83
- Beatriz T. Magalhães, João T. S. Coimbra, Rita S. Santos, Nuno F. Azevedo, Pedro A. Fernandes: Evaluating the diffusion of NAMs across the bacterial envelope. #86
- Filipe Almeida, Fernando Rocha and António Azevedo Ferreira: Continuous gas-liquid mass transfer in an oscillatory flow reactor provided with smooth periodic constrictions. #109
- Mariana B. S. Felgueiras, Manuel F. R. Pereira, Olívia S. G. P. Soares: Screening of supports and metal phases to obtain highly active catalysts for the CO₂ conversion in C₂₊ products. #111
- Gabriela P. Queirós, Clara Pereira and André M. Pereira: Investigation of different gel polymer electrolytes for flexible electrochromic supercapacitors. #119
- Ana Rita F. Pereira, Inês Gomes and Manuel Simões: Are parabens a hushed threat to drinking water microbiological quality? #121
- Rafaela Mulinari Cabral, Claudio Akamatsu, Natiéli Cristina Mendes Ross, Ramiro José Espinheira Martins, Juliana Martins Teixeira de Abreu Pietrobelli: Ecological brick production from water treatment sludge in Brazil. #142
- Thais Theomaris Grabowski and Ramiro José Espinheira Martins: Treatment of effluent from the olive pomace oil extraction industry by coagulation. #146
- Ana C. Afonso, Inês Gomes, Maria José Saavedra, Lúcia Simões and Manuel Simões: *Delftia acidovorans* extracellular metabolites increase the biomass and metabolic activity of drinking water biofilms. #173
- Mariana Gomes, Yana Zamoshchak, Dinesh Dhumal, Ling Peng, Rita S. Santos, Nuno F. Azevedo: Delivering antisense NAMs into bacteria using dendritic lipids. #197
- Ricardo Oliveira, Eva Pinho, Nuno F. Azevedo and Carina Almeida: Selection of nucleic acid mimic (NAM) aptamers: from de novo SELEX to post-SELEX enhancement. #262
- Maria Teresa Oliveira, Isabel Barbosa, Margarida Brito, Cláudia G. Silva and Ricardo J. Santos: CFD design of photocatalytic mesostructured reactors for ammonia production. #268

- Sara Ferreira and Lúcia Santos: Phenolic rich extracts from by-products: promising compounds for the development of value-added foods. #296
- Racha Mansourj, Thais Theomaris Grabowski and Ramiro José Espinheira Martins: Efficient wastewater treatment in olive pomace oil extraction industry using Fenton method. #334
- Rita Marques, Tânia Lopes, Adélio Mendes: Active and stable Iridium-based catalyst for conducting oxygen evolution reaction in a proton exchange membrane electrolyser. #339
- Ingrid D. Soares, Isabel Maria Duque Martins, Júlia C. Kessler, Christianne Elisabete da Costa Rodrigues and Alírio Egídio Rodrigues: Identification of aromatic compounds in cocoa bean shells compared to natural cocoa powder. #340
- Ana Rosa Silva, Diogo Narciso, Luciana Gomes, Fernando Martins, Luís F. Melo and Ana Pereira: Evaluating the impact of thermal disinfection on *Pseudomonas fluorescens* biofilm structures using a CDC biofilm reactor. #341
- Violina B. Barbosa, Laura Cerqueira, João Miranda and Nuno F. Azevedo: Microparticles separation in microchannels. #345
- Paula Esteiro Simón and Elisa González-Romero: Looking for the toxin. #350
- Ana Rita T. Fernandes, Ana Rita Lado Teixeira Ribeiro, Luís M. Madeira and Adrián M.T. Silva: Direct contact membrane distillation-promoted persulfate activation as an innovative approach in water desalination. #351
- Ana M. Chávez, Joaquim L. Faria, Cláudia G. Silva, Adrián M.T. Silva: Photocatalytic activity of phosphorescent strontium aluminate doped with Eu^{2+} and Dy^{3+} . #360
- Barbara Lomba Fernandez, Antía Fdez-Sanromán, Emilio Rosales, Marta Curras and M^a Ángeles Sanromán: Development of different CuFe-MOF/PMS systems for selective treatment of wastewater pollutants. #363
- Mafalda Pina, Yury V. Kolen'ko, O. Salomé G. P. Soares: Reduction of critical raw materials in PEM water electrolysis catalysts for green hydrogen production #366
- Patrícia Ramalho, Salomé Soares and Fernando Pereira: Carbon nanotube-supported bimetallic catalysts with high activity for the selective catalytic reduction of NOx. #370
- Miguel M. Leitão, Manuel Simões and Anabela Borges: Effectiveness of selected aldehydes as inhibitors of the LasI/LasR quorum sensing pathway and enhancers of antibiotic activity against *Pseudomonas aeruginosa* biofilms. #373

The antimicrobial and antibiofilm activity of novel phytochemicals against *Escherichia coli*

Mariana Sousa ^{1,2,*}, Ana Cristina Afonso ^{1,2,3,4}, Lília Soares Teixeira ^{1,2}, Anabela Borges ^{1,2}, Maria José Saavedra ³, Lúcia Chaves Simões ⁴ and Manuel Simões ^{1,2}

¹ LEPABE—Laboratory for Process Engineering, Environment, Biotechnology and Energy, Faculty of Engineering, Department of Chemical Engineering, University of Porto, 4200-465 Porto, Portugal

² ALiCE—Associate Laboratory in Chemical Engineering, Faculty of Engineering, University of Porto, 4200-465 Porto, Portugal

³ CITAB—Centre for the Research and Technology of Agro-Environmental and Biological Sciences, University of Trás-os-Montes e Alto Douro, 5000-801 Vila Real, Portugal

⁴ CEB, LABBELS—Centre of Biological Engineering, Associate Laboratory on Biotechnology and Bioengineering, and Electromechanical Systems, School of Engineering, University of Minho, 4710-057 Braga, Portugal

*Corresponding author: mfsousa@fe.up.pt

Abstract

To overcome the global health problem of antimicrobial resistance, the phytochemicals perillyl alcohol and hydrocinnamic acid were tested for their antimicrobial and antibiofilm activities against *Escherichia coli* CECT 434. Both alone and combinatorial approaches with commercial antibiotics were effective. In addition, a recent bioinformatic tool named Combenefit was used to study the combinatorial effects regarding the inhibition of bacterial growth, allowing to attribute synergism scores and determine the concentrations of phytochemicals and antibiotics with better results.

Author Keywords. Antibiotic resistance, Biofilm control, *E. coli* infections, Plant-based natural product, Combinatorial solutions, Phytochemical-antibiotic interaction.

1. Introduction

The treatment of bacterial infections has been troubled by the increased resistance to antibiotics (Kolář 2022; Terreni, Taccani, and Pregnotato 2021). Thus, it is crucial to discover novel and effective therapies to control and eradicate planktonic and sessile bacterial cells (Ma et al. 2022). Phytochemicals have demonstrated broad-spectrum and effective antibacterial effects as well as antibiotic resistance-modifying activity (Khare et al. 2021). In this study, perillyl alcohol and hydrocinnamic acid were characterized for their antimicrobial and antibiofilm action against *Escherichia coli* CECT 434.

2. Materials and Methods

First, the minimum inhibitory concentrations (MIC) and the minimum bactericidal concentrations (MBC) were determined for two phytochemicals: perillyl alcohol and hydrocinnamic acid and two antibiotics: chloramphenicol and amoxicillin, against one microbial strain: *E. coli* CECT 434. Dual and triple combinations of these phytochemicals with chloramphenicol and amoxicillin were investigated for the first time by the checkerboard microdilution assay and data was analysed by the Combenefit software, which is a powerful and innovative bioinformatic tool that enables the visualization, analysis, and quantification of drug combination effects attributing synergism scores analysis. Regarding the biofilms, the activity of individual treatments (at MIC, 5×MIC and 10×MIC) and the effect of dual and triple combinations (at MIC and 5×MIC) were characterized in terms of biomass removal (through the staining with crystal violet) and culturability of the cells (by the drop plate method). Moreover, the combination amoxicillin/metronidazole was used as a positive control for comparison of the other combinations involving amoxicillin since metronidazole is often used as an adjuvant of amoxicillin.

3. Discussion

Perillyl alcohol had a minimum inhibitory concentration (MIC) of 256 µg/mL and a minimum bactericidal concentration (MBC) of 512 µg/mL. Hydrocinnamic acid had a MIC of 2048 µg/mL and an undetectable MBC (> 2048 µg/mL).

Through the analysis of the checkerboard assay by the Combeneft software, it was observed that the combinations of amoxicillin with each phytochemical resulted in synergism for several concentrations, being more intense for an amoxicillin concentration of 2 µg/mL. Combining chloramphenicol with each phytochemical resulted in synergism at lower concentrations of the antibiotic and a very mild zone of antagonism at intermediate or high concentrations of chloramphenicol.

Both phytochemicals provided total elimination of colony-forming units (CFU) at 5×MIC and 10×MIC. The highest percentages of biomass reduction (61.7% ± 1.6% for 10×MIC) were obtained for *E. coli* treated with amoxicillin. All combinations revealed moderate efficacy in terms of biomass reduction. Considering the culturability of sessile cells, synergism was determined for 20.0% of combinations, additivity for 60.0%, and indifference for 20.0%.

4. Conclusions

The results of this study highlighted the potential of combinatorial therapies for planktonic and biofilm control, where phytochemicals play an important role as resistance-modifying agents.

References

- Khare, Tushar, Utpal Anand, Abhijit Dey, Yehuda G. Assaraf, Zhe-Sheng Chen, Zhijun Liu, and Vinay Kumar. 2021. "Exploring Phytochemicals for Combating Antibiotic Resistance in Microbial Pathogens." *Frontiers in Pharmacology* 12. <https://www.frontiersin.org/articles/10.3389/fphar.2021.720726>.
- Kolář, M. 2022. "Bacterial Infections, Antimicrobial Resistance and Antibiotic Therapy." *Life (Basel)* 12 (4). <https://doi.org/10.3390/life12040468>.
- Ma, R., X. Hu, X. Zhang, W. Wang, J. Sun, Z. Su, and C. Zhu. 2022. "Strategies to prevent, curb and eliminate biofilm formation based on the characteristics of various periods in one biofilm life cycle." *Front Cell Infect Microbiol* 12: 1003033. <https://doi.org/10.3389/fcimb.2022.1003033>.
- Terreni, M., M. Taccani, and M. Pregnolato. 2021. "New Antibiotics for Multidrug-Resistant Bacterial Strains: Latest Research Developments and Future Perspectives." *Molecules* 26 (9). <https://doi.org/10.3390/molecules26092671>.

Acknowledgments

This work was financially supported by LA/P/0045/2020 (ALiCE), UIDB/00511/2020, and UIDP/00511/2020 (LEPABE), funded by national funds through FCT/MCTES (PIDDAC); Project Germirrad-POCI-01-0247-FEDER-072237, funded by FEDER funds through COMPETE2020-Programa Operacional Competitividade e Internacionalização (POCI) and by national funds (PIDDAC) through FCT/MCTES.

Delivery of Nucleic Acid Mimics into bacteria: effect of liposome composition in delivery efficiency

João Santos^{1,3*}, Nuno Guimarães^{1,3}, Eva Pinho^{1,2,3}, Rita S. Santos^{1,3},
Nuno F. Azevedo^{1,3}

¹LEPABE - Laboratory for Process Engineering, Environment, Biotechnology and Energy, Faculdade de Engenharia da Universidade do Porto, Rua Dr. Roberto Frias, 4200-465 Porto, Portugal, FEUP;

²INIAV - National Institute of Agrarian and Veterinary Research;

³ALiCE - Laboratório Associado em Engenharia Química, Faculdade de Engenharia da Universidade do Porto, Rua Dr. Roberto Frias, 4200-465 Porto, Portugal

*Corresponding author: up202103293@fe.up.pt

1. Introduction

The development of antimicrobial resistance (AMR) by bacteria is putting an end to the “golden-era” of antibiotics and is already responsible for thousands of annual deaths worldwide (O’Neill 2014; Bai et al. 2010). This increasing threat to public health requires the development of novel therapeutic solutions (Michael et al. 2014). Nucleic Acid Mimics (NAMs) are chemically modified nucleic acids showing nuclease resistance and high affinity and selectivity for their targets (Santos et al. 2017). NAMs can hybridize with intracellular bacterial RNA and thus have great potential to be applied as therapeutics or as diagnostic tools (Karkare and Bhatnagar 2006).

However, NAMs are charged macromolecules and thus poorly internalized by bacteria, as their envelope poses a stringent permeability barrier (Xue et al. 2018). Therefore, NAMs must be delivered into the bacterial cytosol so that they can fulfil their potential.

2. Materials and Methods

In this work, the influence of the liposomes’ lipid composition on the delivery efficiency of NAMs into important foodborne pathogens (*Escherichia coli* CSH36, *Salmonella enterica* Typhimurium SGSC2523 and *Listeria monocytogenes* ATCC7644) was studied via flow cytometry. Liposomes were composed of the cationic DOTAP, the fusogenic DOPE and the stabilizing DSPE-methoxy-PEG in varied amounts and synthesized following an ethanol dilution method. NAMs were designed to target the essential *acpP* gene and fluorescently labelled with Cy3.

3. Discussion

A high delivery efficiency of NAMs was obtained with over 80% of *E. coli* cells internalizing the NAMs when using a 50:50 ratio of DOTAP/DOPE (without any PEG). However, and for all the tested bacteria, the addition of even a slight percentage of PEG resulted in a significant decrease of this value. Changing the DOTAP/DOPE ratio to 75:25, while including 1% mol PEG seemed to reduce the detrimental effect of the PEGylation.

4. Conclusions

These results show that cationic-fusogenic lipids have potential for the delivery of antisense NAM probes into bacteria. Future work will include the functionalization of lipoNAMs with antibodies, aiming for higher efficiency and specificity of the delivery.

References

- Bai, Hui, Xiaoyan Xue, Zheng Hou, Ying Zhou, Jingru Meng, and Xiaoxing Luo. 2010. “Antisense Antibiotics: A Brief Review of Novel Target Discovery and Delivery.” *Current Drug Discovery Technologies* 7 (2): 76–85. <https://doi.org/10.2174/157016310793180594>.
- Karkare, Shantanu, and Deepak Bhatnagar. 2006. “Promising Nucleic Acid Analogs and Mimics: Characteristic Features and Applications of PNA, LNA, and Morpholino.” *Applied Microbiology and Biotechnology* 71 (5): 575–86. <https://doi.org/10.1007/s00253-006-0434-2>.
- Michael, Carolyn Anne, Dale Dominey-howes, Maurizio Labbate, Christina Maria, and Joseph Elisabeth. 2014. “The Antimicrobial Resistance Crisis: Causes, Consequences, and Management.” *Frontiers in Public Health* 2 (September): 1–8. <https://doi.org/10.3389/fpubh.2014.00145>.
- O’Neill, Jim. 2014. “Antimicrobial Resistance: Tackling a Crisis for the Health and Wealth of Nations.”

- Santos, Rita S., George R. Dakwar, Elisa Zagato, Toon Brans, Céu Figueiredo, Koen Raemdonck, Nuno F. Azevedo, Stefaan C. De Smedt, and Kevin Braeckmans. 2017. "Intracellular Delivery of Oligonucleotides in Helicobacter Pylori by Fusogenic Liposomes in the Presence of Gastric Mucus." *Biomaterials* 138: 1–12. <https://doi.org/10.1016/j.biomaterials.2017.05.029>.
- Xue, Xiao Yan, Xing Gang Mao, Ying Zhou, Zhou Chen, Yue Hu, Zheng Hou, Ming Kai Li, Jing Ru Meng, and Xiao Xing Luo. 2018. "Advances in the Delivery of Antisense Oligonucleotides for Combating Bacterial Infectious Diseases." *Nanomedicine: Nanotechnology, Biology, and Medicine* 14 (3): 745–58. <https://doi.org/10.1016/j.nano.2017.12.026>.

Acknowledgments

This work was supported by LA/P/0045/2020 (ALiCE), UIDB/00511/2020 - UIDP/00511/2020 (LEPABE) funded by national funds through FCT/MCTES (PIDDAC), the FCT grant 2021.0753.BD and the FCT/MCTES (PIDDAC), under the project 2022.07654.PTDC (NAMSaI)

Metal-free sensitization of TiO₂ for photocatalytic removal of pharmaceuticals under solar irradiation

Manuel Peñas-Garzón^{1,2,3}, Almudena Gómez-Avilés³, Javier Álvarez-Conde⁴, Jorge Bedia³, Eva M. García-Frutos⁴, Carolina Belver³

¹LSRE-LCM - Laboratory of Separation and Reaction Engineering – Laboratory of Catalysis and Materials, Faculty of Engineering, University of Porto, Rua Dr. Roberto Frias, 4200-465 Porto, Portugal (manuelpgarzon@fe.up.pt) ORCID 0000-0001-7677-2064

²ALICE - Associate Laboratory in Chemical Engineering, Faculty of Engineering, University of Porto, Rua Dr. Roberto Frias, 4200-465 Porto, Portugal

³Chemical Engineering Department, Universidad Autónoma de Madrid, Campus Cantoblanco, 28049 Madrid, Spain

⁴Instituto Ciencia de Materiales de Madrid, CSIC, Campus Cantoblanco, 28049 Madrid, Spain

Abstract

An azaindole derivative was grafted on TiO₂ as a novel photocatalyst, resulting in the improvement of photocatalyst properties, such as the band gap narrowing and favoring the photogenerated charge separation, as proved by photoluminescence and transient photocurrent tests. Grafted-photocatalyst allowed the removal of different pharmaceuticals in water under solar irradiation, even in a continuous flow regime, thus finding a new strategy to design solar-light-driven photocatalysts for the degradation of pollutants in water.

Author Keywords. Solar irradiation, pharmaceuticals, grafted TiO₂, azaindole.

1. Introduction

The use of TiO₂ as a reference photocatalyst under solar light is constrained by the characteristic large band gap value ($E_g \approx 3.2$ eV). This results in that only the UV contribution from the solar spectrum (i.e., around 5 %) can be harvested to generate the electron/hole pair responsible for the formation of oxidant radicals that may allow the degradation of water contaminants (Agbe et al. 2019). This work aims to prepare a donor-acceptor azaindole compound grafted on TiO₂ (Figure 1a) to enhance the photocatalytic properties and performance in the conversion of pharmaceuticals from aqueous solution under solar and visible irradiations.

2. Materials and Methods

An azaindole derivative (AZA4) was synthesized through different organic reactions starting from 5-bromo-7-azaindole, and finally, it was anchored on TiO₂ by Knoevenagel reaction (Peñas-Garzón et al. 2023). After purification and characterization, the novel TiO₂-AZA4 was used in the conversion of the pharmaceuticals acetaminophen, ibuprofen, and antipyrine, in both batch and continuous flow regimes. Some reaction parameters, such as the initial pH of the solution or the photocatalyst dose were investigated, as well as the likely contribution of radical species was assessed.

3. Discussion

TiO₂-AZA4 showed a remarkable improvement in the photocatalytic performance compared to the non-grafted TiO₂, and even to benchmark P25 under visible light (Figure 1b). This enhancement was ascribed to i) lower E_g value, and ii) higher separation of charge carriers and efficiency for interfacial electron transference as proved by transient photocurrent tests (Figure 1c). The prepared photocatalyst also proved their ability for the elimination of a mixture of pharmaceuticals, including acetaminophen, ibuprofen, and antipyrine in a continuous flow regime for 20 h.

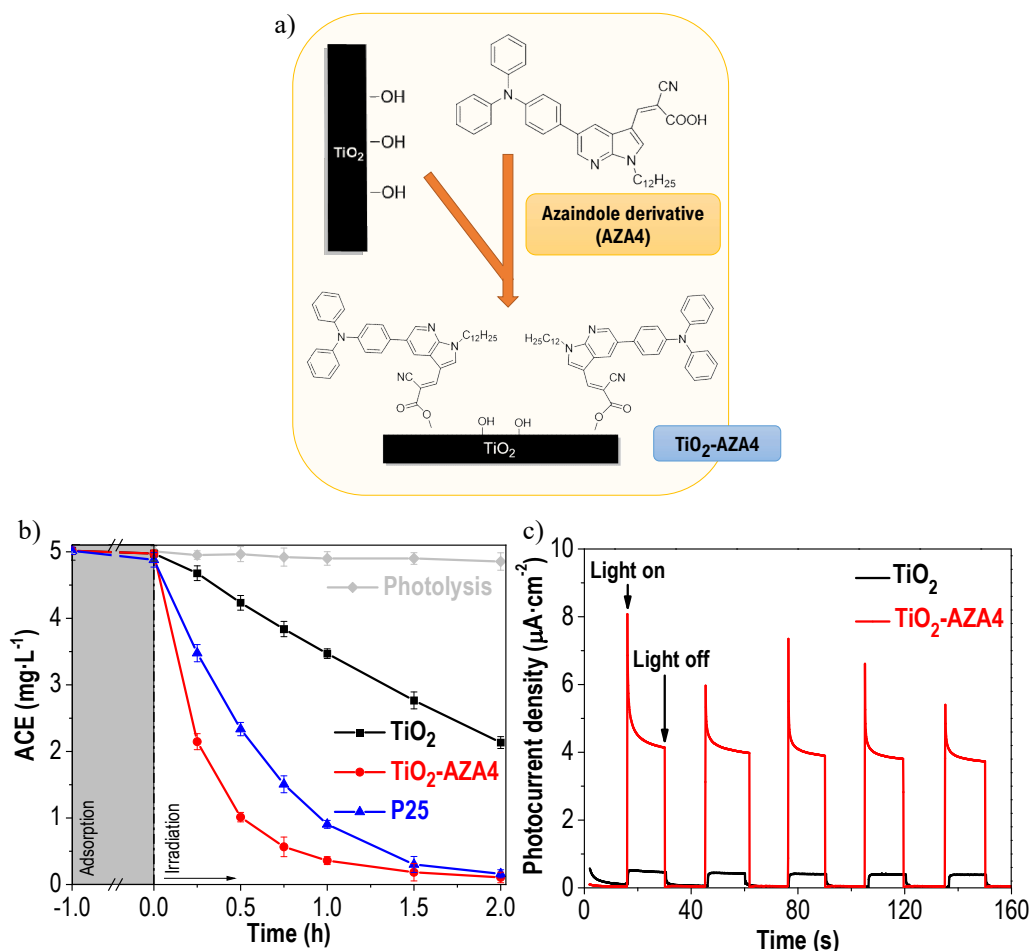


Figure 12: a) Scheme of the azaindole compound grafted on TiO₂; b) evolution of acetaminophen (ACE) concentration using TiO₂, TiO₂-AZA4, and benchmark P25 under visible light; and b) transient photocurrent light/dark cycles of TiO₂ and TiO₂-AZA4.

4. Conclusions

This study presents the photocatalytic performance of a novel azaindole grafted on TiO₂. The synthesized TiO₂-AZA4 represents a new strategy to design solar-light-driven materials for the degradation of aqueous contaminants under solar light in both batch and continuous regime experiments. The proposed band configuration of TiO₂-AZA4 suggests that the photogenerated electrons from the azaindole compound are injected into the conduction band of the TiO₂, allowing the degradation of the pharmaceuticals.

References

- H. Agbe, E. Nyankson, N. Raza, D. Dodoo-Arhin, A. Chauhan, G. Osei, V. Kumar, K.H. Kim. 2019. "Recent advances in photoinduced catalysis for water splitting and environmental applications". *Journal of Industrial and Engineering Chemistry* 72: 31–49, DOI:10.1016/J.JIEC.2019.01.004.
- Peñas-Garzón, Manuel, Almudena Gómez-Avilés, Javier Álvarez-Conde, Jorge Bedia, Eva M. García-Frutos, and Carolina Belver. 2023. "Azaindole grafted titanium dioxide for the photodegradation of pharmaceuticals under solar irradiation". *Journal of Colloid and Interface Science* 629: 593-603. DOI:10.1016/j.jcis.2022.09.005.

Acknowledgments

Spanish Agencia Estatal de Investigación (PID2019- 106186RBI00/AEI/10.13039/501100011033 and PID2019-105479RB-I00 (MCIN/AEI/10.13039/501100011033)). M. Peñas-Garzón acknowledges the postdoctoral fellowship from Fundación Ramón Areces (XXXIV Convocatoria Ciencias de la Vida y de la Materia). J. Álvarez-Conde acknowledges the European Social fund (PEJD-2017-PRE/IND-4536) of the Government of Madrid.

Bioactivity and phenolic composition of chestnut shells extract before and after *in-vitro* simulated gastrointestinal digestion

Diana Pinto^{1,2}, Manuela M. Moreira¹, Anna Vallverdú-Queralt^{3,4},
Cristina Delerue-Matos¹, Francisca Rodrigues^{1,*}

¹REQUIMTE/LAQV, Instituto Superior de Engenharia do Porto, Rua Dr. António Bernardino de Almeida, 4249-015 Porto, Portugal; ²Faculdade de Ciências, Universidade do Porto, Rua do Campo Alegre, 4169-007 Porto, Portugal; ³Nutrition, Food Science and Gastronomy Department, School of Pharmacy and Food Science, University of Barcelona, Barcelona, Spain; ⁴Consorcio CIBER, M.P. Fisiopatología de la Obesidad y la Nutrición (CIBERObn), Instituto de Salud Carlos III (ISCIII), Madrid, Spain. *francisca.rodrigues@graq.isep.ipp.pt

Abstract

The role of bioaccessibility and metabolism on the bioactivity of phenolic compounds has been explored in several studies. The bioactivity of phenolic compounds is not only ascribed to the compounds themselves, but mostly to the metabolites resulting from their passage by the gastrointestinal tract. New insights on the recovery of phenolic compounds from food by-products have been prioritized in the last decades, aiming to employ them as active ingredients for industrial purposes (Pinto et al. 2021). Chestnut shells (CS) are one of the most abundant by-products generated by the Portuguese chestnut fruit industry, highlighting the need to seek for clean and proficient approaches to manage this agro-industrial waste (Lameirão et al. 2020). The current study evaluates the effects of the *in-vitro* simulated human digestion on the phenolic composition, antioxidant/antiradical properties, and radicals scavenging potential of CS extract prepared by Ultrasound-Assisted Extraction (UAE), enlightening on their bioaccessibility. The metabolomic profiling of the CS extract and the digested samples was explored by HPLC-DAD.

The results unveiled a decrease of 41% and 65% in the total phenolic content after gastric and intestinal digestion when compared to the CS extract (355.05 mg gallic acid equivalents (GAE)/g dry weight (dw)). Likewise, the antioxidant activity and radicals counteracting potential were also reduced after digestion (35-50% reduction), indicating that the metabolites formed during the gastrointestinal digestion disclosed lower antioxidant capacity than the original parent compounds. The phenolic composition unveiled the presence of hydroxybenzoic acids, hydroxycinnamic acids, flavanols, flavonols, flavones, and flavanones, along with one alkaloid and one stilbene. Despite the identical phenolic compounds, changes in their concentrations and some biotransformation reactions were identified in digested and undigested extracts, suggesting a lower bioaccessibility of CS extract after digestion.

This study attested the interesting bioactivity of CS extract even after the *in-vitro* digestion, providing a step forward in its valorization as antioxidant ingredient for functional foods. Novel strategies should be explored to enhance the bioaccessibility of phenolic compounds, such as encapsulation techniques.

Keywords: *Castanea sativa*; *in-vitro* digestion; phenolic compounds; bioaccessibility; metabolomic.

References

- Lameirão, F., D. Pinto, E.F. Vieira, A.F. Peixoto, C. Freire, S. Sut, S. Dall'Acqua, P. Costa, C. Delerue-Matos, and F. Rodrigues. 2020. "Green-sustainable recovery of phenolic and antioxidant compounds from industrial chestnut shells using ultrasound-assisted extraction: Optimization and evaluation of biological activities *in vitro*". *Antioxidants*, 9 (3):267. Accessed 28 March, 2023. DOI: 10.3390/antiox9030267.
- Pinto, D., M.d.I.L. Cádiz-Gurrea, A. Vallverdú-Queralt, C. Delerue-Matos, and F. Rodrigues. 2021. "*Castanea sativa* shells: A review on phytochemical composition, bioactivity and waste management approaches for industrial

valorization". *Food Research International*, 144:110364. Accessed 29 March, 2023. DOI: 10.1016/j.foodres.2021.110364.

Acknowledgments

This work received financial support from the projects PTDC/ASP-AGR/29277/2017, 5537 DRI, Sérvia 2020/21 from Portuguese-Serbia Bilateral Cooperation, UIDB/50006/2020, supported by FCT/MCTES and FEDER throughout COMPETE 2020 (POCI-01-0145-FEDER-029277). D.P. is thankful for her Ph.D. grant (SFRH/BD/144534/2019) financed by FCT/MCTES, POPH-QREN, EU and FSE). F.R. (CEECIND/01886/2020) and M.M.M. (CEECIND/02702/2017) are grateful for their contracts financed by FCT/MCTES—CEEC Individual 2020 Program Contract. A.V.-Q. thanks the Spanish Ministerio de Ciencia, Innovación y Universidades for the Ramon y Cajal contract (RYC-2016-19355).

Bioactive composition of goji berries extracted by Ultrasound-Assisted Extraction: Validation of a mathematical model

Filipa Teixeira¹, Ana Margarida Silva¹, Cristina Delerue-Matos¹,
Francisca Rodrigues^{1,*}

¹REQUIMTE/LAQV, ISEP, Polytechnic of Porto, Rua Dr. António Bernardino de Almeida 431, 4249-015 Porto, Portugal (filipamrt237@gmail.com; ana.silva@graq.isep.ipp.pt; cmm@isep.ipp.pt; francisca.rodrigues@graq.isep.ipp.pt) ORCID 0000-0002-9287-8771; 0000-0002-1823-9816; 0000-0002-3924-776X; 0000-0001-8803-0041.

* francisca.rodrigues@graq.isep.ipp.pt

Abstract

Lycium barbarum L. is a species widely used in dietary supplements and natural healthcare products. The berries, also known as goji or wolfberries, mostly grow in China, but its popularity and cultivation have increased around the world due to recent reports that highlighted their remarkable polyphenolic content and outstanding therapeutic properties. This study aims to determine the optimal ultrasound-assisted extraction (UAE) conditions for goji berries and evaluate its antioxidant/antiradical activities. The data obtained suggests that the optimized extract is very promising for nutraceutical proposes.

Author Keywords. *Lycium barbarum*. Response Surface Methodology. Ultrasound-Assisted Extraction. Antioxidant Activity.

1. Introduction

Lycium barbarum L. fruits, also known as goji berries, have been traditionally used as herbal medicine (Donno et al. 2015). The plant mostly grows in Asian regions (Donno et al. 2015; Vidovic et al. 2022) and present a high nutritional value and rich bioactive composition, particularly in phenolic compounds, vitamins, sugars, organic acids, and minerals (Pires et al. 2018). The potential healthy properties of goji berries, such as antioxidant, antimicrobial and anti-inflammatory effects, have been highlighted in recent years (Teixeira et al. 2023), allowing to classify the fruit as a “superfruit” (Vidovic et al. 2022).

This study aims to determine the optimal ultrasound-assisted extraction (UAE) conditions of polyphenolic antioxidants from *L. barbarum* berries using a mathematical model, namely Response Surface Methodology (RSM), and evaluate its antioxidant activity.

2. Materials and Methods

Goji berries were obtained in a local supermarket located in Porto, Portugal. A mathematical model, namely RSM, was used to determine the optimal extraction conditions of goji berries. The impacts of solid-liquid ratio (2.5 – 10.0%, w/v), time (20 – 60 min), and intensity (30 – 70 W/m²) in total phenolic content (TPC) and antioxidant/antiradical activities (assessed by DPPH, ABTS and ferric-reducing antioxidant power (FRAP) assays) were assessed. The optimal extract was characterized regarding its ability to scavenge reactive oxygen species (ROS), namely superoxide dismutase (O₂^{•-}), hypochlorous acid (HOCl), and peroxy radical (ROO[•]), and reactive nitrogen species (RNS), such as peroxy nitrite (ONOO⁻), in the presence and absence of NaHCO₃, and nitric oxide (NO[•]).

3. Discussion

According to the RSM, the optimal extraction conditions were achieved using a solid-liquid ratio of 8.75% (w/v) and an intensity of 59 W/m² for 56.21 min. **Table 1** summarizes the experimental and predicted values for the UAE optimal condition, validating the mathematical model.

	TPC (mg GAE/g)	ABTS (mg AAE/g)	DPPH (mg TE/g)	FRAP (μmol FSE/g)
Experimental value*	23.87 ± 1.47	15.15 ± 1.13	10.25 ± 0.81	105.97 ± 8.20
Predicted value	20.45	13.73	8.29	106.60
p-value	0.066	0.067	0.258	0.266

Table 1: Experimental and predicted value of TPC, ABTS, DPPH and FRAP for the optimal extract. *Results are expressed as mean \pm standard deviation ($n=3$).

The optimal extract was evaluated regarding ROS and RNS scavenging capacity (**Table 2**).

Sample	RNS		ROS		
	ONOO ⁻ without NaHCO ₃	ONOO ⁻ with NaHCO ₃	O ^{• - 2}	HOCl	ROO [•]
	IC50 (μg/mL)	IC50 (μg/mL)	IC50 (μg/mL)	IC50 (μg/mL)	μmol TE/mg dw
Optimal extract	57.78 \pm 4.26 ^b	93.51 \pm 19.65 ^b	225.25 \pm 53.26 ^b	12.99 \pm 1.13 ^c	0.15 \pm 0.01 ^c
Positive controls					
Catechin	0.19 \pm 0.03 ^a	0.29 \pm 0.07 ^a	18.01 \pm 0.77 ^a	0.20 \pm 0.03 ^a	6.37 \pm 2.32 ^a
Gallic acid	0.20 \pm 0.004 ^a	0.28 \pm 0.05 ^a	6.34 \pm 0.53 ^a	2.60 \pm 0.14 ^b	2.45 \pm 0.54 ^b

Table 2: Peroxynitrite (ONOO⁻) in the presence and absence of NaHCO₃, nitric oxide(NO[•]), hydrogen peroxide (H₂O₂), superoxide anion radical (O^{• - 2}), hypochlorous acid(HOCl) and peroxy radical (ROO[•]), scavenging capacities of the optimized extract of goji berries. Results are expressed as mean \pm standard deviation ($n = 3$). Different letters in the same column mean significant differences ($p < 0.05$).

Based on the results presented in **Table 1**, along with the results regarding radical oxygen and nitrogen scavenging capacity summarized in **Table 2**, it is possible to affirm that the optimal extract achieved a high TPC and great antioxidant/antiradical activity.

4. Conclusions

The results obtained emphasize the great antioxidant/antiradical potential of goji berries extracted by UAE for nutraceutical and food industries application. Further studies regarding phenolic composition and *in vitro* intestinal permeation should be performed to clarify the safety of the optimized goji berries extract for nutraceutical use.

References

- Donno, Dario, Gabriele Loris Beccaro, Maria Gabriella Mellano, Alessandro Kim Cerutti, and Giancarlo Bounous. 2015. "Goji berry fruit (*Lycium spp.*): antioxidant compound fingerprint and bioactivity evaluation". *Journal of Functional Foods* 18:1070-1085. Accessed 25 March, 2023. DOI: 10.1016/j.jff.2014.05.020.
- Pires, Tânia C. S. P., Maria Inês Dias, Lillian Barros, Ricardo C. Calhelha, Maria José Alves, Celestino Santos-Buelga, and Isabel C. F. R. Ferreira. 2018. "Phenolic compounds profile, nutritional compounds and bioactive properties of *Lycium barbarum* L.: A comparative study with stems and fruits". *Industrial Crops and Products* 122:574-581. Accessed 25 March, 2023. DOI: 10.1016/j.indcrop.2018.06.046.
- Vidovic, Bojana B., Danijel D. Milincic, Mirjana D. Marcetic, Jelena D. Djuris, Tajana D. Ilic, Aleksandar Z. Kostic, and Mirjana B. Pesic. 2022. "Health Benefits and Applications of Goji Berries in Functional Food Products Development: A Review". *Antioxidants* 11 (2):248. Accessed 25 March, 2023. DOI: 10.3390/antiox11020248.
- Teixeira, Filipa, Ana Margarida Silva, Cristina Delerue-Matos, and Francisca Rodrigues. 2023. "*Lycium barbarum* Berries (Solanaceae) as Source of Bioactive Compounds for Healthy Purposes: A Review". *International Journal of Molecular Sciences* 24 (5):4777. Accessed 22 March, 2023. DOI: 10.3390/ijms24054777.

Acknowledgments

This work received financial support from project EXPL/BAA-GR/0663/2021 – Kiwi4Health – Exploring the Eco-Innovative Re-Use of Kiwiberry, supported by national funds by FCT/MCTES and by the projects UIDB/50006/2020 and UIDP/50006/2020 through national funds. This work was also financed by national funds from FCT - Fundação para a Ciência e a Tecnologia, I.P., in the scope of the project UIDP/04378/2020, UIDB/04378/2020 and the project LA/P/0140/2020. Filipa Teixeira is thankful for the scholarship from project EXPL/BAA- GR/0663/2021. Ana Margarida Silva is thankful for the Ph.D. grant (SFRH/BD/144994/2019) financed by POPH-QREN and subsidized by the European Science Foundation and Ministério da Ciência, Tecnologia e Ensino Superior. Francisca Rodrigues (CEECIND/01886/2020) is thankful for contract financed by FCT/MCTES—CEEC Individual Program Contract.

Microparticles containing *Fragaria Vesca* leaf extract produced with biopolymeric matrices: Binary and ternary blends of alginate, pectin and carrageenan

Yara Bastos, Antónia Gonçalves, Fernando Rocha, Berta Nogueira Estevinho*

LEPABE, Departamento de Engenharia Química, Faculdade de Engenharia da Universidade do Porto, Rua Dr. Roberto Frias, 4200-465 Porto, Portugal

* Corresponding author: Tel: +351225084858 Fax: +351225081449; e-mail: berta@fe.up.pt

Abstract

Valorisation of by-products and maximum utilization of raw material constitute highly relevant topics in the EU and worldwide. The desirable valorisation is not always present. These materials contain different types of phytochemical compounds such as polyphenols, that display a set of biological properties, including chemo-preventive, anti-inflammatory and immune-stimulating.

In this work, the microencapsulation of strawberry (*Fragaria Vesca*) plant extract and its main bioactive compound - quercetin was studied by spray drying using individual biopolymers, binary and ternary blends of pectin, alginate, and carrageenan. Quercetin is widely used in cosmetics, nutraceuticals, and pharmaceuticals due to its high antioxidant and anti-inflammatory potential. Mini Spray-dryer BÜCHI B-290 (Flawil, Switzerland) was used to produce the different microparticles. For the spray drying process were used as independent variables the inlet air temperature (115 °C), the flowrate (30%) and the concentration of encapsulant agent (1% (w/v)).

The microparticles were characterized by size, morphology, and release profile. The quercetin was completely released from the microparticles, with total release times ranging from 200 to 600 s. The microparticles were evaluated by Scanning Electron Microscopy (SEM) and by Coulter showing an average size of 3 µm.

In conclusion, the microstructures prepared present promising characteristics for food, nutraceutical, and cosmetic applications.

Keywords: By-products, *Fragaria Vesca*, Quercetin; Microencapsulation; Spray Drying.

Acknowledgments:

This work was financially supported by LA/P/0045/2020 (ALiCE), UIDB/00511/2020 and UIDP/00511/2020 (LEPABE), funded by national funds through FCT/MCTES (PIDDAC); S4Hort_Soil&Food (NORTE-01-0145-FEDER-000074), supported by Norte Portugal Regional Operational Programme (NORTE 2020), under the PORTUGAL 2020 Partnership Agreement, through the European Regional Development Fund (ERDF).

Evaluating the Diffusion of NAMs Across the Bacterial Envelope

Beatriz T. Magalhães^{1,2}, João T. S. Coimbra³, Rita S. Santos^{1,2}, Nuno F. Azevedo^{1,2}, Pedro A. Fernandes³

¹ LEPABE - Laboratory for Process Engineering, Environment, Biotechnology and Energy, Faculdade de Engenharia, Universidade do Porto, Rua Dr. Roberto Frias, s/n, 4200-465 Porto, Portugal

² ALICE - Associate Laboratory in Chemical Engineering, Faculdade de Engenharia, Universidade do Porto, Rua Dr. Roberto Frias, s/n, 4200-465 Porto, Portugal

³ LAQV, REQUIMTE, Departamento de Química e Bioquímica, Faculdade de Ciências, Universidade do Porto, Rua do Campo Alegre, 687, s/n, 4169-007 Porto, Portugal

*Corresponding author: e-mail address: beatrizmagalhaes95@gmail.com; ORCID ID 0000-0003-4434-6989

Abstract

The antimicrobial resistance (AMR) crisis has been deemed as one of the most concerning health problematics of today (WHO 2022). The inefficacy of the antibiotics traditionally used in the clinical practice urges the development of novel antibacterial drugs. Antisense oligonucleotides can target essential bacterial genes, leading to bacterial death upon hybridization. Chemically modified oligonucleotides, dubbed nucleic acid mimics (NAMs), have the advantage of being resistant to enzymatic degradation (Pereira et al. 2021). However, it is not known whether NAMs can cross the stringent bacterial envelope.

Therefore, our goal was to assess if NAMs could diffuse through bacterial membranes, starting off with lipidic bilayers. We resorted to molecular dynamics (MD) to predict the interaction of NAMs with 1-palmitoyl-2-oleoyl-sn-glycero-3-phosphocholine (POPC)-only and 1-palmitoyl-2-oleoyl-sn-glycero-3-phosphoglycerol (POPG)-only systems.

We employed a charge parameterization protocol for the modified nucleotides using the ANTECHAMBER module from AMBER (D.A. Case 2022). Thereafter, we simulated Locked nucleic acid (LNA) and/or 2'-O-methyl (2'Ome) modified sequences solvated in water and compared the structural properties obtained with those published in the literature to validate our protocol (Yildirim et al. 2014). After validation, we built the POPC-only and POPG-only bilayers with Charmm-Gui (Jo et al. 2008) and equilibrated them with GROMACS (Berendsen, van der Spoel, and van Drunen 1995, Van Der Spoel et al. 2005). Following membrane equilibration, we positioned a 7 mers NAM sequence above the bilayers and simulated the system following a typical MD protocol. After a production of 300 ns, our results showed that the sequence did present some adsorption towards the membranes but did not insert itself into the bilayers. Hence, it seems unlikely than NAMs can cross the bacterial envelope through simple diffusion. Still, umbrella sampling simulations were conducted to obtain the potential of mean force of the sequence across the bilayers and infer possible interactions between the molecule and the lipids. The PMF profile obtained for POPC reveals a high energy barrier for the translocation of the NAMs, which might be related to the dragging of water molecules by the sequence. Umbrella sampling simulations for POPG are ongoing, and additional systems with membranes of different lipidic compositions are being equilibrated. Moreover, delivery vectors will be investigated to reveal potential strategies to effectively deliver NAMs into the bacterial cytosol.

Author Keywords. Molecular Dynamics, Nucleic acid mimics, Diffusion, Antibacterial drugs.

References

- Berendsen, Herman JC, David van der Spoel, and Rudi van Drunen. 1995. "GROMACS: A message-passing parallel molecular dynamics implementation." *Computer physics communications* 91 (1-3):43-56.
- AMBER. University of California, San Francisco.
- Jo, Sunhwan, Taehoon Kim, Vidyashankara G Iyer, and Wonpil Im. 2008. "CHARMM-GUI: a web-based graphical user interface for CHARMM." *Journal of computational chemistry* 29 (11):1859-1865.
- Pereira, Sara, Ruwei Yao, Mariana Gomes, Per Trolle Jørgensen, Jesper Wengel, Nuno Filipe Azevedo, and Rita Sobral Santos. 2021. "Can Vitamin B12 Assist the Internalization of Antisense LNA Oligonucleotides into Bacteria?" *Antibiotics* 10 (4):379.

- Van Der Spoel, David, Erik Lindahl, Berk Hess, Gerrit Groenhof, Alan E Mark, and Herman JC Berendsen. 2005. "GROMACS: fast, flexible, and free." *Journal of computational chemistry* 26 (16):1701-1718.
- WHO, World Health Organization. 2022. "Lack of innovation set to undermine antibiotic performance and health gains." 22 June 2022. <https://www.who.int/news/item/22-06-2022-22-06-2022-lack-of-innovation-set-to-undermine-antibiotic-performance-and-health-gains>.
- Yildirim, Ilyas, Elzbieta Kierzek, Ryszard Kierzek, and George C Schatz. 2014. "Interplay of LNA and 2'-O-methyl RNA in the structure and thermodynamics of RNA hybrid systems: a molecular dynamics study using the revised AMBER force field and comparison with experimental results." *The journal of physical chemistry B* 118 (49):14177-14187.

Acknowledgments

This work was financially supported by LA/P/0045/2020 (ALiCE), UIDB/00511/2020 and UIDP/00511/2020 (LEPABE), funded by national funds through FCT/MCTES (PIDDAC). The work was also supported through the projects 2022.07654.PTDC, UIDB/50006/2020 and UIDP/50006/2020, funded by FCT/MCTES through national funds. BTM is funded through FCT PhD Grant SFRH/BD/143491/2019. JTSC thanks FCT for funding through the Scientific Employment Stimulus – Individual Call (Ref. CEECIND/01374/2018)

Continuous gas-liquid mass transfer in an oscillatory flow reactor provided with smooth periodic constrictions

Filipe Almeida*¹, Fernando Rocha¹, António Ferreira¹

¹LEPABE - Laboratory for Process Engineering, Environment, Biotechnology and Energy, Faculty of Engineering, University of Porto, Rua Dr. Roberto Frias, 4200-465 Porto, Portugal

²ALiCE - Associate Laboratory in Chemical Engineering, Faculty of Engineering, University of Porto, Rua Dr. Roberto Frias, 4200-465 Porto, Portugal

*up201202863@edu.fe.up.pt

Abstract

Over the years airlift, bubble column and stirred tank reactors have been used to enhance gas-liquid mass transfer. Recently, a novel reactor, the oscillatory flow reactor provided with smooth periodic constrictions (OFR-SPC) has been successfully applied to improve the mixing efficiency of several chemical processes either in the presence (Ferreira et al. 2017; Gonçalves et al. 2021) or absence of solids (Ferreira, Teixeira, and Rocha 2015; Almeida et al. 2022). Mixing efficiency implies low power density, and hence, lower operational costs. The OFR-SPC is a multiphase reactor and consists of a column provided with periodic baffles, operating under oscillatory flow mixing, controlled by oscillation amplitude (x_0) and frequency (f) imposed on the liquid (Almeida et al. 2022). As far as it is known the reported results on the OFR are only in semi-batch mode (batch liquid phase and continuous gaseous phase), which is motivation enough to investigate more and improve knowledge using this reactor in continuous mode (continuous liquid phase and continuous gaseous phase). This operation mode applied to the OFR is a new way for industrial applications, namely in microalgal culture, and fermentation bioprocess. Thus, in the present work, the continuous mode operation was used for the first time in an OFR to analyse the influence of the liquid flow rate on gas-liquid mass transfer. The influence of the oscillatory conditions, i.e., oscillation amplitude and frequency were also studied. The parameters evaluated included the volumetric liquid-side mass transfer coefficient ($k_L a$), gas holdup (ε_G), Sauter mean diameter bubbles (d_{32}) and O₂ saturation concentration (C*). The results demonstrated that $k_L a$ increased with oscillatory conditions, consequence of the bubble size decrease. It was found that ε_G increase with oscillation amplitude and frequency due to the increase in bubble residence time, except at low amplitudes where ε_G tended to reduce as frequency increased, which may be a result of the oscillatory velocity imposed on the liquid. An increase in the liquid flow rate promoted a decrease in ε_G , d_{32} and C* and an increase in $k_L a$. Therefore, the liquid flow rate is an important parameter to be optimized in continuous mode since it changes $k_L a$ and C*, both important parameters to be regarded for industrial application like cells growth.

Author Keywords. Gas-liquid Mass transfer, gas holdup, Sauter mean diameter.

References

- Almeida, F, F Rocha, J A Teixeira, and A Ferreira. 2022. "The Influence of Electrolytes in Aqueous Solutions on Gas-Liquid Mass Transfer in an Oscillatory Flow Reactor." *Chemical Engineering Science* 263 (December 2022): 118048–66. <https://doi.org/10.1016/j.ces.2022.118048>.
- Ferreira, A, Patrick O Adesite, J A Teixeira, and F Rocha. 2017. "Effect of Solids on O₂ Mass Transfer in an Oscillatory Flow Reactor Provided with Smooth Periodic Constrictions." *Chemical Engineering Science* 170 (12 October 2017): 400–409. <https://doi.org/10.1016/j.ces.2016.12.067>.
- Ferreira, A, J A Teixeira, and F Rocha. 2015. "O₂ Mass Transfer in an Oscillatory Flow Reactor Provided with Smooth Periodic Constrictions. Individual Characterization of KL and A." *Chemical Engineering Journal* 262 (15 February 2015): 499–508. <https://doi.org/10.1016/j.cej.2014.09.125>.
- Gonçalves, Ana L, Filipe Almeida, Fernando A Rocha, and António Ferreira. 2021. "Improving CO₂ Mass Transfer in Microalgal Cultures Using an Oscillatory Flow Reactor with Smooth Periodic Constrictions." *Journal of Environmental Chemical Engineering* 9 (6): 106505–17. <https://doi.org/10.1016/j.jece.2021.106505>.

Acknowledgements

This work was financially supported by LA/P/0045/2020 (ALiCE), UIDB/00511/2020 and UIDP/00511/2020 (LEPABE), funded by national funds through FCT/MCTES (PIDDAC). F. Almeida would wish to thank to FCT for PhD scholarship 2020.05246.BD.

Screening of supports and metal phases to obtain highly active catalysts for the CO₂ conversion in C₂+ products

Mariana B. S. Felgueiras^{1,2*}, Manuel F. R. Pereira^{1,2}, Olívia S. G. P. Soares^{1,2}

¹ LSRE-LCM – Laboratory of Separation and Reaction Engineering - Laboratory of Catalysis and Materials, Faculty of Engineering, University of Porto, Rua Dr. Roberto Frias, 4200-465 Porto, Portugal.

² ALiCE – Associate Laboratory in Chemical Engineering, Faculty of Engineering, University of Porto, Rua Dr. Roberto Frias, 4200-465 Porto, Portugal.

*E-mail: mbsf@fe.up.pt

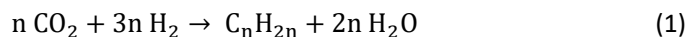
Abstract

Carbon dioxide (CO₂) is one of the main drivers of climate change. The development of technologies to transform excess CO₂ into valuable chemicals and fuels is crucial to protect the environment and reduce dependence on fossil fuels. In this work, the most suitable catalysts supports and metallic active phases for the CO₂ valorization reaction in C₂+ products (products with 2 or more C atoms) were assessed. The catalysts were texturally characterized, and catalytic tests for the CO₂ hydrogenation reactions were carried out at 200 – 350 °C, 15 – 20 bar and under H₂, CO₂ and N₂ flows. AC-supported catalysts recorded the lowest and the CNT-supported catalysts showed the highest CO₂ conversion values. Although Na catalysts demonstrate the highest CO₂ conversion, Fe catalysts are more selective for C₂+ products.

Author Keywords. Carbon dioxide, carbon materials, catalysts, hydrogenation, C₂+ products.

1. Introduction

Carbon dioxide (CO₂) is the most common greenhouse gas, accounting for about 76% of these gases (“Global Emissions” 2019). Most of this pollutant comes from burning fossil fuels in industries and residential or commercial buildings. The increase in these emissions results in global warming, which triggers climate change and has consequences such as shortages of fresh water, rising floods and rising sea levels, which influence livestock, agriculture, and the global food system (William D. Fletcher 2020). The hydrogenation of CO₂ is a versatile route capable of producing various chemicals and C₂+ hydrocarbons (Equation 1) (Wang et al. 2013).



The production of C₂+ products (compounds with 2 or more C atoms) by the hydrogenation of CO₂ would be highly desirable from the viewpoint of utilizing CO₂ as a carbon feedstock to produce chemical products. However, the selectivity for C₂+ products is still low in most of the reported catalysts, so more fundamental studies are needed to develop an efficient catalyst for this purpose. The most used catalysts in the CO₂ hydrogenation reaction through a modified Fischer-Tropsch synthesis (FTS) are essentially metal oxides (ZrO₂, CeO₂, Al₂O₃, Fe₂O₃) and carbon materials: carbon nanotubes (CNT) and activated carbon (AC). Fe and Co based catalysts with alkali metal promoters (especially Na and K) are highly active, with selectivity up to 57% for C₂ – C₄ hydrocarbons and 40 – 60% CO₂ conversion. Both the support and the promoter metal may affect the activity and the selectivity of the catalysts (Ye et al. 2019).

This work aims to find the most suitable supports and combination of metals for both CO₂ conversion and selectivity to C₂+ products.

2. Materials and Methods

Commercial multi-walled carbon nanotubes (CNT), activated carbon (AC), and aluminum oxide (γ – Al₂O₃) were used as support for the metallic phases.

The metallic catalysts were prepared through incipient impregnation using the following metallic precursors: iron nitrate, cobalt nitrate, cerium nitrate, potassium nitrate, sodium carbonate, manganese acetate and ammonia molybdate. The total amount of impregnated metal corresponds to 20 – 37 % (wt. %). In all catalysts, the metallic precursor solution was impregnated in the support

and left for 1.5 h at room temperature in the ultrasonic bath. Finally, the sample was placed in the oven for 24 h at 100 °C. The thermal treatment of the synthesized materials was carried out at 400 °C under a flowrate of N₂ (1 h) and H₂ (3 h) of 100 cm³ min⁻¹ at a heating rate of 10 °C min⁻¹.

The textural properties of the synthesized materials were determined by N₂ adsorption-desorption equilibrium isotherms at -196 °C.

The performance of the catalysts for the CO₂ hydrogenation was evaluated on a Microactivity-Reference (PID) unit. A mass of 200 mg of catalyst was placed in a continuous-flow fixed-bed steel tubular reactor. All the catalysts were reduced under H₂ flow rate (37.5 cm³ min⁻¹) at 400 °C for 1 h. Catalytic evaluation was performed under the reaction conditions of 200 – 350 °C, 15 – 20 bar and a 50% (*vol. %*) H₂, 16.7% (*vol. %*) CO₂ and 33.3% (*vol. %*) N₂ flow rate (30 cm³ min⁻¹) for 1.5 h with a heating rate of 3 °C min⁻¹. Analysis of products was conducted using the Micro GC Fusion® Gas Analyzer chromatograph equipped with a packed Porapak Q column (length of 1 m) followed by a packed 5 A molecular sieve column (5 m) connected to a thermal conductivity detector (TCD).

3. Discussion

AC presents the highest specific surface areas (394 – 966 m²g⁻¹), whereas Al₂O₃ the lowest (70 – 205 m²g⁻¹). The pore volume is higher in the catalysts supported on CNT.

Table 1 shows the CO₂ conversion results obtained at 350 °C.

CNT supported catalyst	X _{CO₂} / %	Al ₂ O ₃ supported catalyst	X _{CO₂} / %	AC supported catalyst	X _{CO₂} / %
NaCo	95	NaCo	85	NaCo	90
NaCoMo	89	NaCoMo	73	NaCoMo	57
Fe	47	Fe	34	Fe	6
FeCoK	43	FeCoK	46	FeCoK	22
FeK	42	FeK	37	FeK	21
FeMnK	37	FeMnK	20	FeMnK	13
FeMn	35	FeMn	33	FeMn	15
FeMnCe	23	FeMnCe	36	FeMnCe	3

Table 1: CO₂ conversion results obtained for the maximum reaction, 350 °C.

It is notable that the AC supported catalysts recorded the lowest CO₂ conversion values, revealing that is not an adequate support for these reactions. Among the catalysts supported on CNT and Al₂O₃, only FeCoK and FeMnCe showed slightly better results when supported on Al₂O₃. Therefore, in the next catalytic tests, AC-supported catalysts will not be included. CNT-supported catalysts have shown to be promising for the reaction under study and will be our focus in the next developments of this work. The reaction products obtained for Fe-impregnated catalysts were carbon monoxide (CO), ethylene (C₂H₄), ethane (C₂H₆), propylene (C₃H₆), propane (C₃H₈) and at least six more C₂+ products that we have not yet been able to identify. On the other hand, catalysts with Na, although presenting higher CO₂ conversions, were less selective to C₂+ products, obtain only CO, methane (CH₄), C₂H₆, C₃H₈ and pentane (C₅H₁₂).

4. Conclusions

The main objective of this study was to decide which support was most suitable for the CO₂ recovery reaction in C₂+ products and which combinations of metals would be more favorable for the CO₂ conversion and the selectivity of C₂+ products. AC-supported catalysts recorded the lowest CO₂ conversion values. The catalysts supported on CNT showed to be promising for the reaction under study and will be our focus in the next developments of this work. Fe-impregnated catalysts were selective for at least 11 C₂+ products. On the other hand, catalysts with Na, although presenting a greater capacity to obtain higher CO₂ conversions were selective to only 5 C₂+ products. Therefore,

the next catalysts will be synthesized using combinations of Fe and Na to find a balance between conversion and selectivity to the CO₂ hydrogenation reaction.

References

- “Global Emissions.” 2019. Center for Climate and Energy Solutions. 2019. <https://www.c2es.org/content/international-emissions/>.
- Wang, Jingjuan, Zhenya You, Qinghong Zhang, Weiping Deng, and Ye Wang. 2013. “Synthesis of Lower Olefins by Hydrogenation of Carbon Dioxide over Supported Iron Catalysts.” *Catalysis Today* 215: 186–93. <https://doi.org/10.1016/j.cattod.2013.03.031>.
- William D. Fletcher, Craig B. Smith. 2020. “Introduction.” In *Reaching Net Zero: What It Takes to Solve the Global Climate Crisis*, 1st ed., 1–8. Candice Janco. <https://doi.org/doi:10.1016/b978-0-12-823366-5.00001-4>.
- Ye, Run Ping, Jie Ding, Weibo Gong, Morris D. Argyle, Qin Zhong, Yujun Wang, Christopher K. Russell, et al. 2019. “CO₂ Hydrogenation to High-Value Products via Heterogeneous Catalysis.” *Nature Communications* 10 (1). <https://doi.org/10.1038/s41467-019-13638-9>.

Acknowledgments

This work was financially supported by LA/P/0045/2020 (ALICE), UIDB/50020/2020, and UIDP/50020/2020 (LSRE-LCM), funded by national funds through FCT/MCTES (PIDDAC) Mariana B. S. Felgueiras acknowledges the PhD research grant from FCT (2022.09616.BD), funded by national funds and by the European Union (EU) through the European Social Fund (ESF). O.S.G.P.S. acknowledges FCT funding under the Scientific Employment Stimulus – Institutional Call CEECINST/00049/2018.

Investigation of different gel polymer electrolytes for flexible electrochromic supercapacitors

Gabriela Queirós¹, André M. Pereira², Clara R. Pereira¹

¹REQUIMTE/LAQV, Department of Chemistry and Biochemistry, Faculty of Sciences, University of Porto, 4169-007 Porto, Portugal

Gabriela Queirós: up201304097@up.pt; ORCID: 0000-0002-6030-970X Clara R. Pereira: clara.pereira@fc.up.pt; ORCID: 0000-0001-9224-1917

²FIMUP – Institute of Physics for Advanced Materials, Nanotechnology and Photonics, Department of Physics and Astronomy, Faculty of Sciences, University of Porto, 4169-007 Porto, Portugal (ampereira@fc.up.pt) ORCID 0000-0002-8587-262X

Abstract

In this work, various gel polymer electrolytes containing different polymers and Li- based salts were prepared and applied in the development of flexible supercapacitors (SCs) and electrochromic supercapacitors (ECSCs). The electrolytes were optimized to improve their ionic conductivity and increase the potential window of operation of the resulting devices. Textile-based SCs were prepared through the assembly of cotton-based electrodes coated with multiwalled carbon nanotubes sandwiching the polymer electrolytes, while the ECSC device was designed using flexible plastic substrates coated with PEDOT:PSS as electrode sandwiching the best-performing polymer electrolyte. The textile-based SC with the best electrochemical performance was designed using the gel polymer electrolyte containing LiClO₄ and polymethyl methacrylate in 1:1.5 mass ratio, exhibiting an energy density of 4.96 μW h cm⁻² at a power density of 910.76 μW cm⁻². Moreover, a flexible ECSC device was developed, with its color changing from colorless to dark blue by application of -1.5/1.5 V potentials.

Author Keywords. gel polymer electrolyte, energy storage, supercapacitors, electrochromism, flexible devices.

1. Introduction

Over the years, the global demand for energy and the exhaustion of fossil fuels have been leading to a quest for clean and safe energy storage devices. Supercapacitors (SCs) are a green and safe energy storage solution, presenting long cycle life, high power density and fast charging. One of the current challenges relies on the development of multifunctional SC technologies with sensing properties in order to monitor in real-time energy consumption. Electrochromic supercapacitors (ECSCs) combine the principles of SCs (energy storage) and electrochromic (EC) devices in a single multitasking device that reversibly changes color under an applied potential. ECSCs have the potential to be applied in wearable electronics for daily applications, such as healthcare monitoring, flexible electronic displays and sensors (Lu et al. 2021).

Gel polymer electrolytes have an important function in the electrochemical performance of SCs and ECSCs, acting both as ion donors and separators, unlike liquid electrolytes that operate in smaller potential windows (~1.2 V) and may suffer corrosion (Kotobuki 2020).

In this work, several gel polymer electrolytes containing different polymers and Li-based salts were prepared and applied in the development of flexible electrical double-layer-type capacitors and an ECSC. The electrolytes were optimized to improve their ionic conductivity and increase the maximum potential window of operation of the resulting devices. Two types of devices were fabricated: (i) textile-based SCs composed of CNT-coated cotton electrodes;

(ii) flexible ECSC composed of two electrodes of PET-ITO (indium tin oxide on polyethylene terephthalate) spray-coated with an electrically-conductive electrochromic polymer of (poly(3,4-ethylenedioxythiophene) polystyrene sulfonate, PEDOT:PSS). All devices were assembled with sandwich-type configuration. This research enabled the development of flexible devices with capacitive and electrochromic features and to grasp the influence of the electrolytes on the devices performance.

2. Materials and Methods

The reagents and solvents used to prepared the polymer electrolytes were lithium perchlorate(LiClO₄, Sigma-Aldrich, 99.99%), lithium chloride (LiCl, Sigma-Aldrich, ≥99%), poly(methylmethacrylate) (PMMA, Sigma-Aldrich), poly(vinyl alcohol) (PVA, Sigma-Aldrich, 99+%), anhydrous polypropylene carbonate (PC, Sigma-Aldrich, 99.7%), acetonitrile (ACN, Honeywell, ≥99.9%), and ultrapure water (Millipore, specific resistivity: 18 MΩ cm).

The textile SCs (TSCs) were prepared through the assembly of two cotton-based electrodes coated with multiwalled carbon nanotubes (MWCNTs), which were previously fabricated through the dip-pad-dry process (Costa et al. 2020). The flexible ECSC devices were designed using two PET-ITO electrodes spray-coated with PEDOT:PSS and assembled in sandwich-type configuration. The electrochemical performance of the devices was evaluated by electrochemical impedance spectroscopy (EIS), cyclic voltammetry and galvanostatic charge/discharge measurements.

3. Discussion

The textile electrodes contained 18 wt% of MWCNTs loading and presented an average electrical resistance of 71 Ω after 8 dip-pad-dry-steps. The fabricated TSCs demonstrated an electric double-layer charge storage mechanism, as revealed by the rectangular-shaped *i*-*V* cycles (Figure 1). The values obtained for the equivalent series resistance at 1 kHz (*RES*, obtained from EIS measurements), areal capacitance, working potential (*V*₀), energy density and power density of the TSCs prepared with the different electrolytes are summarized in Table 1. The gel polymer electrolyte prepared with LiClO₄:PMMA mass ratio of 1:1.5 exhibited the most promising performance, with low *RES* (135.44 Ω), 12.06 mF cm⁻² capacitance at 10 mV s⁻¹, 4.96 μW h cm⁻² energy density and 910.76 μW cm⁻² power density.

Electrolytes	<i>RES</i> (Ω)	Capacitance (mF cm ⁻²) @ 10 mV s ⁻¹	<i>V</i> ₀ (V) @ 0.1 A g ⁻¹	Energy density (μW h cm ⁻²)	Power density (μW cm ⁻²)
LiClO ₄ : PMMA = 1 : 1.5	135.44	12.06	1.72	4.96	910.76
LiClO ₄ : PMMA = 1 : 2	127.37	7.43	1.64	2.79	883.83
LiClO ₄ : PMMA = 1 : 2 (higher volume of ACN)	182.93	7.29	1.24	1.56	350.01
LiClO ₄ : PMMA = 1 : 1.3 (higher volume of ACN)	142.37	7.02	1.57	2.41	720.51
LiClO ₄ : PMMA = 1 : 1.3 (higher volume of PC)	287.35	6.17	1.32	1.48	250.98
LiCl/PVA	207.77	4.90	1.38	1.29	380.91

Table 1: Electrochemical performance of the as-prepared TSCs with different gel polymers electrolytes.

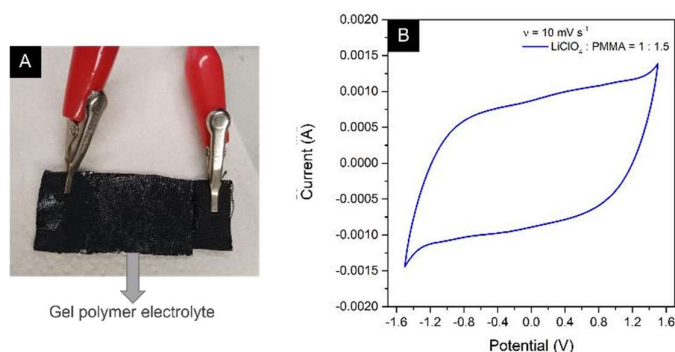


Figure 1: (A) Photograph and (B) *i*-*V* cycle at 10 mV s⁻¹ of the TSC containing the most promising gel polymer electrolyte.

The most promising polymer electrolyte was later used to build a flexible electrochromic supercapacitor device, which changed color from colorless to dark blue with the application of potentials of ±1.5 V (Figure 2).

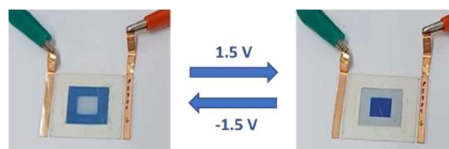


Figure 2. ECSC prepared with the most promising gel polymer electrolyte.

4. Conclusions

EDLC-type textile SCs were successfully prepared using different gel polymer electrolytes. The TSC device with the best electrochemical performance was designed using the gel polymer electrolyte with LiClO₄:PMMA ratio of 1:1.5, exhibiting an energy density of 4.96 $\mu\text{W h cm}^{-2}$ at a power density of 910.76 $\mu\text{W cm}^{-2}$. Subsequently, a flexible ECSC device was successfully developed using the most promising electrolyte, which efficiently changed color from colorless to dark blue by application of -1.5/1.5 V potentials.

References

- Costa, Rui S., Alexandra Guedes, André M. Pereira, and Clara Pereira. 2020. "Fabrication of all-solid-state textile supercapacitors based on industrial-grade multi-walled carbon nanotubes for enhanced energy storage." *Journal of Materials Science* 55 (23):10121-10141. doi: 10.1007/s10853-020-04709-0.
- Kotobuki, Masashi. 2020. "Polymer Electrolytes: State of the Art." In *Polymer Electrolytes: Characterization Techniques and Energy Applications*, edited by Abdul K. Arof TanWinie, and Sabu Thomas. by Wiley-VCH Verlag GmbH & Co. KGaA.
- Lu, Zelin, Xiaolan Zhong, Xueqing Liu, Jinliang Wang, and Xungang Diao. 2021. "Energy storage electrochromic devices in the era of intelligent automation." *Physical Chemistry Chemical Physics* 23 (26):14126-14145. doi: 10.1039/D1CP01398J.

Funding

This work was financially supported by Portuguese funds through Fundação para a Ciência e a Tecnologia (FCT)/MCTES in the framework of the project PTDC/CTM-TEX/4126/2021.

Acknowledgements

Work supported by Portuguese funds through FCT/MCTES in the framework of projects UIDB/50006/2020, UIDP/50006/2020 and UIDB/04968/2020. GQ thanks FCT for the PhD scholarship (UI/BD/151274/2021). CRP thanks FCT for funding through Individual Call to Scientific Employment Stimulus (2021.04120.CEECIND/CP1662/CT0008).

Are parabens a hushed threat to drinking water microbiological quality?

Ana Rita Pereira^{1,2*}, Inês Gomes^{1,2}, Manuel Simões^{1,2}

¹LEPABE - Laboratory for Process Engineering, Environment, Biotechnology and Energy, Faculty of Engineering, University of Porto, Rua Dr. Roberto Frias, 4200-465 Porto, Portugal

² ALiCE - Associate Laboratory in Chemical Engineering, Faculty of Engineering, University of Porto, Rua Dr. Roberto Frias, 4200-465 Porto, Portugal

*Corresponding author: up201505436@edu.fe.up.pt; ORCID 0000-0002-8042-9995

Abstract

Parabens, environmental contaminants found at trace concentrations in drinking water, negatively affect human and aquatic health. The impact of paraben exposure on microorganisms and drinking water microbiological quality is often overlooked. This study investigates the effects of paraben exposure (methylparaben, propylparaben, and butylparaben) on biofilms formed by *Acinetobacter calcoaceticus* and *Stenotrophomonas maltophilia*. Parabens altered biofilm culturability, with significant increases observed in *A. calcoaceticus* biofilms exposed to BP and MIX, while *S. maltophilia* biofilms exhibited varying responses. Parabens may compromise drinking water safety, with polypropylene identified as a critical biofilm growth promoter.

Author Keywords. biofilms, parabens, high-density polyethylene, drinking water

1. Introduction

The presence of parabens as environmental contaminants in water sources has been reported worldwide, even at trace concentrations in drinking water (Wei et al., 2021; Le et al., 2022). These contaminants have been associated to negative effects on human and aquatic organisms' health (Lincho et al., 2021). However, the impact of paraben exposure on microorganisms, including their effects on biofilms and drinking water microbiological quality, has been largely overlooked. This study aims to assess the effects of paraben exposure on biofilms formed by *Acinetobacter calcoaceticus* and *Stenotrophomonas maltophilia*, isolated from drinking water.

2. Materials and Methods

Biofilms were formed on high-density polyethylene (HDPE) coupons for 7 and 26 days, both in the presence and absence of parabens (methylparaben - MP, propylparaben - PP, butylparaben - BP, and a triple combination of each one - MIX) at a concentration of 150 ng/L. The experimental setup and procedures followed the methodology described by Pereira et al. (2023).

3. Discussion

Exposure to parabens had a significant impact on the culturability of the biofilm bacteria. The 26-day-old *A. calcoaceticus* biofilms grown in the presence of BP and MIX at 150 ng/L showed a 3- to 4-fold increase in the number of culturable cells compared to the control. On the other hand, 7-day-old *S. maltophilia* biofilms formed on HDPE exhibited a twofold increase in culturable cells in the presence of MP but a threefold decrease when exposed to MIX. Parabens also influenced the cellular density of biofilms, with an overall increase observed. A double increase was verified for 7-day-old *A. calcoaceticus* biofilms exposed to BP and 26-day-old *A. calcoaceticus* biofilms exposed to MP compared to non-exposed biofilms. Similarly, exposure to MP, PP, and BP at 150 ng/L resulted in increased biofilm cell density in 26-day-old *S. maltophilia* biofilms. However, exposure to MIX for 7 days reduced the total number of *S. maltophilia* biofilm cells by fourfold.

4. Conclusions

This study demonstrates that paraben exposure influences the formation and culturability of biofilms formed by *A. calcoaceticus* and *S. maltophilia*, both commonly found in drinking water. The effects vary depending on the specific paraben, exposure time, and bacterial species. The increased number of biofilm cells induced by parabens raises concerns regarding the potential compromise of drinking water microbiological quality and safety. These findings highlight the importance of considering the effects of parabens on biofilms and microbial communities in water systems. Further research is

needed to fully understand the ecological and public health implications of paraben exposure in the context of drinking water.

References

- Le, Thuy Minh, Phuong Thi Pham, Truong Quang Nguyen, Trung Quang Nguyen, Minh Quang Bui, Hoa Quynh Nguyen, Nam Duc Vu, Kurunthachalam Kannan, and Tri Manh Tran. 2022. "A Survey of Parabens in Aquatic Environments in Hanoi, Vietnam and Its Implications for Human Exposure and Ecological Risk." *Environmental Science and Pollution Research* 29 (31): 46767–77. <https://doi.org/10.1007/s11356-022-19254-3>.
- Lincho, João, Rui C. Martins, and João Gomes. 2021. "Paraben Compounds—Part i: An Overview of Their Characteristics, Detection, and Impacts." *Applied Sciences (Switzerland)* 11 (5): 1–38. <https://doi.org/10.3390/app11052307>.
- Pereira, Ana Rita, Inês B Gomes, and Manuel Simões. 2023. "Impact of Parabens on Drinking Water Bacteria and Their Biofilms: The Role of Exposure Time and Substrate Materials." *Journal of Environmental Management* 332: 117413. <https://doi.org/10.1016/j.jenvman.2023.117413>.
- Wei, Fang, Monika Mortimer, Hefa Cheng, Nan Sang, and Liang Hong Guo. 2021. "Parabens as Chemicals of Emerging Concern in the Environment and Humans: A Review." *Science of the Total Environment* 778 (July). <https://doi.org/10.1016/j.scitotenv.2021.146150>.

Acknowledgments

This work was financially supported by: LA/P/0045/2020 (ALiCE) and UIDB/00511/2020 - UIDP/00511/2020 (LEPABE) funded by national funds through FCT/MCTES (PIDDAC); by the Pereira A. R. PhD scholarship (2021.06226.BD) provided by FCT, by the I. B. Gomes contract (2022.06488.CEECIND) and HealthyWaters (NORTE-01-0145-FEDER-000069), supported by Norte Portugal Regional Operational Programme (NORTE 2020), under the PORTUGAL 2020 Partnership Agreement, through the European Regional Development Fund (ERDF).

Ecological brick production from water treatment sludge in brazil

Rafaela Mulinari Cabral¹, Claudio Akamatsu², Natiéli Cristina Mendes Ross³, Ramiro José Espinheira Martins⁴, Juliana Martins Teixeira de Abreu Pietrobelli⁵

¹ Technology and Management School, Polytechnic Institute of Bragança, 5300-253, Bragança, Portugal (rafaelarmc@hotmail.com)

² Department of Chemical Engineering, University Technology Federal Do Paraná, Rua Doutor Washington Subtil Chueire, 4200-465, Ponta Grossa, Brazil (claudio.akamatsu@gmail.com)

³ Department of Chemical Engineering, University Technology Federal Do Paraná, Rua Doutor Washington Subtil Chueire, 4200-465, Ponta Grossa, Brazil (natielliross@gmail.com)

⁴ Department of Chemical and Biological Technology, Technology and Management School, Polytechnic Institute of Bragança, 5300-253, Bragança, Portugal (rmartins@ipb.pt) ORCID (0000-0003-4327-7782)

⁵ Department of Chemical Engineering, University Technology Federal Do Paraná, Rua Doutor Washington Subtil Chueire, 4200-465, Ponta Grossa, Brazil (jpietrobelli@utfpr.edu.br) ORCID (0000-0002-5804-1644)

Abstract

The accelerated growth of urban areas has led to greater demand for natural resources, mainly water. Conventional water treatment plants are used to treat water that is unsuitable for consumption. However, this process generates sludge, a residue that contains chemical elements that, if improperly disposed, can negatively affect human life and the environment. To solve this problem, an alternative is to use the sludge generated for civil construction applications. The objective of this research was to evaluate the feasibility of partially replacing soil with sludge in the production of ecological bricks using sand, earth, sludge, and cement. Test specimens were manufactured according to the literature and evaluated using the NBR 8491:2012 and NBR 8492:2012 standards with compressive strength and water absorption tests. Under the tested conditions, the bricks displayed high water absorption within the limits of the norm. However, they did not meet the required minimum compressive strengths.

Author Keywords. Water Treatment Plant, Sludge, Civil Construction.

1. Introduction

According to the Brazilian Institute of Geography and Statistics (IBGE), the population of Ponta Grossa has grown by approximately 25% since 2010 (compared to the national growth rate of 8.9%), leading to an increasing demand for water resources. However, the conventional water treatment process employed by Water Treatment Stations (WTS) in Brazil produces a residue called WTP sludge, which contains both organic and inorganic materials with high moisture content and potentially harmful chemical elements. In light of this, several studies have explored the disposal of WTS sludge, including its potential use in civil construction, such as its incorporation into brick manufacturing. Therefore, this study aims to investigate the possibility of utilizing WTP sludge as a partial substitute for soil in brick production, in accordance with the NBR 8491:2012 and 8492:2012 standards for ecological brick production, and testing of compression and water absorption.

2. Materials and Methods

Sludge samples from the Water Treatment Station, soil with a reddish clayey appearance, and sand (gravel from hail deposits with coarse and yellowish particles) were collected or acquired in Ponta Grossa, Paraná, Brazil. The methodology used to manufacture the ecological brick was based on the Booklet for the Production of Soil-Cement Bricks of the Technology Foundation of the State of Acre (FUNTAC, 1999).

To prepare the materials, the soil and sludge were dried separately at 110°C for 48 hours, while the gravel, which had low humidity, was dried, and sieved through a 4.8 mm mesh. The mixture was made with Portland cement (CP-II-F-32 from the Cauê brand) by NBR 10833:2012. Four different mixes were created with a composition of 10% cement, 63% sand, and 27% earth with substitutions of 4%, 9% and 18% of sludge in the soil.

Sand, soil, silt, and cement were homogenized to prepare the mixtures. Water was then added until ideal molding humidity was reached. The ideal humidity parameter for the mixture was verified according to FUNTAC (1999).

The moistened mixtures were sieved manually and subsequently transferred to a manual press hopper to shape the bricks. After the pressing stage, the bricks were cured for seven days (Figure), after which mechanical resistance and water absorption tests were performed to evaluate their properties.



Figure 1: Bricks in curing process

To be considered suitable for use, the bricks must have sharp edges, without any cracks, fractures, or defects that could compromise the laying, strength, and durability of the masonry. To ensure compliance with NBR 8491:2012, which specifies the requirements for soil-cement bricks used in masonry, the compressive strength and water absorption of the bricks were tested, with values between 1.7 MPa and 2.0 MPa, 20% and 22%, respectively. Seven bricks of each mixture were subjected to compression tests, and three bricks of each type were used for absorption tests.

The NBR 8492:2012 standard was used for the methodology of the tests, where in the first test, the bricks were halved and their respective faces were glued together using Portland cement paste. They were then immersed in water for six hours, after which the brick surfaces were dried and transferred to the testing machine. The load was gradually increased at a rate of 500 N/s until the brick failed. In the second test, the bricks were dried at approximately 105°C until a constant mass was achieved. The samples were then immersed in a water tank for 24 h. After this period, the brick surfaces were dried and weighed again.

3. Results and Conclusions

This work is important for studying the feasibility of using WTS sludge in civil construction for the production of ecological bricks.

After curing, the bricks that were not mixed with sludge displayed an average water absorption rate of 18%, whereas those mixed with sludge exhibited a 20% absorption rate for each percentage of the mixture. This is because of their high porosity, which may be attributed to the presence of sand in the brick-making process. This leads to the formation of lumps, particularly in mixtures containing silt, and affects the compressive strength results (which are obtained after immersing the bricks in water). However, the requirements specified by the standards were met (Table 3). The decrease in the strength of the bricks, coupled with the increase in the percentage of sludge, can be attributed to the granules of the sludge (as depicted in Figure 2). It should be noted that adding a material with a lower resistance compared to other components of the mixture can lead to a reduction in the strength of the final product.

Mixture	Breaking Load (N)	Compressive Strength (Mpa)
0	14031.69	0.97
1	7945.26	0.55
2	10085.84	0.70
3	6869.51	0.47

Table 7: Average values of compressive strength in each mixture



Figure 2: Visible granules of sludge

In this study, the bricks did not meet the specifications outlined in NBR 8491:2012, indicating a need for further research to improve their quality. Segantini and Alcântara (2020) identified several factors that significantly affect the properties of soil–cement mixtures, including soil type, cement content, moisture content, compaction, age, and curing period. Future studies should focus on the points highlighted by the authors to investigate this topic further.

References

- HOPPEN, C.; PORTELLA, K. F.; JOUKOSKI, A.. Uso de lodo de estação de tratamento de água centrifugado em matriz de concreto de cimento portland para reduzir o impacto ambiental. *Química nova*, São Paulo, v. 29, n. 1, jan./fev. 2006.
- FUNTAC. Cartilha para produção de tijolo solo cimento. Rio Branco, AC. 1999.
- ABNT (Associação Brasileira de Normas Técnicas). NBR 8491: Tijolo de solo- cimento – Requisitos. Rio de Janeiro, 2012.
- ABNT (Associação Brasileira de Normas Técnicas). NBR 8492: Tijolo de solo cimento – Análise dimensional, determinação da resistência à compressão e da absorção de água – Método de ensaio. Rio de Janeiro, 2012.
- ABNT (Associação Brasileira de Normas Técnicas). NBR 10833: Fabricação de tijolo e bloco de solo-cimento com utilização de prensa manual ou hidráulica. Rio de Janeiro, 2012.
- SEGANTINI, A. A. S; ALCÂNTARA M. A. M. Solo-cimento e Solo – Cal. In: *Materiais de Construção Civil e Princípios de Ciência e Engenharia de Materiais*. São Paulo: IBRACON, 2010, 2ª. Ed. v.2. Cap.27. p.864 – 891.

Acknowledgments

SANEPAR for providing the sludge for this study.

UTFPR-PR for the structure provided, especially Prof. Sandra Mara Kaminski Tramontin responsible for the Destructive and Non-Destructive Testing Laboratory (LabENS).

LSRE-LCM Laboratory of Separation and Reaction Engineering Laboratory of Catalysis and Materials, ALICE Associate Laboratory in Chemical Engineering, FEUP, Porto.

Treatment of effluent from the olive pomace oil extraction industry by coagulation

Thais T. Grabowski¹, Ramiro E. J. Martins^{1,2,3*}

¹Technology and Management School, Polytechnic Institute of Bragança, Campus de Santa Apolónia, 5300-252, Bragança, Portugal.

²LSRE-LCM Laboratory of Separation and Reaction Engineering-Laboratory of Catalysis and Materials, Faculty of Engineering, University of Porto, Rua Dr. Roberto Frias, 4200-465, Porto, Portugal.

³ALICE - Associate Laboratory in Chemical Engineering, FEUP, Porto, Portugal.

*Corresponding author: e-mail address: rmartins@ipb.pt; ORCID ID 0000-0003-4327-7782.

Abstract

This study aimed to find an efficient coagulation/flocculation method for treating wastewater generated from olive oil extraction industry (OOEIW), as untreated discharge of this wastewater can lead to ecological changes in surface water. To achieve this objective, the study utilized aluminum sulfate ($\text{Al}_2(\text{SO}_4)_3$) and Ambifloc 59001 flocculant to reduce the organic matter content in the effluent. The experiments were performed using a Jar Test apparatus with a dosage range of 200 to 3000 mg L^{-1} of $\text{Al}_2(\text{SO}_4)_3$ at pH 7, followed by pH testing at 4.5 and 6 to identify optimal conditions. The dosage of Ambifloc 59001 was then determined using these conditions. It was concluded that the optimal process configuration was 1500 mg L^{-1} of $\text{Al}_2(\text{SO}_4)_3$ and 42 mg L^{-1} of Ambifloc 59001 at pH 6. The supernatant generated from this coagulation/flocculation process exhibited a reduction in COD, TOC, and TPh levels, which suggests a reduction in the organic matter content in the effluent.

Author Keywords. Pomace oil, characterization, discharge, coagulation, aluminum sulfate.

1. Introduction

The olive oil industry utilizes different techniques for producing olive oil, including the two- and three-phase continuous methods, as noted by Domingues et al. (2022). During this process, solid waste, known as olive pomace, is generated, and a second extraction process using organic solvents is performed to remove any remaining oil. The resulting wastewater is referred to as olive oil extraction industry wastewater (OOEIW), which requires treatment, as highlighted by Martins et al. (2022). If discharged without proper treatment, this effluent can cause ecological changes in surface water, including acidification, oxygen depletion, color alteration, and decreased water transparency, as noted by the same authors.

As stated by Khouni et al. (2020), coagulation/flocculation is a popular pre-treatment method due to its affordability and ease of operation when compared to other pre-treatment methods. In addition, coagulation has gained popularity as a tertiary treatment method in effluent treatment systems because of its efficiency in removing suspended solids, organic matter, and phosphorus. The objective of this study is to utilize aluminum sulfate ($\text{Al}_2(\text{SO}_4)_3$) and the flocculant Ambifloc 59001 for the treatment of OOEIW to reduce the organic matter content present in the effluent.

2. Materials and Methods

To conduct the experiments, samples of effluent were collected from an olive pomace oil extraction plant located in Mirandela (northeastern Portugal) on March 15, 2022. The industrial unit receives olive pomace from two-phase olive oil extraction units, and the samples were specifically collected from the stabilization and evaporation pond. The collected OOEIW has a pH of 4.7, with a total nitrogen concentration of 167 $\text{mg NO}_3 - \text{N L}^{-1}$, and a total phosphorus concentration of 509 mg P L^{-1} . It also has a high Biochemical Oxygen Demand (BOD_5) of 6424 mg L^{-1} , a Chemical Oxygen Demand (COD) of 73300 mg L^{-1} , and a total phenolic compound (TPh) concentration of 3862 mg L^{-1} . Additionally, a total organic carbon (TOC) of 26600 mg L^{-1} , total carbon (TC) of 27400 mg L^{-1} , total nitrogen (TN) of 350 mg L^{-1} , total solids (TS) of 36700 mg L^{-1} , and volatile solids (SV) of 22900 mg L^{-1} .

To find an appropriate primary treatment process for the effluent, the coagulation/flocculation technique was assessed at varying dosages of aluminum sulfate $\text{Al}_2(\text{SO}_4)_3$ ranging from 200 to 3000 mg L^{-1} at pH 7. The most effective concentration was then evaluated at pH 6 and 4.5 to determine the best pH for treatment. After identifying the optimal conditions, the dosage of the flocculant Ambifloc 59001 was determined. All experiments were carried out using a coagulation/flocculation apparatus (Jar Test) with a sample size of 300 mL. The procedure involved adding the sample, adjusting the pH, stirring at 150 rpm for 3 minutes, adding the flocculant, and stirring the solution at 20 rpm for 15 minutes. The samples were then left to decant for 2 hours, after which aliquots were taken to measure the COD.

3. Discussion

It was determined that the optimal dosage of the coagulant was 1500 mg L^{-1} in the first stage. Lower dosages resulted in less than 5% removal, while higher dosages yielded only around 8% removal. Thus, the dosage of 1500 mg L^{-1} was the most advantageous, as it resulted in a removal of 10%. (Figure).

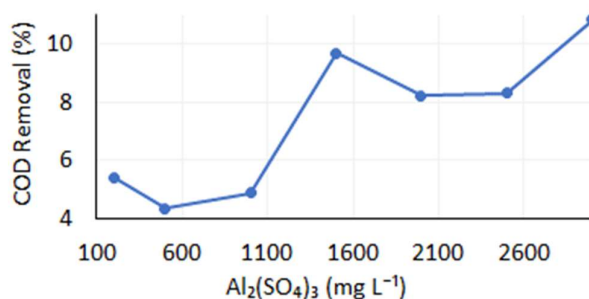


Figure 1: COD removal from the OOEIW after de coagulation process with $\text{Al}_2(\text{SO}_4)_3$ at pH 7

The coagulation process was repeated at pH levels of 4.5 and 6 in the second phase of the study, and the results showed removal rates of 11% and 12%, respectively. Thus, pH 6 was found to be the optimal level. The effectiveness of a flocculant was evaluated by testing different dosages and observing the formation of a thread of coagulates being grouped in the middle. The optimal dosage was determined to be 9 mL, and this dosage was subsequently used to investigate its impact on COD removal. The best COD removal was achieved by adding 25 mL of the flocculant (500 mg L^{-1}). Ultimately, the most effective coagulation/flocculation configuration was determined to be 1500 mg L^{-1} of $\text{Al}_2(\text{SO}_4)_3$ and 42 mg L^{-1} of Ambifloc 59001 at pH 6.

Yazdanbakhsh et al. 2015 conducted experiments to investigate the impact of increasing $\text{Al}_2(\text{SO}_4)_3 \cdot 18\text{H}_2\text{O}$ dosage (ranging from 1000 to 6000 mg L^{-1}) at pH 10 (adjusted before coagulant addition) on the coagulation of OMW with high COD (58800 mg L^{-1}) and TPh (444 mg L^{-1}) concentrations and the authors found the maximum removal of 88% of COD. However, it is important to note that the efficiency of coagulation/flocculation can vary depending on the degree of contamination of the effluent and its matrix. The difference in efficiency observed in this study with OOEIW may be explained by this.

Effluent treated with coagulation/flocculation showed a 15% decrease in total nitrogen (142 $\text{mg NO}_3 - \text{N L}^{-1}$), 55% decrease in total phosphorus (229 mg P L^{-1}) and 16% decrease in COD (61700 mg L^{-1}). The supernatant had a pH of 6, BOD_5 of 6310 mg L^{-1} , high concentrations of TPh (25400 mg L^{-1}) and total solids (45800 mg L^{-1}).

4. Conclusions

The coagulation/flocculation process effectively removed some contaminants from the effluent, but total nitrogen, total phosphorus, and TPh remained high, and only 16% of the COD was removed. Additional treatment processes are needed to fully treat the effluent, such as chemical, physical, and/or biological methods, to meet regulatory requirements. A combination of treatment processes is recommended for safe disposal.

References

- Domingues, Eva, Eryk Fernandes, João Gomes, Sérgio Castro-Silva, and Rui C. Martins. 2022. "Advanced Oxidation Processes at Ambient Conditions for Olive Oil Extraction Industry Wastewater Degradation." *Chemical Engineering Science* 263 (December): 118076. <https://doi.org/10.1016/J.CES.2022.118076>.
- Khouni, Imen, Ghofrane Louhichi, Ahmed Ghrabi, and Philippe Moulin. 2020. "Efficiency of a Coagulation/Flocculation–Membrane Filtration Hybrid Process for the Treatment of Vegetable Oil Refinery Wastewater for Safe Reuse and Recovery." *Process Safety and Environmental Protection* 135 (March): 323–41. <https://doi.org/10.1016/J.PSEP.2020.01.004>.
- Martins, Ramiro J. E., Juliana M. T. de A. Pietrobelli, and Andressa Mazur. 2022. "Effluent Characterization and Waterbody Monitoring from An Olive Pomace Oil Extractor Industry." *International Journal of Engineering Research & Technology* 11 (5): 120–23. <https://doi.org/DOI:10.17577/IJERTV11IS050115>.
- Yazdanbakhsh, Ahmadreza, Fayyaz Mehdipour, Akbar Eslami, Hajar Sharifi Maleksari, and Farshid Ghanbari. 2015. "The Combination of Coagulation, Acid Cracking and Fenton-like Processes for Olive Oil Mill Wastewater Treatment: Phytotoxicity Reduction and Biodegradability Augmentation." *Water Science and Technology* 71 (7): 1097–1105. <https://doi.org/10.2166/wst.2015.080>.

Acknowledgments

This work had financial support: i) Project NORTE-01-0247-FEDER-072124. Bagaço+Valor - Tecnologia Limpa para a Valorização dos Subprodutos do Bagaço na Indústria Extratora de Azeite, funded by the European Regional Development Fund (ERDF) and ii) LA/P/0045/2020 (ALiCE), UIDB/50020/2020 and UIDP/50020/2020 (LSRE-LCM), funded by national funds through FCT/MCTES (PIDDAC).

***Delftia acidovorans* extracellular metabolites increase the biomass and metabolic activity of drinking water biofilms**

Ana C. Afonso^{1,2,3,*}, Inês B. Gomes¹, Maria José Saavedra², Lúcia Simões³, Manuel Simões¹

¹ALICE-LEPABE, Faculdade de Engenharia, Universidade do Porto, Rua Dr. Roberto Frias, 4200-465 Porto, Portugal

²CITAB, Universidade de Trás-os-Montes e Alto Douro, Quinta de Prados Edifício Reitoria Sala D2.30, 5000-801 Vila Real, Portugal

³CEB-LABELS, Universidade do Minho, Campus de Gualtar, 4710-057 Braga, Portugal

*Corresponding author: up202010573@edu.fe.up.pt; ORCID 0000-0002-4926-8935

Abstract

Little is known about the impact of bacterial coaggregation in aquatic biofilms. Thus, in this study, the effect of the presence of bacteria with this ability on drinking water species biofilms was studied. For this, cell-free supernatant of the coaggregating strain *D. acidovorans* was added to each bacterial suspension and biofilms were allowed to grow. A generalized increase in biomass production and metabolic activity of the biofilms was observed when in the presence of these supernatants.

Author Keywords. Bacterial fitness, cell-cell interaction, coaggregation, multispecies biofilm.

1. Introduction

Biofilm formation is one of the main problems in drinking water distribution systems (DWDS) (Simões and Simões 2013). Biofilms commonly appear as multispecies communities and much of their structural and functional dynamics are due to interactions between species (Rickard et al. 2003). Coaggregation is a highly specific form of cell-cell interaction, characterized by the recognition and adhesion of different species to each other (Rickard et al. 2003). This is already considered a key mechanism in multispecies biofilm formation in oral environments (Rickard et al. 2003), but little is known about its role in aquatic biofilms development (Afonso et al. 2021). In previous work, *Delftia acidovorans*, isolated from potable water, was identified as a microorganism with strong coaggregation ability (Afonso et al. 2023). To better understand the role of *D. acidovorans* on the development of DW autochthonous species biofilms, cell-free supernatant (CFS) of *D. acidovorans* were added to each bacterial suspension and biofilms were formed.

2. Materials and Methods

Single-species biofilms and single-species biofilms plus *D. acidovorans* CFS were grown for 24 h and 48 h in 96-well microtiter plates and characterized in terms of biomass production and metabolic activity by crystal violet and resazurin staining assays, respectively.

3. Discussion

In general, there was a directly proportional relationship between time-biomass and time-metabolic activity for both single-species biofilms and single-species biofilms in the presence of CFS. When comparing the biomass of *Citrobacter freundii* and *Pseudomonas putida* biofilms, an increase was observed for biofilms containing CFS at both 24 h and 48 h. Regarding metabolic activity, an increase was observed when CFS was added to *C. freundii* biofilms, both at 24 h and 48 h. This increase in metabolic activity of the 24 h biofilms was almost 5 times higher than the single-species biofilm without CFS, for the same sampling time. There was also an increase in the metabolic activity of *P. putida* biofilms, but not as pronounced.

4. Conclusions

These results suggest the production of extracellular metabolites by *D. acidovorans* that favor the development of biofilms by other DW bacterial species. Furthermore, it provides new insights into the coaggregation mechanism and its impact on DW consortium. That said, understanding coaggregation and identifying other coaggregating strains becomes important given the observations made in this study.

References

- Afonso, Ana C., Inês B. Gomes, Maria José Saavedra, Efstathios Giaouris, Lúcia C. Simões, and Manuel Simões. 2021. "Bacterial Coaggregation in Aquatic Systems." *Water Research* 196 (May). <https://doi.org/10.1016/J.WATRES.2021.117037>.
- Afonso, Ana C., Inês B. Gomes, Maria José Saavedra, Lúcia Simões, and Manuel Simões. 2023. "Drinking-Water Isolated Delftia Acidovorans Selectively Coaggregates with Partner Bacteria and Facilitates Multispecies Biofilm Development." *Science of The Total Environment*, March, 162646. <https://doi.org/10.1016/J.SCITOTENV.2023.162646>.
- Rickard, AH, P Gilbert, NJ High, PE Kolenbrander, and PS Handley. 2003. "Bacterial Coaggregation: An Integral Process in the Development of Multi-Species Biofilms." *Trends in Microbiology*. Elsevier Ltd. [https://doi.org/10.1016/S0966-842X\(02\)00034-3](https://doi.org/10.1016/S0966-842X(02)00034-3).
- Simões, LC, and M Simões. 2013. "Biofilms in Drinking Water: Problems and Solutions." *RSC Advances*. Royal Society of Chemistry. <https://doi.org/10.1039/c2ra22243d>.

Acknowledgments

This work was financially supported by LA/P/0045/2020 (ALiCE), UIDB/00511/2020 and UIDP/00511/2020 (LEPABE), funded by national funds through FCT/MCTES (PIDDAC); UIDB/04469/2020 (CEB) and by LABBELS – Associate Laboratory in Biotechnology, Bioengineering and Microelectromechanical Systems, LA/P/0029/2020; UIDB/04033/2020 (CITAB); Project Biocide_for_Biofilm-PTDC/BII-BTI/30219/2017-POCI-01-0145-FEDER-030219, ABFISH-PTDC/ASP-PES/28397/2017-POCI-01-0145-FEDER- 028397 and Germirrad-POCI-01-0247-FEDER-072237, funded by FEDER funds through COMPETE2020–Programa Operacional Competitividade e Internacionalização (POCI) and by national funds (PIDDAC) through FCT/MCTES; project HealthyWaters (NORTE-01-0145-FEDER-000069)- NORTE 2020/ERDF; and the FCT contract (2022.06488.CEECIND) and FCT grant (2020.04773.BD).

Delivering antisense NAMs into bacteria using dendritic lipids

Mariana Gomes^{1,2,*}, Yana Zamoshchak^{1,2,3}, Dinesh Dhumal⁴, Ling Peng⁴, Rita S. Santos^{1,2}, Nuno F. Azevedo¹

¹LEPABE - Laboratório de Engenharia de Processos, Ambiente, Biotecnologia e Energia, Faculdade de Engenharia da Universidade do Porto, Rua Dr. Roberto Frias, 4200-465 Porto, Portugal

²ALiCE - Laboratório Associado em Engenharia Química, Faculdade de Engenharia da Universidade do Porto, Rua Dr. Roberto Frias, 4200-465 Porto, Portugal

³Faculty of Pharmaceutical, Biomedical and Veterinary Sciences, University of Antwerp, Antwerp, Belgium

⁴CINaM/CNRS - Centre Interdisciplinaire de Nanoscience de Marseille, Centre National de la Recherche Scientifique, Paris, France

*Corresponding author: up201303475@edu.fe.up.pt

1. Introduction

Alternatives to conventional antibiotics are required due to the emergence and growth of antimicrobial resistance (O'Neill 2016). Nucleic acid mimics (NAMs), which can hybridize and thereby prevent the expression of essential bacterial genes in the cytosol, may become such an alternative. The internalization of NAMs and, consequently, their inhibitory potential are severely hampered by the multi-layered bacterial envelopes (Santos et al. 2018). The potential of dendritic lipids (DLs) to transport nucleic acids has been reported; however, most studies to date have focused solely on mammalian cells (Chen et al. 2022). Herein, we evaluate the potential of two DLs (Yu et al. 2012; Dhumal et al. 2021) as bacterial envelope permeabilizers, potentiating their use as delivery systems of NAMs into bacteria.

2. Materials and Methods

For this study, a flow cytometry-based protocol was developed to quantify the membrane damage caused by an antimicrobial agent, using propidium iodide (PI), a membrane impermeant dye. After using a full factorial design of experiments to optimise this protocol, the impact of both DLs was assessed in *E. coli* and compared to the effects of polymyxin (Poly), a membrane-disruptive antibiotic, and of a previous ethanol permeabilization (EtOH).

Additionally, the internalization of LNA- and PNA-based Cy3-labelled NAMs, targeting the essential *acpP* gene in *E. coli*, was evaluated when complexed with each of the DLs, by flow cytometry and epifluorescence microscopy. These results were compared with those of free NAMs as well as of a PNA-based peptide-oligo conjugate (POC), known to successfully reach the cytosol (Santos et al. 2018).

3. Discussion

Regarding permeabilization, both DLs led to significant PI-staining of *E. coli* cells, with the DL with surface tertiary amines (8TA) leading to higher permeabilization ($\approx 82\%$) than that with primary amines (8A) at its surface ($\approx 45\%$).

Regarding the delivery of NAMs into the bacterial cytosol, both DLs led to significant NAM internalization (particularly for LNA-based NAMs), with 8A being more successful ($\approx 90\%$) than 8TA ($\approx 50\%$). The obtained micrographs, which depict cells with a purple-to-pinkish stain brought on by the overlap of Cy3 and DAPI fluorescence, provided additional proof of these findings.

4. Conclusions

Both DLs exhibited promising results, leading to a high percentage of permeabilization. When combined with LNA-based NAMs, both DLs led to significant NAM internalization, highlighting their potential as delivery vectors.

References

Chen, Jiaxuan, Dandan Zhu, Xiaoxuan Liu, and Ling Peng. 2022. "Amphiphilic Dendrimer Vectors for RNA Delivery: State-of-the-Art and Future Perspective." *Accounts of Materials Research* 3 (5): 484–97. <https://doi.org/10.1021/accountsmr.1c00272>.

- Dhumal, Dinesh, Wenjun Lan, Ling Ding, Yifan Jiang, Zhenbin Lyu, Erik Laurini, Domenico Marson, et al. 2021. "An Ionizable Supramolecular Dendrimer Nanosystem for Effective siRNA Delivery with a Favorable Safety Profile." *Nano Research* 14 (7): 2247–54. <https://doi.org/10.1007/s12274-020-3216-8>.
- O’Neill, Jim, ed. 2016. "Tackling Drug-Resistant Infections Globally: Final Report and Recommendations." *Review on Antimicrobial Resistance*. <https://doi.org/10.4103/2045-080X.186181>.
- Santos, Rita S., Céu Figueiredo, Nuno F. Azevedo, Kevin Braeckmans, and Stefaan C. De Smedt. 2018. "Nanomaterials and Molecular Transporters to Overcome the Bacterial Envelope Barrier: Towards Advanced Delivery of Antibiotics." *Advanced Drug Delivery Reviews* 136–137: 28–48. <https://doi.org/10.1016/j.addr.2017.12.010>.
- Yu, Tianzhu, Xiaoxuan Liu, Anne Laure Bolcato-Bellemin, Yang Wang, Cheng Liu, Patrick Erbacher, Fanqi Qu, Palma Rocchi, Jean Paul Behr, and Ling Peng. 2012. "An Amphiphilic Dendrimer for Effective Delivery of Small Interfering RNA and Gene Silencing in Vitro and in Vivo." *Angewandte Chemie - International Edition* 51 (34): 8478–84. <https://doi.org/10.1002/anie.201203920>.

Acknowledgements

This work was financially supported by (i) LA/P/0045/2020 (ALiCE), UIDB/00511/2020 and UIDP/00511/2020 (LEPABE), funded by national funds through FCT/MCTES (PIDDAC); (ii) European Union’s Horizon 2020 research and innovation programme under grant agreement No. 810685; (iii) Project NAMSaI under grant agreement No. 2022.07654.PTDC; and (iv) PhD grant No. 2022.10864.BD, funded by national funds through Fundação para a Ciência e a Tecnologia (FCT).

Selection of nucleic acid mimic (NAM) aptamers: from de novo SELEX to post-SELEX enhancement

Ricardo Oliveira^{1,2,3*}, Eva Pinho^{1,2,3}, Nuno F. Azevedo^{2,3}, Carina Almeida^{1,2,3}

¹INIAV – National Institute for Agrarian and Veterinarian Research, Rua dos Lagidos, 4485-655 Vairão, Vila do Conde, Portugal

²LEPABE – Laboratory for Process Engineering, Environment, Biotechnology and Energy, Faculty of Engineering, University of Porto, Rua Dr. Roberto Frias, 4200-465 Porto, Portugal

³AliCE – Associate Laboratory in Chemical Engineering, Faculty of Engineering, University of Porto, Rua Dr. Roberto Frias, 4200-465 Porto, Portugal

*Corresponding author: e-mail address: up201200365@fe.up.pt; ORCID ID: 0000-0001-9175-4278

Abstract

Aptamers are structurally-defined single-stranded DNA or RNA molecules with ability to bind to a specific target with high affinity and specificity. In this study, an innovative *de novo* systematic evolution of ligands by exponential enrichment (SELEX) methodology for the selection of DNA aptamers against staphylococcal enterotoxin A (SEA) as well as an *in silico* workflow for the prediction of the aptamer-target binding model and the effect of post-SELEX modifications with nucleic acid mimics (NAMs) was developed. A DNA aptamer identified by *de novo* SELEX showed a dissociation constant (K_D) of 13.4 ± 18.6 nM. *In silico* evaluation of the interaction model allowed the identification of 3 potential improved locked nucleic acids (LNA) versions. The post-SELEX modifications decreased the K_D of the original aptamer, but it remained comparable to that of other aptamers described for SEA. However, NAMs allowed to increase the thermal stability of the DNA aptamer. Post-SELEX modifications with NAMs, based on a tailored *in silico*-assisted approach, might be a promising tool to improve DNA aptamers' properties, mainly for *in vivo* purposes.

Author Keywords. Aptamers, nucleic acid mimics, locked nucleic acid, *in silico* modelling, post-SELEX modifications.

1. Introduction

Aptamers are single-stranded nucleic acids with a defined three-dimensional structure that confers them binding characteristics to a target molecule. They are generated using a repetitive *in vitro* approach known as Systematic Evolution of Ligands by Exponential Enrichment (SELEX) (Stoltenburg, Reinemann, and Strehlitz 2007). Aptamers are seen as a versatile solution as diagnostic elements, drugs and drug delivery systems (Keefe, Pai, and Ellington 2010). However, their application in some areas, mainly *in vivo* applications, has so far been hampered by aptamers poor biostability (Gold et al. 2012). To overcome this limitations, post-SELEX modifications with nucleic acids mimics (NAMs), such as locked nucleic acids (LNA), are being used to improve the aptamer's properties (Oliveira, Pinho, Sousa, DeStefano, et al. 2022). Post-SELEX modifications are usually based on trial-and-error approaches that often affect the original aptamer-target interaction. *In silico* approaches have been proposed to assist post-SELEX approaches, saving experimental time in the conventional approaches (Cai et al. 2018). This study summarizes a set of works that encompasses the selection of DNA aptamers for the staphylococcal enterotoxin A (SEA), one of the most reported bacterial toxins in food poisoning outbreaks, through an innovative *de novo* SELEX methodology and the development of an *in silico* workflow for the prediction of the three-dimensional structure of aptamers and consequently application of LNA modifications in a previously selected DNA aptamer.

2. Materials and Methods

In vitro selection of DNA aptamers

A random ssDNA library was incubated with of SEA-coated magnetic beads in binding buffer (BB) at room temperature for 30 min. Binding complexes were collected by magnetic separation, the beads washed, and the bound sequences were eluted by incubating at 95 °C for 10 min. The beads were magnetically separated, and the eluted pool of ssDNA eluted were subject to PCR amplification with

1x Supreme NZYTaQ II 2x Colourless Master Mix, 0.5 μ M forward primer, 0.5 μ M phosphorylated-reverse primer. To recover the ssDNA pool for subsequent selection rounds, dsDNA was then converted in ssDNA with Lambda Exonuclease. Subsequent selection rounds were performed with decreasing incubation time, increasing the number of washing cycles and adding competitors. To eliminate non-specific binding, negative selections were also performed. In total, ten SELEX rounds were performed.

The *in silico* analysis of aptamers' structures was based on the strategy assembled by our group and described in (Oliveira, Pinho, Sousa, Dias, et al. 2022).

Determination of the dissociation constants (K_D), nuclease and thermal stability

The K_D values of the DNA and LNA aptamers for SEA were determined by a non-linear regression based on binding assays with increasing concentrations of each aptamer (1–400 nM) and a constant amount of SEA-coated magnetic beads. To evaluate the effect of temperature on aptamers binding affinity, a single concentration of each aptamer (125 nM) was incubated with a constant amount of SEA-coated beads under the same conditions as for the K_D assays but (1) at 4 °C and (2) at 37 °C. The effect of the insertion of LNA on aptamer's resistance to nuclease degradation was also evaluated. For this, a single concentration of each aptamer (10 nM) was incubated with a DNA endonuclease (DNase I) and a ssDNA exonuclease (Exonuclease VII), and samples were taken over time (5, 10, 20, 30 and 60 minutes). The concentration of aptamer in each assay/condition was determined by qPCR quantification using standard curves.

3. Discussion

The SELEX methodology developed allowed the identification of a DNA aptamer (Apt5) with a $K_D = 13.4 \pm 18.6$ nM, a value in the same range as other aptamers described for SEA (Wang et al. 2016; Huang et al. 2014). The assembled *in silico* workflow allowed the prediction of the three-dimensional structure of the DNA aptamer and based on this, the insertion of various LNAs into its sequences was tested. Three promising LNA versions (LNA13, 14 and 15) were selected based on the *in silico* scores and potential enhancing effect on aptamer's properties. The experimental K_D for the LNA13 was 156.7 ± 39.2 nM, for the LNA14 was 73.7 ± 23.8 nM and for the LNA15 was 142.7 ± 28.0 nM. The K_D of Apt5 was better than the LNA variations. Therefore, the post-SELEX modifications negatively affected the aptamer affinity. Still, the values are in the nM range, comparable to the other aptamers for SEA. Thermal assays reveal that the original Apt5 is negatively affected by increasing temperature (37 °C). Similarly, the LNA13 and LNA15 versions also showed a reduction in affinity at 37 °C compared to the RT assay, although not as much as the reduction seen for the original DNA aptamer. However, a positive effect was observed regarding LNA14. The nuclease assays demonstrate that DNA aptamers as well as LNA variation were rapidly degraded in the presence of endonucleases and exonucleases. The proposed insertion of LNAs were not sufficient to counteract the enzymatic degradation of nucleic acids. Other types of modifications and/or higher number of LNA could be introduced to increase stability to nuclease degradation.

4. Conclusions

In summary, we have successfully demonstrated the selection of DNA aptamers for SEA using an innovative *de novo* SELEX methodology. The identified DNA aptamers show a good affinity for SEA diagnostic applications, such as for the development of aptamer-based biosensors. However, for *in vivo* applications where the incubation temperature (i.e., is typically higher than RT) and enzymatic degradation of natural nucleic acids is a challenge, overcoming these limitations with NAMs is crucial. Post-SELEX modifications together with *in silico* predictions have been shown to be a powerful tool to assist post-SELEX approaches to improve the aptamers' properties, such as thermal stability, while maintaining a good binding affinity for the target molecule. NAMs may also be an option to increase resistance to enzymatic degradation, however, the strategy/number of modifications introduced were not sufficient to increase resistance to nucleases. Still, this study proves the potentiality of selecting functional NAM aptamers with both *in vitro* and *in vivo* applications.

References

- Cai, S., J. Yan, H. Xiong, Y. Liu, D. Peng, and Z. Liu. 2018. "Investigations on the Interface of Nucleic Acid Aptamers and Binding Targets." *Analyst*. The Royal Society of Chemistry. Accessed August 29, 2019. <https://doi.org/10.1039/c8an01467a>.
- Gold, L., N. Janjic, T. Jarvis, D. Schneider, J. J. Walker, S. K. Wilcox, and D. Zichi. 2012. "Aptamers and the RNA World, Past and Present." *Cold Spring Harbor Perspectives in Biology* 4 (3). Accessed December 6, 2022. <https://doi.org/10.1101/CSHPERSPECT.A003582>.
- Huang, Y., X. Chen, Y. Xia, S. Wu, N. Duan, X. Ma, and Z. Wang. 2014. "Selection, Identification and Application of a DNA Aptamer against Staphylococcus Aureus Enterotoxin A." *Anal. Methods* 6 (3): 690–97. Accessed March 19, 2018. <https://doi.org/10.1039/C3AY41576G>.
- Keefe, A. D., S. Pai, and A. Ellington. 2010. "Aptamers as Therapeutics." *Nature Reviews Drug Discovery*. Nature Publishing Group. Accessed February 16, 2021. <https://doi.org/10.1038/nrd3141>.
- Oliveira, R., E. Pinho, A. L. Sousa, J. J. DeStefano, N. F. Azevedo, and C. Almeida. 2022. "Improving Aptamer Performance with Nucleic Acid Mimics: De Novo and Post-SELEX Approaches." *Trends in Biotechnology* 40 (5): 549–63. Accessed February 8, 2023. <https://doi.org/10.1016/J.TIBTECH.2021.09.011>.
- Oliveira, R., E. Pinho, A. L. Sousa, Ó. Dias, N. F. Azevedo, and C. Almeida. 2022. "Modelling Aptamers with Nucleic Acid Mimics (NAM): From Sequence to Three-Dimensional Docking." *PLOS ONE* 17 (3): e0264701. Accessed October 6, 2022. <https://doi.org/10.1371/JOURNAL.PONE.0264701>.
- Stoltenburg, R., C. Reinemann, and B. Strehlitz. 2007. "SELEX-A (r)Evolutionary Method to Generate High-Affinity Nucleic Acid Ligands." *Biomolecular Engineering*. Accessed March 27, 2017. <https://doi.org/10.1016/j.bioeng.2007.06.001>.
- Wang, K., D. Wu, Z. Chen, X. Zhang, X. Yang, C. J. Yang, and X. Lan. 2016. "Inhibition of the Superantigenic Activities of Staphylococcal Enterotoxin A by an Aptamer Antagonist." *Toxicon* 119 (September): 21–27. Accessed May 3, 2021. <https://doi.org/10.1016/j.toxicon.2016.05.006>.

Acknowledgments

This work was financially supported by: LA/P/0045/2020 (ALiCE), UIDB/00511/2020 and UIDP/00511/2020 (LEPABE), funded by national funds through FCT/MCTES (PIDDAC); project POCI-01-0145-FEDER-028659, funded by FEDER funds through COMPETE2020 – Programa Operacional Competitividade e Internacionalização (POCI). The authors also thank FCT for the PhD Fellowship SFRH/BD/138883/2018.

CFD design of photocatalytic mesostructured reactors for ammonia production

M. Teresa Oliveira^{1,2}, Isabel S.O. Barbosa^{1,2}, Margarida S.C.A. Brito^{1,2}, Cláudia G. Silva^{1,2}, Ricardo J. Santos^{1,2}

¹Laboratory of Separation and Reaction Engineering – Laboratory of Catalysis and Materials (LSRE-LCM), Faculty of Engineering, University of Porto, Rua Dr. Roberto Frias, 4200-465 Porto, Portugal

²ALiCE – Associate Laboratory in Chemical Engineering, Faculty of Engineering, University of Porto, Rua Dr. Roberto Frias, 4200-465 Porto, Portugal

Abstract

An elementary configuration of a unit-cell of a mesostructured photocatalytic reactor for green-ammonia production was designed and optimized through computational fluid dynamic (CFD) simulations. A parametric study assessed the best geometry of the cell, based on vorticity and velocity profiles, which ensured higher mixing rates inside the reactor. Mass transfer studies were carried out to evaluate the mass transfer limits in the cell that favor ammonia diffusion and maximize the efficiency of the photocatalytic reaction.

Author Keywords Mesostructured Reactor, Photocatalysis, CFD, Ammonia Production.

1. Introduction

Micro and mesostructured reactors have been under popular research in chemical engineering, due to their potential on enhancing mixing and reaction rates and easy scalability. This type of reactor shows high surface-to-volume ratio, allowing for safer operation and more precise control of reaction variables (Barbosa et al. 2023).

Aside from efficient catalysts and adequate light sources, photocatalytic reactions are much conditioned by the fluid dynamics and the dimensions and geometry of the photoreactor. Small characteristic lengths, which are typical of mesostructured reactors, enable more uniform light and flow distribution (usually in the laminar regime), mitigating the impact of possible stagnant or non-irradiated zones on the reaction efficiency. Light attenuation effect when scaling up the photoreactor must also be kept in consideration (Kayahan et al. 2020). The scale-up from laboratory scale to pilot and industrial devices is usually performed, not through a dimension increase, but by numbering-up the unit elements of the mesostructured network, which keeps constant the surface/volume ratio and does not affect the high characteristic mass and heat transfer performance of these reactors. The static mixer micro/meso-structured reactor NETmix, developed by Laranjeira et al. (2011) has proven to be of success when handling heterogeneous photocatalytic reactions. This reactor's unique inner geometry enables fast and efficient fluid mixing, even under laminar regimes, and contributes to high mass and photon transfer rates.

Apart from integrating flow field dynamics, photocatalytic systems must account for mass transport, reaction kinetics and photon flux distribution, all increasing the complexity of these models. Computational fluid dynamics (CFD) tools arise as an effective numerical approach to the problem, that accounts for the interaction of all these phenomena, and an interesting design strategy to predict and optimize fluid behavior inside the photoreactor. This work reports a CFD study on the design of a structured and immobilized photoreactor with direct application in green-ammonia synthesis, a field in recent advancement, as the search for a more sustainable and low-carbon alternative to Haber-Bosch industrial-scale process is widened.

2. Materials and Methods

Unit-Cell Geometry

The base case geometry of the DeanCell, the structured reactor's unit-cell, was designed to promote secondary flow in the form of dean vortices and enhance fluid mixing inside the reactor. This prismatic geometry, schematized in Figure 1, shows an inlet channel and a main body, on which the

immobilization of the catalyst will occur. The main inlet channel was fixed, presenting characteristic meso dimensions of $1 \times 1 \text{ mm}^2$ (d and w) of cross-sectional area and 3 mm of length (l_{in}), enough to promote a developed flow at the entrance.

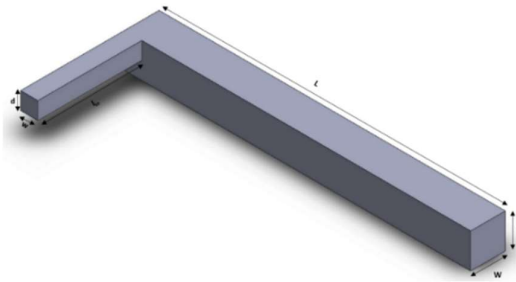


Figure1: Base case geometry of the unit-cell of the mesostructured reactor.

To assess the geometry and the dimensions of the best unitary element configuration, a parametric study was developed, using ANSYS Fluent R 2022. Simulations were held in laminar flow regime and at a Reynolds number (Re) of 100, using the Coupled scheme method for pressure-velocity coupling. Water was set as the working fluid and the following default physical properties were retained: ρ , the mass density, equal to $998.2 \text{ kg}\cdot\text{m}^{-3}$, and ν , the kinematic viscosity, as $1 \times 10^{-6} \text{ m}^2\cdot\text{s}^{-1}$.

The dimensions of the main channel (D , W and L) were under analysis, and vorticity maps were traced in order to optimize these parameters. Vorticity profiles along the length of the cell show that the step drawn on the structure causes an increase in this variable, enhancing mixing in this cell region, and that the vorticity proved to be greater for channel heights equal or above 2mm. The case promoting better vorticity was a cell with 10mm of length, L , D of 2mm and W of 0.5mm, which was kept for all forward simulations as the optimum base geometry.

Mass Transfer Study

Mass transfer from the catalytic plate to the bulk of the cell is evaluated through steady state simulations, for different Re . To assess mass transfer limits, a case of infinite kinetic reaction rate was modelled: considering that the catalyst is immobilized in the surface of two walls in the main channel, the maximum mass fraction of NH_3 in water, at the operating conditions of 1 atm and $20 \text{ }^\circ\text{C}$, was set as the boundary condition in these walls.

Different catalytic immobilization configurations are studied, and the efficiency of the NH_3 diffusion from the catalyst surface to the fluid phase is monitored through a contour of the ammonia concentration at the outlet face. Figure 2 shows a side-view of the unit-cell, corresponding to the case of immobilization of catalyst in the interior and exterior walls. Figure 3 gives an illustration of the vortices formed on a surface of the main channel, through a velocity streamline done in CFD-Post.

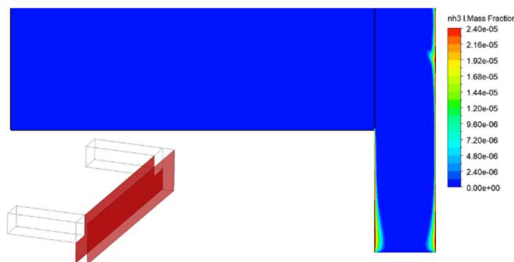


Figure 2 Contour of NH_3 mass fraction in the interior and exterior walls.

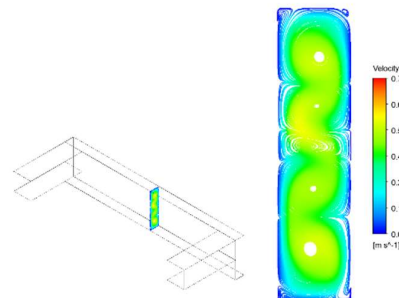


Figure 3 Velocity surface streamline in the main channel.

Considering a well-mixed solution, ΔC , the molar concentration gradient between the catalyst and the bulk of the reactor is the difference between the concentration in the catalytic plate, C_{CP} , and the

monitored concentration value at the outlet face, C_{out} . Equation 1 can be written, where \dot{N} is the molar flux and k is the mass transfer coefficient.

$$\dot{N} = k \cdot \Delta C = k \cdot (C_{CP} - C_{out}) \quad (1)$$

The extent of mass transfer in the cell was further defined by calculating Sherwood numbers (Sh), through the following Equation 2, in which l_{cp} is the catalytic plate length and D is the diffusivity of NH_3 in water, estimated in $2.32 \times 10^{-9} \text{ m}^2 \cdot \text{s}^{-1}$.

$$Sh = \frac{k l_{cp}}{D} \quad (2)$$

3. Conclusions

Based on the simulations performed, the designed cell appears to be effective for use as an elementary cell of a mesostructured photocatalytic reactor. Mass transfer studies show ammonia diffusion through the reactor, which, according to NH_3 mass fraction reports at the outlet face, is only slightly dependent on the localization of the catalytic material. Further studies will assess the mass transfer limiting rates that guarantee the system's operation under chemical regime.

References

- Barbosa, Isabel S. O., João M. Costa, Yaidelin A. Manrique, Madalena M. Dias, Joaquim L. Faria, Ricardo J. Santos, Cláudia G. Silva, and Margarida S. C. A. Brito. 2023. "ChannelCOMB Device for Mesostructured Reactors and Networks of Reactors." *Chemical Engineering & Technology*. <https://doi.org/10.1002/ceat.202200560>.
- Kayahan, Emine, Mathias Jacobs, Leen Braeken, Leen C. J. Thomassen, Simon Kuhn, Tom van Gerven, and M. Enis Leblebici. 2020. "Dawn of a new era in industrial photochemistry: the scale-up of micro- and mesostructured photoreactors." *Beilstein Journal of Organic Chemistry* 16: 2484-2504. <https://doi.org/10.3762/bjoc.16.202>.
- Laranjeira, Paulo E., António A. Martins, Maria Isabel Nunes, José Carlos B. Lopes, and Madalena M. Dias. 2011. "NETmix®, a new type of static mixer: Experimental characterization and model validation." *AIChE Journal* 57 (4): 1020-1032. <https://doi.org/10.1002/aic.12316>.

Acknowledgments

This work was financially supported by LA/P/0045/2020 (ALiCE), UIDB/50020/2020 and UIDP/50020/2020 (LSRE-LCM), and the project SuN2Fuel 2022.04682.PTDC - funded by national funds through FCT/MCTES (PIDDAC). I.S.O. Barbosa acknowledges her FCT grant UI/BD/151092/2021.

Phenolic rich extracts from by-products: promising compounds for the development of value-added foods

Sara M. Ferreira^{1,2*}, Lúcia Santos^{1,2}

¹LEPABE - Laboratory for Process Engineering, Environment, Biotechnology and Energy, Faculty of Engineering, University of Porto, Rua Dr. Roberto Frias, 4200-465 Porto, Portugal

²ALICE - Associate Laboratory in Chemical Engineering, Faculty of Engineering, University of Porto, Rua Dr. Roberto Frias, 4200-465 Porto, Portugal

*Corresponding author: up201604659@fe.up.pt; ORCID ID: 0000-0002-3381-2318

Abstract

Agriculture and food processing have increased as a result of the expansion in the global population. Some of the primary fruits grown in Europe are chestnut, grape, pomegranate, and avocado; they are heavily employed in food processing to produce more appetizing dishes and beverages. This procedure produces significant byproducts, whose improper handling and disposal cause environmental and social issues. Nevertheless, these by-products are rich in bioactive compounds, such as phenolic compounds and fatty acids, which can be extracted and incorporated into foods to develop fortified foods. These extracts have enormous relevance for the food, pharmaceutical, and cosmetic industries. Thereby, allying the development of the food industry with the concept of circular economy and sustainability, the challenge of using extracts obtained from agro-industrial by-products arises to develop value-added and more natural foods, with less environmental impact.

Author Keywords. Phenolic compounds, antioxidants, sustainability, food fortification, circular economy

1. Introduction

Over the past years, consumers have grown interested in natural and functional foods, which created an increase in the demand for new valuable food, as well as the reformulation of others with new or improved functionalities (Gruskiene et al. 2021). Functional foods are defined as those that go beyond simple nutritional requirements to provide particular physiologically beneficial effects and/or lower the risk of chronic illness (Granato et al. 2022). Therefore, the food industry has been focusing on the development of foods with “nature-based” ingredients, not only to increase their nutritional value and functional properties but also to increase the shelf-life of the products.

United Nations is focused on the reduction of food waste and by-product production since its incorrect disposal and treatment are responsible for a large number of environmental problems. Therefore, a strategy to overcome these adverse effects is to extract bioactive compounds, in which these matrixes are rich, such as antioxidants and vitamins, and incorporate them into foods. Phenolic compounds are secondary metabolites of plants, that have a wide range of biological features that make them particularly desirable to many industries, such as food, cosmetics and pharmaceutical (Rodriguez-Lopez et al. 2020). Studies have shown these compounds to have antimicrobial, antiviral, anti-allergic, and anti-cancer activities, but their antioxidant capacity stands out the most. They can act as natural antioxidants due to their ability to reduce oxidative stress (Ferreira and Santos 2022a).

Milk and dairy products, including cheese, yoghurt, and mayonnaise, contain large amounts of fats and oils, mostly healthy. However, these are prone to deterioration due to the oxidation of unsaturated fats, which degrades the food's physicochemical and sensory properties (Bruno et al. 2021). Additionally, these foods are poor in bioactive compounds, hence the interest in incorporating phenolic compounds, to allow the fortification of dairy products. Hence, phenolic compounds can be incorporated into different foods, in order to create value-added products, beneficial to human health, and simultaneously replace the use of synthetic preservatives, such as antioxidants.

Therefore, the present work intends to display how extracts from different by-products can be incorporated into different food matrices, to create functional foods, with extended shelf-life, while promoting sustainability and a circular economy.

2. Materials and Methods

The extracts were obtained through solid-liquid extraction, and they were characterized regarding their antioxidant properties, through the assay with the radical DPPH and ABTS, and total phenolic content. After the incorporation of the extracts into different food matrices, the stability of the products over time was assessed.

3. Discussion

The incorporation of avocado peel phenolic-rich extracts into mayonnaise revealed that the stability of the food was not compromised. The evaluation of the extract revealed its antibacterial and antioxidant capabilities and provided evidence that its addition to mayonnaise might potentially improve its nutritional value for customers. Indeed, the obtained results demonstrated that the incorporation of the extract reduces the oxidation extension compared to the negative control, and displayed similar results to the positive controls in the study, BHT and ascorbic acid. The achieved results indicate that the extract was able to decrease the lipid oxidation of the mayonnaise over time (Ferreira and Santos 2022b). Therefore, the present study shows that it is possible to fortify mayonnaise with the incorporation of avocado peel extract, while preventing lipid oxidation, with a similar performance to synthetic preservatives.

In another assay, a comparison of the effects of adding extracts from different agro-industrial by-products (chestnut shell, grapeseed, and pomegranate peel) into yoghurts was performed, as well as an evaluation of their potential to substitute artificial preservatives (Ferreira and Santos 2023). The physical and chemical stability of the yoghurts was unaffected by the addition of the different extracts, throughout the storage period. All yoghurt samples met the regulatory standards for microbiological safety and were able to stop the development of *S. aureus* and *E. coli*. The best outcomes were shown in yoghurts enhanced with grapeseed and pomegranate peel extract. Regarding the oxidative study, the results showed that increasing the amount of extract added to the yoghurt, allowed similar results to those obtained for the synthetic antioxidant, sorbic acid.

The effect of the incorporation of phenolic chestnut shell extract into fresh cheese was assessed. The results showed that the fortified cheese was shown to have favourable synergistic and water-holding properties. Along with containing phenolic components and the ability to inhibit the DPPH and ABTS radicals, it also demonstrated antioxidant capacity. As a result, adding chestnut shell extract increased the fresh cheese's shelf life. The obtained results appear to emphasize the potential for adding agricultural by-product extracts to fresh cheese, minimizing agricultural industry waste while producing a value-added good with enhanced and intriguing qualities for consumers.

4. Conclusions

Therefore, the present work highlights the potential of the incorporation of phenolic-rich extracts, from different agro-industrial by-products, into different dairy products and mayonnaise to develop functional and value-added foods. Additionally, the results brought to attention the possibility of these extracts replacing or reducing the quantities of synthetic preservatives. In future work, the comparison of the outcomes with the addition of microencapsulated extracts would be interesting.

References

- Bruno, Alessandra De, Rosa Romeo, Antonio Gattuso, Amalia Piscopo, and Marco Poiana. 2021. "Functionalization of a Vegan Mayonnaise with High Value Ingredient Derived from the Agro-Industrial Sector." <https://doi.org/10.3390/foods10112684>.
- Ferreira, Sara M, and Lúcia Santos. 2022a. "A Potential Valorization Strategy of Wine Industry By-Products and Their Application in Cosmetics - Case Study: Grape Pomace and Grapeseed." *Molecules* 27 (3). <https://doi.org/10.3390/molecules27030969>.
- Ferreira, Sara M, and Lúcia Santos. 2022b. "From By-Product to Functional Ingredient: Incorporation of Avocado Peel Extract as an Antioxidant and Antibacterial Agent." *Innovative Food Science & Emerging Technologies*, 103116. <https://doi.org/https://doi.org/10.1016/j.ifset.2022.103116>.
- Ferreira, Sara M, and Lúcia Santos. 2023. "Incorporation of Phenolic Extracts from Different By-Products in Yoghurts to Create Fortified and Sustainable Foods." *Food Bioscience* 51: 102293. <https://doi.org/https://doi.org/10.1016/j.fbio.2022.102293>.
- Granato, Daniel, Márcio Carochó, Lillian Barros, Ioannis Zabetakis, Andrei Mocan, Alexandros Tsoupras, Adriano Gomes Cruz, and Tatiana Colombo Pimentel. 2022. "Implementation of Sustainable Development Goals in the Dairy

Sector: Perspectives on the Use of Agro-Industrial Side-Streams to Design Functional Foods.” *Trends in Food Science and Technology* 124 (December 2021): 128–39. <https://doi.org/10.1016/j.tifs.2022.04.009>.

Gruskiene, Ruta, Alma Bockuviene, and Jolanta Sereikaite. 2021. “Microencapsulation of Bioactive Ingredients for Their Delivery into Fermented Milk Products: A Review.” *Molecules* 26 (15): 1–20. <https://doi.org/10.3390/molecules26154601>.

Rodriguez-Lopez, Antonio D., Bruno Melgar, Carmela Conidi, Lillian Barros, Isabel C.F.R. Ferreira, Alfredo Cassano, and Esperanza M. Garcia-Castello. 2020. *Food Industry By-Products Valorization and New Ingredients: Cases of Study. Cases of Study. Sustainability of the Food System: Sovereignty, Waste, and Nutrients Bioavailability*. Elsevier Inc. <https://doi.org/10.1016/B978-0-12-818293-2.00005-7>.

Acknowledgments

This work was financially supported by: LA/P/0045/2020 (ALiCE), UIDB/00511/2020 and UIDP/00511/2020 (LEPABE), funded by national funds through FCT/MCTES (PIDDAC). Sara M. Ferreira would like to thank the Portuguese Foundation for Science and Technology (FCT) for her PhD grant (2022.10910.BD).

Efficient wastewater treatment in olive pomace oil extraction industry using Fenton method

Racha Mansouri^{1,2*}, Thais T. Grabowski², Ramiro E. J. Martins^{2,3,4}

¹Universite Libre de Tunis (ULT), 1000, Tunisia. Departamento de Engenharia Mecânica, ²Technology and Management School, Polytechnic Institute of Bragança, Campus de Santa Apolónia, 5300-252, Bragança, Portugal.

³LSRE-LCM Laboratory of Separation and Reaction Engineering-Laboratory of Catalysis and Materials, Faculty of Engineering, University of Porto, Rua Dr. Roberto Frias, 4200-465, Porto, Portugal.

⁴ALICE - Associate Laboratory in Chemical Engineering, FEUP, Porto, Portugal.

*Corresponding author: mansouriracha17@gmail.com; ORCID ID 0009-0007-2454-9072

Abstract

The treatment of olive pomace oil extraction industry wastewater is a problem that still does not have an effective solution. The current study aimed to investigate the impact of hydrogen peroxide and iron ion concentrations, as well as the pH level, on effluent treatment. The findings will enable proposing an effective treatment method for the effluent. The Fenton process demonstrated high performance in removing COD (>41%) with good removal of phenolic compound at a pH of 3.5 be achieved (>84%) from the evaluated effluents.

Author Keywords. Wastewater treatment, Fenton, effluent, COD, Phenolic compounds.

1. Introduction

The olive oil industry is an important sector in Europe. The pomace result by the olive oil two or three-phase separation processes can be processed to extract oil, but this still leads to the generation of a highly polluted effluent known as olive oil extraction industry wastewater (OOEIW), creating a new environmental concern (Domingues et al. 2021).

Advanced oxidation processes (AOPs) are recognized for their ability to mineralize various organic compounds in different effluents (Domingues et al. 2021). Among AOPs, Fenton is an AOP involving H₂O₂ and iron source and these are accountable for activating peroxide under acidic conditions without requiring any energy input, and the reaction takes place at room temperature and pressure (Domingues et al. 2021).

The main objective of the present study was to study the removal of organic matter and phenolic compounds by applying the Fenton process in the treatment of wastewater from the olive pomace oil extraction industry.

2. Materials and Methods

To perform the Fenton processes the OOEIW was pre-treat by coagulation/flocculation. In this study, Fenton tests were conducted using 100 ml of OOEIW after the pre-treatment in the Jarrest apparatus. Following the addition of H₂O₂, pH correction and addition of iron in that order, each test was continuously stirred at 80 rpm for 20 minutes. To stop the Fenton reaction at the end of the established reaction time, the pH was raised to 10. The tests were then left to settle overnight, and COD and TPh in the supernatant was subsequently determined.

3. Discussion

Understanding the levels of iron and hydrogen peroxide is crucial in the Fenton reaction. These factors largely influence how effectively the process can degrade organic matter and its associated expenses.

Iron concentration

To ensure the efficient formation of hydroxyl radicals without excessive formation of iron sludge, it is crucial to optimize the iron load. Therefore, a study was conducted to examine the effect of the initial iron concentration on the formation of hydroxyl radicals. The study involved conducting experiments with varying iron concentrations ranging from (0.55 to 7.3 g L⁻¹) while maintaining a constant concentration of H₂O₂ (5 g L⁻¹) and a pH of 3. The findings of the study, which are likely presented in Figure 1, could provide insights into the optimal iron concentration required for the formation of

hydroxyl radicals, which could have significant implications in various fields, including environmental remediation, chemical synthesis, and wastewater treatment.

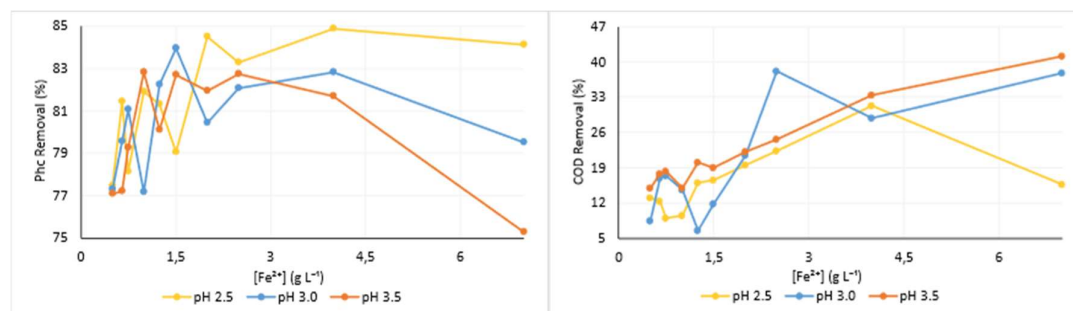


Figure 1. Effect of concentration on COD and total-phenol removal efficiencies during Fenton processes.

After analyzing various curves, it was observed that the highest removal values were achieved at pH 2.5 with 30% COD removal and 84% phenol removal. However, at pH 3, the removal percentages were about 37% for COD and 84% for phenol, while at pH 3.5, the values were 41% for COD and 83% for phenol. Thus, it can be concluded that pH changes do not have a significant impact on removal efficiency. According to a study conducted by Domingues et al. (2021), the concentration of iron ions affects the efficiency of COD and total-phenol removal during Fenton processes. At an iron concentration of 2.5 g L⁻¹, the highest COD removal was approximately 40% and phenolic removal was 84%. Generally, increasing the Fe²⁺ concentration leads to better degradation efficiency of organic pollutants up to a certain limit. However, excessive iron not only results in a loss of iron species but also increases operational costs.

Peroxide concentration

Determining the optimal dosage of hydrogen peroxide is a crucial factor in achieving high efficiency in Fenton processes for degrading pollutants. Excess residual hydrogen peroxide can contribute to COD, so it is important to avoid using excessive amounts. To determine the optimal dosage of H₂O₂, studies were conducted at constant FeSO₄·7H₂O dosage and pH values, with varying amounts of H₂O₂ ranging from 1.5 g L⁻¹ to 20 g L⁻¹. The results of these are demonstrate in Figure 2.

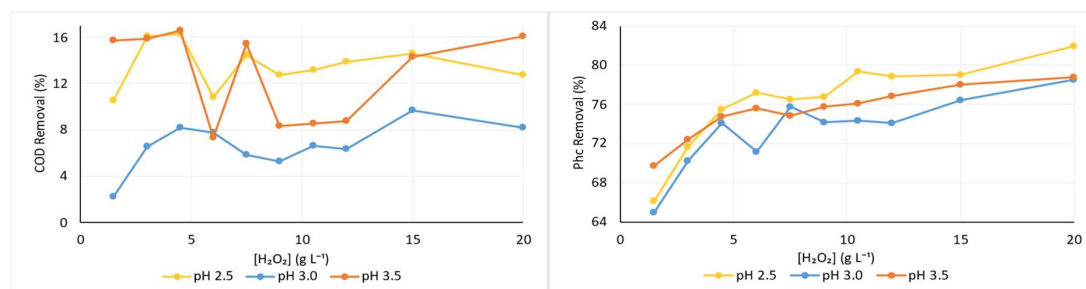


Figure 2. Effect of H₂O₂ concentration on COD and total-phenol removal efficiencies during Fenton processes.

In this study, the highest removal values for COD and phenol were achieved at different pH values, with the best results obtained at pH 2.5 (16% COD removal, 82% phenol removal), pH 3 (10% COD removal, 79% phenol removal), and pH 3.5 (17% COD removal, 83% phenol removal). The phenolic curves displayed similar behavior across the three pH levels, indicating that pH had little effect on phenol removal but had a slight impact on COD removal.

In a study conducted by Domingues et al. (2021), the impact of hydrogen peroxide concentration on COD and total-phenol removal efficiencies during Fenton and Fenton-like processes was investigated. Results showed that both processes were effective in removing COD and phenol, with the Fenton-like process achieving higher removal percentages than the Fenton process at pH 3 (88% COD removal,

91% phenol removal). In Figure 2, it was observed that increasing the concentration of hydrogen peroxide led to greater COD removal without any scavenging effect, indicating that excessive hydrogen peroxide charge may not necessarily lead to destruction of the organic charge.

During the determination process, pH was adjusted between 2.5 and 3.5, and the maximum COD efficiency was obtained at pH 2.5 while the maximum phenol removal was obtained at pH 3.5.

4. Conclusions

The study examined how adding varying amounts of hydrogen peroxide and iron ions to model solutions affected the removal of phenol and COD using the Fenton reagent for chemical oxidation. The results showed that increasing the concentration of H₂O₂ led to higher removal rates for phenol and COD.

References

- Domingues, E., Fernandes, E., Gomes, J., Castro-Silva, S., & Martins, R. C. (2022). Advanced oxidation processes at ambient conditions for olive oil extraction industry wastewater degradation. *Chemical Engineering Science*, 263, 118076.
- Domínguez, Eva, et al. "Olive oil extraction industry wastewater treatment by coagulation and Fenton's process." *Journal of Water Process Engineering* 39 (2021): 101818.

Acknowledgments

This work was financially supported by (i) LA/P/0045/2020 (ALiCE), UIDB/50020/2020 and UIDP/50020/2020 (LSRE-LCM), funded by national funds through FCT/MCTES (PIDDAC), and (ii) Project NORTE-01-0247-FEDER-072124, Bagaço+Valor - Tecnologia Limpa para a Valorização dos Subprodutos do Bagaço na Indústria Extratora de Azeite, funded by the European Regional Development Fund (ERDF). I want to thank the IPB and my University in Tunisia ULT to do the double diploma program and the opportunity to do this work.

Active and stable Iridium-based catalyst for conducting oxygen evolution reaction in a proton exchange membrane electrolyser

Rita Marques^{1,2}, Tânia Lopes^{1,2}, Adélio Mendes^{1,2}

¹LEPABE - Laboratory for Process Engineering, Environment, Biotechnology and Energy, Faculty of Engineering, University of Porto, Rua Dr. Roberto Frias, 4200-465 Porto, Portugal

²ALICE – Associate Laboratory in Chemical Engineering, Faculty of Engineering, University of Porto, Rua Dr. Roberto Frias, 4200-465 Porto, Portugal

*Corresponding author: mendes@fe.up.pt ; ORCID 0000-0003-2472-3265

Abstract

Green hydrogen production by proton exchange membrane (PEM) electrolysis is of great importance in the current energy transition scenario. However, for practical implementation, anode catalysts must be improved towards providing high activity and stability with low iridium content. This work aims to develop a new catalyst with *ca.* 22 wt.% of Iridium (Ir) supported on metal oxide (MO). The results obtained demonstrate that the new supported catalyst displays excellent activity towards oxygen evolution reaction (OER) and enhanced stability.

Author Keywords. Water electrolysis, oxygen evolution reaction, Iridium oxide, tungsten trioxide, activity, stability.

1. Introduction

Proton exchange membrane (PEM) electrolysis is considered a promising route to produce high-purity green hydrogen. However, the widespread commercialization of this technology is limited by the lack of low-cost, active and stable catalysts for the anode side, where the oxygen evolution reaction (OER) takes place [1]. Despite iridium (Ir) oxide being the state-of-the-art catalyst for conducting the OER, its scarcity and high cost boosted the need to significantly reduce its loading. High-valence Ir⁵⁺ and Ir⁶⁺ are incredible OER active centres but display lower stability than Ir³⁺ and Ir⁴⁺ [2]. Hence, an interesting strategy is to disperse Ir particles on supports that can accommodate and stabilise high-valence Ir sites, leading also to smaller average particle size and subsequently higher OER mass-specific activity [3]. In this matter, metal oxides appear as noteworthy electrocatalyst support candidate due to its highly oxidised matrix and excellent stability under an acidic environment, allowing essential structural requirements (activity and stability) to be achieved with lower amounts of Ir [4]. Therefore, this work reports the performance of a low Ir mass loading catalyst (*ca.* 22 wt.% of Ir) supported on a metal oxide (Ir/MO).

2. Materials and Methods

The catalyst was prepared via the polyol method in alkaline media. The synthesis setup consisted of a three-neck round bottom flask placed in a heating plate and connected to a reflux condenser and a thermometer. The synthesis procedure is as follows: NaOH pellets (Sigma Aldrich) were dissolved in ethylene glycol (VWR) to form the reducing medium; after complete dissolution, MO was added to the solution under moderate stirring; then, iridium salt precursor – IrCl₃·xH₂O (Sigma Aldrich) was introduced to the mixture. The obtained slurry was heated under reflux and kept at *ca.* 180 °C for 3 h. After the synthesis, 1 M HNO₃ solution was added drop-wise to adjust the pH until 1-2. A filtration step was used to recover the catalyst nanoparticles, which were then washed with ultrapure water (18.2 MΩ cm, Millipore) and dried under air in a static furnace (80 °C for 5 h).

The catalyst was assessed towards OER in a Zahner IM6-ex using a three-electrode cell configuration (Gamry Instruments) with a rotating disk electrode (RDE710, Gamry Instruments, gold tip, 0.196 cm²) as working electrode. A saturated Ag/AgCl and a graphite rod were used as reference and counter electrodes, respectively. Electrochemical characterisation included cyclic voltammetry (CV), linear sweep voltammetry (LSV) and electrochemical impedance spectroscopy (EIS). To evaluate the catalyst regarding OER stability, an accelerated stress test (AST) was also performed. IrO₂ from Premetek was used as a benchmark catalyst.

3. Discussion

According to **Figure a**), the prepared Ir/MO displays a significantly higher OER activity than the commercial IrO₂ (158.5 vs 5.3 mA·mg_{Ir}⁻¹ @ 1.51 V_{RHE}). In addition, Ir/MO presents an earlier onset at *ca.* 1.48 V_{RHE}, whereas IrO₂ onset potential is at *ca.* 1.60 V_{RHE}. This indicates that OER kinetics are clearly favoured in the supported catalyst since a much lower overpotential is required to overcome the reaction activation energy barrier.

The recorded cyclic voltammograms (**Figure b**)) show that forward and backward scans for Ir/MO are separated by a considerable gap in current density, and both display pronounced and well-shaped redox peaks. For the commercial IrO₂ catalyst, the redox transitions are almost negligible and the recorded current density is also much lower.

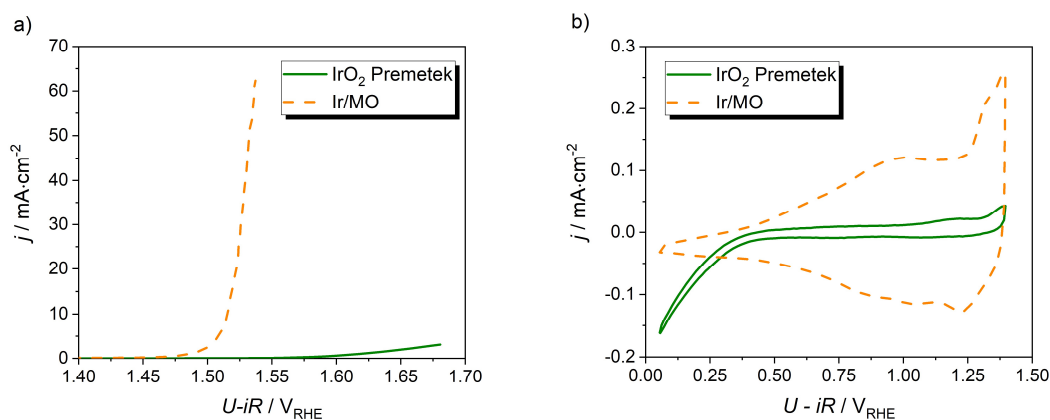


Figure 13: a) Linear sweep voltammograms (LSVs) and b) Cyclic voltammograms (CVs) recorded for the commercial IrO₂ and the prepared Ir/MO.

Regarding the stability (**Table 3**), commercial IrO₂ catalyst presents the worst performance, losing *ca.* 46 % of OER activity. On the other hand, the prepared Ir/MO maintains a remarkable performance after the accelerated stress test (AST), demonstrating almost no loss in OER activity. Accordingly, there should be a strong interaction between Ir active sites and the MO structure, preventing Ir migration from the support and thus improving its stability.

AST	IrO ₂ Premetek	Ir/MO
OER activity before AST (mA·mg _{Ir} ⁻¹)	5.3	158.5
OER activity after AST (mA·mg _{Ir} ⁻¹)	2.3 (- 46 %)	157.9 (- 0.4 %)

Table 8: OER activities before and after AST recorded for the commercial IrO₂ and the prepared Ir/MO.

4. Conclusions

A catalyst consisting of *ca.* 22 wt.% of Ir dispersed in MO was prepared using the polyol synthesis method. The as-prepared catalyst not only displayed higher OER activity (158.5 mA·mg_{Ir}⁻¹) but also an tremendously improved durability compared with the commercial benchmark IrO₂ catalyst. As so, the proposed catalyst has the potential to be incorporated into the anode of PEM electrolyzers. Further studies include the production and testing of membrane electrode assemblies (MEAs) in a single-cell electrolyser to validate the new catalyst performance under real conditions. A patent is now being filled disclosing this new supported catalyst.

References

[1] Carmo, M., et al. 2013. "A comprehensive review on PEM water electrolysis". International Journal of Hydrogen Energy, 38:4901-4934. Accessed 11 April, 2023. DOI: 10.1016/j.ijhydene.2013.01.151

- [2] Pearce, P., et al. 2019. "Revealing the Reactivity of the Iridium Trioxide Intermediate for the Oxygen Evolution Reaction in Acidic Media". *Chemistry of Materials*, 31:5845-5855. Accessed 11 April, 2023. DOI: 10.1021/acs.chemmater.9b01976
- [3] Hansaem, J. and Jaeyoung, J. 2020. "Iridium oxide fabrication and application: A review". *Journal of Energy Chemistry*, 46: 152-157. Accessed 11 April, 2023. DOI: 10.1016/j.jechem.2019.10.026
- [4] Navarrete, E., et al. 2020. "Tungsten trioxide nanowires decorated with iridium oxide nanoparticles as gas sensing material". *Journal of Alloys and Compounds*, 812:152156. Accessed 11 April, 2023. DOI: 10.1016/j.jallcom.2019.152156

Acknowledgements

This work was financially supported by: LA/P/0045/2020 (ALiCE), UIDB/00511/2020 and UIDP/00511/2020 (LEPABE), funded by national funds through FCT/MCTES (PIDDAC); project Baterias 2030, with the reference POCI-01-0247-FEDER-046109, co-funded by Operational Programme for Competitiveness and Internationalisation (COMPETE 2020), under the Portugal 2020 Partnership Agreement, through the European Regional Development Fund (ERDF). Rita Marques and Tânia Lopes are grateful to the Portuguese Foundation for Science and Technology (FCT) for their grants (ref. 2021.06496.BD and CEECIND/02385/2021, respectively).

Identification of aromatic compounds in cocoa bean shells compared to natural cocoa powder

Ingrid Denardi Soares¹, Isabel Maria Duque Martins², Júlia Cristiê Kessler³,
Christianne Elisabete da Costa Rodrigues⁴, Alírio Egídio Rodrigues⁵

^{1,4}Separation Engineering Laboratory (LES), Department of Food Engineering (ZEA-FZEA), University of São Paulo (USP), Av. Duque de Caxias Norte, 13635-900 Pirassununga, Brazil
^{2,3,5}LSRE-LCM - Laboratory of Separation and Reaction Engineering – Laboratory of Catalysis and Materials, Faculty of Engineering, University of Porto, Rua Dr. Roberto Frias, 4200-465 Porto, Portugal

^{2,3,5}ALiCE - Associate Laboratory in Chemical Engineering, Faculty of Engineering, University of Porto, Rua Dr. Roberto Frias, 4200-465 Porto, Portugal

* **Corresponding author:** ingrid.soares@usp.br; ORCID 0000-0003-1276-9178

Abstract

The present study aimed to compare the aromatic profile of natural cocoa powder (NCP) with cocoa bean shells (CS), a cocoa industry residue. Headspace solid-phase microextraction (HS-SPME) and gas chromatography coupled to mass spectrometry (GC-MS) were used, and results were expressed regarding relative composition. The aromatic fractions of CS and NCP were composed of acids, alcohols, aldehydes, pyrazines, terpenes, and ketones. The predominant class in CS was acids ($39.6 \pm 0.5\%$), whereas, in NCP, this class represented $22 \pm 1\%$ of the volatile fraction. The predominant class in NCP was pyrazines and pyrrole ($27 \pm 1\%$), while this class in the CS was only $2.5 \pm 0.2\%$. However, CS had a higher percentage of aldehydes ($26.5 \pm 0.3\%$) than NCP ($13 \pm 1\%$). Despite the punctuated differences, the aroma of CS resembles that of NCP, which can generate application opportunities to add value to this residue.

Author Keywords. volatile fraction, flavor, headspace.

1. Introduction

Cocoa bean shell (CS) is a coproduct of the cocoa industry treated as waste and commonly used as fuel for boilers, agricultural compost, or animal feed. However, this material is of great nutritional interest due to its dietary fiber content of approximately 50%, in addition to proteins, lipids, and bioactive compounds. It can be studied for application in the food, pharmaceuticals, cosmetics, or agricultural industries, which characterizes a significant economic interest in its valorization (Balentic et al., 2018). Several studies are being developed on enhancing CS through application in food matrices, such as chocolates (Barisic et al., 2021) and cookies (Soares et al., 2023). However, knowledge of the aromatic characteristics of CS compared to the characteristics of commercial coproducts, such as natural cocoa powder (NCP), is essential to help determine the applicability of this underused material in human food. Therefore, the present study aimed to identify the volatile compounds responsible for the aromatic profile of CS and NCP and to compare both materials.

2. Materials and Methods

The volatile compounds were extracted by headspace solid phase microextraction (HS-SPME) (Kessler et al., 2022) and identified by chromatography coupled to mass spectrometry (GC-MS) (Barbosa-Pereira et al., 2019). For this, about 1 g of sample in a 20 mL sealed headspace vial was incubated at 60 ± 1 °C for 20 minutes for stabilization. Then, the SPME fiber was exposed to the headspace for 57 minutes at the same temperature. The chromatography's injector and interface temperatures were maintained at 250 and 270 °C, respectively. An oven program ranging from 32 to 240 °C was used. The identification of the compounds was carried out through the database of the National Institute of Standards and Technology (NIST 21, 27, 107, 147).

3. Discussion

The volatile compounds identified in the volatile fractions of CS and NCP are presented in Table 1, in

terms of their relative composition.

Volatile compound	Relative composition (%)	
	CS	NCP
<i>Acids</i>		
Acetic acid	37.2 ± 0.3 a	21 ± 1 b
3-methyl-butanoic acid	2.4 ± 0.2 a	1.21 ± 0.01 b
<i>Alcohols</i>		
2,3-butanediol	11.2 ± 0.8 a	6.8 ± 0.2 b
1,3-butanediol	4.4 ± 0.1 a	2.57 ± 0.07 b
3-furanmethanol	n.d.	4.1 ± 0.2
Phenylethyl Alcohol	2.90 ± 0.01 a	2.5 ± 0.2 a
<i>Aldehydes</i>		
2-methyl-butanal	n.d.	0.21 ± 0.01
Furfural	13.7 ± 0.1	n.d.
Benzaldehyde	3.3 ± 0.1 b	6.7 ± 0.8 a
Benzeneacetaldehyde	3.21 ± 0.06 a	1.0 ± 0.1 b
Nonanal	5.79 ± 0.01 a	4.5 ± 0.1 b
Decanal	0.47 ± 0.04 a	0.59 ± 0.06 a
<i>Terpenes</i>		
α-pinene	0.80 ± 0.05 b	1.2 ± 0.1 a
Camphene	0.31 ± 0.02 b	0.53 ± 0.01 a
β-myrcene	0.99 ± 0.03 b	1.55 ± 0.06 a
3-Carene	0.45 ± 0.03 b	0.71 ± 0.06 a
D-Limonene	4.3 ± 0.3 b	8 ± 2 a
Linalool oxide	0.24 ± 0.01	n.d.
<i>Pyrazines and pyrrole</i>		
Pyrrole	n.d.	3.9 ± 0.3
Methyl-pyrazine	0.34 ± 0.01 b	9.0 ± 0.3 a
2,5-dimethyl-pyrazine	n.d.	5.1 ± 0.2
Ethyl- pyrazine	n.d.	0.57 ± 0.05
2,3-dimethyl-pyrazine	n.d.	0.16 ± 0.01
2-ethyl-5-methyl-pyrazine	n.d.	1.3 ± 0.1
2-ethyl-3-methyl-pyrazine	n.d.	1.36 ± 0.01
2,3-dimethyl-5-ethyl-pyrazine	0.35 ± 0.01 b	2.9 ± 0.2 a
Tetramethyl-pyrazine	1.8 ± 0.2 b	2.6 ± 0.1 a
<i>Ketones</i>		
2-butanone	0.94 ± 0.01	n.d.
Acetophenone	0.39 ± 0.03	n.d.
2-nonanone	n.d.	0.53 ± 0.01
<i>Others</i>	4.4 ± 0.2 b	8.4 ± 0.8 a

n.d. = not detected; means followed by equal lowercase letters on the same row do not differ from each other at the 95% confidence level by the Duncan Test (Duncan, 1955).

Table 1: Relative composition of the volatile fraction of cocoa bean shells (CS) and natural cocoa powder (NCP).

The aromatic fractions of CS and NCP were composed of acids, alcohols, aldehydes, pyrazines, terpenes, and ketones. Comparing the CS to the NCP, it was noted that the main difference occurs in the pyrazines group. In addition, regarding the pyrazines in cocoa powder, only three were identified in the CS (methyl-pyrazine, 2,3-dimethyl-5-ethyl-pyrazine, and tetramethyl-pyrazine). Pyrazines are the main components of cocoa aroma, especially tetramethyl-pyrazine, responsible for the flavor notes of nuts, toast, and chocolate (Menezes et al., 2016). These compounds are products of the Maillard reaction during the cocoa bean roasting (Barbosa-Pereira et al., 2019).

In contrast, CS had a higher relative percentage of aldehydes. An aromatic fraction rich in aldehydes is desirable since these compounds are related to cocoa quality, producing a characteristic cocoa aroma and fruity notes (Menezes et al., 2016). Another difference observed was the higher percentage of acetic acid present in CS. This acid is usually associated with an unpleasant odor due to its rancid and sour vinegary notes (Barbosa-Pereira et al., 2019).

4. Conclusions

Through the identification of volatile compounds of cocoa bean shell (CS) and natural cocoa powder (NCP) it was possible to compare the aromatic profile of both materials. It was observed that the main difference between the volatile fractions of CS and NCP is the lower percentage of pyrazines and the greater presence of acetic acid in CS. However, CS has a higher relative percentage of aldehydes, also responsible for forming cocoa aroma. Therefore, despite the differences in relative composition, CS aroma can be related to cocoa derivatives, generating application opportunities to add value to this residue.

References

- Balentic, J. P.; Ackar, D.; Jokic, S.; et al. Cocoa Shell: A By-Product with Great Potential for Wide Application. *Molecules*, v. 23, 1404, 2018. doi:10.3390/molecules23061404
- Barisic, V.; Petrovic, J.; Loncarevic, I.; et al. Physical Properties of Chocolates Enriched with Untreated Cocoa Bean Shells and Cocoa Bean Shells Treated with High-Voltage Electrical Discharge. *Sustainability*, v.13, 2620, 2021. <https://doi.org/10.3390/su13052620>
- Barbosa-Pereira, L.; Rojo-Poveda, O.; Ferrocino, I.; et al. Assessment of volatile fingerprint by HS-SPME/GC-qMS and E-nose for the classification of cocoa bean shells using chemometrics. *Food Res. Int.*, v. 123, p. 689-696, 2019. <https://doi.org/10.1016/j.foodres.2019.05.041>
- Duncan, D. B. Multiple F and multiple "F" test. *Biometrics*, v. 11, 1955.
- Kessler, J. C.; Vieira, V.; Martins, I. M.; et al. Chemical and organoleptic properties of bread enriched with *Rosmarinus officinalis* L.: The potential of natural extracts obtained through green extraction methodologies as food ingredients. *Food Chem.*, v. 384, 132514, 2022. <https://doi.org/10.1016/j.foodchem.2022.132514>
- Menezes, A. G. T.; Batista, N. N.; Ramos, C. L.; et al. Investigation of chocolate produced from four different Brazilian varieties of cocoa (*Theobroma cacao* L.) inoculated with *Saccharomyces cerevisiae*. *Food Res. Int.*, v.81, p.83-90, 2016. <http://dx.doi.org/10.1016/j.foodres.2015.12.036>
- Soares, I. D.; Cirilo, M. E. M.; Junqueira, I. G.; et al. Production of Cookies Enriched with Bioactive Compounds through the Partial Replacement of Wheat Flour by Cocoa Bean Shells. *Foods*, v 12, 436, 2023. <https://doi.org/10.3390/foods12030436>

Acknowledgments

This work was financially supported by LA/P/0045/2020 (ALiCE), UIDB/50020/2020, and UIDP/50020/2020 (LSRE-LCM), funded by Portuguese national funds through FCT/MCTES (PIDDAC) and Brazilians by FAPESP (2022/05656-0, 2019/02251-7, 2014/21252-0), CAPES (Finance code 001) and CNPq (306020/2022-0).

Evaluating the impact of thermal disinfection on *Pseudomonas fluorescens* biofilm structures using a CDC biofilm reactor

Ana Rosa Silva^{1,2}, Diogo Narciso^{1,2}, Luciana Gomes^{1,2}, Fernando Martins^{1,2}, Luís F. Melo^{1,2} and Ana Pereira^{1,2}

¹LEPABE – Laboratory for Process Engineering, Environment, Biotechnology and Energy, Faculty of Engineering, University of Porto, Rua Dr. Roberto Frias, 4200-465 Porto, Portugal (arms@fe.up.pt, dnarciso@fe.up.pt, luciana.gomes@fe.up.pt, fgm@fe.up.pt, lmelo@fe.up.pt, aalex@fe.up.pt)

²ALiCE – Associate Laboratory in Chemical Engineering, Faculty of Engineering, University of Porto, Rua Dr. Roberto Frias, 4200-465 Porto, Portugal

Abstract

Temperature-based strategies are commonly applied to control microbial growth, but the impact of those procedures on biofilm structure is usually not evaluated. This study aimed to understand how thermal disinfection procedures affect pre-established *Pseudomonas fluorescens* biofilms, formed in a Center for Disease Control (CDC) biofilm reactor under 125 and 225 rpm. The biofilm regrowth potential was evaluated over 24 h. Biofilms structure was assessed at the microscale by Confocal Laser Scanning Microscopy (CLSM) and at the mesoscale through Optical Coherence Tomography (OCT). Results showed that the impact of the thermal disinfection on the biofilm structure depends on the hydrodynamic conditions, which are also critical to the biofilm structural rearrangement upon regrowth.

Author Keywords. Biofilm regrowth, disinfection, temperature shock, water systems

1. Introduction

Thermal disinfection approaches are widely applied to control microorganisms' growth (Nocker et al. 2021). This disinfection procedure can be used in engineered water systems to reduce the levels of waterborne pathogens like *Legionella* (Mouchtouri et al. 2007). Field-based studies have been performed to evaluate thermal disinfection effectiveness (Mouchtouri et al. 2007), mostly on planktonic microorganisms. The role of biofilms in shielding such microorganisms against harsh conditions has been ignored (Pereira et al. 2021). From the operational point-of-view of engineered hot water networks, understanding what happens to the biofilm structure upon thermal disinfection and under different flow velocities can lead to a better design and implementation of thermal procedures. This work aimed to evaluate the impact of thermal shocks on the biofilm structure under microscale (Confocal Laser Scanning Microscopy, CLSM) and mesoscale imaging (Optical Coherence Tomography, OCT).

2. Materials and Methods

Pseudomonas fluorescens ATCC 13525 was grown overnight in nutrient broth. On day 0, the Center for Disease Control (CDC) biofilm reactor was inoculated with 1 mL of the overnight culture (10^8 CFU/mL *P. fluorescens*) in 500 mL of sterile nutrient medium. The baffle was set to rotate at either (a) 125 (0.0205 N/m^2) or (b) 225 (0.0573 N/m^2) rpm. Biofilm was formed for 8 days and then subjected to a thermal shock (70°C over 15 min). The regrowth potential was evaluated 1 and 24 hours after thermal shock. Figure 1 shows the experimental setup.

Biofilm structural parameters (such as thickness and surface coverage) were evaluated with microscale (Confocal Laser Scanning Microscopy, CLSM) and mesoscale imaging (2D-Optical Coherence Tomography, OCT).



Figure 14: Experimental installation for biofilm growth using the CDC reactor.

3. Discussion

The biofilms grown at 125 rpm were thicker than the biofilms formed at 225 rpm (Figure 2a and 2b). A thickness reduction of 80 % was found after the shock for biofilms formed under 125 rpm (Figure 2a), however there was no significant biofilm sloughing off for the 225 rpm (Figure 2b). Surface coverage was reduced by 65 % and 6 % after the thermal shock for 125 and 225 rpm (Figures 2c and 2d), respectively. Results showed that the impact of the thermal disinfection on the biofilm structure depends on the hydrodynamic conditions, which are also critical to the biofilm structural rearrangement upon regrowth.

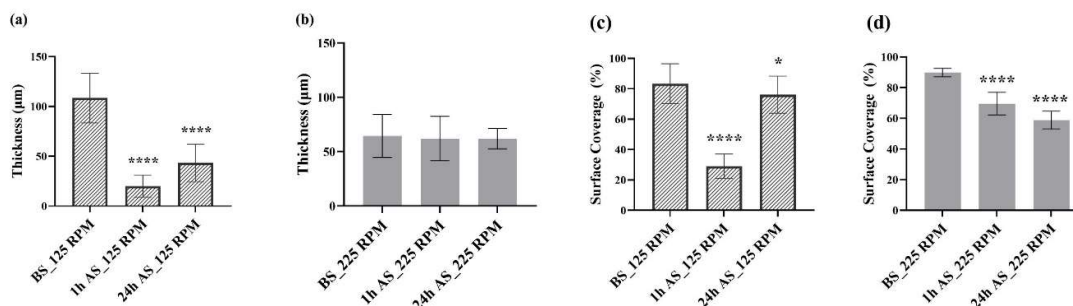


Figure 2: Thickness of 8-days-old biofilms developed under 125 RPM (a) and 225 RPM (b), before shock (BS) and 1 (1h AS) and 24 (24h AS) hours after shock (AS). Surface coverage of 8-days-old biofilms developed under 125 RPM (a, c) and 225 RPM (b, d) before shock (BS) and 1 (1h AS) and 24 (24h AS) hours after shock (AS). The means \pm standard deviation are shown. Statistically significant differences are represented for $p < 0.05$ by * and < 0.0001 by **** when compared with BS samples.

4. Conclusions

The overall results showed that the effect of thermal shock on the biofilm structure seems to depend on the prevailing hydrodynamic conditions. We demonstrated that there is a different spatial arrangement of the biofilm structure after the thermal shock. Using a reproducible biofilm model, assessed with a micro- and mesoscale analysis, this work provides new insights on the need of studying biofilm structure.

References

- Mouchtouri, Varvara, Emmanuel Velonakis, and Christos Hadjichristodoulou. 2007. "Thermal Disinfection of Hotels, Hospitals, and Athletic Venues Hot Water Distribution Systems Contaminated by Legionella Species." *American Journal of Infection Control* 35 (9): 623–27. <https://doi.org/https://doi.org/10.1016/j.ajic.2007.01.002>.
- Nocker, Andreas, Elisa Lindfeld, Jost Wingender, Simone Schulte, Matthias Dumm, and Bernd Bendinger. 2021. "Thermal and Chemical Disinfection of Water and Biofilms: Only a Temporary Effect in Regard to the Autochthonous Bacteria." *Journal of Water and Health* 19 (5): 808–22. <https://doi.org/10.2166/wh.2021.075>.
- Pereira, Ana, Ana R Silva, and Luis F Melo. 2021. "Legionella and Biofilms—Integrated Surveillance to Bridge Science

and Real-Field Demands." *Microorganisms* 9 (6):1212. <https://doi.org/10.3390/microorganisms9061212>.

Acknowledgments

This work was supported by LA/P/0045/2020 (ALiCE), UIDB/00511/2020 and UIDP/00511/2020 (LEPABE), funded by national funds through FCT/MCTES (PIDDAC). This work is also financially supported by national funds through the FCT/MCTES (PIDDAC), under the project 2022.03523.PTDC. Funding from the European Union—Horizon 2020 research and innovation program under grant agreement No 952471 (SurfSAFE). Ana Rosa Silva thanks the Portuguese Foundation for Science and Technology (FCT) for the financial support of the PhD grant (2020.08539.BD).

Microparticles separation in microchannels

Barbosa Violina B.^{1,3*}, Cerqueira Laura^{3,1}, Miranda João^{2,3}, Azevedo Nuno F.^{1,3}

¹LEPABE—Laboratory for Process Engineering, Environment, Biotechnology and Energy, Department of Chemical Engineering, Faculty of Engineering of University of Porto, Rua Dr. Roberto Frias, s, /n 4200-465 Porto, Portugal

²CEFT—Transport Phenomena Research Center, Department of Chemical Engineering, Faculty of Engineering of University of Porto, Rua Dr. Roberto Frias, s, /n 4200-465 Porto, Portugal

³ALICE—Associate Laboratory in Chemical Engineering, Faculty of Engineering, University of Porto, Porto, Portugal

*Corresponding author: violina.barbosa@gmail.com

Abstract

In this work, we assessed microparticle separation using a deterministic lateral displacement in a microfluidic channel. The separation occurs because microparticles flow in specific trajectories along the microchannel. Also, calculating the critical diameter (D_c) allows to predict microparticle separation. The experimental results confirmed that particles above D_c (3.36 μm) were separated from smaller particles that were below this value.

Author Keywords. Microfluidics, separation, microparticles, food safety.

1. Introduction

In food microbiology, culture-based methods are considered as “gold standard” for microorganism detection and identification. These methods are low-cost and allow specific, sensitive detection and identification of microorganisms of interest. However, these are demanding procedures and require initial sample enrichment for microbial concentration, which could last for several days. Alternatively, using microfluidic technology, target microorganisms can be efficiently separated and concentrated from heterogenous mixtures (Sande 2020). Thus, we used microparticles to optimise flow conditions and to investigate the separation in microfluidic channels intended for food safety application.

2. Materials and Methods

The proposed microchannel was designed with AutoCAD® and fabricated in elastomer (polydimethylsiloxane-PDMS) by soft-lithography. The configuration and dimensions were confirmed with scanning electron microscopy. Then, the microchannel was used to separate fluorescence polystyrene microparticles of diameter 2 μm and 6 μm . These particles were previously suspended in 0.1% (wt/vol) sodium dodecyl sulfate (SDS) alone or supplemented with 15% (wt/vol) dextran. Finally, microparticle separation was visualized through streak line photography.

3. Discussion

The critical particle diameter (D_c) (Davis 2006) in the proposed microchannel is 3.36 μm . This value was determined from the array tilt angle, gap size, micropillar diameter, array pitch and row shift. The inlet flow rate of 0.2 $\mu\text{L}/\text{min}$ in a cross section of 100 \times 30 μm was set, which was equivalent to an inlet velocity of 0.001 m/s. The laminar flow profile was confirmed by the dimensionless Re number ($Re = 0.11$). The density of SDS supplemented with 15% (wt/vol) dextran matched the density of the fluorescence polystyrene particle, which resulted in reduced microparticles sedimentation. Finally, the experimental data, acquired with streak line photography, revealed that 6 μm microparticles were displaced, while 2 μm particles were not, which is consistent with the microchannel critical diameter.

4. Conclusions

Overall, the results demonstrate that fluid properties have an important role on particle flow profile and subsequent separation in microfluidic channel. Moreover, acquired data from particle experiments will be used for subsequent validation tests with microorganisms.

References

Sande, M.G.; Caykara, T.; Silva, C.J.; Rodrigues, L.R. New solutions to capture and enrich bacteria from complex samples.

Med Microbiol Immunol 2020, 209, 335–341, DOI:10.1007/s00430-020-00659-1.

Davis, J.A.; Inglis, D.W.; Morton, K.J.; Lawrence, D.A.; Huang, L.R. Chou SY, Sturm JC, Austin RH. Deterministic hydrodynamics: taking blood apart. *Proc Natl Acad Sci U S A*. 2006;103(40):14779-84. DOI: 10.1073/pnas.0605967103

Looking for the Toxin

Paula Esteiro^{1,3,*}, Emilio Rosales², Marta Calvo-Catoira^{3,4} and Elisa González-Romero¹

¹Department of Analytical and Food Chemistry and ²CINTEX – University of Vigo, Campus As Lagoas-Marcosende, Vigo, 36310, Spain

³Zendal S. A., Lugar La Relva, 36410, O Porriño, Spain

⁴School of Architecture & Polytechnic., European University of Valencia, 46022 Valencia, Spain

*Corresponding author: paula.esteiro@uvigo.es and eromero@uvigo.es

Abstract

The quality and safety of medicines has been the main concern of both, the industry, and regulatory agencies. Indeed, to ensure these product characteristics, the concept of Quality by Design (QbD), an innovative pharmaceutical quality system during production, which allows monitoring production in real time, was born. The aim of this study was the development of a sensitive and selective methodology to control the production of a clostridial toxin while it is produced as a component of the clostridial polyvalent vaccine. The results obtained demonstrated the capability of electrochemical techniques to monitor the toxin, allowing to relate the observed signal to the production stage.

Author Keywords. Quality by Design, Electroanalysis, Clostridial Bacteria, Toxin

1. Introduction

The importance of animal health has been increased by the One Health concept (McEwen and Collignon 2018), an approach that recognizes that the health of people is related to animals' health and to the environment. Indeed, healthier animals will have a direct impact on healthier human, beings through diet or through simple contact between both. As a result, animals are administered with preventive treatments. An example of this are polyvalent vaccines for the prevention of clostridial diseases that affect animals and also, humans.

Clostridial polyvalent vaccines are made from the inactivated toxins produced by clostridial bacteria. These bacteria are cultivated until they are stressed to release the corresponding toxin. Once the toxin is obtained, usually, it goes through an inactivation process, so that the toxin does not suppose a risk to the organism while, a response from the immune system is obtained. Finally, the inactivated toxin (toxoid) is purified through processes such as centrifugation and/or filtration to eliminate residues from the production process that may suppose a risk for the use of the vaccine (Walker 1992).

Quality by Design (QbD) was born at the beginning of the last century as a consequence of the permanent concern of the pharmaceutical industry together with regulatory agencies, to ensure the safety and efficacy of its products (J. M. Juran 1992). QbD is an innovative pharmaceutical quality system during production, which allows monitoring production in real time. These advance aims to guarantee the quality of pharmaceutical products using statistical, analytical and risk management methodologies during design, development, and manufacturing of the product (International Council for Harmonisation of Technical Requirements for Pharmaceuticals for Human Use 2004).

The aim of this project is to develop sensitive, selective, simple, and reproducible methodologies based on electroanalytical techniques that allow the control of the culture of a clostridial toxin. For this, initially the electrochemical study of the immunopurified toxoid will be carried out. Once the toxoid has been characterized, the study of the toxoid will continue in the different step of production from the toxin in the culture medium, until the final product, a complex matrix that will produce a large amount of interference.

2. Materials and Methods

Biological production samples, analysed without any pre-treatment, were from the production of a clostridial toxoid from the pharmaceutical company ZENDAL.

Cyclic Voltammetry (CV) measurements were performed with a portable potentiostat μ Stat 100 (DropSens Company), SPE Connector (2 mm banana, PalmSens) for Screen-Printed Electrode (SPE) and controlled by PalmSensLite Software (PSLite 1.6.1.0). CV is the technique used to carry out the

electrochemical process study attending to the following conditions: potential range from -1.2 to 1.2 V and scan rate $100 \text{ mV}\cdot\text{s}^{-1}$.

3. Discussion

Initially, an immunopurified sample was analyzed. This analysis made it possible to ensure that the signal observed was the protein of interest, as it is shown in Figure 15. With the signal already identified, production samples were analyzed from the end of production to the beginning of the culture. In this sequencing it was expected that the toxoid/toxin signal would be similar, and that it would maintain a proportionality between the processes to which they were subjected and the intensity of the signal.

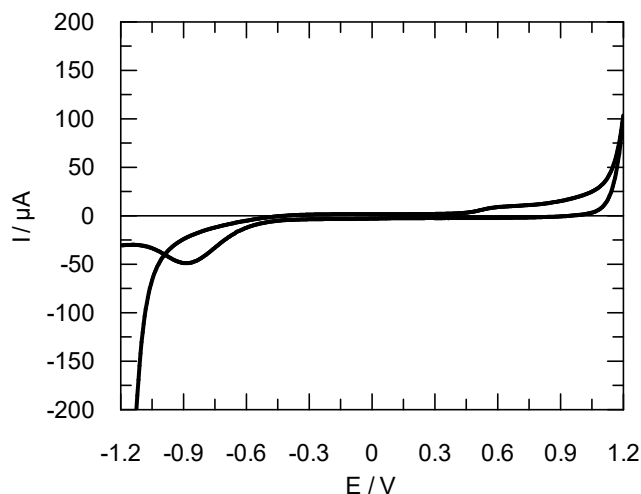


Figure 15: Voltammograms obtained for the immunopurified toxoid

Subsequently, during the first batch, it was possible to monitor the toxoid since the end of the inactivation process until the final product. The signals obtained for the different stages were related with different procedures the toxin or toxoid had suffered. Nevertheless, the electrochemical activity of the toxoid was also influenced by the media.

Voltammograms obtained for the second batch (Figure 16), where it can be seen that, there is an increase in signal intensity during the culture, which subsequently begins to decrease, until reaching the most concentrated point, where the signal increases in intensity again.

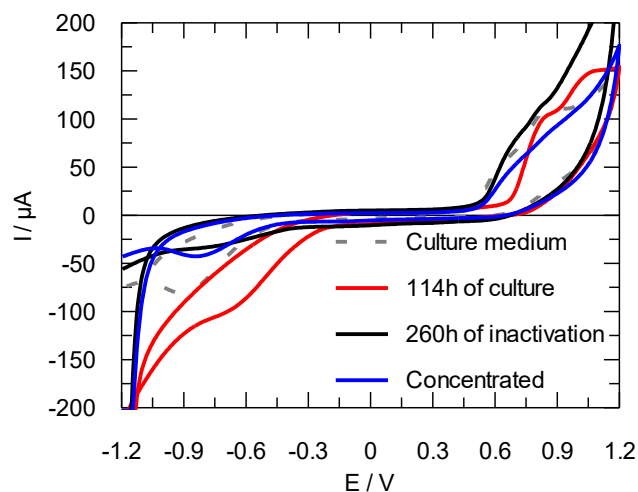


Figure 16: Voltammograms obtained during the production of the toxoid.

After obtaining samples from different productions, it was possible to conclude that both the toxin and the toxoid are reduced, generating cathodic peaks.

4. Conclusions

Electrochemical techniques, specifically voltammetric techniques, have demonstrated their ability to measure the toxin or toxoid of a clostridial bacteria during its production. These techniques seem to be promising techniques to implement production control methods under the QbD concept, although it is necessary to continue optimizing the methodology while scaling the analysis.

References

- International Council for Harmonisation of Technical Requirements for Pharmaceuticals for Human Use. 2004. "ICH Q8 (R2) Pharmaceutical Development - Scientific Guideline."
- J. M. Juran. 1992. *Juran on Quality by Design: The New Steps for Planning Quality Into Goods and Services*.
- McEwen, Scott A., and Peter J. Collignon. 2018. "Antimicrobial Resistance: A One Health Perspective." *Microbiology Spectrum* 6 (2). <https://doi.org/10.1128/microbiolspec.arba-0009-2017>.
- Walker, P D. 1992. "Bacterial Vaccines: Old and New, Veterinary and Medical." *Vaccine* 10 (14): 977–90.

Acknowledgments

The authors are highly indebted to the Institutions for financial support like the Project PID2020-113667GB-I00 funded by the Spanish Ministry of Sciences and Innovation MCIN/AEI/10.13039/501100011033 and European Union Next Generation EU/ PRTR (PDC2021-121394-100 and PCI2022-132941), as well as, to the many colleagues and coworkers who did this research a reality, especially to A. Alonso (from the company Cualitis), for his formation's course on Risks associated with exposure to biological agents. Paula Esteiro is grateful to the company ZENDAL for her PhD contract.

Direct contact membrane distillation-promoted persulfate activation as an innovative approach in water desalination

A. Rita T. Fernandes^{1,2,*}, Ana R. Lado Ribeiro^{1,2}, Luís M. Madeira^{2,3},
Adrián M. T. Silva^{1,2}

¹LSRE-LCM - Laboratory of Separation and Reaction Engineering – Laboratory of Catalysis and Materials, Faculty of Engineering, University of Porto, Rua Dr. Roberto Frias, 4200-465 Porto, Portugal

²ALiCE - Associate Laboratory in Chemical Engineering, Faculty of Engineering, University of Porto, Rua Dr. Roberto Frias, 4200-465 Porto, Portugal

³LEPABE – Laboratory for Process Engineering, Environment, Biotechnology and Energy, Faculty of Engineering, University of Porto, Rua Dr. Roberto Frias, 4200-465 Porto, Portugal

*Corresponding author: arfernandes@fe.up.pt ORCID ID: 0000-0002-0188-5758

Abstract

Due to population growth, urbanization and intensification of industrial processes, several substances that end up in aquatic compartments can be considered contaminants of emerging concern, with potential adverse effects on ecosystems and human health. Over the years, the scientific community has developed more efficient processes for both the removal of these contaminants from water and the desalination of seawater. This work aims to study how two processes (direct contact membrane distillation and thermal activation of persulfate) can be integrated to enhance their advantages in simultaneous seawater desalination and decontamination. In this context, venlafaxine was added to ultrapure water and seawater as a model pharmaceutical compound frequently found in water compartments. Its complete removal was rapidly achieved using sodium persulfate (SPS) at 80 °C in a batch reactor. The integration of these processes was evaluated to verify their efficiency for the recovery of clean water.

Author Keywords: persulfate, thermal activation, integrated treatment, membrane distillation, clean water recovery.

1. Introduction

Water plays an essential role in ecosystems and several human activities (Barbosa et al. 2016), but population growth, climate change, urbanization and the intensification of industrial processes have led to an increased demand for water (Gude 2017). Additionally, many compounds are released daily into the environment, including pharmaceuticals, hormones, illicit drugs, pesticides, personal care products, industrial products, among others (Barbosa et al. 2016; Morin-Crini et al. 2022). Nevertheless, conventional wastewater treatment plants (WWTPs) cannot completely remove these recalcitrant organic compounds. Due to these limitations, organic pollutants are persistently released into the environment at very low concentrations (ranging from ng L^{-1} to $\mu\text{g L}^{-1}$). However, these compounds may have a toxic and adverse effect on ecosystems and human health (Morin-Crini et al. 2022).

Over the years, the scientific community has made several efforts to develop more efficient processes for the removal of pollutants from water. Advanced oxidation processes (AOPs) are among the most promising technologies for the treatment of these contaminants because of their efficiency and simplicity in many cases (Morin-Crini et al. 2022). In particular, the thermal activation of persulfate is gaining major attention. By increasing the temperature (above 40 °C), it is possible to promote the degradation of persulfate and generate radicals ($\text{SO}_4^{\bullet-}$ and HO^{\bullet}) that can attack and remove different organic compounds from water.

On the other hand, membrane distillation (MD) is an emerging non-isothermal separation process that combines distillation and membrane processes. It is based on the liquid-vapor equilibrium and requires heat to be supplied to the feed solution. The driving force of the MD process is the difference in vapor pressure between the two sides of a hydrophobic and microporous membrane (Khayet 2011).

The main goals of this work are: (i) to evaluate the efficiency of an AOP (activated SPS) in the degradation of contaminants of emerging concern in ultrapure water and in seawater, and (ii) to

integrate such AOP with the MD process and evaluate the quality of the recovered water through the integrated system.

2. Materials and Methods

The venlafaxine solutions were prepared using ultrapure water and seawater, with a contaminant concentration of $250 \mu\text{g L}^{-1}$. The batch experiments were performed in 100 mL amber bottles containing 50 mL of the previously prepared solution under constant stirring. Temperature was one of the parameters under study and the bottles were placed in an oil bath to reach the desired operating temperature. The parameters studied were the SPS concentration, temperature, and pH. All experiments were performed in duplicate.

To quantify the degradation of venlafaxine, samples were collected at specific times (0, 5, 10, 15, 30, 45, 60, 90, 120 and 180 min). At each of these times, 200 μL of the sample was withdrawn and instantly placed at $-20 \text{ }^\circ\text{C}$ to stop the reaction. The samples were analyzed using high-performance liquid chromatography (HPLC) coupled with a fluorescence detector (FD). The injection volume was 30 μL and the temperature was maintained at $30 \text{ }^\circ\text{C}$. The excitation wavelength of the FD was 230 nm and the emission wavelength was 300 nm.

During the direct contact membrane distillation (DCMD) experiments, the feed and distilled water were contained in glass tanks and operated in counter-current mode entering the membrane module at a given flow rate using two peristaltic pumps. The inlet and outlet temperatures were continuously monitored using two thermocouples connected to a digital device, and the amount of water recovered was measured using a digital balance placed under the distilled water flask (Silva et al. 2018).

3. Discussion

Thermal activation of persulfate has been extensively reported in the literature. However, its integration with DCMD has not been investigated in seawater desalination. In this study, venlafaxine was chosen as a model pollutant to follow the degradation by the thermal activation of persulfate, taking advantage of the required high temperatures in the DCMD feed. A parametric study was conducted to evaluate the effects of the different variables (temperature, sodium persulfate concentration and pH) and select those that maximize the removal of the organic pollutant.

The effect of temperature *per se* on pollutant degradation was also evaluated. After 24 h at $80 \text{ }^\circ\text{C}$, venlafaxine concentration remained constant, suggesting that the compound did not undergo thermal degradation (*i.e.*, without SPS). Subsequently, the effect of SPS concentration on venlafaxine degradation was evaluated in amber bottles. Experiments were performed at $80 \text{ }^\circ\text{C}$, and the respective controls at room temperature. The concentration of SPS ranged between 50 mg L^{-1} and 250 mg L^{-1} and showed that with an increase in concentration, the rate of degradation of venlafaxine increased, and the pollutant was degraded after 5 and 30 min for the highest and lowest concentrations of SPS, respectively. Regarding the effect of temperature, it was observed that with an increase in the reaction temperature, the reaction rate also increased. The effect of pH was tested and no significant changes were observed in the rate of venlafaxine degradation in the range studied (pH from 2.1 to 10.5). Furthermore, the process was efficient in removing venlafaxine, even when using a real matrix (seawater).

Finally, experiments were performed with seawater and the pollutant in a DCMD system. The influence of different parameters (temperature, feed flow rate, and operating time) was evaluated to optimize the permeate flux, water recovery and quality of the recovered water. The retentate (concentrated seawater) and permeate (distilled water) were analyzed to verify the efficiency of the integrated treatment process.

4. Conclusions

In this study, the thermal activation of persulfate was evaluated for the degradation of venlafaxine. A parametric study enabled us to determine the conditions under which the process provided the best results. The efficiency of this process was verified, even when a real water matrix was used, and venlafaxine was successfully removed.

The MD process, in which the feed is heated to generate a temperature difference between the retentate and permeate sides, was integrated with the thermal activation of persulfate.

References

- Barbosa, Marta O., Nuno F.F. Moreira, Ana R. Ribeiro, Manuel F.R. Pereira, and Adrián M.T. Silva. 2016. "Occurrence and Removal of Organic Micropollutants: An Overview of the Watch List of EU Decision 2015/495." *Water Research* 94 (May): 257–79.
- Gude, Veera Gnanaswar. 2017. "Desalination and Water Reuse to Address Global Water Scarcity." *Reviews in Environmental Science and Biotechnology* 16 (4): 591–609.
- Khayet, Mohamed. 2011. "Membranes and Theoretical Modeling of Membrane Distillation: A Review." *Advances in Colloid and Interface Science* 164 (1–2): 56–88.
- Morin-Crini, Nadia, Eric Lichtfouse, Marc Fourmentin, Ana Rita Lado Ribeiro, Constantinos Noutsopoulos, Francesca Mapelli, Éva Fenyvesi, et al. 2022. "Removal of Emerging Contaminants from Wastewater Using Advanced Treatments. A Review." *Environmental Chemistry Letters*. Springer.
- Silva, Tânia L.S., Sergio Morales-Torres, Carla M.P. Esteves, Ana R. Ribeiro, Olga C. Nunes, José L. Figueiredo, and Adrián M.T. Silva. 2018. "Desalination and Removal of Organic Micropollutants and Microorganisms by Membrane Distillation." *Desalination* 437 (July): 121–32.

Acknowledgments

This work was financially supported by: LA/P/0045/2020 (ALiCE), UIDB/50020/2020 and UIDP/50020/2020 (LSRE-LCM), UIDB/00511/2020 and UIDP/00511/2020 (LEPABE), funded by national funds through FCT/MCTES (PIDDAC). A.R.T.F. is grateful for her PhD research grant (2022.12141.BD) from FCT, funded by national funds and by the European (EU) through the European Social Fund (ESF). A.R.L.R. acknowledges FCT funding under the Scientific Employment Stimulus - Individual Call (2022.00184.CEECIND).

Photocatalytic activity of phosphorescent strontium aluminate doped with Eu²⁺ and Dy³⁺

Ana M. Chávez^{1,2*}, Joaquim L. Faria², Cláudia G. Silva², Adrián M.T. Silva²

¹Departamento de Ingeniería Química y Química Física, Instituto Universitario del Agua, Cambio Climático y Sostenibilidad (IACYS), Universidad de Extremadura, 06006 Badajoz, Spain.

²LSRE-LCM – Laboratory of Separation and Reaction Engineering – Laboratory of Catalysis and Materials (LSRE-LCM), Faculdade de Engenharia, Universidade do Porto, Rua Dr. Roberto Frias s/n, 4200-465 Porto, Portugal.

³ALICE – Associate Laboratory in Chemical Engineering, Faculdade de Engenharia, Universidade do Porto, Rua Dr. Roberto Frias s/n, 4200-465 Porto, Portugal.

*Corresponding author: achavez@fe.up.pt; ORCID ID 0000-0001-8781-5154

Abstract

Strontium aluminate doped with europium and dysprosium (SAED) is widely employed as a long afterglow phosphorescent solid material. It has been also combined with photocatalysts for the degradation of pollutants in water, but with low stability. This study demonstrates that the absence or presence of some anions (*i.e.*, chloride and sulfates) and pH may affect the stability, leaching strontium into the media. On the contrary, phosphates prevent hydrolysis and maintain the photoluminescent properties. The photocatalytic activity of SAED-based photocatalysts was enhanced in phosphate-buffered solutions, the SAED-coupled carbon nitride being the most promising photocatalyst.

Author Keywords. Phosphorescent, photoluminescence, stability, water treatment.

1. Introduction

Photocatalysis is based on the photo-excitation of a material generating electron/hole pairs under radiation provided by UV lamps, sunlight or visible-light LEDs. Recently, phosphorescent materials have been coupled with photocatalysts, reducing the electron/hole recombination or actuating as self-luminous light source (Kang et al. 2021). Strontium aluminate doped with europium and dysprosium (SAED) is a persistent luminous material widely employed in paints, inks, and ceramics. In water decontamination, SAED has been used in combination with photocatalysts (PCs) such as TiO₂, WO₃ and carbon nitride (CN); however, some stability problems in water have been found (Guo et al. 2007).

2. Materials and Methods

SAED (Sigma-Aldrich 98%, ref: 756539, CAS 883150-73-0), TiO₂ (Fluka) and WO₃ (Alfa Aesar). were used without any further purification. CN was synthesized with urea in a muffle furnace according to a previous study (Lima et al. 2017). SAED-coupled materials were prepared by mixing SAED:PC in a ratio 1:1 and post-thermally treated at 400 °C for 4 hours (initial heating ramp 5 °C/min).

The stability of the SAED material was tested in the presence of different anions in solution (provided by 0.01 M of HCl, H₂SO₄ and H₃PO₄) at initial pH 4, 7 and 10 under stirring for 24 h. The solid samples were collected by centrifugation, dried at 100 °C, and analyzed with a spectrofluorometer (JASCO FP 8300) and other techniques. The leached Sr was determined by ionic chromatography (Metrohm 881 compact IC pro).

The photocatalytic activity of the coupled materials was studied with tramadol as target pollutant (5 mg L⁻¹) in non-buffered or H₃PO₄ buffered solution and using a solar simulator as radiation source (550 W m⁻²).

3. Discussion

The stability tests performed in presence of different ions (Cl⁻, SO₄²⁻ and PO₄³⁻) reveals that SAED maintains its photoluminescence with phosphates in the media (results not shown). Moreover, phosphates also prevent the hydroxylation of SAED better than sulfates and chloride. However, pH is also an important factor that has to be considered, since SAED demonstrated to be more stable at basic than acidic pH, as revealed by the released amount of Sr (**Erro! A origem da referência não foi encontrada.**). Almost no leaching was found at pH = 10 in the phosphate buffer solution.

SAED-coupled photocatalysts were tested for the degradation of tramadol in water under solar simulated radiation. Comparing the experiments in ultrapure water and buffered solutions, the efficiency of the treatments is negatively affected by the low stability of the SAED materials in water. Therefore, the photoluminescence might play an important role on the photocatalytic degradation of water pollutants. The SAED-CN solid was found to be the most promising SAED-based photocatalyst.

	Cl ⁻			SO ₄ ²⁻			HPO ₄ ⁻ /PO ₄ ²⁻			
pH ₀	4	7	10	4	7	10	4	7	10	free
pH _f	11.5	11.5	11.5	11.6	11.7	11.6	5.3	7.0	10.0	11.8
Sr, ppm	353.2	366.0	88.3	27.9	22.7	23.4	66.7	9.8	1.5	310.6

Table 9: Final pH (pH_f) and leached Sr after 24 h of suspended SAED in contact with different anions and at different initial pH values (pH₀).

4. Conclusions

The SAED material was demonstrated to be more stable in presence of phosphates > sulfates >> chloride and at higher pH values. In addition, SAED only preserves the photoluminescence in phosphate buffered solutions, resulting in a better photocatalytic performance.

References

- Guo, Chongfeng, Lin Luan, Dexiu Huang, Qiang Su, and Yuhua Lv. 2007. "Study on the Stability of Phosphor SrAl₂O₄:Eu²⁺, Dy³⁺ in Water and Method to Improve Its Moisture Resistance." *Materials Chemistry and Physics* 106 (2–3): 268–72. <https://doi.org/10.1016/J.MATCHEMPHYS.2007.05.052>.
- Kang, Fengwen, Guohuan Sun, Philippe Boutinaud, Haoyi Wu, Fei Xiang Ma, Jian Lu, Jiulin Gan, Haidong Bian, Fei Gao, and Sanshui Xiao. 2021. "Recent Advances and Prospects of Persistent Luminescent Materials as Inner Secondary Self-Luminous Light Source for Photocatalytic Applications." *Chemical Engineering Journal* 403 (January): 126099. <https://doi.org/10.1016/J.CEJ.2020.126099>.
- Lima, Maria J., Adrián M.T. Silva, Cláudia G. Silva, and Joaquim L. Faria. 2017. "Graphitic Carbon Nitride Modified by Thermal, Chemical and Mechanical Processes as Metal-Free Photocatalyst for the Selective Synthesis of Benzaldehyde from Benzyl Alcohol." *Journal of Catalysis* 353 (September): 44–53. <https://doi.org/10.1016/J.JCAT.2017.06.030>.

Acknowledgments

Ana M. Chávez is grateful to Ministerio de Ciencia, Innovación y Universidades of Spain through Universidad de Extremadura (UEX) for her postdoctoral fellowship "Ayudas para la recualificación del sistema universitario español. Modalidad Margarita Salas" for young Ph.D. researchers (MS-17, UEX, call 2021). This work was also supported by LA/P/0045/2020 (ALICE), UIDB/50020/2020 and UIDP/50020/2020 (LSRE-LCM), funded by national funds through FCT/MCTES (PIDDAC), and by Project NORTE-01-0145-FEDER-000069 (Healthy Waters) supported by NORTE 2020, under the PORTUGAL 2020 Partnership Agreement, through ERDF.

Development of different CuFe-MOF/PMS systems for selective treatment of wastewater pollutants

Bárbara Lomba-Fernández^{1*}, Antía Fdez-Sanromán¹, Marta Pazos¹,
Emilio Rosales¹ and M^a Ángeles Sanromán¹

¹CINTECX, Department of Chemical Engineering, Universidade de Vigo, Campus Universitario As Lagoas-Marcosende, 36310 Vigo, Spain

*Corresponding author: barbara.lomba.fernandez@uvigo.gal; ORCID: 0009-0005-0083-1941

Abstract

This study presents the solvothermal synthesis of three CuFe-MOFs. Different metallic salts and temperatures (90 or 150 °C) were used in the synthesis of different CuFe-MOFs. The characterization of the materials revealed different morphologies and properties. The MOFs were named CuFe-MOF_n, where n is 1 for the highest ratio and 3 for the lowest ratio. Optimal conditions of pH, peroxymonosulfate (PMS) concentration and catalyst dosage were determined by removing Rhodamine B. Under these conditions, the degradation of a mixture of drugs such as sulfamethoxazole (SMX) and antipyrine (ANT) was evaluated and the results revealed a degradation of 80% of both drugs after 30 minutes for the CuFe-MOF with high iron content. High antibacterial activity was also attained with the system CuFe-MOF₁/PMS due to the high copper content concerning the others.

Author Keywords. CuFe-MOFs, Rhodamine B degradation, drugs degradation, antibacterial activity.

1. Introduction

Water is widely recognized as a natural, limited and very valuable resource. Overpopulation and industrial activity have resulted in an increase in many organic pollutants, known as emerging pollutants, and pathogens. This has prompted the search for more effective water treatment techniques to ensure water quality, such as advanced oxidation processes (AOPs). Within these processes, PMS activation has received considerable attention to produce sulfate radicals. These radicals have much greater redox potential and greater adaptive capacity in contrast to other reactive species such as hydroxyl radicals. Therefore, their use results in superior degradation of organic pollutants.

The activation of PMS can be possible by different methods such as heating, ultrasound, light and transition metals. Nowadays it stands out the use of transition metals, however, their use as homogeneous catalysts presents several problems due to their difficult recovery and recycling. Thus, heterogeneous catalysts are preferred for PMS activation and Metal-organic frames (MOFs), highly ordered structures composed of organic and inorganic components, exhibit excellent catalytic properties due to the abundance of oxygen vacancies (as active sites), synergistic mechanisms and high efficiency (Fdez-Sanromán *et al.* 2022).

2. Materials and Methods

Synthesis CuFe-MOF_n: was carried out by solvothermal methods. In the synthesis of several reagents were used: dimethylformamide, ethanol, 2-aminoterephthalic acid (NH₂BDC), iron (II) sulfate heptahydrate, copper (II) acetate, copper (II) chloride hexahydrate and iron (III) chloride hexahydrate. All the chemicals mentioned were purchased from Sigma Aldrich. The procedure is based on the work of Fu *et al.* (2022) and Khosravi *et al.* (2022).

Degradation of Rhodamine B: the influence of the initial pH, which was evaluated between 3 and 9, the CuFe-MOF concentration, between 0.125 and 0.5 g/L, and the PMS, whose values were 0.1 to 1 mM.

Degradation of the drug mixture: Fenton-like, photo-PMS, photolysis, photoadsorption and photocatalysis processes were evaluated operating at the previous optimal conditions.

Disinfection: *E. coli* CECT 102 inactivation experiments were carried out at 0.1 mM PMS and 0.25 g/L concentrations of the three CuFe-MOFs.

3. Discussion

First, the tests carried out on Rhodamine B established that the optimal conditions for conducting the experiments were 0.25 g/L catalyst, 1mM PMS and an initial pH value of 6. Under these conditions, the catalytic capacity to degrade drugs was analyzed, CuFe-MOF₂ and CuFe-MOF₃ were found to have a high catalytic capacity. Particularly in UV/PMS/CuFeMOF (Figure 17) and PMS/CuFeMOF systems drug degradation reached about 80% in 30 min.

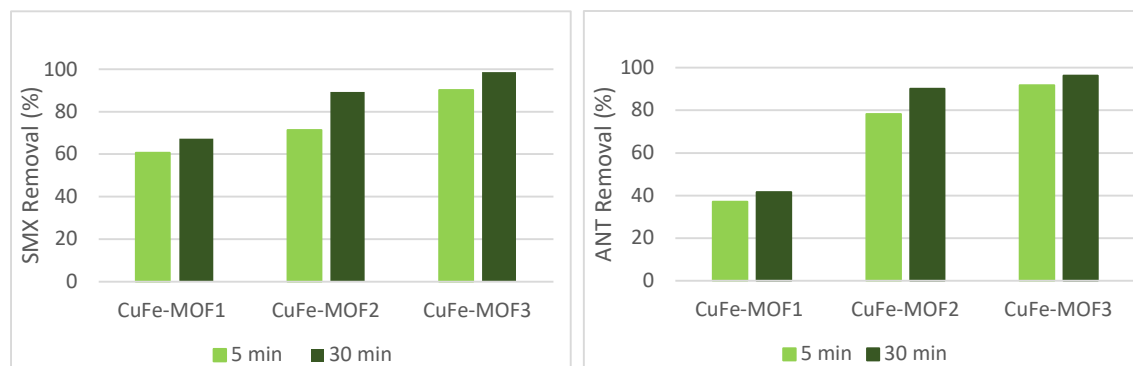


Figure 17: Degradation of SMX (left) and ANT (right) using UV-PMS-MOF system.

Second, by disinfecting *E. coli*, CuFe-MOF₁ was the only catalyst that allows the complete elimination of this pathogen in less than 1 h, while the other two catalysts cannot degrade more than 50%. This fact can be explained by the different copper content of the CuFe-MOFs.

4. Conclusions

Three CuFe-MOF with different morphologies and properties have been successfully synthesized. These properties allow a different application. It was detected that materials with high iron content had better results in the degradation of Rhodamine B and drugs (SMX and ANT), while those with high copper content showed better efficiency in the disinfection processes. In addition, these CuFe-MOFs could be easily recycled and reused in successive cycles keeping their catalytic activity so they could be used in the continuous treatment of contaminated effluents.

References

- Fdez-Sanromán, A., Rosales, E., Pazos, M., Sanromán, A. 2022. "Metal-Organic Frameworks as Powerful Heterogeneous Catalysts in Advanced Oxidation Processes for Wastewater Treatment." *Applied sciences*.
- Fu, A., Liu, Z., Sun, Z. 2022. "Cu/Fe oxide integrated on graphite felt for degradation of sulfamethoxazole in the heterogeneous electro-Fenton process under near-neutral conditions." *Chemosphere* 297: 1-12.
- Khosravi, F., Gholinejad, M., Sansano, J. M., Luque, R. 2022. "Bimetallic Fe-Cu metal organic frameworks for room temperature catalysis." *Applied Organometallic Chemistry* 36: 1-22.

Acknowledgments

This research was funded through the join 2019-2020 Biodiverse & Water JPI joint call for research proposals, under the BiodivRestore ERA-Net COFUND program with the Project PCI2022-132941 funded by MCIN/AEI/10.13039/501100011033 and PID2020-113667GBI00, funded by MCIN/AEI/10.13039/501100011033 and Xunta de Galicia, and the European Regional Development Fund (ED431C 2021-43). Antía Fdez-Sanromán thanks Ministerio de Ciencias e Innovación (PRE2021-098540) for her predoctoral fellowships.

Reduction of critical raw materials in PEM water electrolysis catalysts for green hydrogen production

Mafalda Pina^{1,2,3*}, Yury V. Kolen'ko³, O. Salomé G. P. Soares^{1,2}

¹ LSRE-LCM - Laboratory of Separation and Reaction Engineering – Laboratory of Catalysis and Materials, Faculty of Engineering, University of Porto, Rua Dr. Roberto Frias, 4200-465 Porto

² ALiCE - Associate Laboratory in Chemical Engineering, Faculty of Engineering, University of Porto, Rua Dr. Roberto Frias, 4200-465, Porto, Portugal

³ Nanochemistry Research Group, International Iberian Nanotechnology Laboratory (INL), Avenida Mestre José Veiga, 4715-330 Braga, Portugal

*Corresponding author: up202200553@fe.up.pt; <https://orcid.org/0000-0001-7286-1617>

Abstract

Green hydrogen can be produced from water electrolysis. The state-of-the-art catalysts used depend on critical raw materials, namely platinum in the cathode and iridium and/or ruthenium in the anode. The development of Pt-free and Ir-reduced catalysts is described with promising results. To replace Pt, a simple method to produce transition metal phosphides (TMP) supported on carbon materials was used. Incipient wet impregnation was used to add iron into the carbon support, followed by phosphorization with red phosphorus as the P source. The reduction of Ir loading on the anode catalyst was studied using commercial ATO powder as support for iridium oxide. The electrochemical catalysts' activity was tested in a three-electrode setup, under acidic conditions (0.5 M H₂SO₄).

Author Keywords. PEM electrolyzers, water electrolysis, green hydrogen.

1. Introduction

Climate crisis is propelling the green economy. After the Paris agreement, a limit for temperature increase was set, goals for renewable energy production, and a shift towards use of more abundant materials were determined, and several organizations and governments designed roadmaps. Hydrogen is pointed as a crucial molecule to achieve carbon neutrality by 2050, being used as an energy vector and energy source with zero emissions (Dunn et al. 2020). Hydrogen can be produced by a simple and green method: water electrolysis powered by electricity from renewables. While this process is fairly simple and has zero carbon emissions, the catalysts used to promote water splitting depend on critical raw materials (CRMs). A race for producing earth-abundant catalysts is in place, with many research groups focusing on replacing and decreasing the loading of platinum (Pt), iridium (Ir) and ruthenium (Ru) CRMs. These materials are the catalysts currently used in proton exchange membrane electrolyzers (PEMEL), with Pt being deployed on the cathode to catalyze hydrogen evolution reaction (HER) and Ir and Ru oxides in the anode side to catalyze oxygen evolution reaction (OER). In a PEMEL, from the two half-cell reactions that comprise the water electrolysis ($2 \text{H}_2\text{O} \rightarrow 2 \text{H}_2 + \text{O}_2$), the OER is the limiting reaction. Due to the oxidation mechanism and the acidic medium, replacing CRM catalysts is more challenging than in HER side – where carbon supports can be used to increase the superficial area of the active catalyst (Chatenet et al. 2022).

In this work, Pt-free HER catalysts from earth-abundant materials were prepared, while a reduction of IrOx loading in OER catalysts was investigated.

2. Materials and Methods

Synthesis of HER catalyst

Iron(III) nitrate nonahydrate was used as transition metal precursor. Carbon black Vulcan XCmax 22 (CABOT) was used as conductive carbon support. Incipient wet impregnation method was used, adding an aqueous solution containing the transition metal (iron) dropwise onto the carbon support in an ultrasonic bath. After 60 min of sonication, the prepared materials were dried in an oven at 100 °C overnight. Weight loading tested were 15, 20 and 25 % of metal. The process was followed by a thermal treatment in a vertical furnace under nitrogen atmosphere for 1 h with subsequent reduction under hydrogen atmosphere at 400 °C for 3 h, with 100 cm³/min gas flow. After cooling down to room

temperature under nitrogen flow, 0.3 g of the samples were transferred into a horizontal furnace where phosphorization takes place. Inside the same reactor, 0.25 g of red phosphorus was also placed, and it was heated to 500 °C for 1 h followed by a reduction of temperature to 250 °C for 12 h. Phosphorization was conducted under 100 cm³/cm nitrogen flow. (Brito et al. 2022)

Synthesis of OER catalyst

Iridium oxide was prepared adapting reported procedure (Ruiz Esquius et al. 2020). In a round bottom flask, 1 mmol of IrCl₃ and 8 mmol of Li₂CO₃ was dissolved in 25 mL of deionized water and stirred overnight at room temperature. The yellow solution was then refluxed for 3 h, and the obtained blue precipitate was centrifuged several times with deionized water. Afterwards, it was left to dry at room temperature, and the obtained blue powder was crushed in a mortar and stored. Commercial conductive antimony-doped tin oxide (ATO) from Thermo Scientific was used as support, being added to the IrCl₃ and Li₂CO₃ solution prior to reflux.

Electrochemical testing

For the electrochemical characterization, a three-electrode setup was used. As counter and reference electrodes, a platinum wire and calomel electrode were used, respectively, and the acidic electrolyte medium was 0.5 M H₂SO₄. Carbon paper was used as working electrode for HER catalyst, where 1 cm² was coated with the HER catalyst ink, obtaining a loading of 1 mg/cm² of catalyst. For OER, a glassy carbon electrode with 3 mm of diameter was used as working electrode and the loading was 100 µg/cm². The ink formulation was very similar for both reactions. For HER, 5 mg of catalyst was mixed with 750 µL ethanol, 250 µL of deionized water and 10 µL of Nafion. The solution was sonicated for over 1 h before drop casting onto the working electrode using a micropipette. For OER, the only different parameter was the amount of catalyst used (only 2.5 mg). The instrument used for all electrochemical measurements was a Biologic VMP-3 potentiostat/galvanostat, and cyclic voltammetry (CV) and linear sweep voltammetry (LSV) curves were obtained after an initial catalyst's activation.

3. Discussion

Figure 18a shows the powder X-ray diffraction (XRD) patterns obtained for the Fe/C catalyst before and after the phosphorization. The black pattern indicates that the Fe/C is a phase mixture of metallic iron (ICDD 04-012-6482) and iron oxide (ICDD 00-006-0615). The red pattern indicates that the phosphorization was successful, forming iron phosphide HER catalyst (ICDD 00-039-0809) supported on carbon (FeP/C). In **Figure 18b** the XRD patterns for the synthesized iridium oxide, commercial ATO and IrOx supported on ATO catalysts are shown. The IrOx pattern suggests an amorphous material, with no defined crystalline phase. The ATO and the ATO supported catalysts present a defined antimony-tin oxide phase (ICDD 01-086-4569).

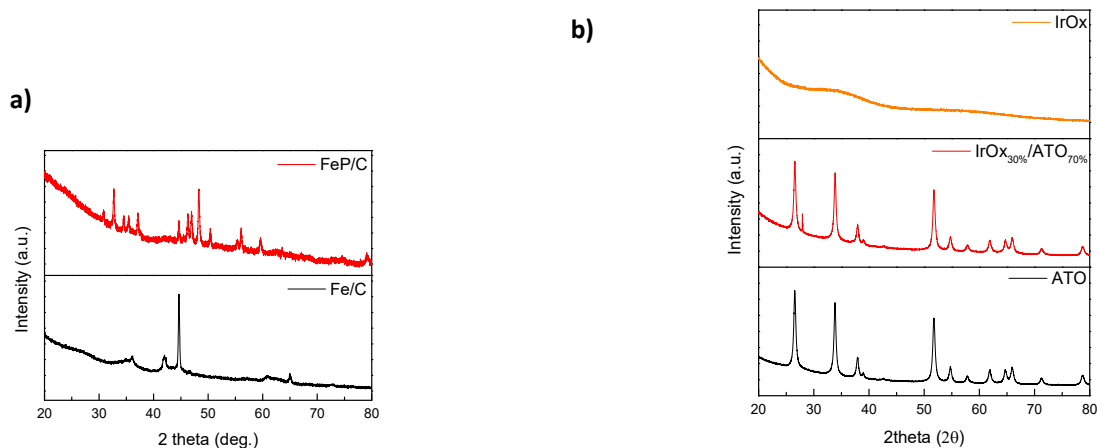


Figure 18: Collected XRD patterns for **a)** Fe/C precursor material (black pattern) and final FeP/C HER catalyst (red pattern) synthesized by phosphorization, and for **b)** synthesized iridium oxide (orange pattern), iridium oxide with different loadings of commercial ATO (blue and red patterns) and ATO (black pattern).

The obtained LSV curves for the different prepared catalysts were plotted against RHE reference value. The obtained graph for the iron phosphides is represented in

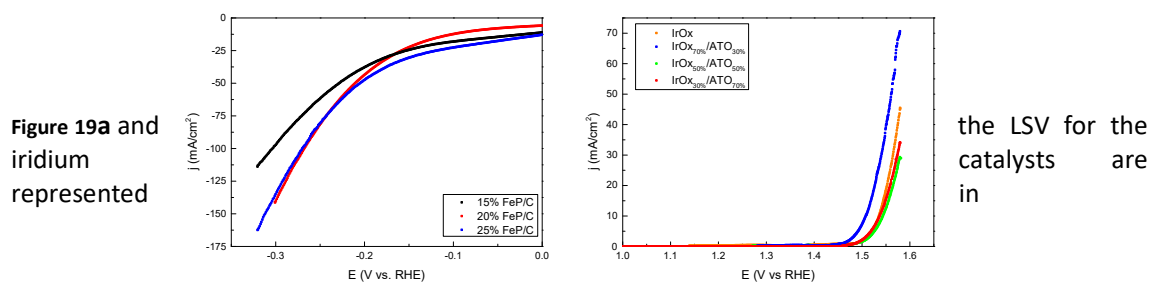


Figure 19a and **iridium** represented

the LSV for the catalysts are in

Figure 19b.

a) **b)**

Figure 19: **a)** HER cathodic polarization curve recorded for the synthesized FeP/C catalysts, **b)** OER anodic polarization curves recorded for the synthesized IrOx catalysts. All polarization curves are 85% *iR*-compensated. Scan rate = 5 mV/s. Electrolyte = 0.5 M H₂SO₄.

4. Conclusions

It was possible to prepare catalysts without CRMs or with a reduced CRM loading. Iron phosphide supported on conductive carbon (FeP/C) proved to be a good alternative to substitute commercial Pt/C catalyst for acidic HER. The method used for the preparation of state-of-the-art IrOx OER catalyst also proved to be efficient, achieving a high-performing catalyst for acidic OER. The composite iridium oxide supported on the conductive antimony-doped tin oxide (IrOx/ATO) with reduced content of IrOx

presented results comparable to the IrOx in LSV characterisation. In the future, the performance of the most promising HER and OER catalysts will be assessed in single-cell PEMEL, by the fabrication of membrane electrode assemblies (MEAs) with the selected synthesized catalysts.

References

- Brito, João, João Restivo, Juliana P.S. Sousa, Natalia C.M. Spera, D. S. Falcão, Amadeu Rocha, A. M.F.R. Pinto, Manuel Fernando R. Pereira, and Olívia Salomé G.P. Soares. 2022. "Implementation of Transition Metal Phosphides as Pt-Free Catalysts for PEM Water Electrolysis." *Energies* 15 (5). <https://doi.org/10.3390/en15051821>.
- Chatenet, Marian, Bruno G. Pollet, Dario R. Dekel, Fabio Dionigi, Jonathan Deseure, Pierre Millet, Richard D. Braatz, et al. 2022. "Water Electrolysis: From Textbook Knowledge to the Latest Scientific Strategies and Industrial Developments." *Chemical Society Reviews* 51 (11): 4583–4762. <https://doi.org/10.1039/D0CS01079K>.
- Dunn, R. J.H., D. M. Stanitski, N. Gobron, and K. M. Willett. 2020. "Global Climate." *Bulletin of the American Meteorological Society*. American Meteorological Society. <https://doi.org/10.1175/BAMS-D-20-0104.1>.
- Ruiz Esquius, Jonathan, David J. Morgan, Ioannis Spanos, Daniel G. Hewes, Simon J. Freakley, and Graham J. Hutchings. 2020. "Effect of Base on the Facile Hydrothermal Preparation of Highly Active IrOx Oxygen Evolution Catalysts." *ACS Applied Energy Materials* 3 (1): 800–809. <https://doi.org/10.1021/acsaem.9b01642>.

Acknowledgments

This work was financially supported by LA/P/0045/2020 (ALiCE), UIDB/50020/2020, and UIDP/50020/2020 (LSRE-LCM), funded by national funds through FCT/MCTES (PIDDAC). Mafalda Pina acknowledges the PhD research grant from FCT (2021.08790.BD), funded by national funds and by the European Union (EU) through the European Social Fund (ESF). O.S.G.P.S. acknowledges FCT funding under the Scientific Employment Stimulus – Institutional Call CEECINST/00049/2018.

Carbon nanotube-supported bimetallic catalysts with high activity for the selective catalytic reduction of NO_x

Patrícia S. F. Ramalho^{1,2*}, O.S.G.P. Soares^{1,2}, and M.F.R. Pereira^{1,2}

¹LSRE-LCM – Laboratory of Separation and Reaction Engineering – Laboratory of Catalysis and Materials, Faculty of Engineering, University of Porto, Rua Dr. Roberto Frias, 4200-465 Porto, Portugal.

²ALiCE – Associate Laboratory in Chemical Engineering, Faculty of Engineering, University of Porto, University of Porto, Rua Dr. Roberto Frias, 4200-465 Porto, Portugal.

*up200605969@edu.fe.up.pt ORCID: 0000-0002-5547-8066

Abstract

Nitrogen oxides are involved in environmental pollution phenomena, making it important to develop techniques for treating the emissions of these gases. The selective catalytic reduction of NO_x with carbon is an alternative technology to the more common reduction processes using NH₃. This work's main objective is the synthesis of carbon catalysts, catalytically active in NO reduction. The carbon nanotubes (CNT) were subjected to appropriate treatments to modify their surface chemistry (introduction of nitrogen, oxygen functionalities and metallic phase). The presence of copper and potassium in the catalysts is indispensable for obtaining high activities. The introduction of nitrogen surface groups further enhances their performance. The best results were obtained for nitrogen-doped CNT and impregnated with copper and potassium, obtaining a NO reduction of 100 % for a $T = 360$ °C. The catalyst stability was evaluated by carrying out a long-term reaction test. Some catalyst deactivation was observed after 41h of reaction.

Author Keywords. Nitric oxide, selective catalytic reduction, carbon nanotube, copper, potassium

1. Introduction

The reduction of nitrogen oxide (NO_x) emissions is one of the main environmental concerns, as they can cause global warming, acid rain, the greenhouse effect, and several problems for human health. Thus, it is imperative to develop advanced technologies and catalysts to control NO_x emissions to comply with increasingly stringent legislation (Bahrami et al. 2017).

Selective catalytic reduction (SCR) is a means of converting NO_x with the aid of a catalyst into N₂. At low temperatures, carbon-based catalysts show greater catalytic activity in reducing NO_x than conventional catalysts; therefore, selective catalytic reduction with carbon (SCR-C) is an excellent alternative for NO_x reduction, with the additional advantage of avoiding the need for an external reducing agent (Illán-Gómez et al. 2001).

To further improve the reactivity of carbon to NO_x, transition metals (Cu, Ni, Fe, Co) and alkali metals (K, Na) have been reported as catalysts, increasing the ability of NO_x adsorption on activated carbon and decreasing the activation energy of NO_x reduction (Gonçalves and Figueiredo 2004; Ramalho et al. 2023). Recent studies have shown that NO can be reduced to N₂ at temperatures below 500 °C, using carbon materials impregnated with transition metals (Ramalho et al. 2023). Recently, there has been a growing interest in N-doped carbon materials. Ramalho et al. (Ramalho et al. 2023) prepared activated carbon catalysts containing transition metals and nitrogen precursors for NO reduction. They observed that the presence of transition metals in the structure was essential for the catalytic activity, which was enhanced by introducing nitrogen surface groups.

The main objective of this work is to study the reduction of NO using carbon nanotubes (CNT) as a catalyst or as a support for the metallic phases.

2. Materials and Methods

CNT was used as the starting material for subsequent treatments: the CNT surface chemistry was modified by oxidation in the liquid phase with 7M of nitric acid, into which 6g of sample was placed. The acid was heated to the boiling temperature, and the system was refluxed for 3 h. After this period, the material was washed with distilled water until the pH of the washing solution was close to the natural pH of the water and dried at 110 °C in an oven for 24 h (sample CNT_HNO₃). Nitrogen-doped

samples are obtained by mixing 0.6 g of CNT with 0.39 g of melamine (M) which was used as N-precursor. CNT was ground in a ball-milling with a constant vibration frequency of 15 vibrations per second for 4 h. After mechanical mixing, the samples were submitted to thermal treatment under N₂ (100 cm³ min⁻¹) until 600 °C and kept at that temperature for 1 h (CNT_M_BM). The catalysts were prepared by the incipient wetness impregnation method of the prepared supports (described above). The support was placed under ultrasonic vibration and a solution of copper nitrate (Cu) or copper nitrate with potassium nitrate (CuK) was added to reach 10 wt% by weight of Cu or 5 wt% by weight of Cu with 5 wt% by weight of K. After impregnation, the samples were dried at 100 °C for 24 h and heat-treated at 460 °C under an N₂ flow for 1 h and an H₂ flow for 3 h.

The resulting catalysts and their supports were characterized by various techniques such as N₂ adsorption isotherms, determined at – 196 °C, X-ray photoelectron spectroscopy (XPS), transmission electron microscopy (TEM), elemental analysis (EA) and inductively coupled plasma-optical emission spectrometry (ICP-OES).

The catalytic tests were carried out in a fixed-bed U-shaped microreactor, where 200 mg of the catalyst. NO reduction was performed under a total flow rate of 100 cm³ min⁻¹ with a concentration of 1000 ppm NO in He.

3. Discussion

The treatments carried out modified the textural properties of CNT. The samples submitted to oxidative treatments had specific surface areas slightly higher (S_{BET} : 255 m² g⁻¹) than the original material (S_{BET} : 320 m² g⁻¹). This increase can be explained by the fact that these treatments remove impurities that may be blocking the access of nitrogen to the pores. With the introduction of the N-precursor the CNT_M_BM sample showed a smaller surface area (S_{BET} : 228 m² g⁻¹) due to the introduction of nitrogen groups that partially block N₂ access to the pores. Metal-based catalysts also presented a low surface area (S_{BET} : 189 m² g⁻¹) too compared to the original sample.

Table 1 presents the catalytic results obtained for the catalysts developed.

Catalyst	X _{NO} (%)	T (°C)
CNT	2	460
CNT@10Cu	26	460
CNT_M_BM	78	460
CNT_M_BM@5Cu5K	100	360

Table 10: NO conversion to reach full conversion for the developed catalysts.

CNT does not show significant catalytic activity in the reduction of NO. When incorporating copper the performance is a little better, obtaining a conversion of 26 %. The introduction of nitrogen surface groups (CNT_M_BM) further increases the catalytic activity, thus observing that the nitrogen incorporated into carbon nanotubes increases their catalytic activity, thus showing a NO reduction of 78 %. The effect of adding potassium to copper on both types of support for the reduction of NO was investigated and it was verified that the addition of potassium significantly improves its catalytic performance. Among the samples, the best results were obtained for nitrogen-doped CNT and impregnated with copper and potassium (CNT_M_BM@5Cu5K), obtaining a NO reduction of 100 % for a T = 360 °C.

4. Conclusions

The main objective of this work was to prepare, and test CNT catalysts with a wide range of textural and surface chemical properties, catalytically active for NO reduction.

It was observed that the incorporation of metal is essential for the reduction of NO. The introduction of N-surface groups further enhances the catalytic activity, with CNT_M_BM@5Cu5K being the best catalyst for NO reduction into N₂, presenting a 100% conversion at 360 °C.

In the stability test, the CNT_M_BM@5Cu5K catalyst is stable for 41h, losing its activity after that time.

References

- Bahrami, Soudabe, Aligholi Niaei, María José Illán-Gómez, Ali Tarjomannejad, Seyed Mahdi Mousavi, and Vicente Albaladejo-Fuentes. 2017. "Catalytic reduction of NO by CO over CeO₂-MO_x (0.25) (M=Mn, Fe and Cu) mixed oxides—Modeling and optimization of catalyst preparation by hybrid ANN-GA." *Journal of Environmental Chemical Engineering* 5 (5): 4937-4947. <https://doi.org/https://doi.org/10.1016/j.jece.2017.09.023>.
- Gonçalves, Filomena, and J. L. Figueiredo. 2004. "Development of carbon supported metal catalysts for the simultaneous reduction of NO and N₂O." *Applied Catalysis B: Environmental* 50 (4): 271-278. <https://doi.org/https://doi.org/10.1016/j.apcatb.2004.01.014>.
- Illán-Gómez, M. J., S. Brandán, C. Salinas-Martínez de Lecea, and A. Linares-Solano. 2001. "Improvements in NO_x reduction by carbon using bimetallic catalysts." *Fuel* 80 (14): 2001-2005. [https://doi.org/https://doi.org/10.1016/S0016-2361\(01\)00091-6](https://doi.org/https://doi.org/10.1016/S0016-2361(01)00091-6).
- Ramalho, P. S. F., O. S. G. P. Soares, J. L. Figueiredo, and M. F. R. Pereira. 2023. "Catalytic reduction of NO over copper supported on activated carbon." *Catalysis Today* 418: 114044. <https://doi.org/https://doi.org/10.1016/j.cattod.2023.114044>.
- Shu, Yun, Fan Zhang, Fan Wang, and Hongmei Wang. 2018. "Catalytic reduction of NO_x by biomass-derived activated carbon supported metals." *Chinese Journal of Chemical Engineering* 26 (10): 2077-2083. <https://doi.org/https://doi.org/10.1016/j.cjche.2018.04.019>.

Acknowledgments

This work was financially supported by LA/P/0045/2020 (ALICE), UIDB/50020/2020, and UIDP/50020/2020 (LSRE-LCM), funded by national funds through FCT/MCTES (PIDDAC) and project 2SMART: NORTE-01-0145-FEDER-000054, supported by Norte Portugal Regional Operational Programme (NORTE 2020), under the PORTUGAL 2020 Partnership Agreement, through the European Regional Development Fund (ERDF). Patrícia S.F. Ramalho acknowledges the PhD research grant from FCT (SFRH/BD/149838/2019), funded by national funds and by the European Union (EU) through the European Social Fund (ESF). O.S.G.P.S. acknowledges FCT funding under the Scientific Employment Stimulus – Institutional Call CEECINST/00049/2018.

Effectiveness of selected aldehydes as inhibitors of the LasI/LasR quorum sensing pathway and enhancers of antibiotic activity against *Pseudomonas aeruginosa* biofilms

Miguel M. Leitão^{1,2}, Fernanda Borges³, Manuel Simões^{1,2,4*}, Anabela Borges^{1,2,4*}

¹LEPABE—Laboratory for Process Engineering, Environment, Biotechnology and Energy, Faculty of Engineering, University of Porto, Rua Dr. Roberto Frias, 4200-465 Porto, Portugal

²ALICE—Associate Laboratory for Innovation in Chemical Engineering, Faculty of Engineering, University of Porto, Rua Dr. Roberto Frias, s/n, 4200-465 Porto, Portugal

³CIQUP—Department of Chemistry and Biochemistry, Faculty of Sciences, University of Porto, Porto, Portugal.

⁴DEQ—Department of Chemical Engineering, Faculty of Engineering, University of Porto, Rua Dr. Roberto Frias, s/n, 4200-465 Porto, Portugal.

*Corresponding author: Manuel Simões-(mvs@fe.up.pt) ORCID 0000-0002-3355-4398, and Anabela Borges-(apborges@fe.up.pt) ORCID 0000-0001-6929-6805

Abstract

Quorum sensing (QS) is an important bacterial communication mechanism that regulates the expression of virulence factors, biofilm formation and contributes to antimicrobial resistance. This study investigated the effectiveness of three aldehydes (p-hydroxybenzaldehyde, vanillin and syringaldehyde) in interrupting the LasI/LasR QS system of *Pseudomonas aeruginosa* using bioreporter strains. The aldehydes were also combined with the antibiotic tobramycin to evaluate their ability to prevent and control biofilms, which were characterised in terms of biomass, metabolic activity, and cell culturability reduction. Results indicates that the aldehydes showed potential to inhibit the 3-oxo-C12-HSL-dependent QS system by over 80%, even at sub-inhibitory concentrations. Moreover, the combination of the aldehydes with tobramycin resulted in an improvement of the antibiotic biofilm prevention and disruption efficacy. In conclusion, this study demonstrated that the tested aldehydes show promise as QS inhibitors and enhancer agents of the antibiofilm activity of antibiotics against *P. aeruginosa*.

Author Keywords. Aldehydes, antibiofilm activity, antimicrobial combination, antimicrobial resistance, quorum sensing inhibition

1. Introduction

Bacterial resistance to antibiotics, especially when a biofilm is formed, is a major problem in the treatment and prevention of infectious diseases. To date, there are no effective therapies for the treatment of infections associated with biofilms (Borges, *et al.* 2012, Gonçalves *et al.* 2023). Therefore, new therapeutic alternatives are needed that aim to interact with the bacterial systems responsible for pathogenicity/virulence. At this regard, quorum sensing (QS) mechanism is a intercellular communication system mediated by extracellular signalling molecules called autoinducers (Ais) (Borges *et al.* 2017). The main function of this phenomenon is the regulation of gene expression, which plays an important role in the formation and maintenance of biofilms, as well as antibiotic resistance in bacteria. The high degree of pathogenicity of *Pseudomonas aeruginosa* is mainly caused by QS (Gonçalves *et al.* 2023). Natural QS inhibitors (QSI) could represent a promising strategy for the prevention and control of biofilms. Aldehydes are a group of secondary plant metabolites, *i.e.* phytochemicals, that exhibit a broad spectrum of antibiotic activity and have excellent properties in modulating bacterial cell-cell communication in biofilm communities (Gonçalves *et al.* 2023). Besides, some aldehydes are important intermediates for the production of various chemical products of industrial value (pharmaceuticals, dyes and fragrances) (Zhang, Ke, and Zhu). It has been stated that applying QSI can improves the antibiofilm activity of antibiotics so that lower doses can be used. In this work, the activity of three selected aldehydes (p-hydroxybenzaldehyde, vanillin and syringaldehyde) was evaluated for their interfering ability with the 3-oxo-C12-HSL-dependent QS system of *P.*

aeruginosa (LasI/LasR). The evaluation of aldehydes in biofilm prevention and control alone and in combination with antibiotic tobramycin was also studied.

2. Materials and Methods

2.1 Bacterial strains, phytochemicals, and antibiotics

P. aeruginosa ATCC 10145, *P. aeruginosa* PA14 wild-type and *P. aeruginosa* PA14-R3 were used in this study. The phytochemicals p-hydroxybenzaldehyde, vanillin, syringaldehyde and antibiotic tobramycin were purchased from Sigma-Aldrich. The minimum inhibitory concentration (MIC) of each compound to be tested was determined using the broth microdilution method according to (Borges *et al.* 2013). In this work, each phytochemical was tested at concentrations ranging from 6.25 to 1000 $\mu\text{g mL}^{-1}$ prepared in 10% dimethyl sulfoxide (DMSO). Tobramycin was tested at subinhibitory concentrations (0.25-1 $\mu\text{g mL}^{-1}$) prepared in water. Negative controls were performed with 10% DMSO.

2.2 QS Inhibition Screening

The evaluation of the aldehydes ability to interfere with the QS response of *P. aeruginosa* will be performed using a high-throughput QS inhibition screening system based on a co-culture assay (using biosensor *P. aeruginosa* PA14-R3 and *P. aeruginosa* PA14 wild -type) (Borges *et al.* 2017).

2.3 Biofilm assays

Biofilms were developed using a modified microtiter plate test (Borges *et al.* 2012). For biofilm prevention assays, overnight batch cultures were grown for 24h (at 37°C and 150 rpm) in the presence of each aldehyde (500 $\mu\text{g mL}^{-1}$) or antibiotic tobramycin (0.25-1 $\mu\text{g mL}^{-1}$), as well as a combination of the two. Whereas for biofilm control studies, 24h pre-established biofilms were exposed to aldehydes (at 10000 $\mu\text{g mL}^{-1}$), tobramycin (at 0.5-1 $\mu\text{g mL}^{-1}$) and combinations for 24h at 37°C with agitation (150 rpm). Then for both conditions, the biofilms were examined in terms of biomass (production/removal), metabolic activity reduction and biofilm culturable cells quantification.

3. Results and Discussion

QSI can act at the level of synthesis, transport, and detection of the autoinducer 3-oxoC12-HSL through competitive binding or structural modification. For example, the addition of a compound with inhibitory activity will lead to a decrease in bioluminescence emitted by *P. aeruginosa* PA14-R3. A compound that reduces bioluminescence by at least 50% without significantly affecting cell growth (<20%) is considered a promising inhibitor (Borges *et al.* 2017). In this sense, the MIC of the aldehydes for the three strains of *P. aeruginosa* was calculated. None of the compounds showed bacterial growth inhibition at different concentrations tested (6.25-1000 $\mu\text{g mL}^{-1}$). Therefore, the same concentration range was used for the QS tests. The results of the QS inhibition screen performed with sub-MICs of the aldehydes (6.25-1000 $\mu\text{g mL}^{-1}$) are shown in Figure 1. The three aldehydes inhibited the *P. aeruginosa* 3-oxo-C12-HSL dependent QS system, and the effect was dose-dependent. Vanillin was the most effective, with an 85% reduction in bioluminescence at a concentration of 400 $\mu\text{g mL}^{-1}$, without affecting bacterial growth. Inhibition of QS may be an important strategy to

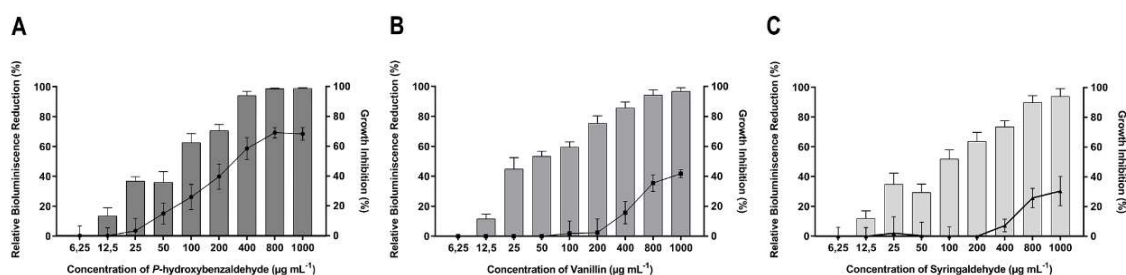


Figure 1 - Effect of increasing concentrations of p-hydroxybenzaldehyde (A), Vanillin (B) and Syringaldehyde (C) (6.25–1000 $\mu\text{g mL}^{-1}$) on the *P. aeruginosa* 3-oxo-C12-HSL-dependent QS system (primary y-axis; bars) and on growth inhibition (secondary y-axis; dashed line).

prevent and control biofilms and increase sensitivity to antibiotics. In this study, tobramycin (at 0.5 $\mu\text{g mL}^{-1}$) in combination with the three selected aldehydes (500 $\mu\text{g mL}^{-1}$) displayed higher preventive effect, in terms of both metabolic activity and biomass reduction. In turn, no effect was observed at the level of culturable cells for all aldehydes. On the other hand, the tobramycin-aldehydes combination was also shown to be effective in disrupting pre-established biofilms with significant reduction of metabolic activity (about 80%). It is of note that the application of tobramycin alone (at 0.5 $\mu\text{g mL}^{-1}$) had no effect on metabolic activity. In terms of biomass removal, the application of aldehydes individually was more effective than the combination, with the exception of syringaldehyde, which resulted in twice the reduction compared to the antibiotic and to its individual application. Regarding biofilm cells culturable, the application of the combination of tobramycin with either p-hydroxybenzaldehyde or vanillin showed a higher reduction of the number of culturable cells (2.5 log (CFU/cm²)) compared to the antibiotic alone at the same concentration.

4. Conclusions

Aldehydes seem to be promising products for anti QS strategies. These compounds have been shown to have the potential to inhibit bacterial communication systems. This study also highlights the potential of aldehydes to increase the susceptibility of biofilms to antibiotics. This allows the use of lower antibiotic doses and avoids the misuse of broad-spectrum or last line antibiotics. Additional studies are underway to investigate the interference of selected aldehydes with other *P.aeruginosa* QS systems.

References

- Borges, Anabela, Carla Ferreira, Maria J Saavedra, and Manuel Simões. 2013. "Antibacterial activity and mode of action of ferulic and gallic acids against pathogenic bacteria." *Microbial drug resistance* 19 (4):256-265.
- Borges, Anabela, Maria J Saavedra, and Manuel Simões. 2012. "The activity of ferulic and gallic acids in biofilm prevention and control of pathogenic bacteria." *Biofouling* 28 (7):755-767.
- Borges, Anabela, Pedro Sousa, Alexandra Gaspar, Santiago Vilar, Fernanda Borges, and Manuel Simões. 2017. "Furvina inhibits the 3-oxo-C12-HSL-based quorum sensing system of *Pseudomonas aeruginosa* and QS-dependent phenotypes." *Biofouling* 33 (2):156-168.
- Gonçalves, Ariana SC, Miguel M Leitão, Manuel Simões, and Anabela Borges. 2023. "The action of phytochemicals in biofilm control." *Natural Product Reports*.
- Zhang, Xingguang, Xuebin Ke, and Huaiyong Zhu. "Photocatalysts of Zeolite Supported Gold Nanoparticles for Selective Oxidation of Aromatic Alcohols to Aldehydes."

Acknowledgments

This work was supported by LA/P/0045/2020 (ALiCE), UIDP/00511/2020 (LEPABE) and FCT – Portuguese Foundation for Science and Technology through the Scientific Employment Stimulus—Individual Call—[CEECIND/00823/2021] and PhD fellowship (2021.07145.BD).

AUTHORS INDEX

Index of authors and the pages of this Book of Abstracts that they appear in

Afonso, Ana C.	105, 136
Akamatsu, Claudio	130
Albuquerque, Daniela	34
Almeida, Andreia	81
Almeida, Carina	89,140
Almeida, Filipe	120
Álvarez, Pedro M.	42
Álvarez-Conde, Javier	109
Alves, Arminda	13
Alves, Manuel A.	60
Amin, Mohsin	92
Azevedo, Ana	92
Azevedo, Nuno F.	87, 89, 107, 118, 138, 140, 161
Barbosa, Ana	87
Barbosa, Isabel S.O.	39, 69, 143
Barbosa, José R.M.	10
Barbosa, Violina B.	161
Barros, Rita A. M.	45
Bastos, Yara	115
Bedia, Jorge	109
Belver, Carolina	109
Bolaños-Vázquez, M.	51
Borges, Anabela	100, 105, 180
Borges, Fernanda	180
Bourbon, Ana I.	94
Brandão, Sofia	72
Brito, Margarida S.C.A.	72, 143
Burmølle, Mette	92
Cabral, Rafaela Mulinari	130
Calvo-Catoira, Marta	163
Campos, J.B.L.M.	60, 66
Cancela, Joana	39
Caruncho-Pérez, Sara	31
Carvalho, Fábio M.	92
Cerqueira, Laura	87
Cerqueira, Miguel A.	94
Chávez, Ana M.	42, 169
Coimbra, João T. S.	118
Costa, João M.	69
Costa, Paulo C.	84, 75
Crespo, João G.	13
Cristóvão, Maria B.	13
Cristóvão, Raquel O.	45
Dele, Cristina	81

Delerue-Matos, Cristina	75, 84, 111, 113
Dhumal, Dinesh	138
Dias, Madalena M.	69
Díez, Aida M.	28, 51
El-Hachemi, Zoubir	57
Escudero-Curiel, Silvia	54
Esteiro, Paula	163
Estevinho, Berta N.	84, 85, 86, 103, 115
Faria, Joaquim L.	28, 39, 42, 45, 69, 169
Faria, Rui P. V.	19
Fdez-Sanromán, Antía	171
Felgueiras, Mariana B. S.	122
Fernandes, A. Rita T.	166
Fernandes, Isabel	63
Fernandes, Pedro A.	118
Ferreira, Alexandre F.P.	10
Ferreira, António	72, 120
Ferreira, Karoline Kaiser	16
Ferreira, Sara M.	97, 146
Figueiredo, José Luís	37
Flouris, Andreas D.	57
Francisca Rodrigues1	84
Francisca Rodrigues2	111
García-Frutos, Eva M.	109
Goeres, Darla M.	87
Gomes, Inês B.	128, 136
Gomes, Luciana C.	92, 94, 158
Gomes, Mariana	138
Gomes, Sandra M.	34
Gómez-Avilés, Almudena	109
Gonçalves, Antónia	115, 117
Gonçalves, Ariana S. C.	100
Gonçalves, Liliana P. L.	25
González-Romero, Elisa	31, 163
Gorito, Ana M.	13
Gouveia, Teresa I.A.	13
Grabowski, Thais T.	22, 133, 149
Guimarães, Nuno	107
Guiomar, Raquel	89
Ignacio-Meijoeiro, María	31
Jong, Ed.d. De	94
Joy, Amala	39
Kessler, Júlia Cristiê	155
Kolen'ko, Yury V.	173
Laiño-Rodríguez, V.	51
Lamuela-Raventós, Rosa	81
Laura, Cerqueira	161
Leitão, Miguel M.	180

Lima, Marta	92, 94
Lomba-Fernández, Bárbara	171
Lopes, Tânia	152
López-Yerena, Anallely	81
Loureiro, Joana A.	78
Madeira, Luís M.	166
Magalhães, Beatriz T.	118
Magalhães, Duarte J. Junqueira	37
Malaquias, André Fonseca	66
Manrique, Yaidelin A.	69
Mansouri, Racha	149
Marques, Rita	152
Marrocos, Paulo Henrique	63
Martins, Fernando	158
Martins, Isabel Maria Duque	155
Martins, Ramiro E. J.	22, 130, 133, 149
Melo, Luís F.	158
Mendes, Adélio	152
Mergulhão, Filipe J.	92, 94
Messias, Mariana	97
Miranda, João	161
Miranda, João Mário	66
Montes-Paradela, Xoel	31
Morais, Rafael G.	37
Moreira, Manuela M.	111
Narciso, Diogo	158
Nunes, Débora	78
Oliveira, Catarina M.	48
Oliveira, M. Teresa	143
Oliveira, Ricardo	89
Orge, Carla A.	10
Pacheco, Pedro	60
Paiva, Júlio	60
Pané, Salvador	57
Pastrana, Lorenzo	94
Pazos, M.	28, 31, 51, 54, 171
Peñas-Garzón, Manuel	109
Peng, Ling	138
Pereira, Ana	158
Pereira, Ana Rita	128
Pereira, André M.	125
Pereira, Clara R.	125
Pereira, Manuel F. R.	10, 13, 16, 25, 37, 122, 177
Pereira, Maria Carmo	78
Pereira, Rui	116
Pereira, Vanessa J.	13
Pietrobelli, Juliana Martins Teixeira de Abreu	130
Pina, Mafalda	173

Pinho, Eva	89, 107, 140
Pinto, Diana	81, 111
Pires, José C.M.	48
Pituco, Mateus	63
Puigmartí-Luis, Josep	57
Queirós, Gabriela	125
Querido, Ana Rita	25
Ramalho, Patrícia S. F.	177
Regufe, Maria João	10
Restivo, João	10
Rey-Raap, Natalia	37
Ribeiro, Ana Mafalda	10
Ribeiro, Ana R.	13, 166
Ribeiro, Lucília S.	16
Ribeiro, Rui S.	37
Ricardo Oliveira1	140
Rocha, Fernando	115, 120
Rodrigues, Alírio E.	19, 155
Rodrigues, Christianne Elisabete da Costa	155
Rodrigues, Francisca	75, 113
Rodríguez, Xacobe López	54
Romeu, Maria J.	94
Rosales, Emilio	171, 163
Ross, Natiélli Cristina Mendes	130
Saavedra, Maria José	105, 136
Sampaio, Maria J.	39, 45
Sanromán, M. Ángeles	28, 31, 51, 54, 171
Santos, João	107
Santos, Lúcia	34, 97, 146
Santos, Marlei V.	22
Santos, Mónica S.F.	13
Santos, Ricardo J.	39, 63, 69, 72, 143
Santos, Rita S.	107, 118, 138
Sarmento, Bruno	81
Sevim, Semih	57
Silva, Adrián M.T.	13, 28, 42, 166, 169
Silva, Ana Margarida	84, 75, 113
Silva, Ana Rosa	158
Silva, Cláudia G.	28, 39, 42, 45, 69, 143, 169
Silva, Luís	63
Simões, Lúcia Chaves	105
Simões, Manuel	100, 105, 128, 136, 180
Sjollema, Jelmer	92, 94
Sjollema, Jelmer	94
Soares, Ingrid Denardi	155
Soares, Olívia S. G. P.	10, 25, 122, 173, 177
Sorrenti, Alessandro	57
Sousa, Mariana	105

Tavares, Loleny	97
Teixeira, Filipa	84, 113
Teixeira, Lília Soares	105
Teixeira-Santos, Rita	92, 94
Torres-Pinto, André	28, 42
Valcarcel, Jesus	94
Vale, João Pedro	57
Vallverdú-Queralt, Anna	81, 111
Vázquez, José A.	94
Vilar, Vítor	63
Vindeirinho, João	89
Wahed, Ahmed Abd El	89
Walgode, Pedro M.	19
Whitehead, Kathryn A.	92
Zamoshchak, Yana	138



ISBN: 978-972-752-306-1



9 789727 523061 >

🏠 www.fe.up.pt/dce

✉ dce@fe.up.pt